Modulating the Global Conformations of c-Src Kinase

by

Michael Paul Agius II

A dissertation submitted in partial fulfillment
of the requirements for the degree of
Doctor of Philosophy
(Medicinal Chemistry)
in the University of Michigan
2017

Doctoral Committee:

Assistant Professor Matthew B. Soellner, Chair
Assistant Professor Amanda L. Garner
Professor Anna K. Mapp
Professor Brent R. Martin

Michael Paul Agius II

mpagius@umich.edu

ORCID: 0000-0003-2356-4274

DEDICATION

To

My Family: Mom, Dad, & Matt

My Friends: Nick, Brittany, & Cassie

ACKNOWLEDGEMENTS

First and foremost, I would like to thank my advisor, Prof. Matthew Soellner, for his support and guidance throughout graduate school. I especially thank him for allowing me to diversify my skillset to better understand how the research we do in the lab can make a larger impact in the world. His openness and enthusiasm for drug discovery truly enabled me to find a passion in science again. I have grown up so much while in his lab and I need to thank him for being supportive through every one of my phases. I would also like to thank my dissertation committee members Profs. Amanda Garner, Anna Mapp, and Brent Martin for their helpful discussions and suggestions as I progressed though my thesis projects. Specifically I'd like to thank Dr. Anna Mapp for her intellectual contributions and suggestions toward this work.

I would like to thank the current lab members Eric Lachacz and Sameer Phadke. I have seen them both 6 days a week for 5 years, and they have provided a ton of support both in and out of the lab. I also want to thank former lab member, Dr. Kristin Ko, as she has had a tremendous influence in my thesis projects. More importantly she has provided incredible support in professional development, scientific ideas (for all our startup ideas), and as a lifting partner. I specifically need to thank her for our trips exploring food around Ann Arbor and all of the local employees we have became friends with along the way (inventor of the 'Charged Chai-der', Lindsey Lohan, Ahmos Owner, ect.). I hope we one day fulfill our dreams of running a biotech company together.

The College of Pharmacy & the Department of Medicinal Chemistry has provided tremendous support for me during my time here. I need to thank Antionette Hopper, Sarah Lloyd, and Elaine Griffin for their administration support. I also need to thank Jenn Rohl for her incredible guidance toward my professional development. She has

introduced me to U-M alumni and staff who have been very influential players during my graduate school experience. I want to thank her for the amazing enthusiasm she has for helping students, connecting people, and being a great mentor.

I spent a large portion of my time at The Ross School of Business my last year at U-M. I specifically need to thank Mike Johnson for his introduction to the Zell Lurie Commercialization Fund (ZLCF), his mentorship while on the fund, and aid in my professional development. ZLCF was one of the most valuable experiences I've had at U-M and I thank him for the skill set I have acquired in venture capital and technology assessment. The integration with MBA students was not only incredible to obtain a new perspective with a diverse set of students, but I have made some amazing friends along the way.

I have had the opportunity to meet some amazing mentors through the Office of Technology Transfer. Firstly, I need to thank Mutsumi Yoshida and Anne Juggernaut for their support as my supervisors for the fellows program and for introducing me to Mike Johnson from Ross. I also need to thank Dave Repp for his time meeting to discuss all of my career interests and helping with any career preparation. It has been inspiring to work with many of the innovative life-science technologies emerging from the OTT, and the fellows program has provided me a lens of how our discoveries in the lab can eventually make an impact in the clinic.

My friends have been very encouraging during my time at U-M. I want to thank Nick, Brittany, Cassie, for their support, enthusiasm, and encouragement during graduate school. Thank you for understanding all the times I 'had lab.'

Finally, my family has been an incredible support system these past 5 years. They are a constant reminder that life is more than just a list of accomplishments. I need to thank them for all our Sunday dinners and letting me be a forth roommate my last year here. I love you Mom, Dad, and Matt!

TABLE OF CONTENTS

DEDICATION ii

ACKNOWLEDGEMENTS iii

LIST OF TABLES ix

LIST OF FIGURES x

LIST OF SCHEMES xiv

LIST OF APPENDICES xv

ABSTRACT xvii

CHAPTER

I. Protein Kinases Signal Via Catalytic & Non-Catalytic Mechanisms 1

Abstract 1

Kinase Domain Conformation Regulates Catalytic Function 1

Kinases also Signal Through Non-Catalytic Functions 3

Using Kinase Inhibitors to Perturb Non-Catalytic Functions 4

Methods for Elucidating Changes in Quaternary Kinase Conformation 6

Conclusions 8

References 10

II. Development of Selective Proteolysis Methodology to Elucidate Global Kinase Conformations 13

Abstract 13

Introduction 13

Conformational Changes of c-Src Impact its Sensitivity to Thermolysin 17

Expanding Selective Proteolysis to Diverse Kinases Including c-Abl 19

Conclusions 22

Materials and Methods 22

References 25

III. Characterization of Clinical c-Src Mutations Reveals Changes in Global Kinase Conformation 27

Abstract 27

Introduction 27

Clinical c-Src Mutations Show Changes in Global Conformation 30

Non-Clinical Mutations also Influence c-Src's Global Conformation 31

c-Src Conformation can Influence Kinase Catalytic Function 32

Open Mutations can Avoid Down Regulation by Csk 33

The Closed Conformation Resists Phosphorylation at Y530 35

Matching Inhibitor Conformation to Kinase Conformation as a Targeting Strategy 36

Conclusions 38

Materials and Methods 38

References 51

IV. Design of 'Tunable' Conformation-Selective ATP-Competitive Inhibitors 54

Abstract 54

Introduction 54

Conformation Selective Inhibitors can Stabilize Global c-Src Conformations 56

Structure-Conformation Relationship of a Panel of Pyrazolopyrimidine Inhibitors 59

Conformation Analysis of FDA Approved Inhibitors 62

Conclusions 63

Materials and Methods 63

References 79

V. Identification of Allosteric Hotspots that can Modulate the Global Conformation of c-Src Kinase 82

Abstract 82

Introduction 82

MixMd to Identify Allosteric Hotspots 84

Identification of Novel Druggable Hotspots of c-Src 86

Conclusions 89

Materials and Methods 89

References 92

VI. The Future of Inhibiting Kinase Signaling: Modulating both the Catalytic and Non-Catalytic Functions 94

Abstract 94

Introduction 94

Selective Proteolysis of c-Src as a Potential Drop-in Platform Technology 95

Kinase Mutations as Genetic Tools for Elucidating Signaling Pathways 96

Modulating Non-catalytic Functions with Kinase Inhibitors 97

Identifying Allosteric Inhibitors of c-Src Kinase 98

Conclusions 100

References 101

APPENDICES 103

LIST OF TABLES

TABLE		
3.1	Src mutations added onto the down regulated, Src^{SH2Eng} construct shows mutations stabilizing the open conformation (eg. W121R) are a novel mechanism for escaping down regulating processes.	35
3.2	K_{on} determinations using BODIPY labeled conformation-selective probes **3.3** and **3.4** show that matching inhibitor conformation to kinase to be a promising therapeutic strategy for targeting mutations that affect kinase conformation.	37
4.1	Select FDA approved inhibitors screened using selective proteolysis reveals changes in the global conformations of c-Src	62
B.1	Comprehensive Half-Life Table for All Mutations	122
B.2	Comprehensive Table for V_{max} of c-Src Mutants	132
B.3	Comprehensive Table for Substrate K_m of c-Src Mutants	133
B.4	Comprehensive Table for ATP K_m of c-Src Mutants	143
B.5	Comprehensive Table for K_d of SH2-FITC Peptide with c-Src Mutants	144
B.6	Comprehensive Table for c-Src Mutant Melting Temperatures	145
B.7	Initial Phosphorylation Rates of Irreversible Bound Constructs	149
C.1	Comprehensive Table of All Inhibitor Half-Lives	168

LIST OF FIGURES

FIGURE

1.1 (Left) All protein kinases contain a catalytic kinase domain responsible for phosphorylation of down stream protein targets. (Right) Three catalytic residues are essential for catalysis to occur, and conformational changes of these residues are common regulatory mechanisms of protein kinases 2

1.2 c-Src's regulatory SH2 and SH3 domains participate in a number of non-catalytic functions including pathway activation through binding of EGFR or Fak, and additionally participate in auto-inhibitory mechanisms. 3

1.3 Conformation-selective inhibitors of c-Src that bind the αC-helix-in conformation can modulate the activation of EGFR in a non-catalytic manner. 5

1.4 Methods for determining the global conformations of kinases typically used biophysical approaches (X-Ray Crystallography & SAXS) and often required expensive equipment and highly trained technicians. Biochemical approaches lack in their applicability to diverse kinases and for investigating mutations. 7

2.1 The global conformations of c-Src are regulated via phosphorylation states. Phosphorylation at Y419 by a Src Family Kinase (SFK) stabilizes an open conformation (PDB: 1Y5F). Phosphorylation at Y530 by Csk stabilizes a closed conformation (PDB: 2SRC). 14

2.2 The only biochemical method used to determine the global conformation of c-Src. Enrichment via the SH3 domain using an SH3 ligand can be used to determine c-Src's global conformation. Unfortunately, its utility for analyzing mutations or investigating other kinases are major setbacks. 15

2.3 c-Src in the closed conformation and the open conformation. The SH2-Kd linker (red) is highly shielded in the closed and highly accessible in the open conformation, increasing the sensitive of Gly257 (blue) by the protease thermolysin. 16

2.4 Treatment of the open (pY419) and closed (pY530) phosphorylated constructs show differences in the cleavage rate by the protease thermolysin, validating this as a novel method for identifying conformational changes in c-Src. 17

2.5 Conformation selective inhibitors **2.1** and **2.2** are shown to stabilize the open or closed c-Src conformations respectfully and further validate using thermolysin as a method for identifying conformational changes in c-Src. 19

2.6 Sequence alignment of kinases possessing a SH2-Kd linker afforded 9 diverse kinases that could also be investigated using this methodology. 20

2.7 The global conformations of c-Abl can also be determined with this methodology. These results confirm reported observations with the Myristate binding peptide stabilizing the closed conformation (red) and Imatinib the open conformation (blue). The conformation selective Dasatinib analogs **2.1** and **2.2** were also assessed along with the allosteric inhibitor, GNF-2. 21

3.1 c-Src's non-catalytic functions are regulated though its phosphorylation state. Phosphorylation at Y530 on the c-terminal tail by Csk renders a closed kinase conformation, unable to participate in vital protein-protein interactions. Phosphorylation at Y419 renders an open kinase conformation that can form complexes with many protein partners including Fak and EGFR. 28

3.2 Clinical Mutations (Red Spheres) documented from the CCLE and COSMIC databases reveal many that exist distal from the ATP binding pocket and are hypothesized to be modulating the global kinase conformation. 30

3.3 A small panel of clinical c-Src mutants was characterized using selective proteolysis and reveal clinical mutations that can stabilize the open or closed conformations of c-Src. 31

3.4 A panel of non-clinical c-Src mutants was characterized using selective proteolysis and reveal additional mutations that can stabilize the open or closed conformations of c-Src. 32

3.5 All mutants were characterized kinetically and show that closed kinase conformations always displayed a decrease in catalytic function. Open kinase conformation showed more variation, but generally displayed an increase in catalytic activity. 33

3.6 Stabilization of the open and closed conformations, using irreversible conformation-selective Dasatinib inhibitors **3.1** and **3.2**, show differential 36

phosphorylation rates at Y530 by Csk. However, no change in phosphorylation rate was observed at Y419 when using Hck.

4.1 IRE1α has both catalytic kinase function and ribonucleic activity. The ribonuclease activity can additionally be inhibited using a αC-Helix-out inhibitor (through inhibition of oligermization of riboneuclease domain). However, stabilization of the active kinase conformation still inhibits kinase function, but activate ribonuclease activity, showcasing the power of utilizing conformation-selective inhibitors. 55

4.2 Conformation-Selective Dasatinib analogs were designed to stabilize the αC-Helix-in (**4.1**) and αC-Helix-out (**4.2**) conformations to additionally modulate the quaternary structure of c-Src kinase. The binding modes were validated by X- Ray Crystallography PDB: 4YBJ & 4YBK. 57

4.3 Design elements from the Conformational-selective Dasatinib can be adopted by many diverse inhibitor scaffold to modulate the non-catalytic functions of any kinase of interest 58

4.4 Select inhibitors that were utilized to stabilize the open c-Src conformation. Inhibitors **4.5** and **4.7** stabilize the open conformation the most as these inhibitors can stabilize the αC-helix-in conformation using h-bond donors on the inhibitor. 60

4.5 Select inhibitors were designed to stabilize the αC-helix-out conformation through disruption of the catalytic Glu313 and Lys298 salt-bridge. 60

4.6 The full panel of 23 'tunable' conformation-selective inhibitors designed to stabilize various open and closed global conformations of c-Src kinase. 61

5.1 (Left) c-Abl bound to the allosteric inhibitor GNF-2 (blue), which can inhibit catalytic function and stabilize c-Abl in the closed conformation. (Right) c-Src has no known allosteric modulators, however is structurally similar to c-Abl. 83

5.2 MixMD simulations rely on clustering of small organic solvents (triangles), including acetonitrile, isopropanol, and pyrimidine, to identify potential ligand binding 'hotspots.' 85

5.3 MixMD simulations on c-Src afforded 6 potential 'hotspot.' Hotspots 4,5, and 6 will be specifically probed using tryptophan mutations due to their optimal location between the kinase domain and its regulatory SH2/SH3 domains. 87

5.4 Selective proteolysis of 6 tryptophan c-Src mutants. Q365W and T293W (blue) both stabilized the closed conformation and validated pockets 5 & 6 88

as potential allosteric sites. Q254W (green) displayed no change in conformation. Mutations is red could not be expressed.

6.1 Studies to study the effect of global conformational changes independent of catalytic function be carried out utilizing CRISPR-CAS9 technology. 97

6.2 'Tunable' ATP competitive inhibitors can be utilized and adapted to target any kinase of interest. 98

6.3 Identified hotspots can be used to generate PH4 models in which *in-silico* docking experiments can be performed to find allosteric modulators of c-Src. 99

A.1 Mass Spectrometry Data for Selective Proteolysis 104

A.2 Half-Life Determination of c-Src Constructs 105

A.3 Half-Life Curves for Compounds **2.1** and **2.2** bound c-Src 107

A.4 Half-Life Curves for small molecules bound to c-Abl 108

B.1 Selective Proteolysis for Clinical Mutations 111

B.2 Selective Proteolysis for Non-Clinical Mutations and Complexes 115

B.3 V_{max} & Substrate K_m Determinations for c-Src Mutations/Constructs 123

B.4 ATP K_m Determination for c-Src Mutants 134

B.5 Phosphorylation Rate Determination with **3.1** and **3.2** c-Src 146

B.6 K_{off} Rates for BODIPY Compounds **3.3** & **3.4** 154

B.7 K_d Determination for BODIPY Compounds 3.3 & 3.4 157

C.1 Selective Proteolysis Results for c-Src Inhibitors 160

D.1 Analytical Data for Half-Life Determination of c-Src Mutants 185

LIST OF SCHEMES

SCHEME

3.1	Synthetic Route for Compound **3.1**	43
3.2	Synthetic Route for Compound **3.2**	44
3.3	Synthesis of Compound **3.7**	44
3.4	Synthesis of Compound **3.9**	45
3.5	Synthesis of Compound **3.10**	46
3.6	Synthesis of Compound **3.1**	46
3.7	Synthesis of Compound **3.11**	47
3.8	Synthesis of Compound **3.12**	48
3.9	Synthesis of Compound **3.13**	49
3.10	Synthesis of Compound **3.2**	49
4.1	Synthetic Route for Intermediate **4.29**	64
4.2	Synthetic Route for Intermediate **4.30**	65
4.3	General Synthetic Route for Select Pyrazolopyrimidine Compounds	65
4.4	Synthesis of Compound **4.5**	66
4.5	Synthesis of Compound **4.11**	66
4.6	Synthesis of Compound **4.12**	67
4.7	Synthesis of Compound **4.13**	68
4.8	Synthesis of Compound **4.14**	68
4.9	Synthesis of Compound **4.16**	69
4.10	Synthesis of Compound **4.17**	70
4.11	Synthesis of Compound **4.18**	70
4.12	Synthesis of Compound **4.20**	71
4.13	Synthesis of Compound **4.21**	72
4.14	Synthesis of Compound **4.22**	73
4.15	Synthesis of Compound **4.23**	74
4.16	Synthesis of Compound **4.6**	74
4.17	Synthesis of Compound **4.24**	75
4.18	Synthesis of Compound **4.25**	76
4.19	Synthesis of Compound **4.26**	76
4.20	Synthesis of Compound **4.27**	77
4.21	Synthesis of Compound **4.28**	78

LIST OF APPENDICES

APPENDIX

A. Supplemental Information for Chapter II 103

Mass Spectrometry Data for Selective Proteolysis 104

Analytical Data for Half-Life Determination of c-Src Constructs 105

Analytical Data for **2.1** & **2.2** bound c-Src 107

Analytical Data for Small Molecules bound c-Abl 108

B. Analytical Data and Supplemental Information for Chapter III 110

Selective Proteolysis for Clinical Mutations 111

Selective Proteolysis for Non-Clinical Mutations & Complexes 115

V_{max} & Substrate K_m Determinations for c-Src Mutations/Constructs 123

ATP K_m Determination for c-Src Mutants 134

Phosphorylation Rate Determination of 3.1 & 3.2 Src Complexes 146

Spectral Data of Compounds 3.1, 3.2, 3.7, 3.9 – 3.12 150

K_{off} Rates for BODIPY Compounds 3.3 & 3.4 154

K_d Determination for BODIPY Compounds 3.3 & 3.4 157

C. Analytical Data and Supplemental Information for Chapter IV 159

Selective Proteolysis Results for c-Src Inhibitors 160

Spectral Data for Compounds 4.5, 4.11 – 4.14, 4.16 – 4.18, 4.20 - 4.28 169

D. Supplemental Information for Chapter V 184

Analytical Data for Half-Life Determination of c-Src Mutants 185

ABSTRACT

Protein Kinases are key regulators of important cellular processes and have been a validated therapeutic target for cancer over the past two decades. Kinase signaling is a combination of its catalytic function, through post-translational phosphorylation, and non-catalytic functions, often through protein-protein interactions. The design of kinase inhibitors to inhibit kinase signaling has solely focused on inhibition of the catalytic process. However, evidence of inhibitors modulating non-catalytic functions, through stabilizing distinct kinase conformations, has uncovered a novel strategy for modulating of both arms of kinase signaling. Unfortunately, the lack of tools to elucidate kinase conformational changes has stalled the targeting of these non-catalytic processes.

The work herein highlights methods, both ligand and mutation induced, to modulate the global conformation of c-Src kinase. Characterization of these conformational changes was made possible by the development of our novel 'Selective Proteolysis' methodology that takes advantage of c-Src's sensitivity to the protease thermolysin. Using this methodology we have characterized a panel of clinical c-Src mutations and have uncovered W121R to be a potential activating c-Src mutation. To improve the targeting strategies of c-Src, we developed series of ATP competitive, conformation-tunable inhibitors, to inhibit the catalytic function of c-Src, while simultaneously modulating its non-catalytic functions. Furthermore, we utilized MixMD methodology to identify two novel allosteric hotspots of c-Src that can be utilized to identify allosteric modulators of c-Src.

This work demonstrates that inhibitors of c-Src can be used to modulate both catalytic and non-catalytic functions simultaneous. Additionally, that clinical mutations may be activating through stabilization of district protein conformations. We hope that others utilize this work as a stepping-stone towards developing the next generation of kinase targeted therapies with improved signaling modulation.

Chapter I

Protein Kinases Signal Via Catalytic & Non-Catalytic Mechanisms

Abstract

Protein Kinases are key regulators of important cellular processes and have been a validated therapeutic target for cancer over the past two decades. Kinase signaling is a combination of catalytic function, through post-translational phosphorylation, and non-catalytic functions, often through protein-protein interactions. Both catalytic and non-catalytic functions are regulated through conformational changes in the kinase domain or regulatory domains respectfully. The focus on modulating kinase signaling, using kinase inhibitors, has been solely on the catalytic process. However, more evidence of inhibitors modulating non-catalytic functions, through stabilizing distinct kinase conformations, has revealed a novel strategy for modulating of both arms of kinase signaling. Unfortunately, the lack of tools to elucidate kinase conformational changes has stalled the progress for targeting these non-catalytic processes. Thus, the development of tools, that can be easily implemented and used on many diverse kinases, will enable researchers to begin modulating kinase signaling to its fullest extent.

Kinase Domain Conformation Regulates Catalytic Function

Protein Kinases (PKs) function as key regulators of important cellular processes such as cell growth and survival through post-translational phosphorylation.[1-3] The PK superfamily is one of the largest protein families, encoding a total of 518 protein kinases.[4] All PKs consist of a highly conserved catalytic domain responsible for phosphorylation of their protein substrates. Mapping of these downstream phosphorylation pathways have provided researchers a clearer understanding how messages from the extracellular environment can propagate and eventually lead to global changes gene expression.[5-7]

Structurally, all protein kinases possess a catalytic domain responsible for catalyzing the phosphorylation reaction of their downstream targets. While sequence

identity will differ vastly between kinases, they structurally all contain key regulatory motifs used to modulate their catalytic activity.[8] The active kinase conformation involves 3 catalytic residues to sit in the correct orientation for catalysis to occur (Figure 1.1). The first includes a catalytic aspartate that points into the ATP binding site and coordinates a Mg^{2+} cation.[9] The magnesium cation is responsible for de-shielding the localized negative charge associated with the beta and gamma phosphates of ATP. This aspartate resides on a key kinase motif, known as the 'DFG'-motif, and is speculated to be a common regulatory loop among the kinome.[10, 11]

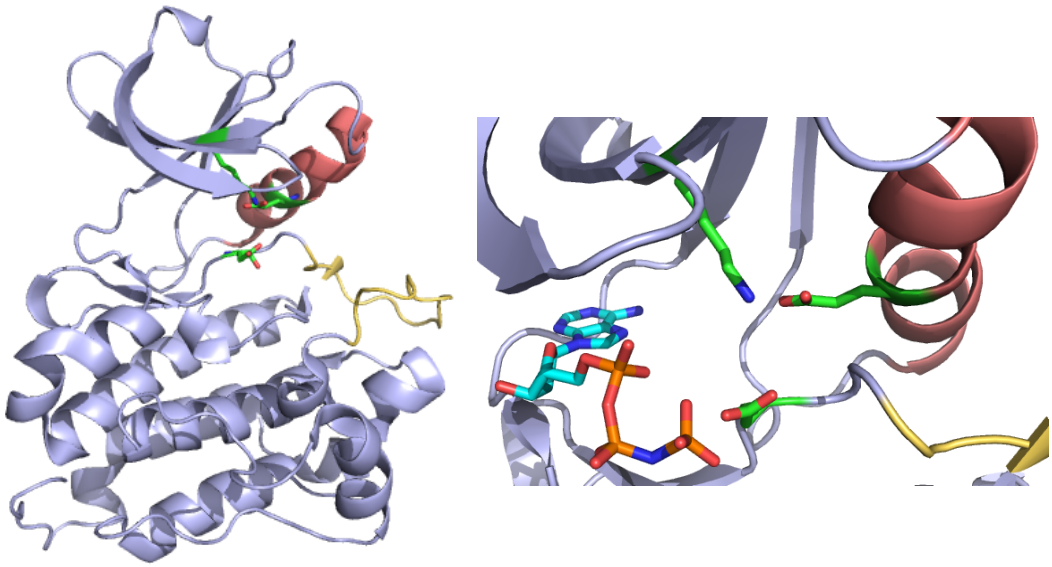

Figure 1.1. (Left) All protein kinases contain a catalytic kinase domain responsible for phosphorylation of down stream protein targets. (Right) Three catalytic residues are essential for catalysis to occur, and conformational changes of these residues are common regulatory mechanisms of protein kinases.

The second residue includes a catalytic lysine (on the roof of the ATP pocket), which is responsible for forming a key electrostatic interaction with the α-phosphate of ATP.[12] The third residue is a catalytic glutamate that is located on the αC-helix of the kinase domain. This glutamate interacts and stabilizes the catalytic lysine through

formation of a salt-bridge.[13] Additionally, Modulating the conformation of the αC-helix is a common regulatory mechanism seen in a number of diverse kinases including c-Src and CDKs.[14, 15] The outwards shift of this helix (though a physiological or inhibitor induced event) breaks the salt bridge to the catalytic lysine and renders the kinase inactive. While the kinome is often depicted with a highly organized phylogenetic tree, we should be aware that these groupings of related kinases leave out an important feature: kinases' regulatory domains.[16]

Kinases also Signal Through Non-Catalytic Functions

In addition to the catalytic kinase domain, protein kinases often possess key regulatory domains that remain underappreciated when discussing kinase signaling.[17, 18] These regulatory domains often help coordinate kinase signaling within the cell and can function independently of a kinase's catalytic ability.

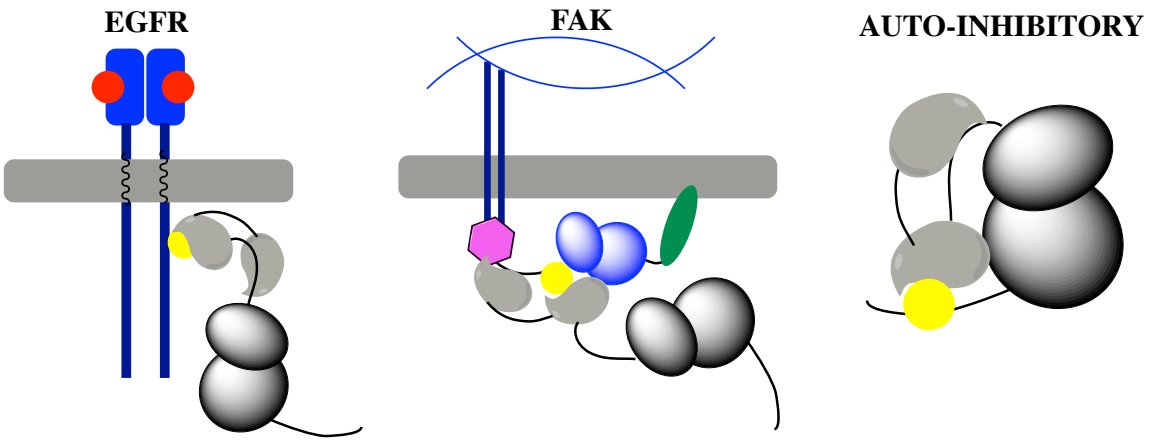

Figure 1.2. c-Src's regulatory SH2 and SH3 domains participate in a number of non-catalytic functions including pathway activation through binding of EGFR or Fak, and additionally participate in auto-inhibitory mechanisms.

For example, these regulatory domains can be seen as protein binding domains such as the SH2 or SH3 domains in the kinases c-Abl, Btk, and the Src family kinases.[19-21] These regulatory domains have many diverse functions, and when used in tandem with

the kinase's catalytic function, encompass the entirety of kinase signaling (Figure 1.2). The SH2 and SH3 domains have been shown to enable kinases to form protein complexes as these domains can bind phospho-tyrosine residues and specific poly-proline sequences respectfully.[22, 23] They are used to coordinate cellular localization and can also aid in cell membrane recruitment or internalization processes.[24, 25] Finally, they have also been observed in auto-inhibitory mechanisms as a method to inhibit their intrinsic catalytic activity.[16]

Other kinases possess regulatory domains with their own intrinsic catalytic activity, including the kinase IRE1α, which possesses ribonuclease activity that is activated in the unfolded protein response.[26] Receptor tyrosine kinases, including EGFR and VEGFR, contain extracellular ligand binding domains, which are responsible for sensing and binding the extracellular ligands EGF and VEGF.[27, 28] Finally, many kinases, including the MAP family kinases, possess no regulatory domains. They however, can still signal through non-catalytic mechanisms, including Erk2, which can activate the phosphatase DUSP6 via a key protein-protein interaction.[29, 30]

Kinases' ability to participate in these non-catalytic mechanisms enable their signaling to be both highly intricate and tightly regulated.[31] Unfortunately, their catalytic ability still remains the focus when investigating kinase signaling. The combination of both the catalytic and non-catalytic signaling mechanisms encompasses the entirety of kinase signaling. In diseases, especially cancer, where kinase signaling is often dysregulated or perturbed, targeting strategies that focus on modulating both signaling arms should be considered when developing targeted therapies. Luckily, progress towards the inhibition of these non-catalytic functions have just began to surface in the literature and has been proven to be a successful targeting strategy for many diseases.

Using Kinase Inhibitors to Perturb Non-Catalytic Functions

Over the past decade, the success of kinase target therapies in the clinic has been seen with the over 32 FDA approved inhibitors in 2016.[32] The dysregulation of kinase signaling has been a major hallmark for nearly every cancer type.[33] Thus, the use of kinase inhibitors has been a powerful tool for elucidating these complex signaling pathways and treating diseases in the clinic. Still today, the focus on developing kinase

inhibitors still remains on modulating catalytic function through the development of ATP-competitive inhibitors. Only recently has it been showcased that ATP competitive inhibitors additionally have the ability to modulate non-catalytic functions simultaneously.[31]

Previously mentioned was the ribonuclease activity of IRE1α involved in the unfolded protein response. The Maly group has since reported a series of IRE1α inhibitors that can additionally inhibit ribonuclease activity in addition to the catalytic kinase activity.[34] Crystal structures showcased these inhibitors stabilizing an inactive kinase conformation, or αC-helix-out conformation, where the ligand bound kinase is stabilizing a conformation where the αC-helix was rotated outward (breaking the Glu-Lys salt bridge needed for catalysis). This data demonstrated one of the first examples of ATP competitive inhibitors modulating non-catalytic functions, however IRE1α was not simply an isolated case.

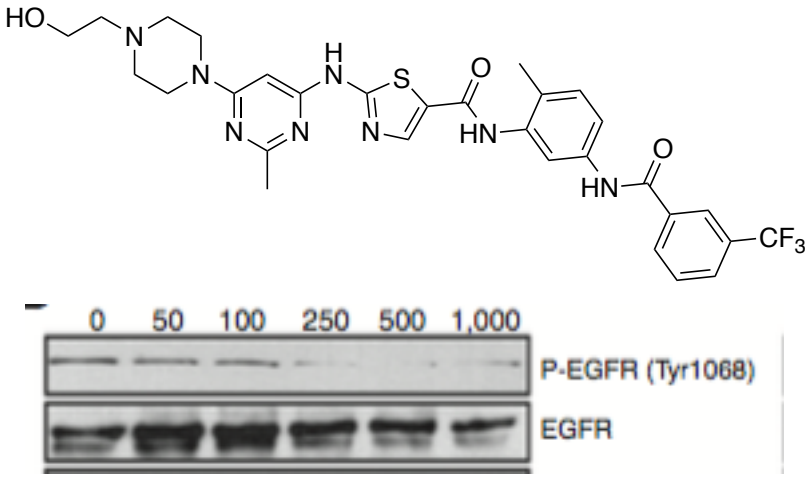

Figure 1.3. Conformation-selective inhibitors of c-Src that bind the αC-helix-in conformation can modulate the activation of EGFR in a non-catalytic manner.

The serine/threonine kinase Erk2 possesses no regulatory domains and it can be hypothesized to be difficult to disrupt any non-catalytic processes due to the lack of regulatory domains. However, it has been shown that ATP-competitive inhibitors of

Erk2 additionally have the ability to inhibit non-catalytic roles. The Maly lab additionally reported Erk2 inhibitors that stabilize an inactive conformation in which the inhibitor causes a conformational change in the kinase's activation loop (commonly referred to DFG-out).[35] This conformational change was observed to cause a decrease in activation of Erk2 by disrupting the orientation of two residues that become phosphorylated during activation of the kinase. Additionally, Erk2 bound in this in-active DFG-out conformation, inhibited the activation of the phosphatase DUSP6 without modulating the biding affinity to Erk2. This data demonstrate that even kinases without having modular regulatory domains can still be targeted using conformation-selective inhibitors.

Finally, c-Src was the first proto-oncogene identified and still remains a popular drug target for a number of cancer types.[36] Stabilization of the αC-helix-in or αC-helix-out has been shown to regulate the accessibility of its regulatory SH2 and SH3 domains, and is of large focus in the upcoming chapters.[37, 38] Clinically, our lab has identified c-Src to be an important target for treating triple-negative breast cancer. Recently reported is a clinical candidate based off the Dasatinib scaffold that additionally binds the αC-helix-in conformation.[39] Modulation of c-Src's αC-helix is shown to stabilize an open kinase conformation, and empirically we have shown it to inhibit EGFR signaling in a non-catalytic fashion, with decrease in phosphorylation at Y1068 (not seen when using Dasatinib, the αC-helix 'neutral' analog) (Figure 1.3).

These examples showcase that designing inhibitors to modulate kinase signaling can be expanded to perturb more than catalytic activity, thus impacting kinase signaling to a greater extent. These data also showcase that influencing a kinases' non-catalytic functions can be easily accomplished through probing of the ATP binding pocket, an area that researchers have become very effective at targeting. Unfortunately, these non-catalytic functions are often regulated though conformational changes in quaternary structure. Thus, the lack of tools to easily and rapidly assess protein conformational changes has stalled the exploration of this targeting strategy.

Methods for Elucidating Changes in Quaternary Kinase Conformation

The challenge of assessing a kinase's global conformation has stalled the efforts of researchers looking to modulate kinase non-catalytic functions. Existing methods to determine the global conformations of multi-domain kinases rely upon complex biophysical techniques (Figure 1.4). X-ray crystallography can often capture unique kinase conformational changes as seen with c-Src (e.g., PDB: 2SRC, 1Y57).[38, 39] However, these structures can be influenced through crystal packing, experimental conditions (e.g., pH, detergent) and stabilization of energy minimum conformations, which may not accurately depict solution phase conformations. More recently, SAXS and NMR spectroscopy have been utilized to observe conformation in solution. For example, SAXS analysis of c-Src confirmed the conformations observed by X-ray crystallography.[40] NMR spectroscopy has been utilized to see changes in tertiary structure of c-Src (changes in the αC-helix).[41] These techniques are far superior to X-ray crystallography as it provides insight to structure in the solutions phase. However, these techniques both require large quantities of purified protein, a highly skilled technician, expensive equipment, and often take weeks for experiment optimization.

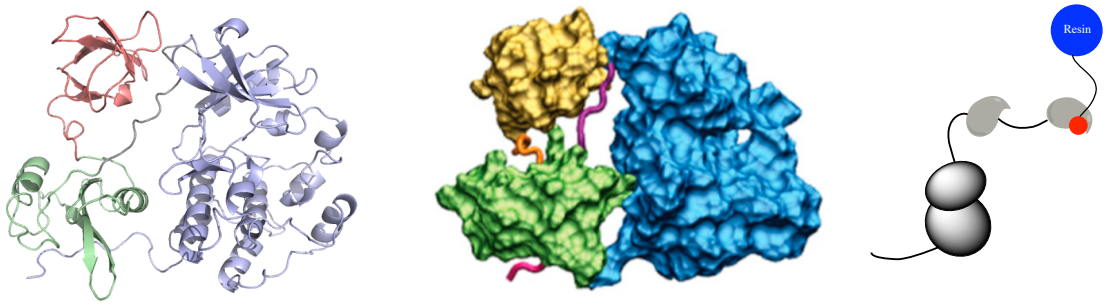

Figure 1.4. Methods for determining the global conformations of kinases typically used biophysical approaches (X-Ray Crystallography & SAXS) and often required expensive equipment and highly trained technicians. Biochemical approaches lack in their applicability to diverse kinases and for investigating mutations.

Only recently, biochemical approaches for c-Src are being utilized involving enrichment through its SH3 domain with an SH3 ligand.[42] While much simpler than

alternative techniques, it lacks application to other kinases to those without an SH3 or similar binding domain. Additionally, it requires a domain with a significant conformational change, and one that has an available ligand, with modest potency, to implement the enrichment experiment with. Finally, any mutations introduced to these kinases can affect the enrichment experiment if these mutations are on or near the binding site of the pull-down. Therefore, a more robust method, applicable to many diverse kinases and not sensitive to mutagenesis, would be highly valuable for elucidating conformational changes in c-Src and thus begin exploring the non-catalytic functions.

Conclusions

Kinase's catalytic functions and downstream phosphorylation pathways have been used for decades to map and understand their complex signaling pathways.[2] Catalytic residues that reside in the ATP binding site can modulate a kinase's catalytic function.[9-11] Conformational changes of these residues, to inactive the kinase, has been seen as a regulatory mechanism both physiologically as well as ligand induced. More recently however, these ligand-induced conformations are now beginning to be appreciated for modulating non-catalytic signaling as well. These non-catalytic functions have additionally been determined to play a crucial role in signaling mechanisms.[31] Thus, modulating both catalytic and non-catalytic mechanism simultaneously is a unique strategy for targeting kinase signaling, and has even been demonstrated in the literature with IRE1α, Erk2, and c-Src.[34, 35, 42] However, as non-catalytic functions are regulated through large conformational changes in protein structure, they still remain a challenge for researchers to investigate.

The work herein reveals novel methodology that can be utilized to observe changes in the global conformation of c-Src. With this method, we have begun revealing how best to modulate c-Src's global conformation toward targeting c-Src's non-catalytic functions. Furthermore, we have showcased, using both mutagenesis and inhibitor based methods, how c-Src's global conformation can be used to alter cellular signaling, escape down regulation mechanisms, and present a unique strategy for targeting using conformation-selective inhibitors. These data presented in this dissertation will enable researchers to begin developing methodologies and conformation-selective kinase

inhibitors of their own, to begin modulating both catalytic and non-catalytic functions of their respected targets.

References

1. Hunter T. Protein kinases and phosphatases: the yin and yang of protein phosphorylation and signaling. *Cell*. **1995**, *80* (2), 225-36.
2. Manning G, Whyte DB, Martinez R, Hunter T, Sudarsanam S. The Protein Kinase Complement of the Human Genome. *Science***. 2002**, 298 (5600), 1912-34.
3. Hunter T. A Thousand and One Protein Kinases. *Cell*. **1987**, 50 (6), 823-9.
4. Manning G, Whyte DB, Martinez R, Hunter T, Sudarsanam S. The Protein Kinase Complement of the Human Genome. *Science***. 2002**, 298 (5600), 1912-34.
5. Su B, Karin M. Mitogen-activated Protein Kinase Cascades and Regulation of Gene Expression. Current opinion in Immunology. **1996**, 8 (3), 402-11.
6. Yoon S, Seger R. The Extracellular Signal-Regulated Kinase: Multiple Substrates Regulate Diverse Cellular Functions. *Growth factors*. **2006**, 24(1), 21-44.
7. Marshall CJ. Specificity of Receptor Tyrosine Kinase Signaling: Transient Versus Sustained Extracellular Signal-Regulated Kinase Activation. *Cel*l. **1995**, 80(2), 179-85.
8. Vulpetti A, Bosotti R. Sequence and Structural Analysis of Kinase ATP Pocket Residues. *Il Farmaco*. **2004,** 59(10), 759-65.
9. Nolen B, Taylor S, Ghosh G. Regulation of Protein Kinases: Controlling Activity Through Activation Segment Conformation. *Molecular Cell*. **2004**, 15(5), 661-75.
10. Kornev AP, Haste NM, Taylor SS, Ten Eyck LF. Surface Comparison of Active and Inactive Protein Kinases Identifies a Conserved Activation Mechanism. *Proceedings of the National Academy of Sciences*. **2006**, 103(47), 17783-8.
11. Treiber DK, Shah NP. Ins and Outs of Kinase DFG motifs. *Chemistry & BIology*. **2013**, 20(6), 745-6.
12. Carrera AC, Alexandrov K, Roberts TM. The Conserved Lysine of the Catalytic Domain of Protein Kinases is Actively Involved in the Phosphotransfer Reaction and not Required for Anchoring ATP. *Proceedings of the National Academy of Sciences.* **1993**, 90(2), 442-6.
13. Johnson LN, Noble ME, Owen DJ. Active and Inactive Protein Kinases: Structural Basis for Regulation. *Cell*. **1996**, 85(2), 149-58.
14. Roskoski R. Src Protein–Tyrosine Kinase Structure and Regulation. *Biochemical and Biophysical Research Communications*. **2004**, 324(4), 1155-64.
15. Huang H, Zhao R, Dickson BM, Skeel RD, Post CB. αC Helix as a Switch in the Conformational Transition of Src/CDK-like Kinase Domains. *The Journal of Physical Chemistry B*. **2012,** 116(15), 4465-75.
16. Soderling TR. Protein kinases. Regulation by Autoinhibitory Domains. *Journal of Biological Chemistry*. **1990**, 265(4), 1823-6.
17. Taylor SS, Kornev AP. Protein Kinases: Evolution of Dynamic Regulatory Proteins. *Trends in Biochemical Sciences*. **2011**, 36(2), 65-77.
18. Corbalán-García S, Gómez-Fernández JC. Protein kinase C Regulatory Domains: the Art of Decoding many Different Signals in Membranes. *Biochimica et Biophysica Acta (BBA)-Molecular and Cell Biology of Lipids*. **2006**, 1761(7), 633-54.
19. Nagar B, Hantschel O, Seeliger M, Davies JM, Weis WI, Superti-Furga G, Kuriyan J. Organization of the SH3-SH2 Unit in Active and Inactive Forms of the c-Abl Tyrosine Kinase. *Molecular cell*. **2006**, 21(6), 787-98.

20. Park H, Wahl MI, Afar DE, Turck CW, Rawlings DJ, Tam C, Scharenberg AM, Kinet JP, Witte ON. Regulation of Btk Function by a Major Autophosphorylation Site Within the SH3 domain. *Immunity*. **1996**, 4(5), 515-25.
21. Young MA, Gonfloni S, Superti-Furga G, Roux B, Kuriyan J. Dynamic Coupling Between the SH2 and SH3 Domains of c-Src and Hck Underlies their Inactivation by C-terminal Tyrosine Phosphorylation. *Cell*. **2001**, 105(1), 115-26.
22. Koch CA, Anderson D, Moran MF, Ellis C, Pawson T. SH2 and SH3 domains: Elements that Control Interactions of Cytoplasmic Signaling Proteins. *Science*. **1991** , 252(5006), 668-75.
23. Pawson T, Gish GD. SH2 and SH3 Domains: from Structure to Function. *Cell*. **1992**, 71(3), 359-62.
24. Buday L. Membrane-targeting of Signaling Molecules by SH2/SH3 domain-Containing Adaptor Proteins. *Biochimica et Biophysica Acta (BBA)-Reviews on Biomembranes*. **1999**, 1422(2), 187-204.
25. Yamazaki T, Zaal K, Hailey D, Presley J, Lippincott-Schwartz J, Samelson LE. Role of Grb2 in EGF-stimulated EGFR Internalization. *Journal of Cell Science*. **2002**, 115(9), 1791-802.
26. Chen Y, Brandizzi F. IRE1: ER Stress Sensor and Cell Fate Executor. *Trends in Cell Biology*. **2013**, 23(11), 547-55.
27. Herbst RS. Review of Epidermal Growth Factor Receptor Biology. *International Journal of Radiation Oncology* Biology* Physics*. **2004**, 59(2), S21-6.
28. Jeffers M, LaRochelle WJ, Lichenstein HS. Fibroblast Growth Factors in Cancer: Therapeutic Possibilities. *Expert opinion on Therapeutic Targets*. **2002**, 6(4), 469-82.
29. Saxena M, Williams S, Taskén K, Mustelin T. Crosstalk Between cAMP-Dependent Kinase and MAP Kinase through a Protein Tyrosine Phosphatase. *Nature cell Biology*. **1999**, 1(5).
30. Owens DM, Keyse SM. Differential Regulation of MAP kinase Signalling by Dual-Specificity Protein Phosphatases. *Oncogene***. 2007**, 26(22), 3203.
31. Kung JE, Jura N. Structural Basis for the Non-catalytic Functions of Protein Kinases. *Structure*. **2016**, 24(1), 7-24.
32. Wu P, Nielsen TE, Clausen MH. Small-Molecule Kinase Inhibitors: an Analysis of FDA-Approved Drugs. *Drug Discovery Today*. **2016**, 21(1), 5-10.
33. Blume-Jensen P, Hunter T. Oncogenic Kinase Signalling. *Nature*. 2001, 411(6835), 355.
34. Maly DJ, Papa FR. Druggable Sensors of the Unfolded Protein Response. *Nature Chemical Biology*. **2014**, 10(11), 892-901.
35. Hari SB, Merritt EA, Maly DJ. Conformation-Selective ATP-competitive Inhibitors Control Regulatory Interactions and Noncatalytic Functions of Mitogen-Activated Protein Kinases. *Chemistry & Biology*. **2014**, 21(5), 628-35.
36. Martin GS. The Road to Src. *Oncogene*. **2004**, 23(48), 7910.
37. Xu W, Doshi A, Lei M, Eck MJ, Harrison SC. Crystal structures of c-Src Reveal Features of its Autoinhibitory Mechanism. *Molecular Cell*. **1999,** 3(5), 629-38.
38. Cowan-Jacob SW, Fendrich G, Manley PW, Jahnke W, Fabbro D, Liebetanz J, Meyer T. The Crystal Structure of a c-Src Complex in an Active Conformation Suggests Possible steps in c-Src Activation. *Structure***. 2005**, 13(6, 861-71.

39. Gilani RA, Phadke S, Bao LW, Lachacz EJ, Dziubinski ML, Brandvold KR, Steffey ME, Kwarcinski FE, Graveel CR, Kidwell KM, Merajver SD. UM-164: a Potent c-Src/p38 Kinase Inhibitor with in Vivo Activity Against Triple-Negative Breast Cancer. *Clinical Cancer Research*. **2016**, 22(20), 5087-96.
40. Bernadó P, Pérez Y, Svergun DI, Pons M. Structural Characterization of the Active and Inactive States of Src kinase in Solution by Small-angle X-ray Scattering. *Journal of Molecular Biology*. **2008**, 376(2), 492-505.
41. Ulmer TS, Werner JM, Campbell ID. SH3-SH2 Domain Orientation in Src kinases: NMR studies of Fyn. *Structure*. **2002**, 10(7), 901-11.
42. Krishnamurty R, Brigham JL, Leonard SE, Ranjitkar P, Larson ET, Dale EJ, Merritt EA, Maly DJ. Active Site Profiling Reveals Coupling Between Domains in SRC-family kinases. *Nature Chemical Biology*. **2013**, 9(1), 43-50.

CHAPTER II

Development of Selective Proteolysis Methodology to Elucidate Global Kinase Conformations

Abstract

Methods to evaluate changes in the global conformations of kinases involve complex biophysical or biochemical techniques that prevent both its adoption among scientists and its use in a high-throughput fashion. Identifying changes in the accessibility of the SH2-Kinase domain linker, in the open and closed conformation of c-Src, provided a promising site to interrogate changes in c-Src's global conformation. The bacterial protease thermolysin was previously reported to selectively cleave this linker and provided a novel tool to better elucidate global conformational changes in a handful of diverse kinases. We utilized model kinases, c-Src & c-Abl, and have displayed that kinase conformation using our developed, 'selective proteolysis methodology', align well with highly validated kinase constructs (using both phosphorylated and ligand bound states). The development of this method has paved the way for ongoing studies to further reveal the effects that global conformation have in both cell signaling pathways and targeting strategies of protein kinases.

Introduction

While a variety of methods exist that can evaluate the catalytic activity of kinases, the development of methods to evaluate kinase conformation is still in its infancy and rely on techniques used to study the structure of any protein of interest. Existing methods to determine the global conformations of multi-domain kinases rely upon complex biophysical techniques. X-ray crystallography is often the most utilized of techniques and can often capture unique kinase conformational changes as seen with c-Src (e.g., PDB: 2SRC, 1Y57).[1,2] Figure 2.1 displays c-Src adopting two very distinct global conformations with its SH2 and SH3 domains bound (left) or unbound (right) to the

kinase domain. While c-Src's global conformations can be elucidated from these structures, the conformations of other multi-domain kinases can be influenced through crystal packing, experimental conditions (e.g., pH, detergent) and stabilization of energy minimum conformations, which may not accurately depict relevant, solution phase conformations. Thus, investigating global kinase conformation using protein in the solution phase would provide a more physiological accurate and dynamic model of how these protein conformations are behaving.

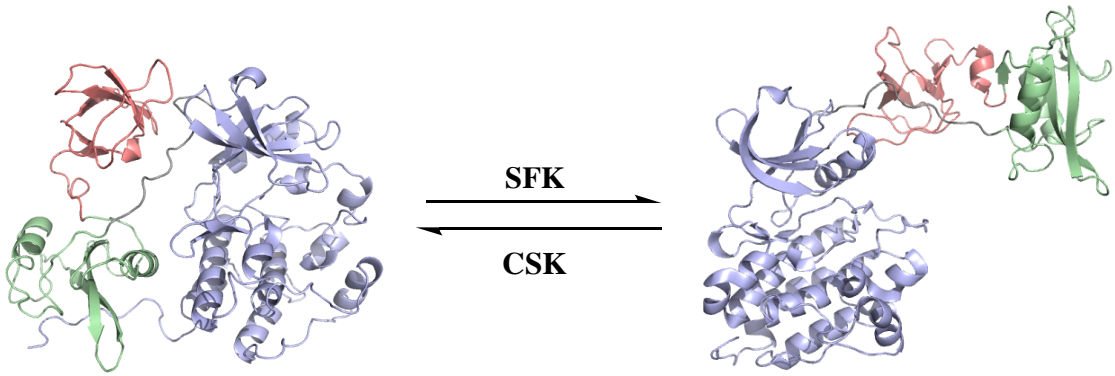

Figure 2.1. The global conformations of c-Src are regulated via phosphorylation states. Phosphorylation at Y419 by a Src Family Kinase (SFK) stabilizes an open conformation (PDB: 1Y5F). Phosphorylation at Y530 by Csk stabilizes a closed conformation (PDB: 2SRC).

More recently, SAXS and NMR spectroscopy have been utilized to observe conformation in solution. The Pons lab have preformed the SAXS analysis of c-Src and successfully confirmed the conformations observed using X-ray crystallography methods.[3] SAXS analysis of the kinase c-Abl also identified unique global conformations of c-Abl when bound to the FDA approved inhibitors, Dasatinib and Imatinib.[4] Additionally, NMR spectroscopy has been a useful biophysical application and can be utilized to see changes in tertiary structure of c-Src that are known to change when

adopting distinct global conformations (e.g. changes in αC-helix).[5] Unfortunately, these techniques both require large quantities of purified protein (which are easy to obtain when analyzing only the kinase domain), which remain a difficult challenge when obtaining multi-domain kinase constructs. Additionally, a highly skilled technician and expensive equipment are needed to preform the analysis of SAXS, X-Ray crystallography, and NMR studies. Finally, these experiments often take weeks for experiment optimization and thus does not make them amenable for use in a high-throughput fashion.

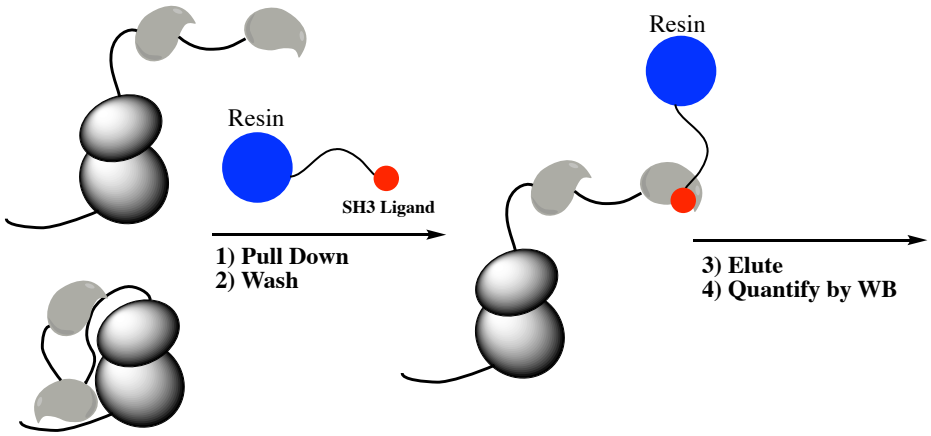

Figure 2.2. The only biochemical method used to determine the global conformation of c-Src. Enrichment via the SH3 domain using an SH3 ligand can be used to determine c-Src's global conformation. Unfortunately, its utility for analyzing mutations or investigating other kinases are major setbacks.

More recently, biochemical approaches for c-Src are being utilized involving enrichment through its SH3 domain (with an SH3 ligand) recently reported by the Maly Lab (Figure 2.2).[6] This methodology relies upon c-Src's SH3 domain becoming more accessible in the 'open' conformation (solvent exposed) and shielded in the 'closed' conformation (bound to SH2-KD linker). While this technique is much simpler than alternative methods mentioned above, it lacks the broad application to other kinases. This methodology requires a target kinase to possess a domain with a significant

conformational change, in which the said domain has an existing high-affinity ligand that can be immobilized onto resin, to implement the enrichment experiment with. Toward a goal of making a high-throughput & robust assay to decipher kinase conformation of any full-length, multi-domain kinase of interest, we set out to develop a technique that has none of the limitations inherent in other techniques mentioned above.

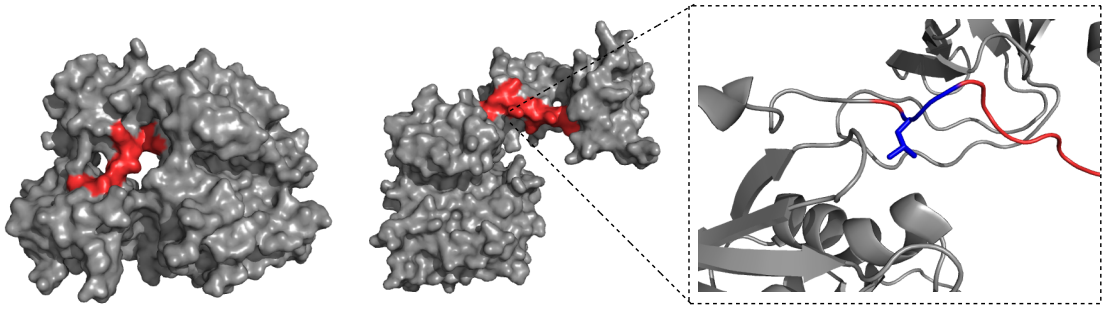

Figure 2.3. c-Src in the closed conformation and the open conformation. The SH2-Kd linker (red) is highly shielded in the closed and highly accessible in the open conformation, increasing the sensitive of Gly257 (blue) by the protease thermolysin.

In 1989, the Cooper laboratory reported that c-Src was selectively cleaved by the bacterial protease thermolysin.[7] After analysis by SDS-PAGE, it was hypothesized that the cleavage site was found somewhere within the linker region that connects the kinase and SH2 domains. Observing the existing crystal structures of c-Src, we have identified two distinct global conformations that showcase open/extended (PDB: 1Y57) and closed/compact (PDB: 2SRC) conformations. A feature of the mechanism by which c-Src goes from open to closed is the SH3 domain binding to the SH2-KD linker. Thus, the SH2-KD linker of c-Src is protected by the SH3 domain in the closed conformation, and solvent-accessible in the open conformation. We hypothesized that the SH2-KD linker cleavage rate by thermolysin could provide an indication of the c-Src's global conformation, and be an amenable method to use for determining changes in global conformations across the kinome.

Conformational Changes of c-Src Impact its Sensitivity to Thermolysin

As descried above, c-Src's global conformations *in-vivo* are regulated via the phosphorylation state of c-Src.[8,9] Activation of c-Src occurs though phosphorylation of the activation loop at Y419 by either autophosphorylation, or transphosphorylation by another SFK.[10] This event stabilizes c-Src in a catalytically active state and renders the SH2 and SH3 domains to adopt a more extended or 'open' conformation. Inactivating c-Src occurs through phosphorylation at tyrosine 530, by CSK, which resides on the C-Terminal tail.[11] This event causes a global conformational change in which the SH2 domain binds the phosphor-tyrosine of pY530 and the SH3 domain docks to the SH2-KD linker.[12]

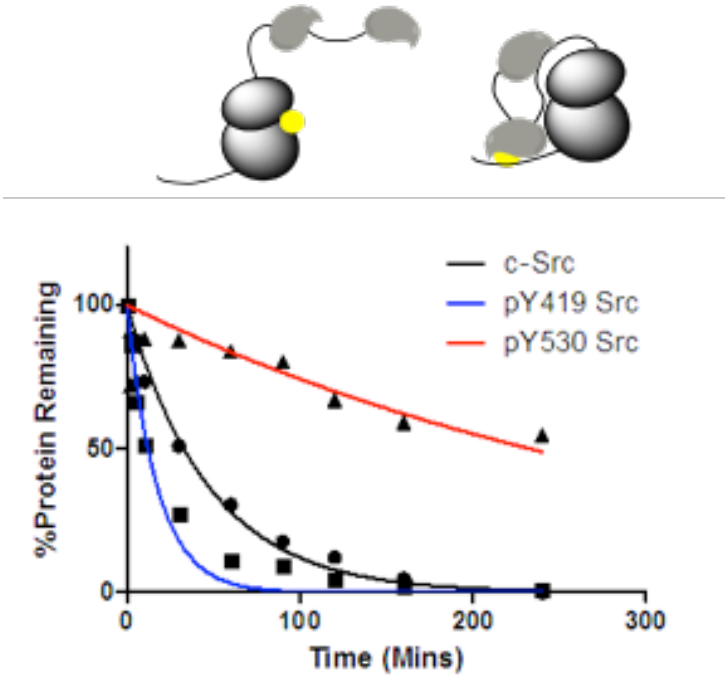

Figure 2.4. Treatment of the open (pY419) and closed (pY530) phosphorylated constructs show differences in the cleavage rate by the protease thermolysin, validating this as a novel method for identifying conformational changes in c-Src.

We first treated wt c-Src with the protease thermolysin in a 30:1 ratio and only a single cut site was observed after analysis by SDS-PAGE electrophoresis. Mass spectrometry analysis identified the primary cleavage site to reside on the linker as originally hypothesized, specifically between Gly257 and Leu258. We rationalized that c-Src in the open conformation would undergo selective proteolysis more rapidly than the closed conformation, due to an increase in accessibility of this site by disengagement of the SH3 domain. As phosphorylation of c-Src at Y419 (Src^{Act}) and Y530 ($Src^{Inactive}$) stabilize the open and closed conformations respectfully, proteolysis of Src^{Act} and $Src^{Inactive}$ by thermolysin was monitored over time. As hypothesized, Src^{Act} was degraded faster than wt-Src, with half-lives of 12 min versus 33 min, respectively. $Src^{Inactive}$, with its known 'closed' conformation, was degraded slower, with a half-life of 241 min. With excellent correlation between the known 'open' and 'closed' forms of c-Src, we next assessed an additional construct of c-Src known to be 'closed', Src^{SH2Eng}. Src^{SH2Eng} mimics Y530 phosphorylation by replacing the c-terminal tail with a high affinity poly-anion SH2 sequence.[13] Gratifyingly, we confirmed that Src^{SH2Eng} also adopts a closed kinase conformation, with a half-life of 356 mins.

It was recently reported by the Maly Lab, that in addition to phosphorylation, conformation selective ATP-competitive inhibitors can also stabilize open or closed conformations of c-Src.[14,15] As described in more detail in chapter III, ligands that interact with a regulatory structural motif, the αC-helix, is known to influence the global conformation of a number of diverse kinases. For c-Src specifically, type II inhibitors (or DFG-out inhibitors) have been reported to stabilize the open conformation upon binding through stabilizing the 'αC-helix in' conformation. Inhibitors stabilizing the αC-helix in an extended, or 'αC-helix-out' conformation, have been reported to stabilize the closed conformation. To increase the validity of this method, we performed selective proteolysis of c-Src in the presence of conformation-selective Dasatinib analogues, **2.1** and **2.2**, that bind the αC-helix in or αC-helix out conformations respectfully.[16] As expected the **2.1** treated c-Src was degraded by thermolysin very rapidly with a half-life of only 2 mins, corresponding to stabilization of an open conformation. Alternatively, the **2.2** treated c-Src stabilized a more closed conformation with an observed half-life of 83 minutes.

This selective proteolysis methodology has afforded results matching those using previously reported and orthogonal methods. However, the robustness of the method will be increasingly more attractive if it can be applied to other diverse kinases.

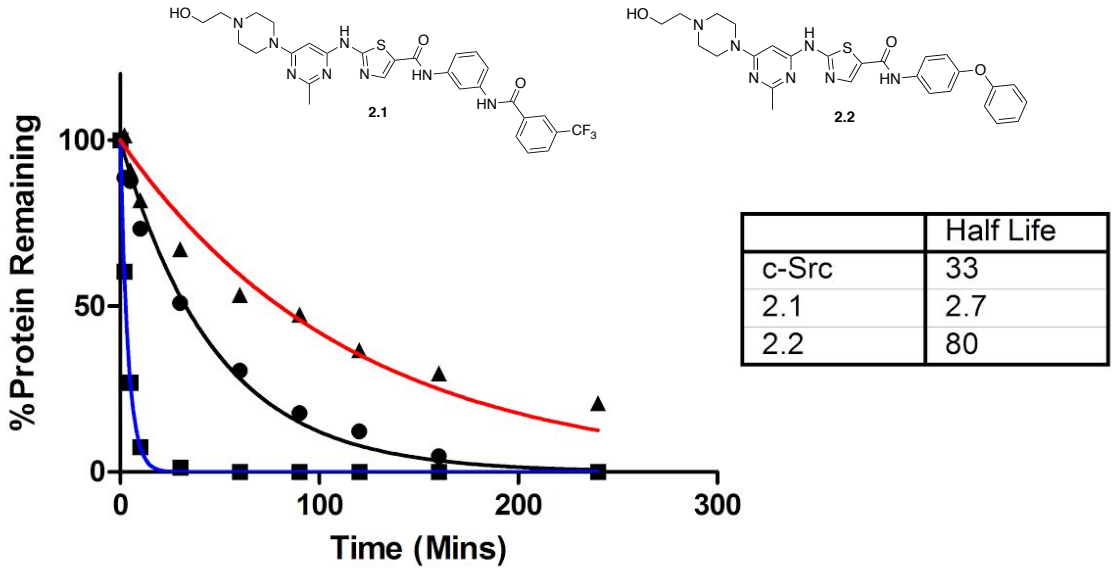

Figure 2.5. Conformation selective inhibitors **2.1** and **2.2** are shown to stabilize the open or closed c-Src conformations respectfully and further validate using thermolysin as a method for identifying conformational changes in c-Src.

Expanding Selective Proteolysis to Diverse Kinases Including c-Abl

In addition to c-Src, many PKs contain regulatory domains (e.g., SH2 and SH3 domains) that serve in scaffolding and regulatory roles.[17-19] The applicability of this method outside of just c-Src would be a great advantage to other existing methods. Given that we know the exact cleavage site within the linker, we wanted to use this knowledge to apply our method to diverse protein kinases. Sequence alignment of the linker region resulted in number of other kinases that could be amenable to this method (Figure 2.5). Each of these diverse kinases has high sequence identity with the linker region. In support of this analysis, we identified the kinase, c-Abl, to be a suitable proof-of-concept kinase. The kinase c-Abl has been an important drug target for the treatment of CML for

over a decade.[20-22] Additionally, c-Abl is known to regulate kinase signaling though changes in the global conformation, and includes a regulatory SH2 and SH3 domain similar to that of c-Src.[23] Thus, we determined applying our methodology to c-Abl would provide a useful tool to eventually begin understanding how these conformations may aid in the progression of diseases including CML.

ABL	NKPTVY**GV**SPN-YDKW
ABL2	NKPTVY**GV**SPI-HDKW
SRC	-PTSKPQTQ**GL**AKDAW
YES	-PTVKPQTQ**GL**AKDAW
FGR	-TIMKPQTL**GL**AKDAW
ITK	-RQKAPVTA**GL**RYGKW
BTK	-NKNAPSTA**GL**GYGSW
TEC	-GKNAPTTA**GF**SYEKW
TXK	-GSCLPATA**GF**SYEKW

Figure 2.6. Sequence alignment of kinases possessing a SH2-Kd linker afforded 9 diverse kinases that could also be investigated using this methodology.

Previous studies have identified c-Abl to also adopt unique global conformations as a means of regulation. X-Ray crystallography has revealed an inhibitory mechanism that c-Abl undergoes after posttranslational modification through myristolyation on the c-Terminal tail.[24] This modification results in the myristoyl group binding within a pocket located on the bottom of the kinase domain (myristate pocket) and causes c-Abl to adopt a closed conformation similarly to that of pY530-Src (with additionally masking of the SH2-linker by c-Abl's SH3 domain).[23] Alternatively, SAXS analysis has reported that binding of the FDA approved inhibitor Imatinib showcases c-Abl adopting an 'open' or extended conformations, similarly to that of the active pY419-Src.[4] We believed these to be well-validated controls in order to determine the validity of selective proteolysis upon c-Abl.

Selective proteolysis was preformed with c-Abl in the presence of a myrisotylated peptide (mimicking a myristoylated c-terminal tail) and the inhibitor Imatinib. These results were as predicted with c-Abl in the presence of the myristoylated peptide[25] having

a very long half-life of 192 mins indicating stabilization of the closed conformations. Alternatively, c-Abl in the presence of Imatinib had a very short half-life of only 3.3 mins. These data display the robustness of this method to expand beyond that of only c-Src. However, we also wanted to showcase it's utility with c-Abl in the presence of small molecules.

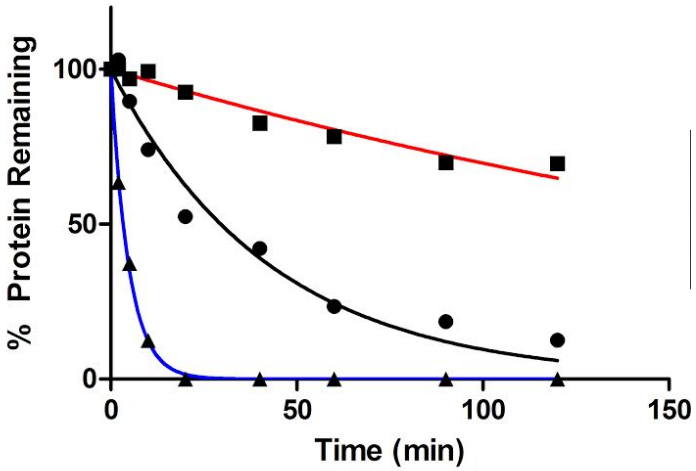

	Half Life
3 Domain Abl	30
+ Myristate	192
+ Imatinib	3.3
+ 2.1	2.2
+ 2.2	47
+ GNF	173

Figure 2.7. The global conformations of c-Abl can also be determined with this methodology. These results confirm reported observations with the Myristate binding peptide stabilizing the closed conformation (red) and Imatinib the open conformation (blue). The conformation selective Dasatinib analogs **2.1** and **2.2** were also assessed along with the allosteric inhibitor, GNF-2.

To assess the conformational changes c-Abl would adopt in the presence of conformation selective inhibitors, selective proteolysis was preformed in the presence of **2.1** and **2.2** as preformed previously with c-Src. Abl in the presence of **2.1** displayed a half-life of 2.2 mins, which is no surprise as Imatinib and **2.1** both bind the same αC-Helix-In. To our surprise, c-Abl in the presence of **2.2** displayed a half-life of 47 mins, which is indicative of stabilizing a more closed conformation. This is the first evidence of a kinase inhibitor that stabilizes c-Abl in the αC-helix out conformation to additionally

stabilize the closed global conformation. We also assessed the allosteric inhibitor GNF-II as it speculated to also stabilize the closed conformation due to similarities in the binding of mode to myristolyation.[26] The half-life of c-Abl in the presence of GNF-II was 173 mins, additionally confirming inhibitors that bind far outside the ATP binding site can also stabilize unique protein conformations. These data provide interesting leads toward developing the next-generation of c-Abl inhibitors for the treatment of CML.

Conclusions

The current techniques to evaluate large conformational changes of kinases inhibit conformational analysis in a high-throughput fashion, and in some cases are not amenable to other diverse kinase. After evaluation of the unique structural differences of the SH2-linker between c-Src's open and closed conformations, and previous observations of this site's sensitivity to the protease thermolysin, we were able to develop a robust method that is superior to those currently reported. This method has replaced the need for highly trained technicians, copious amounts of proteins, and can be easily amenable to other protein targets. We hypothesize that those kinases not sensitive to thermolysin can also be evaluated using one of many identified proteases and will enable the study of global conformational changes to be accessible by any lab. The data herein has additionally confirmed the conformational changes in c-Src that occur in the differential phosphorylation and ligand bound states that have been observed through orthogonal approaches. This method has also identified new strategies for stabilization of c-Abl's closed conformation through inhibitors that stabilize the αC-helix out conformation or those that bind allosterically (GNF-2) in the miristoyl-binding pocket. Using selective proteolysis, we can now begin understand the role that global conformations, of c-Src specifically, can play in both affecting signaling pathways (Chapter III) and developing novel targeting strategies for c-Src (Chapter IV & Chapter V).

Materials and Methods

Cut-Site Determination

5 μM WT 3D Src and 5 μM WT 3D Src treated with thermolysin (60nM final concentration) for 2 hours were submitted to the University of Michigan Mass Spectrometry Facility for analysis. Samples were run using a Waters MicromassZQ mass spectrometer.

Generation of Src^{Act} (pY419) and $Src^{Inactive}$ (pY530) Constructs

c-Src^{Y530F} (for Src^{Act}) or c-Src^{Y419F} (for $Src^{Inactive}$) was diluted in reaction buffer (50mM Tris-HCl pH 8.0, 100mM NaCl, 0.1 mM $MgCl_2$, 0.1% TritonX) to yield a final protein concentration of 2 μM. For Src^{Act} the reaction was initiation with ATP for a final ATP concentration of 1 mM and reacted at 90 C for 1.5 hours. The resulting mixture was suspended in reaction buffer (5 mL), concentrated using [Concentrators], and washed 3 additional times to afford Src^{Act}. For $Src^{Inactive}$, GST labeled Csk was added to a final concentration of 200 nM and reaction was initiated with ATP to a final volume of 1 mM and reacted at 90 C for 1.5 hours. GST-Resin was added to the reaction and the mixture was cooled to 0 and shaken for 1 hour. The supernatant was decanted, concentrated using [Concentrators], and washed 3 additional with reaction buffer times to afford $Src^{Inactive}$.

Selective Proteolysis of c-Src General Method

c-Src and c-Src constructs were diluted in proteolysis buffer (50 mM Tris-HCl pH 8.0, 100 mM NaCl, 0.5 mM $CaCl_2$) to yield a final protein concentration of 2 μM. If inhibitor was being used, 1 μL of a 10 mM DMSO stock was added and incubated with c-Src for 15 mins at room temperature. Thermolysin (purchased from Promega, catalog number: V4001) from a 3.8 μM stock solution was added to the reaction mixture to a final concentration of 60 nM. 15 μL of the proteolysis reaction was added to 5 μL of 50 mM EDTA to quench proteolysis at various time points (0, 2, 5, 10, 30, 60, 90, 120, 180, and 240 mins) and stored at -20 °C. The quenched samples were analyzed by SDS-PAGE (12 % Bis-Tris gel in MES running buffer, staining with comassie blue). Band intensities were analyzed by ImageJ imaging software. Percent protein remaining was plotted against time and fit to an exponential decay equation using GraphPad Prism 6 software to obtain half-lifes of each protein. The Exponential Decay curve for each protein was fit

using the equation Y=(Y0 - Plateau)*exp(-K*X) + Plateau X = time(mins) and Y = normalized band intensity.

Selective Proteolysis of c-Abl General Method

c-Abl was diluted in proteolysis buffer (50 mM Tris-HCl pH 8.0, 100 mM NaCl, 0.5 mM $CaCl_2$) to yield a final protein concentration of 2 μM. If inhibitor was being used, 1 μL of a 10 mM DMSO stock was added and incubated with c-Abl for 15 mins at room temperature. Thermolysin (purchased from Promega, catalog number: V4001) from a 3.8 μM stock solution was added to the reaction mixture to a final concentration of 20 nM. 15 μL of the proteolysis reaction was added to 5 μL of 50 mM EDTA to quench proteolysis at various time points (0, 2, 5, 10, 30, 60, 90, 120, 180, and 240 mins) and stored at -20 °C. The quenched samples were analyzed by SDS-PAGE (12 % Bis-Tris gel in MES running buffer, staining with comassie blue). Band intensities were analyzed by ImageJ imaging software. Percent protein remaining was plotted against time and fit to an exponential decay equation using GraphPad Prism 6 software to obtain half-lifes of each protein. The Exponential Decay curve for each protein was fit using the equation Y=(Y0 - Plateau)*exp(-K*X) + Plateau X = time(mins) and Y = normalized band intensity.

General Syntheitc Methods

All reagents were obtained via commercial sources without further purification. **2.1** and **2.2** have been previously synthesized and characterized using the following protocol.[16]

Individual Contributions

Dr. Taylor K. Johnson prepared the c-Abl that was used in the selective proteolysis assay. Additionally she prepared the Myristate peptided used alongside c-Abl.

References

1. Xu W, Harrison SC, Eck MJ. Three-dimensional structure of the Tyrosine Kinase c-Src. *Nature*. **1997**, 385(6617), 595.
2. Cowan-Jacob SW, Fendrich G, Manley PW, Jahnke W, Fabbro D, Liebetanz J, Meyer T. The Crystal Structure of a c-Src Complex in an Active Conformation Suggests Possible Steps in c-Src Activation. *Structure.* **2005**, 13(6), 861-71.
3. Bernadó P, Pérez Y, Svergun DI, Pons M. Structural Characterization of the Active and Inactive States of Src Kinase in Solution by Small-angle X-ray Scattering. *Journal of Molecular Biology*. **2008**, 376(2), 492-505.
4. Nagar B, Hantschel O, Seeliger M, Davies JM, Weis WI, Superti-Furga G, Kuriyan J. Organization of the SH3-SH2 unit in Active and Inactive Forms of the c-Abl Tyrosine Kinase. *Molecular Cell*. **2006**, 21(6), 787-98.
5. Xie Q, Fulton DB, Andreotti AH. A Selective NMR Probe to Monitor the Conformational Transition from Inactive to Active Kinase. *ACS Chemical Biology*. **2014** Sep 26, 10(1), 262-8.
6. Krishnamurty R, Brigham JL, Leonard SE, Ranjitkar P, Larson ET, Dale EJ, Merritt EA, Maly DJ. Active Site Profiling Reveals Coupling Between Domains in SRC-Family Kinases. *Nature Chemical Biology*. **2013**, 9(1), 43-50.
7. MacAuley AL, Cooper JA. Structural Differences Between Repressed and Derepressed Forms of p60c-src. *Molecular and Cellular Biology*. **1989**, 9(6), 2648-56.
8. Huse M, Kuriyan J. The Conformational Plasticity of Protein Kinases. *Cell*. **2002**, 109(3), 275-82.
9. Cooper JA, Howell B. The When and how of Src Regulation. *Cell*. **1993**, 73(6), 1051-4.
10. Irby RB, Yeatman TJ. Role of Src Expression and Activation in Human Cancer. *Oncogene.* **2000**, 19(49), 5636.
11. Okada M, Nada S, Yamanashi Y, Yamamoto T, Nakagawa H. CSK: a Protein-tyrosine Kinase Involved in Regulation of Src Family Kinases. *Journal of Biological Chemistry.* **1991**, 266(36), 24249-52.
12. Okada M. Regulation of the SRC Family Kinases by Csk. *International Journal of Biological Sciences.* **2012**, 8(10), 1385.
13. Lerner EC, Smithgall TE. SH3-dependent Stimulation of Src-family Kinase Autophosphorylation Without tail Release from the SH2 domain in vivo. *Nature Structural & Molecular Biology*. **2002,** 9(5), 365-9.
14. Krishnamurty R, Brigham JL, Leonard SE, Ranjitkar P, Larson ET, Dale EJ, Merritt EA, Maly DJ. Active Site Profiling Reveals Coupling Between Domains in SRC-Family Kinases. *Nature Chemical Biology*. **2013,** 9(1), 43-50.
15. Leonard SE, Register AC, Krishnamurty R, Brighty GJ, Maly DJ. Divergent Modulation of Src-family Kinase Regulatory Interactions with ATP-competitive Inhibitors. *ACS Chemical Biology*. **2014**, 9(8), 1894-905.
16. Kwarcinski FE, Brandvold KR, Phadke S, Beleh OM, Johnson TK, Meagher JL, Seeliger MA, Stuckey JA, Soellner MB. Conformation-selective Analogues of Dasatinib Reveal Insight into Kinase Inhibitor Binding and Selectivity. *ACS Chemical Biology*. **2016**, 11(5), 1296-304.

17. Soderling TR. Protein kinases. Regulation by Autoinhibitory Domains. *Journal of Biological Chemistry*. **1990**, 265(4), 1823-6.
18. Gonfloni S, Weijland A, Kretzschmar J, Superti-Furga G. Crosstalk Between the Catalytic and Regulatory Domains allows Bidirectional Regulation of Src. *Nature Structural & Molecular Biology*. **2000**, 7(4), 281.
19. Kung JE, Jura N. Structural Basis for the Non-catalytic Functions of Protein Kinases. *Structure***. 2016**, 24(1), 7-24.
20. Clark SS, McLaughlin J, Crist WM, Champlin R, Witte ON. Unique Forms of the Abl Tyrosine Kinase Distinguish Ph1-positive CML from Ph1-positive ALL. *Science*. **1987**, 235, 85-9.
21. Gambacorti-Passerini C, Le Coutre P, Mologni L, Fanelli M, Bertazzoli C, Marchesi E, Di Nicola M, Biondi A, Corneo GM, Belotti D, Pogliani E. Inhibition of the ABL Kinase Activity Blocks the Proliferation of BCR/ABL+ Leukemic Cells and Induces Apoptosis. *Blood Cells, Molecules, and Diseases*. **1997**, 23(3), 380-94.
22. Bedi A, Zehnbauer BA, Barber JP, Sharkis SJ, Jones RJ. Inhibition of Apoptosis by BCR-ABL in Chronic Myeloid Leukemia. *Blood*. **1994**, 83(8), 2038-44.
23. Nagar B, Hantschel O, Seeliger M, Davies JM, Weis WI, Superti-Furga G, Kuriyan J. Organization of the SH3-SH2 Unit in Active and Inactive forms of the c-Abl Tyrosine Kinase. *Molecular Cell*. **2006,** 21(6), 787-98.
24. Hantschel O, Nagar B, Guettler S, Kretzschmar J, Dorey K, Kuriyan J, Superti-Furga G. A Myristoyl/Phosphotyrosine Switch Regulates c-Abl. *Cell*. **2003**, 112(6), 845-57.
25. Zhang J, Adrián FJ, Jahnke W, Cowan-Jacob SW, Li AG, Iacob RE, Sim T, Powers J, Dierks C, Sun F, Guo GR. Targeting Wild-type and T315I Bcr-Abl by Combining Allosteric with ATP-site Inhibitors. *Nature*. **2010**, 463(7280), 501.
26. Adrián FJ, Ding Q, Sim T, Velentza A, Sloan C, Liu Y, Zhang G, Hur W, Ding S, Manley P, Mestan J. Allosteric Inhibitors of Bcr-Abl-Dependent Cell Proliferation. *Nature Chemical Biology*. **2006**, 2(2), 95.

CHAPTER III

Characterization of Clinical c-Src Mutations Reveals Changes in Global Kinase Conformation

Abstract

Kinase signaling is traditionally mapped by monitoring downstream phosphorylation pathways, however their 'non-catalytic' functions remain less appreciated as critical mechanisms of kinase signaling. The proto-oncogene, c-Src, regulates its non-catalytic functions through large conformational changes of its regulatory domains. We have previously demonstrated that changes in c-Src's global conformations can be elucidated through monitoring cleavage by the protease thermolysin at glycine 257. We further utilized this methodology to investigate changes in global conformation of a number of clinical and non-clinical mutations of c-Src, and revealed a potential activating mutation, W121R, that has the ability to escape classical down-regulation mechanisms. We finally showcase that matched conformation-selective inhibitors to be a promising strategies for targeting mutations that stabilize distinct c-Src conformations. This methodology additionally can be expanded to a number of potential TKs, and emphasizes the importance of considering kinase conformation in targeting strategies.

Introduction

Protein Kinases (PKs) function as key regulators of important cellular processes such as cell growth and survival through post-translational phosphorylation.[1-3] The PK superfamily is one of the largest protein families, encoding a total of 518 protein kinases.[4] All PKs consist of a highly conserved catalytic domain responsible for phosphorylation of their protein substrates. More recently, PK's 'non-catalytic' functions have been identified to play critical roles in cellular processes, independent of their catalytic functions.[5] These 'non-catalytic' functions are commonly observed as protein-protein

interactions (PPIs), and are often controlled through large conformational changes.[6] Unfortunately, the difficulty in measuring protein conformations using biochemical approaches has stalled the investigation of kinase's non-catalytic functions.

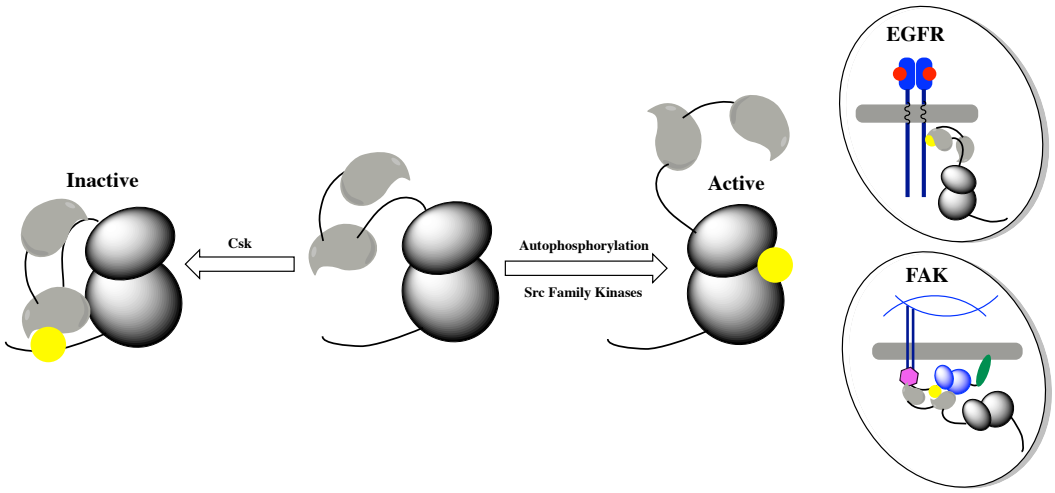

Figure 3.1. c-Src's non-catalytic functions are regulated though its phosphorylation state. Phosphorylation at Y530 on the c-terminal tail by Csk renders a closed kinase conformation, unable to participate in vital protein-protein interactions. Phosphorylation at Y419 renders an open kinase conformation that can form complexes with many protein partners including Fak and EGFR.

The tyrosine kinase, c-Src, has been validated as a prominent target for many solid tumors via genomic knockdown (e.g. siRNA).[7] However, pharmacological inhibition (both in the clinic and in pre-clinical models) leads to a divergent signaling phenotype and has not recapitulated c-Src as an important target. In addition to the catalytic function of c-Src, the full signaling profile of c-Src relies on protein–protein interactions to other signaling proteins, including: EGFR, FAK, and STAT3.[8-10] The regulatory SH2 and SH3 domains of c-Src are responsible for scaffolding to signaling proteins, and changes in the accessibility of these regulatory domains are influenced by the global conformation of c-Src.[11] Moreover, the biological modulation of c-Src's conformation is dependent upon the phosphorylation state of c-Src (Figure 3.1).[12]

Specifically, phosphorylation at Y419 (Tyr 419 is on c-Src's activation loop), stabilizes an 'open' or 'extended' conformation where the SH2 and SH3 domains are amenable to scaffolding signaling proteins.[13] Downregulation of c-Src, via phosphorylation at Y530 (c-terminal tail), stabilizes a 'closed' or 'compact' conformation, rendering the SH2 and SH3 domains inaccessible and fully engaged to the kinase.[14] These large changes in quaternary structure enable modulation of the non-catalytic functions of c-Src, and are now a common mechanism of regulation found in many diverse kinases.

Mutations within the catalytic domain of PKs have long been understood to impact kinase signaling by altering catalytic activity.[15] However, many patient-derived mutations reside outside the catalytic domain, without any explanation for their ability to impact cell signaling. We hypothesize that non-catalytic domain mutations alter cell signaling via changes in kinase conformation (and subsequently noncatalytic kinase function). Data collected from genome wide sequencing databases, has uncovered c-Src to harbor a number of uncharacterized mutations that exist outside the ATP binding site. c-Src has been previously observed by the Cooper lab in 1989 to be sensitive to degradation by the bacterial protease thermolysin.[16] In Chapter II this simple observation enabled us to develop novel methodology to elucidate changes in the quaternary structure of c-Src.

Herein we utilize selective proteolysis methodology to identify conformational changes of c-Src caused by both somatic and non-clinical mutations. These mutations will be explored in terms of their catalytic efficiencies and ability to participate in regulatory mechanisms. The data herein has enabled us to investigate characteristics of 'open' and 'closed' c-Src conformations, and has uncovered a potential gain-of-function mutation, W121R. Due to the robust nature of this assay, in chapter 2 we have additionally showcased its use for the kinase c-Abl, and hypothesize its utility with other PTKs including Btk and Fgr. Our results have provided tools to enable deeper understanding of the signaling mechanisms of c-Src that are independent of its traditional catalytic functions.

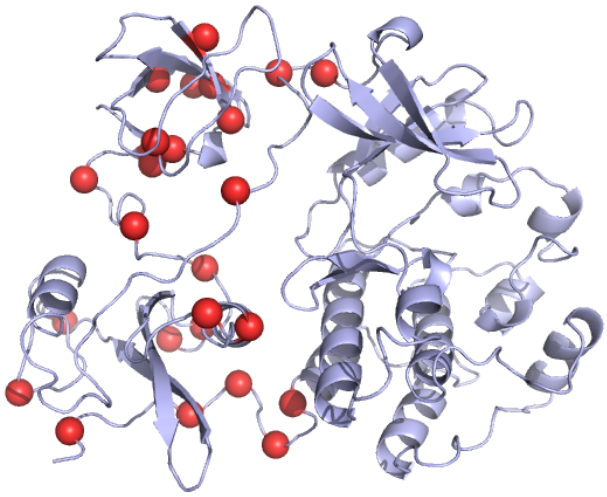

Figure 3.2. Clinical Mutations (Red Spheres) documented from the CCLE and COSMIC databases reveal many that exist distal from the ATP binding pocket and are hypothesized to be modulating the global kinase conformation.

Clinical c-Src Mutations Show Changes in Global Conformation

Single amino acid mutations in kinases have been transformative in a number of solid tumors including lung, breast, and colon.[17-19] Data collected from genome wide sequencing databases of various tumor samples, including: COSMIC, NIH Center of Genomics, and the Cancer Cell Line Encyclopedia (CCLE), have uncovered c-Src to harbor a number of uncharacterized mutations that are distal to the ATP binding pocket (Figure 3.2).[20-22] Due to the great attention to the kinase domain, and the lack of bench top methods to decipher protein conformation, most of these mutations still remain uncharacterized. Utilizing our selective proteolysis method to identify changes in c-Src's global conformation, a small panel of clinical mutations was expressed, purified, treated with thermolysin, and cleavage was monitored over time. Surprisingly, many of these single amino acid mutations influence the conformation of c-Src, highlighting the intricacy of the hydrogen bond network that stabilizes kinase conformation (Figure 3.3). Mutations stabilizing the active conformation included: W121R, R163W and D407H. With the exception of D407H, these mutations are located on the interface between regulatory domain and the kinase domain. It is hypothesized that these mutations act through destabilization of the inactive conformation through a steric (W121R),

electrostatic (R163W) mechanism, or interaction with the αC-helix (D407H). Mutations stabilizing the closed conformation include: K298E, T341R, Q529H, E527K, & P307R, and are positioned to interact with the αC-helix or the SH2 domain, both known to influence the closed conformation. With these mutations characterized, they can now be utilized as genetic tools to begin elucidating how c-Src global conformation may be influencing complex signaling pathways and driving tumor progression.

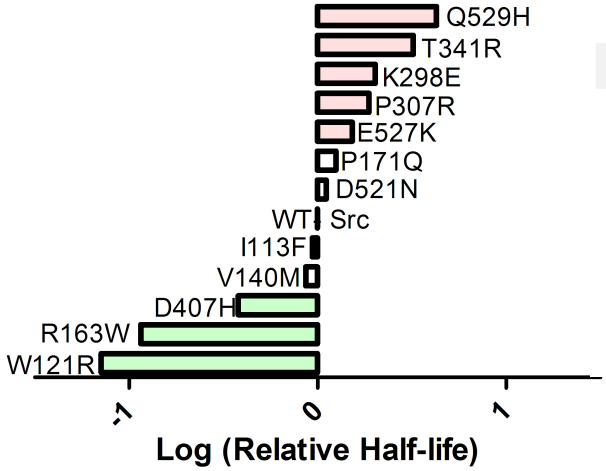

Mutation	Half-life	Mutation	Half-life
I113F	31	P307R	62
W121R	2	T341R	106
V140M	29	D407H	13
R163W	4	D521N	37
P171Q	41	E527K	50
K298E	67	Q529H	141

Figure 3.3 A small panel of clinical c-Src mutants was characterized using selective proteolysis and reveal clinical mutations that can stabilize the open or closed conformations of c-Src.

Non-Clinical Mutations also Influence c-Src's Global Conformations

A number of c-Src mutations have been reported in the literature that has been utilized to interrogate both the structure and function of protein kinases. Genetic manipulation of kinases, including the mutations K298M, T341G, and F408G, has been a powerful approach for elucidating their complex signaling pathways.[23-25] Drug resistant mutations, including the gatekeeper mutations T341M, T341I, and T341R, are useful models to begin understanding how mutations play a role in avoiding therapeutic intervention.[26,27] v-Src mutations, including D117N and R95W (D120N & R98W human numbering), were identified as mutations that could avoid down-regulation by CSK.[28]

Finally, residues that are important for maintaining the intricate hydrogen-bond network, W263A, D407N, F408A, were also investigating using our selective proteolysis methodology (Figure 3.4).[29, 30]

Of this panel, 5 mutations were found to stabilize the open conformation: D120N, R98W, K298M, W263A, and D407N. The two v-Src mutations, D120N and R98W, are also both highly active and may begin to uncover the mechanism of avoiding downregulation by CSK. The kinase dead mutation, K298M, was also found to stabilize the open conformation, and we believe to not be the ideal choice when considering using a 'kinase dead' construct (F408G could be better suited as no change in conformation was observed). Finally, W263A stabilizing the open conformation confirms its importance in acting as a master regulator between c-Src's open and closed global conformations as originally reported. These mutations highlight the importance of taking global conformation into consideration when using genetic approaches to study kinase structure function relationships.

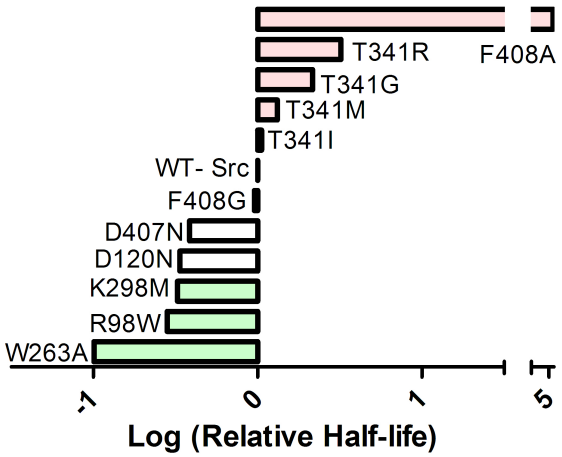

Figure 3.4. A panel of non-clinical c-Src mutants was characterized using selective proteolysis and reveal additional mutations that can stabilize the open or closed conformations of c-Src.

c-Src Conformation can Influence Kinase Catalytic Function

Having identified a number of mutations that stabilize c-Src's open and closed conformation, we next investigated the relationship between the kinase's conformation and its catalytic activity. The catalytic activity of these mutations was assessed via a self-reporting activity assay utilizing a synthetic peptide substrate (Figure 3.5).[31] Kinetic parameters including ATP K_m and substrate K_m were also measured (Appendix B). The open c-Src mutants displayed a V_{max} equal to or greater than that of wt-Src, while the closed c-Src mutants always displayed a decrease in V_{max}. It has been reported that SH3 engagement to the SH2-linker is an auto-inhibitory mechanism of Src family kinases. We speculate that the open c-Src mutations destabilize this auto-inhibitory conformation, and can result in an increase in the V_{max}. Alternatively, closed c-Src mutations would increase the SH3-linker interaction, via a proximity-based mechanism, thus decreasing the observed V_{max}. It is now even more apparent that mutations distal to the ATP binding site can additionally affect intrinsic catalytic activity in addition to their effect on global kinase conformation.

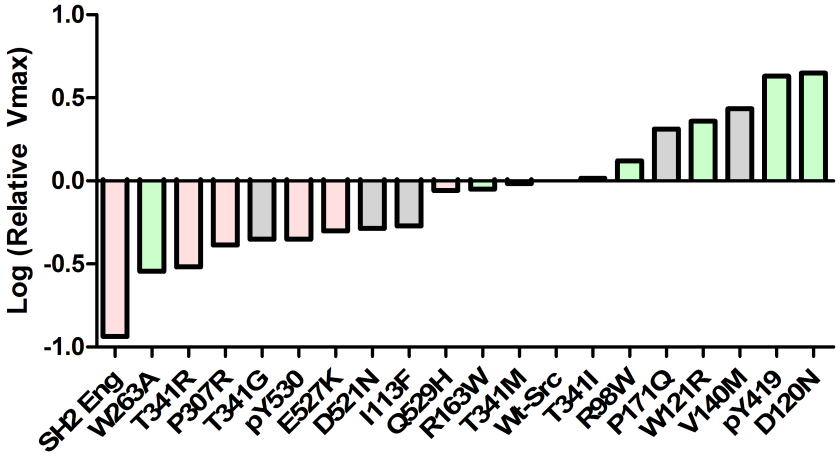

Figure 3.5. All mutants were characterized kinetically and show that closed kinase conformations always displayed a decrease in catalytic function. Open kinase conformation showed more variation, but generally displayed an increase in catalytic activity.

Open Mutations can Avoid Down Regulation by Csk

It has been reported that v-Src mutants, R95W and D117N, have the ability to escape down-regulation when co-expressed with Csk in S. Pombe.[28] These mutations on c-Src, R98W and D120N, stabilize open conformations when assessed using our selective proteolysis methodology. We hypothesized that clinical mutations stabilizing the open conformation may also be able to escape down-regulation by Csk. We added a small panel of mutations onto the down-regulated construct of c-Src, Src^{SH2Eng}, as phosphorylation at Y530 biochemically would also promote autophosphorylation at Y419.[32] The 'SH2-Engaged' construct involves the c-terminal tail replaced with a high affinity sequence, and mimics phosphorylation at Y530 (Table 3.1). Analysis via the selective proteolysis and kinetic parameters verifies this construct as an acceptable pY530 mimetic.

The mutation T341M was added to this construct, $T341M^{SH2Eng}$, and served as T341M had very little conformational changed observed by this mutation. As expected $T341M^{SH2Eng}$ still appears to stabilize a closed conformation along with a decrease in catalytic activity. As R95W in v-Src was observed to escape down-regulation, we analyzed the affect this mutation on c-Src, $R98W^{SH2Eng}$, would have on the downregulated construct. This mutation was now observed to stabilize an open kinase conformation as hypothesized, and additionally displays increased its catalytic activity. We next introduced the clinical mutation W121R onto this construct ($W121R^{SH2Eng}$). Surprisingly, $W121R^{SH2Eng}$ had the largest change in conformation and catalytic activity, mimicking properties of the original W121R mutation. This data has revealed global conformation to be novel mechanism of escaping down-regulation by CSK, and has identified a potential 'gain-of-function' mutation of c-Src. While it is unsure whether all opening mutations has this ability, or if it is unique to W121R, it should stress the importance of the impact of c-Src (and all kinases) global conformations may have on regulating mechanisms. This resistance mechanism may also be a phenomenon with other protein kinases, including c-Abl & Btk, and are currently under investigation by our group.

	$Src^{Inactive}$	Src^{SH2Eng}	$T341M^{SH2Eng}$	$R98W^{SH2Eng}$	$W121R^{RSH2Eng}$
Half-Life	241	356	283	42	4
Vmax (RFU/Min)	25 ± 6	6.5 ± 0.5	11 ± 4	70 ± 21	118 ± 7

Table 3.1. Src mutations added onto the down regulated, Src^{SH2Eng} construct shows mutations stabilizing the open conformation (eg. W121R) are a novel mechanism for escaping down regulating processes.

The Closed Conformation Resists Phosphorylation at Y530

c-Src activation or in-activation can also be accomplished by other intracellular kinases including Hck and Csk.[33,34] We next investigated if the global conformation of c-Src could influence activation or inactivation by monitoring phosphorylation at Y419 and Y530. As c-Src will undergo autophosphorylation in the presence of ATP, we utilized irreversible conformation-selective inhibitors to lock c-Src in the open (**3.1**) or closed (**3.2)** conformations, while 3additionally inhibiting its ability to undergo autophosphorylation.

Wt c-Src & Y530F c-Src (to inhibit tail phosphorylation biochemically) was incubated with the irreversible analogs **3.1** and **3.2**, purified, and were utilized as substrates for the phosphorylation reaction with Hck and Csk (Figure 3.6). The **Src^{Y530F} – 3.1** and **Src^{Y530F} – 3.2** complexes were incubated with Hck, the reaction was initiated with ATP, and phosphorylation was monitored over time. As depicted, no change in the initial phosphorylation rates were observed between the open or closed c-Src conformation using both kinase domain and 3-domain Hck Constructs (Figure). This data suggests that the accessibility of Y419 remains unchanged between the open and closed conformations of c-Src.

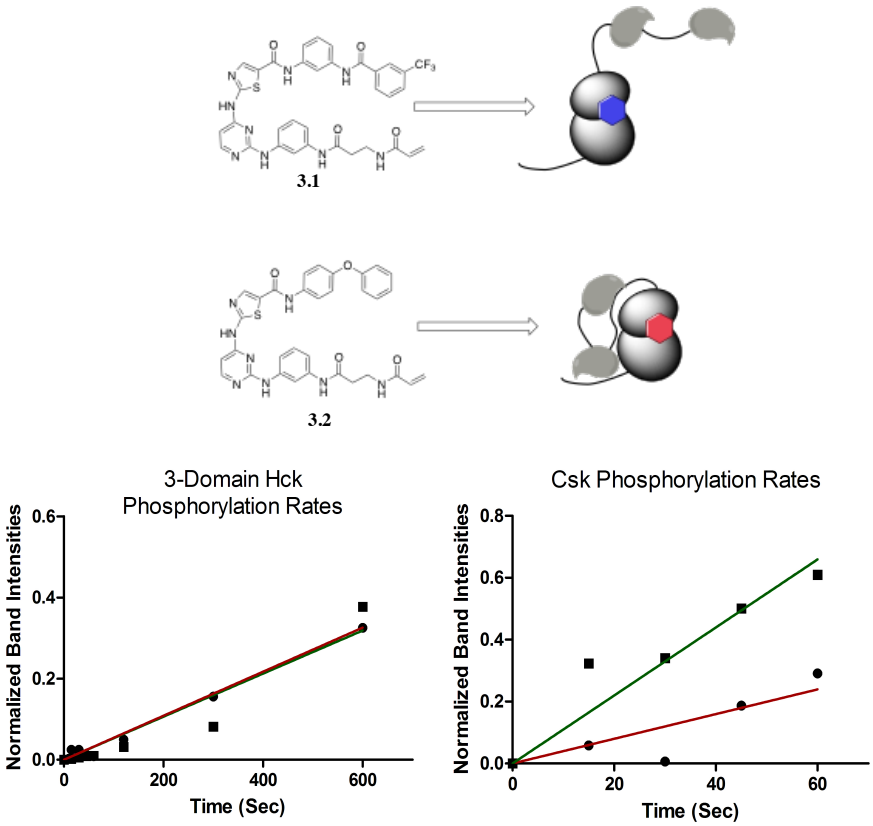

Figure 3.6. Stabilization of the open and closed conformations, using irreversible conformation-selective Dasatinib inhibitors **3.1** and **3.2**, show differential phosphorylation rates at Y530 by Csk. However, no change in phosphorylation rate was observed at Y419 when using Hck.

This method was repeated with the kinase Csk in order to monitor phosphorylation at Y530. **Src – 3.1** and **Src – 3.2** complexes were incubated with Csk, the reaction was initiated with ATP, and phosphorylation was monitored over time. Gratifying, the open complex **Src – 3.1**, had a faster initial phosphorylation rate than the closed complex, **Src – 3.2**. We hypothesize that the decrease in accessibility at Y530 in the closed conformation is reflected in the decrease in phosphorylation rate by Csk. This data encouragingly supports previously reported observation that shows decreased phosphatase activity at this site.

Matching Inhibitor Conformation to Kinase Conformation as a Targeting Strategy

ATP-comptitive kinase inhibitors have recently been recognized to stabilize distinct kinase conformations.[35] Thus, 'conformation-selective' kinase inhibitors have exciting implications for modulating signaling beyond catalytic function. In an effort to improve targeting clinical mutations that also alter global conformation, we hypothesized mutations that stabilized the open or closed conformations could be targeted with matching conformation-selective inhibitors. Using previously reported conformation selective BODIPY probes, we calculated the K_{on} rates of both DAS-DFGO-BODIPY, **3.3**, and DAS-CHO-BODIPY, **3.4**, with an open (Src^{Act}) and closed (Src^{SH2Eng}) kinase construct (Table 3.2).[35] We hypothesized that the inhibitor would no longer need to pay an entropy cost due to the protein conformation already being pre-set. Thus, it would be reflected with faster K_{on} rates versus its 'un-matching' counterpart. The K_{on} values were calculated from experimentally determined K_d and K_{off} values and as hypothesized, the **3.3** probe binds the Src^{Act} most quickly. Alternatively, the **3.4** prefers the Src^{SH2Eng} construct with a faster K_{on}. This data showcases a new approach to targeting clinical kinase mutations using matched conformation selective inhibitors.

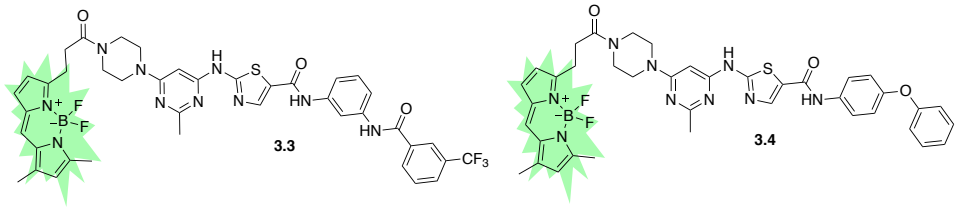

	wt-Src		pY419-Src		Src^{SH2Eng}	
	3.3	**3.4**	**3.3**	**3.4**	**3.3**	**3.4**
K_{off} ($x10^{-2}$)	1.04	1.07	0.58	1.01	2.4	2.2
Half-Life (mins)	66.65	65.04	118.7	68.88	29.03	31.37
K_d (nM)	10.5	5.8	3.1	2.4	2.5	5.3
K_{on} ($x10^{-2}$)	**0.1**	**0.18**	**0.19**	**0.42**	**0.96**	**0.42**

Table 3.2. K_{on} determinations using BODIPY labeled conformation-selective probes **3.3** and **3.4** show that matching inhibitor conformation to kinase to be a promising therapeutic strategy for targeting mutations that affect kinase conformation.

Conclusions

Due to the many disadvantages using current available methods, the protease thermolysin was utilized as a method to quickly and confidently detect changes in the global conformation of c-Src. This method relies upon the differences in accessibility of G257 & L258 located on the SH2-linker in the 'open' and 'closed' conformations. The analysis of a number of clinical and non-clinical mutations showcases the tightly controlled network that regulates protein shape and conformation. Additionally, mutations that stabilize an open kinase conformation may have the potential to escape down-regulation by the kinase Csk. Thus, designing conformation selective ligands that complement the open/closed conformation can improve the therapeutic targeting of c-Src and other protein kinases. This method has been additionally showcased with c-Abl kinase, and has the potential to be expanded to other TK's including Fgr and Btk. Methods such as these enable the rapid identification of changes in protein conformation, thus a better appreciation of c-Src's signaling mechanism to eventually elucidate kinase's non-catalytic functions.

Materials and Methods

Production of c-Src Mutants

Human c-Src 3-domain in pET28a, modified with a TEV protease cleavable N-terminal 6x-His tag was prepared as previously reported.[36] The desired mutations were added to this plasmid using iterative rounds of mutagenesis using the Agilent QuikChange II kit. The plasmid was transformed by electroporation into Bl21DE3 electrocompetent cells containing YopH in pCDFDuet-1. Cell growth, expression, and protein purification were performed using modified literature protocols for expression of wild-type c-Src 3-domain.

General Kinetic Data Procedures

Black, opaque-bottom 96 well plates were purchased from Nunc. All proteins were expressed in *E.coli* using previously published procedures.[36] Data were obtained

using Biotek Synergy Mx and Biotek Synergy 4 plate readers. Curve fitting was done using Graphpad Prism 6 software.

Selective Proteolysis of c-Src Mutants/Constructs General Method

c-Src mutants or c-Src constructs were diluted in proteolysis buffer (50 mM Tris-HCl pH 8.0, 100 mM NaCl, 0.5 mM $CaCl_2$) to yield a final protein concentration of 2 μM. If inhibitor was being used, 1 μL of a 10 mM DMSO stock was added and incubated with c-Src for 15 mins at room temperature. Thermolysin (purchased from Promega, catalog number: V4001) from a 3.8 μM stock solution was added to the reaction mixture to a final concentration of 60 nM. 15 μL of the proteolysis reaction was added to 5 μL of 50 mM EDTA to quench proteolysis at various time points (0, 2, 5, 10, 30, 60, 90, 120, 180, and 240 mins) and stored at -20 °C. The quenched samples were analyzed by SDS-PAGE (12 % Bis-Tris gel in MES running buffer, staining with comassie blue). Band intensities were analyzed by ImageJ imaging software. Percent protein remaining was plotted against time and fit to an exponential decay equation using GraphPad Prism 6 software to obtain half-lifes of each protein. The Exponential Decay curve for each protein was fit using the equation Y=(Y0 - Plateau)*exp(-K*X) + Plateau X = time(mins) and Y = normalized band intensity.

General procedure for ATP Km determination

A continuous fluorescence assay was used to determine Km values.[(old ref)] Reaction volumes of 100 μL were used in 96-well plates. 85 μL of enzyme in buffer was added to each well. 2.5 μL of DMSO was then added followed by 2.5 μL of a substrate peptide ("compound 3" as described in Wang et al)[2] solution (1.8 mM in DMSO). The reaction was initiated with 10 μL of the appropriate ATP dilution (typically 1000, 500, 250, 125, 62.5, 31.3, 15.6, 7.8, 3.9, 2.0 μM in H_2O) and reaction progress was immediately monitored at 405 nm (ex. 340 nm) for 10 minutes. Reactions had final concentrations of 30 nM enzyme, 45 μM peptide substrate, 100 μM Na_3VO_4, 100 mM Tris buffer (pH 8), 10 mM $MgCl_2$, 0.01% Triton X-100. The initial rate data collected was used for determination of Km values. For Km determination, the kinetic values were obtained directly from nonlinear regression of substrate-velocity curves in the presence of varying

concentrations of ATP. The equation Y = (Vmax * X)/(Km + X), X = substrate concentration (μM) and Y = enzyme velocity (RFU/s); was used in the nonlinear regression. Each ATP Km value was determined using at least three independent experiments.

General procedure for Peptide Substrate Km determination

The previously described fluorescence assay was used to determine Km values.[36] Reaction volumes of 100 μL were used in 96-well plates. 85 μL of enzyme in buffer was added to each well. 2.5 μL of DMSO was then added followed by 2.5 μL of a substrate peptide dilution (450, 225, 112.5, 56.3, 28.0, 14.1, 7.0, 3.5, 0, μM in DMSO) ("compound 3" as described in Wang et al)[36] solution. The reaction was initiated with 10 μL of 50mM ATP and reaction progress was immediately monitored at 405 nm (ex. 340 nm) for 10 minutes. Reactions had final concentrations of 30 nM enzyme, 5mM ATP, 100 μM Na3VO4, 100 mM Tris buffer (pH 8), 10 mM $MgCl_2$, 0.01% Triton X-100. The initial rate data collected was used for determination of K_m values. For Km determination, the kinetic values were obtained directly from nonlinear regression of substrate-velocity curves in the presence of varying concentrations of ATP. The equation Y = (Vmax * X)/(Km + X), X = substrate concentration (μM) and Y = enzyme velocity (RFU/s); was used in the nonlinear regression. Each ATP Km value was determined using at least three independent experiments.

General Procedure for Determining Melting Temperature of c-Src Mutants

WT 3D-Src, mutants, and irreversibly charged constructs were mixed with a 1mM stock of ANS (in DMSO). A total assay volume of 5uL were plated in quadruplicate into a 384 well plate to yield a final concentration of 2μM Src, 50μM ANS, 5% DMSO. 1.5μL of Silicon Oil (Sigma Aldrich) was added to each well to prevent evaporation and the plate was centrifuged at 1000 x g for 1 minute. The experiment was performed in a ThermoFluor instrument (Johnson & Johnson Pharmaceutical Research and Development L.L.C) using continuous ramping mode from 30 °C to 80 °C in increments of 1 °C holding 1 minute at each temperature. Data were analyzed using ThermoFluor^{++} version 1.3.7 software.

General Procedure for Generating Covalently Modified c-Src

WT Src or Y530F Src was incubated with inhibitor **3.3** or **3.4** for 1 hour at room temperature at final concentrations of 10 μM enzyme and 100 μM inhibitor in 25 μL of total volume (5% DMSO). Excess inhibitor was washed with Buffer D (100 mM Tris buffer pH 8, 10 mM $MgCl_2$, 5% Glycerol) through [Spin filter concentrators]. Concentrations were determined via absorbance at 280 nm, and then assayed as previously described.

Activation/Inactivation with Hck or Csk General Procedure

Covalently modified WT 3-D Src or Y530F 3D-Src with Inhibitor **3.3** or **3.4** was diluted in reaction buffer (100 μM Na3VO4, 100 mM Tris buffer (pH 8), 10 mM MgCl2, 0.01% Triton X-100), followed by addition of Hck Kd or GST-Csk to a final concentration of 100nM. Reaction was initated with 50mM ATP at room temperature to give a final concentration of 100 μM (for Kd Hck) or 500 μM (for 3D Hck). 15 μL of the proteolysis reaction was added to 7 μL of SDS-PAGE loading dye to quench proteolysis at various time points (0, 15, 30, 45, 60sec, 2, 5, 10, 30, and 60 mins) and stored at -20 °C. The quenched samples were analyzed by SDS-PAGE (12 % Bis-Tris gel in MES running buffer) and stained according to the Phospho-ProQ Diamond Stain. Gels were imaged with a Typhoon 9410 using an excitation of 532 nm (green laser) and emission filter of 560 nm. Afterwards, the gel was post stained with Invitrogen Sypro Ruby protein gel stain as per instructions, and imaged on Typhoon 9410 using an excitation of 532 nm (green laser) and emission filter of 610 nm. Band intensities were analyzed by ImageJ imaging software and normalized to band intensities measured from the Sypro Ruby Stain. Initial velocities were plotted fit to a [X] equation using GraphPad Prism 6 software to obtain velocities.

General Procedure for BODIPY Probe K_{off} Determination

A multiple time point read fluorescence assay was used to determine dasatinib analogue BODIPY (**3.3** and **3.4)** off rates. Briefly, 60 μL of total volume with 700 nM enzyme and 500 nM probe in buffer A 1× (master mix) was incubated at rt for 4 h along

with 60 μL of 500 nM probe alone in buffer A 1× (blank mix). Following this incubation period, 4 μL of the master mix was added into five wells and 4 μL of the blank mix was added into two wells via multichannel pipet into 116 μL of buffer A 1× containing 5 μM (final concentration) unlabeled dasatinib (120 μL total, 30-fold dilution). Additionally, 4 μL of master mix was added into a single well of 116 μL of buffer A 1× containing 100 nM (final concentration) probe to maintain consistent plate reader gain values over the course of the fluorescent reads. Master mix dilutions with competitor had final concentrations of 23 nM enzyme, 17 nM BODIPY-probe, 5 μM unlabeled dasatinib, 100 mM Tris buffer, pH 8, and 10 mM MgCl2. Reads (ex/em 485/535 nm) were taken every 10 min for the first 2 h, every 20 min for the next 2 h, and finally every 30 min for the remainder of the assay (12 h total). The values for koff determination were obtained directly from the nonlinear regression fits for one-phase decay curves (using blanked data). The equation Y = (Y0 − Plateau) exp(−KX) + Plateau was used in the nonlinear regression. An average of five wells at each time point was utilized for the final fit values produced

General Procedure for BODIPY Probe K_d Determination

A fluorescence polarization was used to determine K_d values. Reaction volumes of 50 μL were used in 96-well plates. 34 μL of buffer (50 mM Tris buffer (pH 8), 10 mM NaCl, 5% Glycerol, 1 mM DTT) was added to a single row, followed by 15 μL of enzyme (3.3X concentration) in buffer with 2-fold dilutions (typically 150, 75, 37.5, 18.75, 9.375, 4.69, 2.34, 1.17, 0.586, 0.293, and 0 nM final well concentration). Then, 1 μL of a 500 nM stock of the appropriate dasatinib analog BODIPY probe in DMSO was added (2% DMSO final). Wells were incubated on ice for 30 minutes prior to fluorescence polarization read (ex/em 485/535 nm). Reactions had final concentrations of 10 nM BODIPY-probe, 50 mM Tris buffer (pH 8), 10 mM NaCl, 5% Glycerol, 1 mM DTT. For K_d determination, the Polarization values (normalized to the 0 nM protein control) were plotted vs. varying protein concentrations. The equation Y = (Bmax * X)/(Kd + X), X = Protein concentration and Y = FP response; was used in the nonlinear regression.

General Synthetic Methods

All reagents were obtained via commercial sources without further purification. **3.3** and **3.4** has been synthesis from previous published protocol.(old ref) Additionally, the synthesis of **3.5**, **3.6**, and **3.8**, have been syntehsis from previously published protocols.[37-39]

Synthesis of Compounds: 3.1 & 3.2

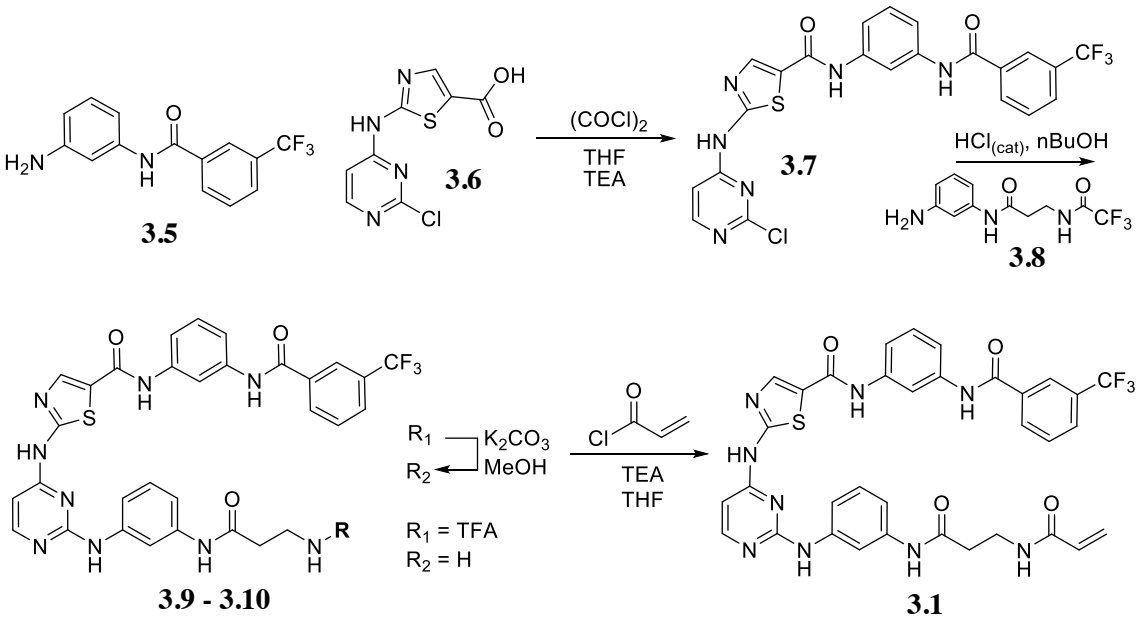

Scheme 3.1. Synthetic Route for Compound **3.1**

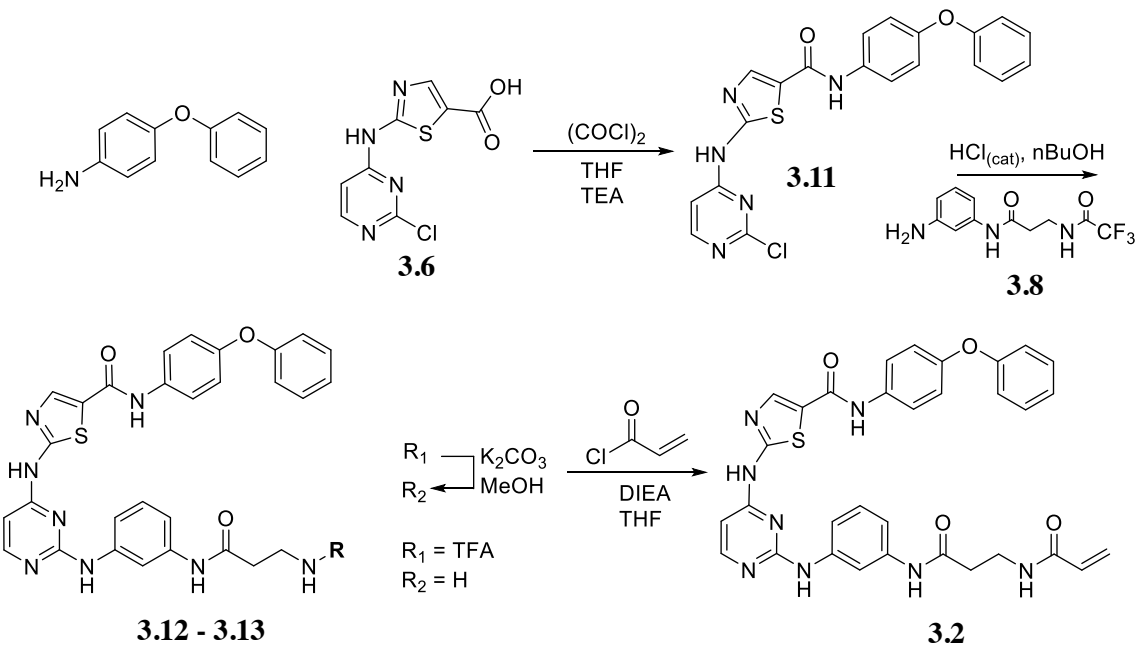

Scheme 3.2. Synthetic Route for Compound **3.2**

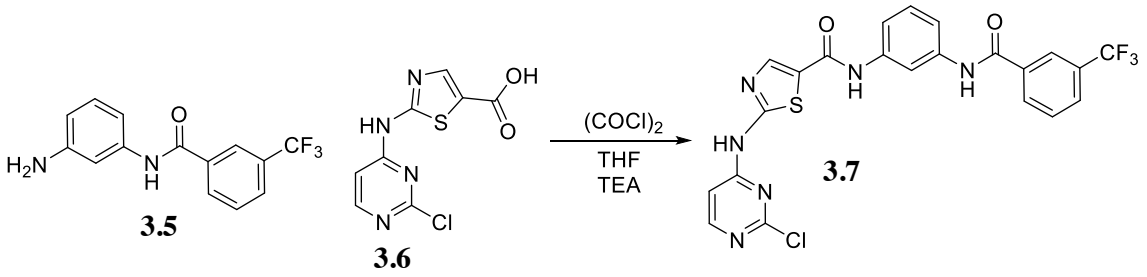

Scheme 3.3. Synthesis of Compound **3.7.**

Synthesis of 3.7. Compound **3.6** (1000 mg, 3.9 mmol) was dissolved in THF (30mL), cooled to 0°C, and stirred under N_2 atmosphere. Oxalyl Chloride (0.46 mL, 5.3 mmol) was added drop wise followed by a drop of DMF. The contents were stirred for 3 hours at 0°C. The THF was removed under reduced pressure and compound **3.5** (992 mg, 3.54 mmol) was added and suspended in THF (30 mL). TEA (0.74 mL, 5.3 mmol) was added and the suspension was stirred at RT under N_2 atmosphere for 16 hours. THF was removed under reduced pressure and re-suspended in EtOAc. The organic mixture was washed with aqueous saturated $NaHCO_3$ (1 x 75 mL), brine (1 x 75 mL), dried over anhydrous $MgSO_4$ (s) and filtered. Solvent was removed under reduced pressure to yield

crude **3.7.** The product was purified by automated silica gel chromatography (linear gradient of 25 – 80% ethyl acetate in hexanes) to yield **S3** (1.3 g, 64.3% yield) as tan solid. **Spectral data.** ^{1}H NMR (500 MHz, DMSO-d_6): δ12.49 (s, 1H), 10.53 (s, 1H), 10.31 (s, 1H), 8.48 – 8.36 (m, 2H), 8.34 – 8.24 (m, 3H), 7.98 (d, J = 7.7 Hz, 1H), 7.80 (t, 1H), 7.56 – 7.43 (m, 2H), 7.35 (t, J = 8.1 Hz), 7.08 (d, J = 5.5 Hz, 1H).

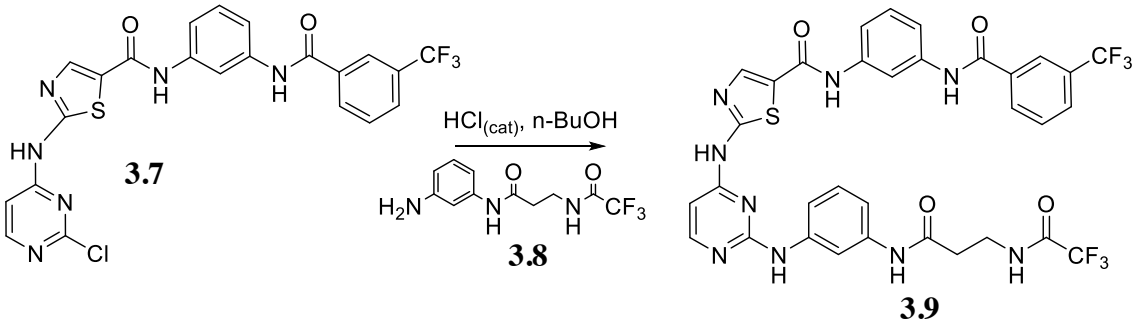

Scheme 3.4. Synthesis of Compound **3.9**

Synthesis of 3.9. Compound **3.7** (290 mg, 0.56 mmol) was added to a flame-dried flask that was flushed with N_2, followed by addition of dioxane (10mL), compound **3.8** (169 mg, 0.61 mmol) and 2 drops of HCl. The contents of the flask were refluxed for 13 h and cooled to R.T. Saturated $NaHCO_3$ (10mL) was added to the reaction flask, and the dioxane was removed under reduced pressure. Aqueous layer was extracted with EtOAC (3 x 30 mL), washed with brine (1 x 50 mL), dried under), dried over anhydrous $MgSO_4$ (s) and filtered. Solvent was removed under reduced pressure to yield crude **3.9.** The product was purified by automated silica gel chromatography (linear gradient of 25 – 80% ethyl acetate in hexanes) to yield **3.9** as a tan solid (318 mg, 75% yield). **Spectral data.** ^{1}H NMR (500 MHz, DMSO-d_6): δ 11.80 (s, 1H), 10.53 (s, 1H), 10.20 (s, 1H), 9.93 (s, 1H), 9.53 (t, 1H), 9.43 (S, 1H), 8.33 (s, 1H), 8.31 – 8.27 (m, 2H), 8.24 (s, 1H), 8.20 (d, J = 5.6 Hz, 1H), 8.00 – 7.92 (m, 2H), 7.80 (t, J = 7.8 Hz, 1H), 7.51 (d, 1H), 7.45 (t, J = 9.4 Hz, 2H), 7.34 (t, J = 8.1 Hz, 1H) 7.28 (d, J = 8.3 Hz, 1H), 7.21 (t, J = 8.1 Hz, 1H), 6.54 – 6.47 (m, 1H), 3.46 (q, J = 6.7 Hz, 2H), 2.59 (t, J = 6.9 Hz, 2H).

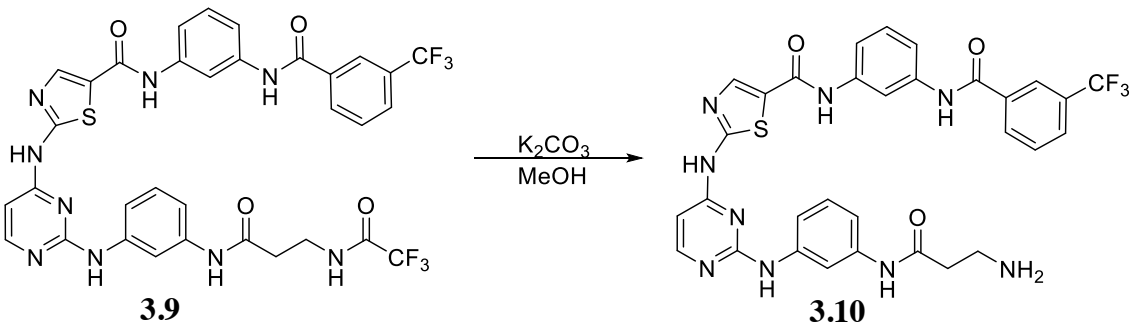

3.9 **3.10**

Scheme 3.5. Synthesis of Compound **3.10**

Synthesis of 3.10. Compound **3.9** (250 mg, 0.33 mmol) was added to a flask and suspended in MeOH. K_2CO_3 (223 mg, 1.65 mmol) was added to the flask and suspension was allowed to reflux for 8 h. MeOH was removed under reduced pressure. Solid was filted and washed with H_2O (20 mL) and dried via lyophilization overnight to yeild **3.10** (160 mg, 73% yeild) as a white solid, which was taken forward without further purification.

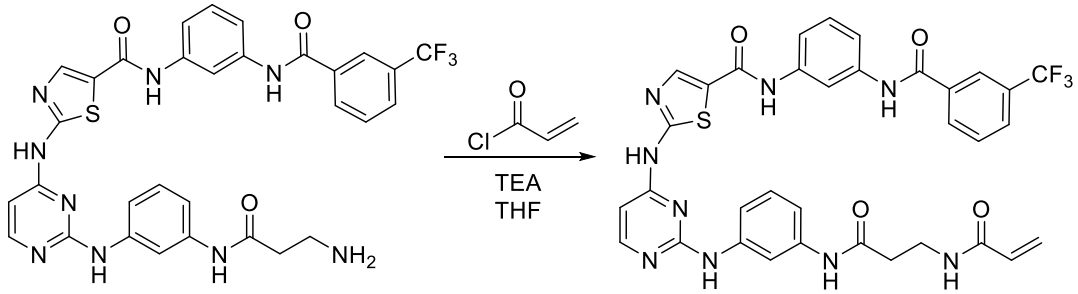

3.10 **3.1**

Scheme 3.6. Synthesis of Compound **3.1**

Synthesis of 3.1. Compound **3.10** (20 mg, 0.32 mmol) was added to a flame-dried flask that was flushed with N_2, followed by THF (3 mL) and TEA (5.05 µL, 0.36 mmol) addition. Reaction was cooled to 0°C prior to addition of acrolyl chloride (2.93 µL, 0.36 mmol). The reaction was allowed to stir for 1.5 h. Solvent was removed under reduced pressure to provide the crude product, which was purified via reverse-phase chromatography (linear gradient of 5 – 100% CH_3CH in H_2O) to yield compound **3.1** as a white solid (4.2 mg, 19.2% yield). **Spectral data.** ^{1}H NMR (500 MHz, DMSO-d_6): δ

10.53 (s, 1H), 10.18 (s, 1H), 10.01 (s, 1H), 8.46 (d, J = 5.8 Hz, 1H), 8.31 (s, 2H), 8.28 (d, J = 7.7 Hz, 1H), 8.22 (s, 1H), 8.18 (t, J = 5.7 Hz, 1H), 7.98 (d, J = 7.5 Hz, 1H), 7.82 – 7.78 (m, 1H), 7.58 (s, 1H), 7.48 (d, J = 15.5 Hz, 3H), 7.38 – 7.32 (m, 1H), 6.95 (d, J = 7.6 Hz, 1H), 6.58 – 6.48 (m, 1H), 6.30 (dd, J = 16.9, 1.7 Hz, 1H), 6.23 – 6.14 (m, 1H), 6.05 (dd, J = 17.1, 2.1 Hz, 1H), 5.76 (d, 1H), 5.53 (dd, J = 10.2, 2.2 Hz, 1H), 3.38 – 3.35 (q, 2H), 2.51 (t, 2H). ^{13}C NMR (125 MHz, DMSO-d6): δ 170.01, 166.43, 165.08, 164.49, 160.01, 159.91, 157.95, 141.55, 140.48, 139.47, 136.21, 132.33, 132.14, 131.35, 130.15, 129.81, 129.46, 129.19, 128.56, 125.37, 124.72, 123.29, 118.74, 118.22, 116.48, 113.03, 109.99, 79.67, 79.40, 79.14, 36.68, 35.36.

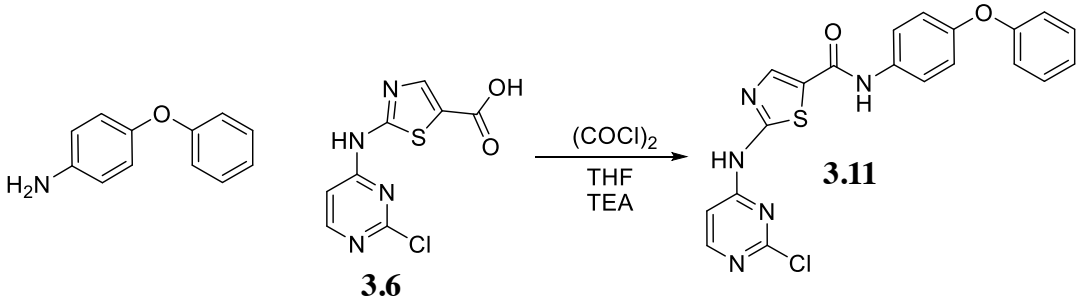

Scheme 3.7. Synthesis of Compound **3.11**

Synthesis of 3.11. Compound **3.6** (1000 mg, 3.9 mmol) was dissolved in THF (30mL), cooled to 0°C, and stirred under N_2 atmosphere. Oxalyl Chloride (0.46 mL, 5.3 mmol) was added drop wise followed by a drop of DMF. The contents were stirred for 3 hours at 0°C. The THF was removed under reduced pressure and 4-phenoxyaniline (656 mg, 3.54 mmol) was added and suspended in THF (30mL). TEA (0.74 mL, 5.3 mmol) was added and the suspension was stirred at RT under N_2 atmosphere for 16 hours. THF was removed under reduced pressure and re-suspended in EtOAc. The organic mixture was washed with aqueous saturated $NaHCO_3$ (1 x 75 mL), brine (1 x 75 mL), dried over anhydrous $MgSO_4$ (s) and filtered. Solvent was removed under reduced pressure to yield crude **S7.** The product was purified by automated silica gel chromatography (linear gradient of 25 – 80% ethyl acetate in hexanes) to yield **S7** (602 mg, 36.4 % yield) as a tan solid, and was taken forward without further purification.

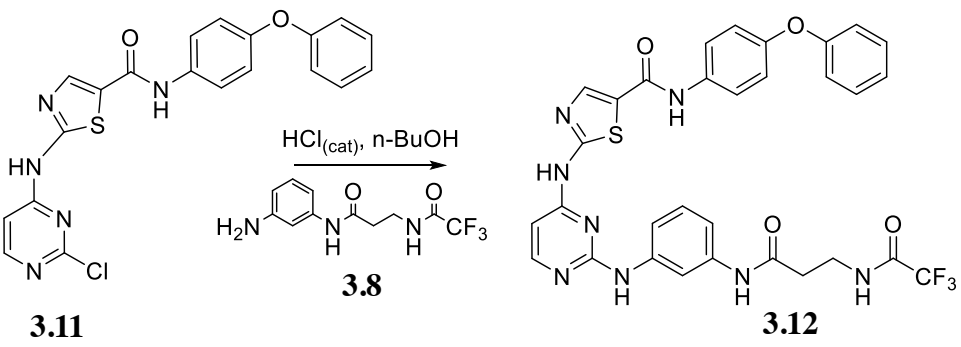

Scheme 3.8. Synthesis of Compound **3.12**

Synthesis of 3.12. Compound **3.11** (424 mg, 1.0 mmol) was added to a flame-dried flask that was flushed with N_2, followed by addition of dioxane (10mL), compound **3.8** (287 mg, 1.1 mmol) and 2 drops of HCl. The contents of the flask were refluxed for 13 h and cooled to R.T. Saturated $NaHCO_3$ (10mL) was added to the reaction flask, and the dioxane was removed under reduced pressure. Aqueous layer was extracted with EtOAC (3 x 30 mL), washed with brine (1 x 50 mL), dried over anhydrous $MgSO_4$ (s) and filtered. Solvent was removed under reduced pressure to yield crude **3.12.** The product was purified by automated silica gel chromatorgraphy (linear gradient of 25 – 80% ethyl acetate in hexanes) to yield **3.12** (371.5 mg, 57.3 % yeild) as a brown solid. **Spectral data.** ^{1}H NMR (500 MHz, DMSO-d_6) δ 11.86 (s, 1H), 10.15 (s, 1H), 9.94 (s, 1H), 9.59 – 9.46 (m, 2H), 8.29 (s, 1H), 8.19 (d, J = 5.6 Hz, 1H), 7.95 (s, 1H), 7.71 (d, J = 8.9 Hz, 2H), 7.39 (q, J = 7.5 Hz, 3H), 7.29 (d, J = 8.2 Hz, 1H), 7.22 (t, J = 8.0 Hz, 1H) 7.12 (t, J = 7.4 Hz, 1H), 7.04 (d, J = 8.9 Hz, 2H), 6.99 (d, J = 7.9 Hz, 2H), 6.51 (d, 1H), 3.46 (t, J = 6.1 Hz, 3H), 2.59 (t, J = 7.0 Hz, 2H).

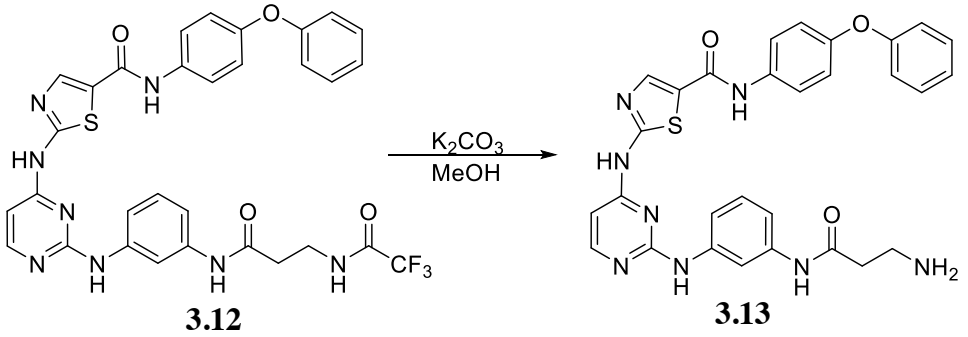

Scheme 3.19. Synthesis of Compound **3.13**

Synthesis of 3.13. Compound **3.12** (320 mg, 0.5 mmol) was added to a flask and suspended in MeOH. K_2CO_3 (345 mg, 2.5 mmol) was added to the flask and suspension was allowed to stir at reflux for 8 h. MeOH was removed under reduced pressure. Solid was filtered and washed with H_2O (20 mL) and dried via lyophilization overnight to yield **3.13** (237 mg, 87 % yield) which was taken forward without further purification.

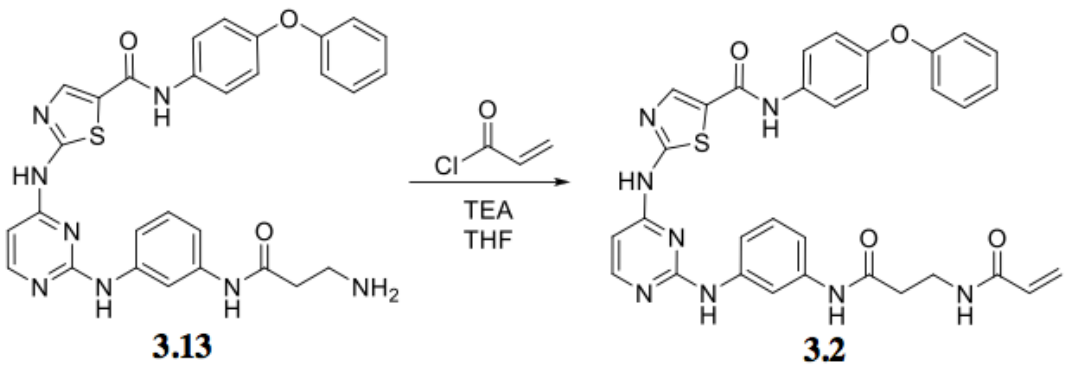

3.13 **3.2**

Scheme 3.10. Synthesis of Compound **3.2**

Synthesis of 3.2. Compound **3.13** (11.2 mg, 0.020 mmol) was added to a flame-dried flask that was flushed with N_2, followed by THF (3 mL) and TEA (3.3 µL, 0.024 mmol) addition. Reaction was cooled to 0°C prior to addition of acrolyl chloride (1.9 µL, 0.024 mmol). The reaction was allowed to stir for 1.5 h. Solvent was removed under reduced pressure to provide the crude product, which was purified via reverse-phase chromatography (linear gradient of 5 – 100% CH_3CH in H_2O) to yield compound **3.2** as a white solid (11.8 mg, 96% yield). **Spectral data.** ^{1}H NMR (500 MHz, DMSO-d_6): δ 10.14 (s, 1H), 9.88 (s, 1H), 9.40 (s, 1H), 8.28 (s, 1H), 8.25 – 8.17 (m, 2H), 7.96 (s, 1H), 7.72 (d, J = 8.8 Hz, 3H), 7.49 – 7.34 (m, 4H), 7.30 (d, J = 8.2 Hz, 1H), 7.20 (t, J = 8.0 Hz, 1H), 7.12 (t, J = 7.3 Hz, 1H), 7.04 (d, J = 8.8 Hz, 2H), 6.99 (d, J = 8.2 Hz, 2H), 6.49 (d, 1H), 6.28 – 6.17 (m, 1H), 6.07 (d, J = 18.8 Hz, 1H), 5.56 (d, J = 10.2 Hz, 1H), 3.40 (q, J = 6.3 Hz, 3H), 2.53 (t, 3H). ^{13}C NMR (125 MHz, DMSO-d6): δ 169.70, 165.09, 162.44, 160.10, 159.46, 157.72, 157.53, 157.46, 152.45, 141.09, 140.69, 139.61, 135.19, 132.20,

130.42, 128.76, 125.41, 123.48, 122.22, 119.79, 118.41, 116.15, 113.74, 111.93, 99.68, 36.66, 35.55, 25.15.

Individual Contributions

Dr. Kristin Ko aided greatly in the mutagenesis and production of the c-Src mutations. Dr. Frank Kwarcinski synthesized and characterized both the irreversible-Conformation selective Dasatinib inhibitors as well as the Conformation Selective BODIPY probes. Dr. Taylor K. Johnson provided support in the initial K_{off} determinations as well as experiments not included in this thesis.

References

1. Hunter T. Protein Kinases and Phosphatases: the Yin and Yang of Protein Phosphorylation and Signaling. *Cell*. **1999**, 80.2, 225-236.
2. Marshall CJ. Specificity of Receptor Tyrosine Kinase Signaling: Transient Versus Sustained Extracellular Signal-regulated Kinase Activation. *Cell.* **1995**, 80(2), 179-85.
3. Chang L, Karin M. Mammalian MAP Kinase Signalling Cascades. *Nature*. **2001**, 410(6824), 37.
4. Manning G, Whyte DB, Martinez R, Hunter T, Sudarsanam S. The Protein Kinase Complement of the Human Genome. *Science*. **2002**, 298(5600), 1912-34.
5. Kung JE, Jura N. Structural Basis for the Non-catalytic Functions of Protein Kinases. *Structure.* **2016**, 24(1), 7-24.
6. Huse M, Kuriyan J. The Conformational Plasticity of Protein Kinases. *Cell*. **2002**, 109(3), 275-82.
7. Bjorge JD, Pang AS, Funnell M, Chen KY, Diaz R, Magliocco AM, Fujita DJ. Simultaneous siRNA Targeting of Src and Downstream Signaling Molecules Inhibit Tumor Formation and Metastasis of a Human Model Breast Cancer Cell Line. *PLoS One*. **2011**, 6(4), e19309.
8. Maa MC, Leu TH, McCarley DJ, Schatzman RC, Parsons SJ. Potentiation of Epidermal Growth Factor Receptor-mediated Oncogenesis by c-Src: Implications for the Etiology of Multiple Human Cancers. *Proceedings of the National Academy of Sciences*. **1995**, 92(15), 6981-5.
9. Avizienyte E, Frame MC. Src and FAK Signalling Controls Adhesion Fate and the Epithelial-to-mesenchymal Transition. *Current Opinion in Cell Biology*. **2005**, 17(5), 542-7.
10. Xi S, Zhang Q, Dyer KF, Lerner EC, Smithgall TE, Gooding WE, Kamens J, Grandis JR. Src Kinases Mediate STAT Growth Pathways in Squamous cell Carcinoma of the Head and Neck. *Journal of Biological Chemistry*. **2003**, 278(34), 31574-83.
11. Cooper JA, Howell B. The when and how of Src Regulation. *Cell*. **1993**, 73(6), 1051-4.
12. Boggon TJ, Eck MJ. Structure and Regulation of Src Family Kinases. *Oncogene*. **2004**, 23(48), 7918.
13. Cowan-Jacob SW, Fendrich G, Manley PW, Jahnke W, Fabbro D, Liebetanz J, Meyer T. The Crystal Structure of a c-Src Complex in an active Conformation Suggests Possible steps in c-Src Activation. *Structure*. **2005**, 13(6), 861-71.
14. Xu W, Harrison SC, Eck MJ. Three-dimensional Structure of the Tyrosine Kinase c-Src. *Nature.* **1999,** 385(6617), 595.
15. Greenman C, Stephens P, Smith R, Dalgliesh GL, Hunter C, Bignell G, Davies H, Teague J, Butler A, Stevens C, Edkins S. Patterns of Somatic Mutation in Human Cancer Genomes. *Nature*. **2007,** 446(7132), 153.
16. MacAuley AL, Cooper JA. Structural Differences Between Repressed and Derepressed Forms of p60c-src. *Molecular and Cellular Biology*. **1989**, 9(6), 2648-56.
17. Zhang J, Kalyankrishna S, Wislez M, Thilaganathan N, Saigal B, Wei W, Ma L, Wistuba II, Johnson FM, Kurie JM. SRC-family Kinases are Activated in Non-small Cell

Lung Cancer and Promote the Survival of Epidermal Growth Factor Receptor-dependent Cell Lines. *The American Journal of Pathology*. **2007**, 170(1), 366-76.
18. Ottenhoff-Kalff AE, Rijksen G, Van Beurden EA, Hennipman A, Michels AA, Staal GE. Characterization of Protein Tyrosine Kinases from Human Breast Cancer: Involvement of the c-Src Oncogene Product. *Cancer Research*. **1992**, 52(17), 4773-8.
19. Irby RB, Mao W, Coppola D, Kang J, Loubeau JM, Trudeau W, Karl R, Fujita DJ, Jove R, Yeatman TJ. Activating SRC Mutation in a subset of Advanced Human Colon Cancers. *Nature Genetics*. **1999**, 21(2).
20. Bamford S, Dawson E, Forbes S, Clements J, Pettett R, Dogan A, Flanagan A, Teague J, Futreal PA, Stratton MR, Wooster R. The COSMIC (Catalogue of Somatic Mutations in Cancer) Database and Website. *British Journal of Cancer*. **2004**, 91(2), 355.
21. MacArthur J, Bowler E, Cerezo M, Gil L, Hall P, Hastings E, Junkins H, McMahon A, Milano A, Morales J, Pendlington ZM. The New NHGRI-EBI Catalog of Published Genome-wide Association Studies (GWAS Catalog). *Nucleic Acids Research*. **2017**, 45(D1), D896-901.
22. Barretina J, Caponigro G, Stransky N, Venkatesan K, Margolin AA, Kim S, Wilson CJ, Lehár J, Kryukov GV, Sonkin D, Reddy A. The Cancer Cell Line Encyclopedia Enables Predictive Modelling of Anticancer Drug Sensitivity. *Nature.* **2012,** 483(7391), 603-7.
23. Schwartzberg PL, Xing L, Hoffmann O, Lowell CA, Garrett L, Boyce BF, Varmus HE. Rescue of Osteoclast Function by Transgenic Expression of Kinase-deficient Src insrc−/− Mutant Mice. *Genes & Development*. **1997,** 11(21), 2835-44.
24. Liu Y, Shah K, Yang F, Witucki L, Shokat KM. Engineering Src Family Protein Kinases with Unnatural Nucleotide Specificity. *Chemistry & Biology*. **1998**, 5(2), 91-101.
25. Bukhtiyarova M, Karpusas M, Northrop K, Namboodiri HV, Springman EB. Mutagenesis of p38α MAP Kinase Establishes Key Roles of Phe169 in Function and Structural Dynamics and Reveals a Novel DFG-OUT State. *Biochemistry*. **2007**, 46(19), 5687-96.
26. Blencke S, Zech B, Engkvist O, Greff Z, Őrfi L, Horváth Z, Kéri G, Ullrich A, Daub H. Characterization of a Conserved Structural Determinant Controlling Protein Kinase Sensitivity to Selective Inhibitors. *Chemistry & Biology*. **2004**, 11(5), 691-701.
27. Azam M, Seeliger MA, Gray NS, Kuriyan J, Daley GQ. Activation of Tyrosine Kinases by Mutation of the Gatekeeper Threonine. *Nature Structural & Molecular Biology***. 2008**, 15(10), 1109-18.
28. Brabek J, Mojzita D, Novotny M, Puta F, Folk P. The SH3 domain of Src can Downregulate its Kinase Activity in the Absence of the SH2 domain-pY527 Interaction. *Biochemical and Biophysical Research Communications*. **2002**, 296(3), 664-70.
29. Meng Y, Roux B. Computational Study of the W260A Activating Mutant of Src Tyrosine Kinase. *Protein Science*. **2016**, 25(1), 219-30.
30. Foda ZH, Shan Y, Kim ET, Shaw DE, Seeliger MA. A Dynamically Coupled Allosteric Network Underlies Binding Cooperativity in Src Kinase. *Nature Communications*. **2015**, 6.
31. Sharma V, Wang Q, Lawrence DS. Peptide-based Fluorescent Sensors of Protein Kinase Activity: Design and Applications. *Biochimica et Biophysica Acta (BBA)-Proteins and Proteomics*. **2008,** 1784(1), 94-9.

32. Lerner EC, Smithgall TE. SH3-dependent Stimulation of Src-family Kinase Autophosphorylation Without Tail Release from the SH2 Domain in vivo. *Nature Structural & Molecular Biology*. **2002**, 9(5), 365-9.
33. Abram CL, Courtneidge SA. Src Family Tyrosine Kinases and Growth Factor Signaling. *Experimental Cell Research*. **2000**, 254(1), 1-3.
34. Okada M, Nada S, Yamanashi Y, Yamamoto T, Nakagawa H. CSK: a Protein-Tyrosine Kinase Involved in Regulation of Src Family Kinases. *Journal of Biological Chemistry*. **1991,** 266(36), 24249-52.
35. Agius MP, Soellner MB. Modulating Noncatalytic Function with Kinase Inhibitors. *Chemistry & Biology*. **2014**, 21(5), 569-71.
36. Seeliger MA, Young M, Henderson MN, Pellicena P, King DS, Falick AM, Kuriyan J. High Yield Bacterial Expression of Active c-Abl and c-Src Tyrosine Kinases. *Protein Science*. **2005,** 14(12), 3135-9.
37. Kwarcinski FE, Brandvold KR, Phadke S, Beleh OM, Johnson TK, Meagher JL, Seeliger MA, Stuckey JA, Soellner MB. Conformation-selective Analogues of Dasatinib Reveal Insight into Kinase Inhibitor Binding and Selectivity. *ACS Chemical Biology*. **2016**, 11(5), 1296-304.
38. Kwarcinski FE, Fox CC, Steffey ME, Soellner MB. Irreversible Inhibitors of c-Src Kinase that Target a Nonconserved Cysteine. *ACS Chemical Biology*. **2012**, 7(11), 1910-7.

CHAPTER IV

Design of 'Tunable' Conformation-Selective ATP-Competitive Inhibitors

Abstract

Kinase targeted drugs have shown immense clinical utility for diverse indications. While 32 kinase inhibitors have been approved (and many more in clinical trials), it remains unclear whether clinical efficacy is observed solely through target inhibition, or whether modulation of non-catalytic functions has a role in their efficacy. A series of pyrazolopyrimidine kinase inhibitors designed to impact global kinase conformation of c-Src was synthesized and characterized using our selective proteolysis methodology. We further displayed these design elements could be adopted by many diverse chemical scaffolds. Finally, a panel of FDA approved kinase inhibitors that bind c-Src was also assessed to provide insight into their binding modes.

Introduction

The development of potent and selective ATP competitive kinase inhibitors has been a breakthrough in cancer-targeted therapies and improving patient outcomes.[1-3] Modulating kinase signaling, through inhibition of downstream phosphorylation, has been a successful therapeutic strategy for a number of cancer types. However, more evidence suggests that kinase signaling through 'non-catalytic' mechanisms is as important as their catalytic role.[4] This non-catalytic signaling is often observed as protein-protein interactions, localization changes, and is typically modulated through large protein conformational changes.[5,6] While it has been reported (and showcased in Chapter's II & III) that ATP competitive kinase inhibitors can modulate these non-catalytic kinase functions, only recently is their therapeutic benefit being identified.

For example, the nuclear kinase IRE1α in an important signaling molecule during the unfolded protein response.[7] Its implication in diabetes, neurodegeneration, and cancer, makes IRE1α a promising therapeutic kinase target.[8-10] In addition to its canonical

catalytic activity, IRE1α also possesses ribonuclease activity. Upon dimerization in the nuclease, IRE1α's ribonuclease is activated, and the cleavage of RNA leads to the activation of a number of gene targets involved in the unfolded protein response.[11] Recently, ATP-competitive conformation selective inhibitors have been used to interrogate the signaling of IRE1α through inhibition of the kinase activity.[12] Surprisingly, some these inhibitors were also shown to have the ability to inhibit ribonuclease activity (Figure 4.1). X-Ray structures of these inhibitors showcased that they were stabilizing a Src-like/Cdk inactive conformation with the αC-helix of IRE1α in the extended conformation. This is speculated to inhibit the dimerization event required for ribonuclease activity to occur. Other examples in the literature point that modulating αC-helix movement to be a promising method of modulating 'non-catalytic' functions of kinases.

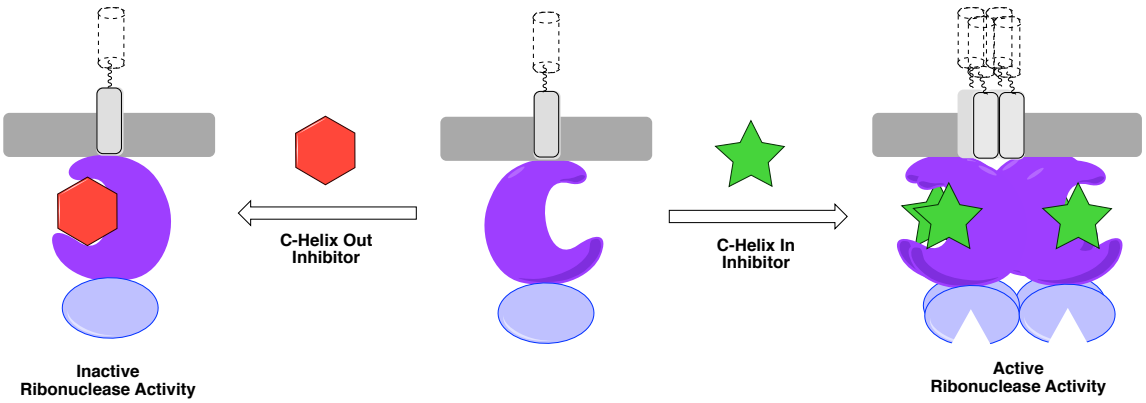

Figure 4.1. IRE1α has both catalytic kinase function and ribonucleic activity. The ribonuclease activity can additionally be inhibited using a aC-Helix-out inhibitor (through inhibition of oligermization of riboneuclease domain). However, stabilization of the active kinase conformation still inhibits kinase function, but activate ribonuclease activity, showcasing the power of utilizing conformation-selective inhibitors.

Cyclin-dependent-kinases, or CDKs, have been a promising therapeutic target for metastatic breast cancer.[13] However, It catalytic activity is dependent upon the binding of a small protein, cyclin.[14] The binding site of cyclin occurs on top of the αC-helix of

CDKs and stabilizes a αC-Helix-In conformation which activates catalytic activity. Thus, it is no surprise that when inhibited with a conformation-selective inhibitor, stabilizing the 'αC-Helix-out' conformation, that cyclins can no longer bind.[15]

Additionally, conformation-selective inhibitors have been used to overcome inhibitor resistance mechanisms in cancer. The Shokat Lab recently reported that modulating the αC-helix of Her2 to be advantageous in not only inhibiting the catalytic function of Her2, but specifically the Her2-Her3 heterodimers that were resistant to Lapatinib treatment.[16] Crystal structure analysis showcases stabilization of this αC-helix-In conformation in the Her2-Her3 heterodimer. It is speculated that heterodimer formation, through increase levels of Her3, is what eventually leads to inhibitor resistance as αC-helix out inhibitors (eg. Lapatinib) cannot bind these complexes. Thus, conformation-selective αC-Helix-in inhibitors were validated as a novel strategy for targeting these complexes and avoiding inhibitor resistance mechanisms. These examples of IRE1α, Cdk, and Her2, showcase the power of modulating kinase signaling beyond the catalytic event, and furthermore can aid in developing the next generation of kinase targeted therapies.

Conformation Selective Inhibitors Can Stabilize Global c-Src Conformations

Recently, ATP-competitive inhibitors have been shown to modulate the global conformations of protein kinases, including c-Src.[17] We noted that stabilization of c-Src's αC-Helix (a key regulatory helix within the kinase domain) in the 'in' or 'out' conformation can promote a global 'open' or 'closed' conformation, respectfully. Furthermore, αC-Helix modulation has been observed to influence the non-catalytic function of many diverse protein kinase, including: IRE1α, CDK, and Her2. To validate that αC-Helix conformation can influence the global conformation of c-Src, we designed and synthesized a matched set of conformation-selective kinase inhibitors based on the Dasatinib scaffold (Figure 4.2).

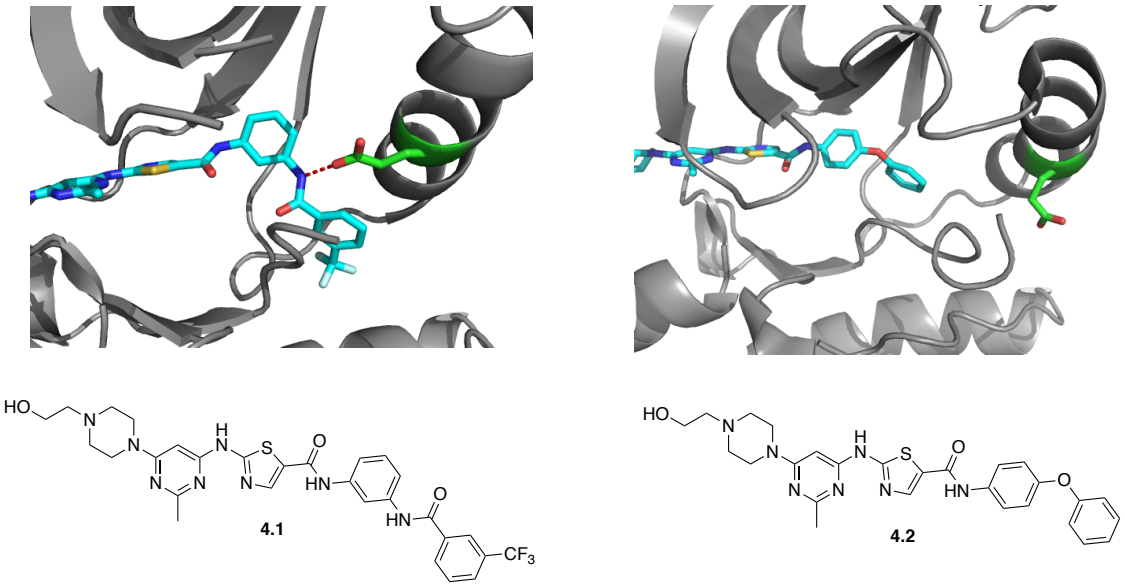

Figure 4.2. Conformation-Selective Dasatinib analogs were designed to stabilize the αC-Helix-in (**4.1**) and αC-Helix-out (**4.2**) conformations to additionally modulate the quaternary structure of c-Src kinase. The binding modes were validated by X- Ray Crystallography PDB: 4YBJ & 4YBK.

As we reported in 2016, x-ray crystallography verified that the DAS-IN analog (**4.1**) stabilizes the c-helix in the 'in' conformation (PDB: 4YBJ), and DAS-OUT (**4.2**) in the 'out' conformation (PDB: 4YBK).[18] We utilized our selective-proteolysis method with our matched set of conformation selective Dasatinib analogs. The observed half-life for **4.1** is 3 min, confirming stabilization of the 'open' conformation. Meanwhile, the half-life of **4.2** is 82 min, confirming stabilization of the 'closed' conformation. These data verify our hypothesis that the small changes in the αC-Helix, stabilized by our matched set, can control the quaternary structure of c-Src. We have characterized this set of conformation-selective kinase inhibitors across the kinome and found that each analog is a potent inhibitor of ~40 diverse protein kinases.

We hypothesize that design elements from our matched set of conformation-selective Dasatinib analogs can be mapped onto other diverse inhibitor scaffolds. The quinazoline scaffold has been used in number of FDA approved drugs including Lapatinib and Gefetinib.[19, 20] Additionally, the pyrazolopyrimidine kinase scaffold has been found as the core of many kinase inhibitors, including Ibrutinib, an FDA-approved

Btk inhibitor.[21] Thus we designed and synthesized both quinazoline and pyrazolopyrimidine analogs that can stabilize the αC-helix 'in' and 'out' conformation (Figure 4.3). Quinazoline containing compounds, **4.3** and **4.4**, were observed to stabilize the open and closed conformations with half-lifes of 4 mins and 100 mins respectfully. Pyrazolopyrimidine containing compounds, **4.5** and **4.6**, were found to have half-lives of 2 mins and 71 mins, respectfully. These data showcase that conformation-selective elements, designed to interact with the αC-helix, can be transposed onto many inhibitor scaffolds of choice. Providing researchers with the ability to beginning targeting non-catalytic function of any number of kinases.

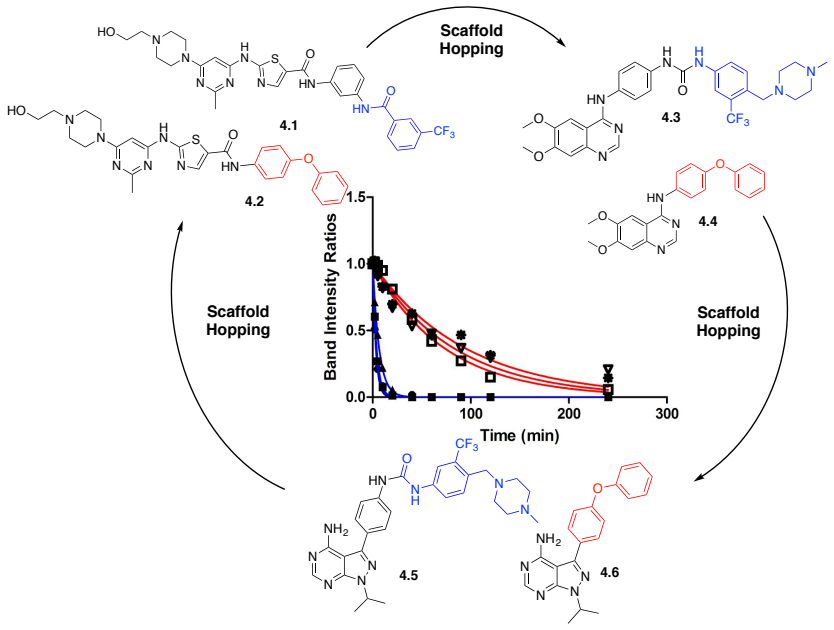

Figure 4.3. Design elements from the Conformational-selective Dasatinib can be adopted by many diverse inhibitor scaffold to modulate the non-catalytic functions of any kinase of interest

Consistent with our hypothesis, specific interactions with the αC-helix result in the stabilization of specific kinase conformations. PP2, a widely-used c-Src inhibitor does not interact with the αC-helix and was found to have a thermolysin half-life of 13 mins,

corresponding to a 'neutral' conformation (not 'open' or 'closed').[22] On the basis of these data, we hypothesize that chemically 'tuning' the interaction between the inhibitor and the αC-helix could afford 'conformation-tunable' inhibitors (that is, inhibitors that stabilize conformations across the 'open' vs 'closed' global conformations observed).

Structure-Conformation Relationship of a Panel of Pyrazolopyrimidine Inhibitors

To enable better conformational control using small molecule inhibitors, we hypothesized that modulating the interaction between the inhibitor and the αC-helix could afford 'conformation-tunable' inhibitors. 23 inhibitors were rationally designed, synthesized, and the conformation of c-Src when inhibitor bound was determined using selective proteolysis (Figure 4.6). Most of the design elements were adopted from existing small molecules used to interrogate kinase signaling. This enabled us to aid in the characterization of these ligands with the αC-helix, while maintaining a high degree of chemical diversity to explore.

When designing inhibitors that bind the open/active c-Src conformation, it was speculated that molecules that had the ability to hydrogen bond to the Glu313 (located on the αC-Helix) of c-Src could stabilize the open conformation. We synthesized a number of molecules with hydrogen bond-donor groups (-OH, -NH2, ect.) that we predicted would hydrogen bond to Glu313 with various strengths. Those that stabilized the most open conformation were **4.5** and **4.7** with half-life values of 2 and 3 mins respectfully (Figure 4.4). Masking of the hydrogen donor group, through methylation of the 3-hydroxy, afforded **4.11** that bound to a less open construct, comparable to inhibitor **4.10,** which contains no hydrogen-bond donor groups. Surprisingly inhibitor **4.17** had an observed half-life of 36 mins (indicative of binding the apo construct), which depicts the importance of correctly positioning the hydrogen-bond donor groups to correctly stabilize an open c-Src conformation.

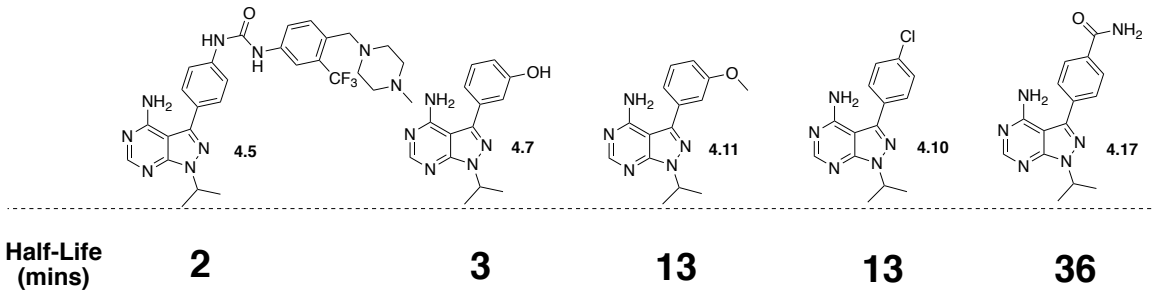

Figure 4.4. Select inhibitors that were utilized to stabilize the open c-Src conformation. Inhibitors **4.5** and **4.7** stabilize the open conformation the most as these inhibitors can stabilize the αC-helix-in conformation using h-bond donors on the inhibitor.

When designing inhibitors that bind the closed/inactive c-Src conformation, it has been observed that large, hydrophobic groups, are known to break the Glu313 - Lys298 salt bridge and stabilize a αC-helix-out conformation (Figure 4.5).[17] Thus, we synthesized a number of molecules that masked any hydrogen-bond donor groups by installing aryl ethers that could stabilize various αC-helix out conformations. Compounds **4.27** and **4.28** stabilized the most closed conformation with half-lives of 94 mins and 160 mins respectfully. Surprisingly, compound **4.19** appeared to be our 'bulkiest' compound, however only displayed a half-life of 44 mins, indicating both the available room in the back hydrophobic pocket, and the importance of ligand positioning to stabilize the αC-helix out conformation.

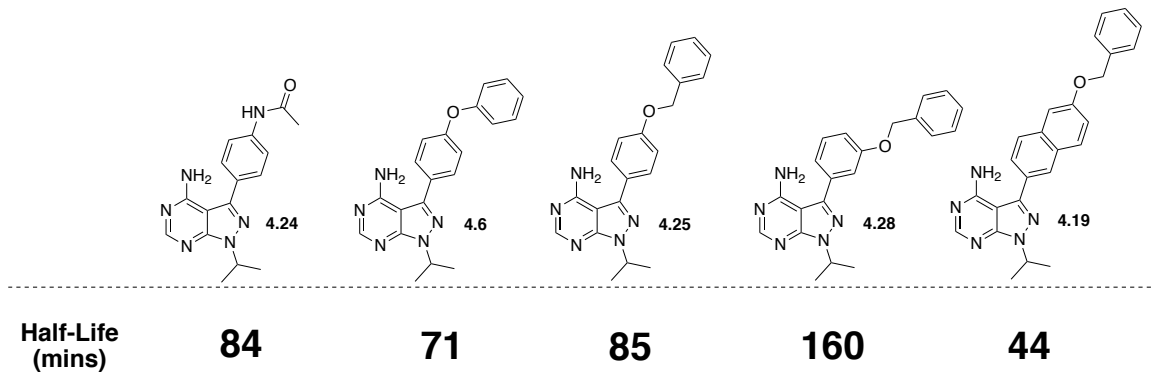

Figure 4.5. Select inhibitors were designed to stabilize the αC-helix-out conformation through disruption of the catalytic Glu313 and Lys298 salt-bridge.

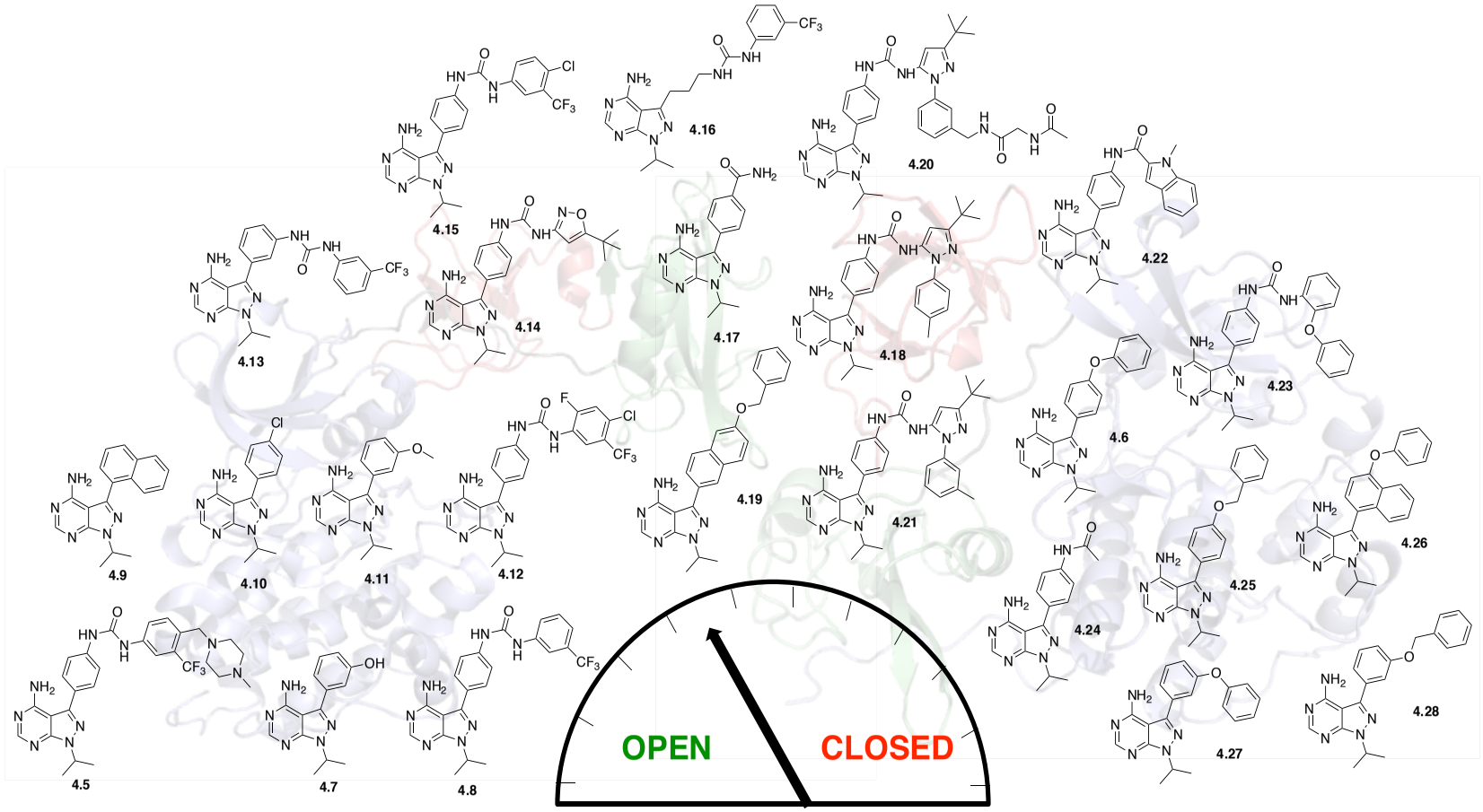

Figure 4.6. The full panel of 23 'tunable' conformation-selective inhibitors designed to stabilize various open and closed global conformations of c-Src kinase.

Conformation Analysis of FDA Approved Inhibitors

Over the past decade, the success of kinase inhibitors in the clinic has now produced 32 FDA kinase inhibitors to date.[23] However, the focus on targeting this protein class remains predominantly on targeting the catalytic functions using ATP competitive inhibitors. The modulation of kinase's non-catalytic functions, through small molecule inhibitors, has only recently been appreciated as a targeting strategy.[24] As we showcased how a number ATP-competitive inhibitors to be conformation selective for c-Src, we speculated whether the success of current FDA approved inhibitors could also be from modulating non-catalytic functions as well. Thus we screened a small panel of FDA approved inhibitors that can bind c-Src, to characterize their effect on modulating global kinase conformation (Table 4.1).

	DMSO	Dasatinib	Ponatinib	Bosutinib	Saracatinib	4.6
Half-Life	33	3.1	2.5	4.5	6.9	71

Table 4.1. Select FDA approved inhibitors screened using selective proteolysis reveals changes in the global conformations of c-Src

Our panel included FDA approved inhibitors Dasatinib, Saracatinib, Bosutinib, Ponatinb.[25-28] We also included **4.6** as it structurally binds identically to FDA approved Ibrutinib. Surprisingly, all FDA approved inhibitors bind the open conformation indicative of stabilizing the αC-helix in conformation. While none of these are approved for solely targeting c-Src, it is unclear weather stabilization of the αC-helix in conformation may have an effect on their targets 'non-catalytic functions.' **4.6**, previously investigated above, stabilizes the αC-helix out or closed c-Src conformation. This raises new hypotheses, such as: is inhibition of Btk, in the αC-helix out conformation, required for clinical efficacy? Fortunately, with the characterization and development of tunable conformation-selective inhibitors, such questions can be answered.

Conclusions

Kinase inhibitors have only recently been shown to additionally modulate non-catalytic functions via stabilization of kinase global conformations. Nearly all examples in the literature achieve this through modulation of the kinase's αC-helix, displaying how the αC-helix is used as a common regulatory domain of all kinases. Here we displayed how modulating αC-helix movement, with conformation-selective Dasatinib analogs can stabilize c-Src's open and closed conformations. We further showcased that tuning the interaction with the αC-helix, through the addition of hydrogen bond donors or hydrophobic groups, can modulate the global conformation of c-Src with varying degrees. We further displayed the modularity of this approach by showcasing that design elements from these inhibitors can be easily designed onto other diverse chemical scaffolds to target the kinome.

FDA approved kinase inhibitors have been designed to modulate kinases catalytic functions. Characterization of a small panel of FDA approved inhibitors showcase how these inhibitors have αC-helix modulation character. It remains a mystery whether the clinical efficacy of kinase inhibitors is from solely inhibition of catalytic activity, or if they additionally modulate non-catalytic functions as well. These chemical tools described herein can give researchers insight to better design kinase inhibitors that can additionally affect non-catalytic functions of kinases.

Materials and Methods

Selective Proteolysis of c-Src General Method

c-Src was diluted in proteolysis buffer (50 mM Tris-HCl pH 8.0, 100 mM NaCl, 0.5 mM $CaCl_2$) to yield a final protein concentration of 2 μM. 1 uL of a 10 mM DMSO stock of the inhibitor was added and incubated with c-Src for 15 mins at room temperature. Thermolysin (purchased from Promega, catalog number: V4001) from a 3.8 μM stock solution was added to the reaction mixture to a final concentration of 60 nM. 15 μL of the proteolysis reaction was added to 5 μL of 50 mM EDTA to quench proteolysis at various time points (0, 2, 5, 10, 30, 60, 90, 120, 180, and 240 mins) and stored at -20

°C. The quenched samples were analyzed by SDS-PAGE (12 % Bis-Tris gel in MES running buffer, staining with comassie blue). Band intensities were analyzed by ImageJ imaging software. Percent protein remaining was plotted against time and fit to an exponential decay equation using GraphPad Prism 6 software to obtain half-lifes of each protein. The Exponential Decay curve for each protein was fit using the equation Y=(Y0 - Plateau)*exp(-K*X) + Plateau X = time(mins) and Y = normalized band intensity.

General Synthetic Methods

Unless otherwise noted, all reagents were obtained via commercial sources and used without further purification. ^{1}H NMR and ^{13}C NMR spectra were measured with a Varian MR400 or Inova 500 spectometer. Compounds **4.1**, **4.2**, **4.4**, **4.7**, **4.8**, **4.9**, **4.10**, **4.15**, **4.19**, **4.29**, **4.30** were synthesized using previously reported methods.[18, 30-35]

Synthetic Schemes

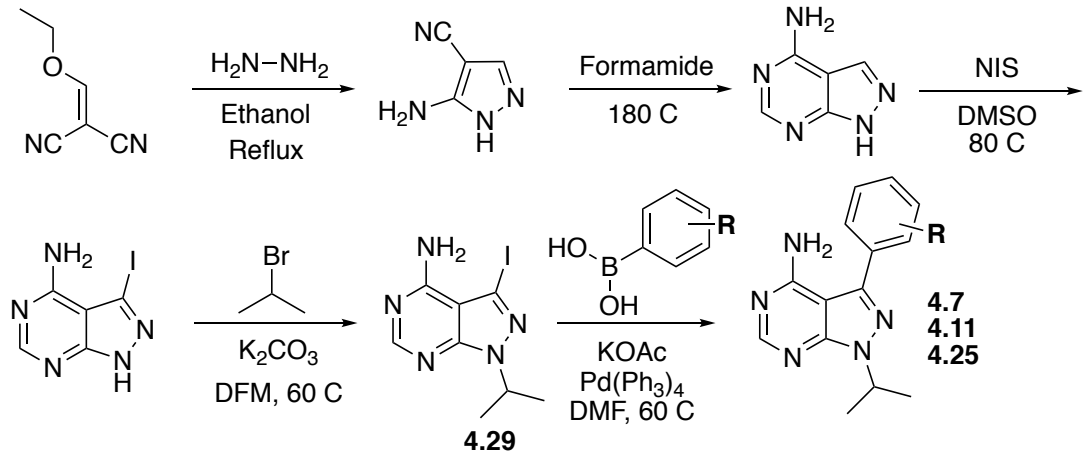

Scheme 4.1. Synthetic Route for Intermediate **4.29**

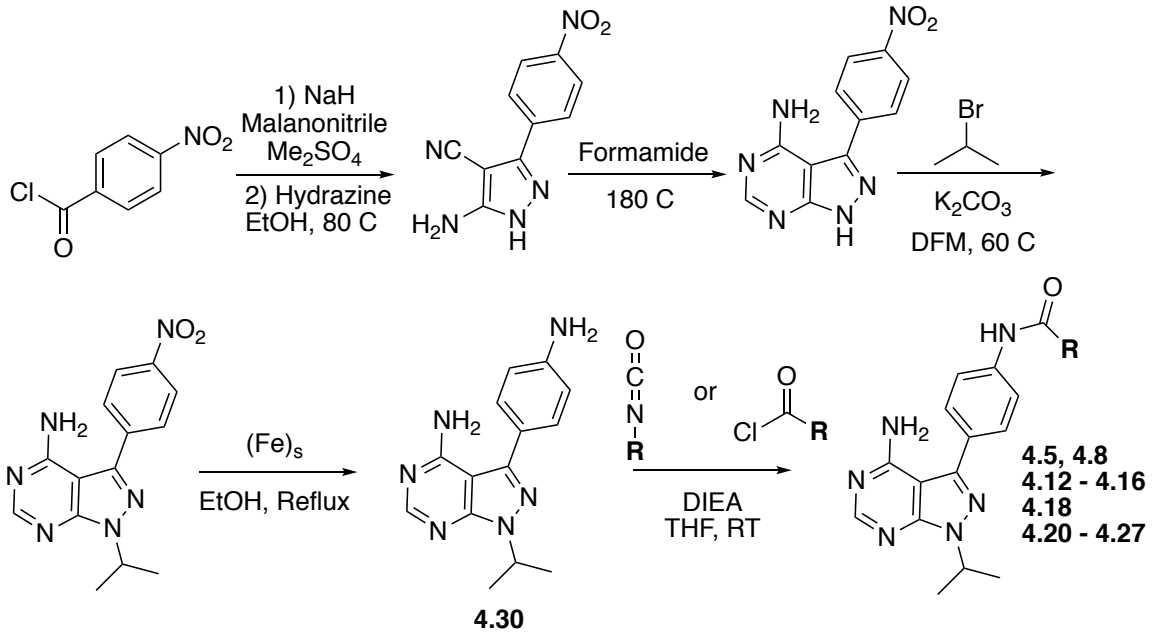

Scheme 4.2. Synthetic Route for Intermediate **4.30**

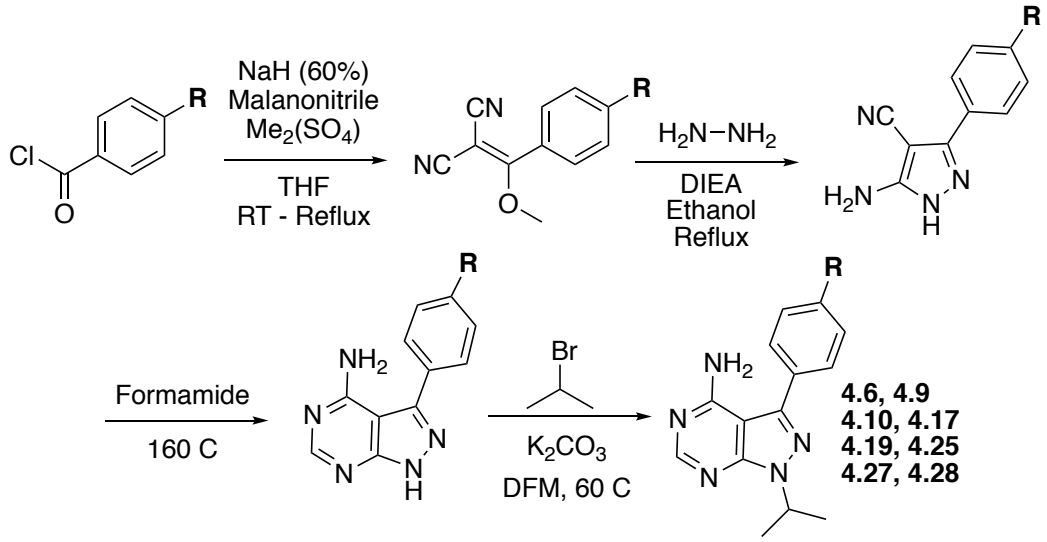

Scheme 4.3. General Synthetic Route for Select Pyrazolopyrimidine Compounds

Synthetic Protocols

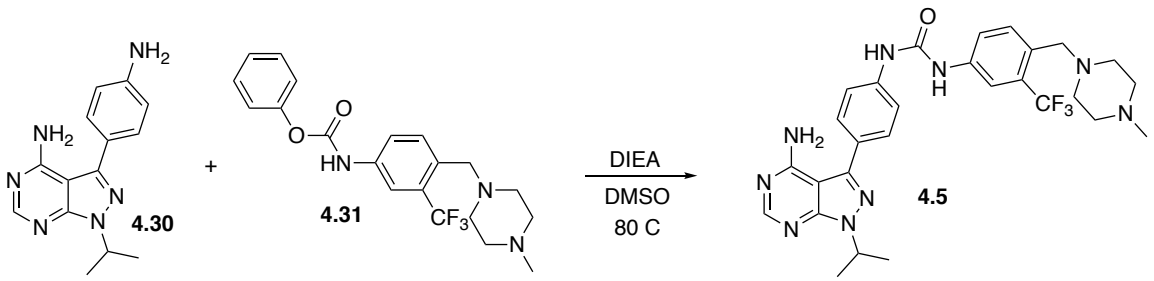

Scheme 4.4. Synthesis of Compound **4.5**

1-(4-(4-amino-1-isopropyl-1*H*-pyrazolo[3,4-*d*]pyrimidin-3-yl)phenyl)-3-(4-((4-methylpiperazin-1-yl)methyl)-3-(trifluoromethyl)phenyl)urea (**4.5**). In a 5 mL round bottom flask, **4.30** (25 mg, 0.09 mmol) and **4.31** (35 mg, 0.09 mmol) was dissolved in 2 mL of DMSO. Compound **4.31** was synthesized as previously described.[36] DIEA (31 µL, 0.18) mmol) was added and the reaction was stirred at 80 C for 2 hours. The reaction was cooled to room temperature and immediately purified by reverse phase HPLC using a linear 30% - 90% CAN in H_2O gradient to afford **4.5** as a white solid (10 mg, 0.02 mmol). Yield = 20%. ^{1}H NMR (500 MHz, DMSO-*d*6) δ 9.33 (s, 1H), 9.26 (s, 1H), 8.22 (s, 1H), 8.03 – 7.97 (m, 1H), 7.65 (d, *J* = 8.6 Hz, 2H), 7.63 – 7.56 (m, 4H), 5.05 (p, *J* = 6.7 Hz, 1H), 3.53 (s, 2H), 2.36 (s, 8H), 2.15 (s, 3H), 1.49 (d, *J* = 6.7 Hz, 6H).^{13}C NMR (126 MHz, DMSO) δ 159.81, 159.53, 159.26, 158.99, 154.45, 153.02, 151.71, 149.77, 145.88, 141.13, 139.97, 132.25, 129.34, 125.59, 123.63, 121.97, 119.13, 115.58, 97.11, 56.88, 53.03, 49.71, 49.41, 42.53, 22.16.

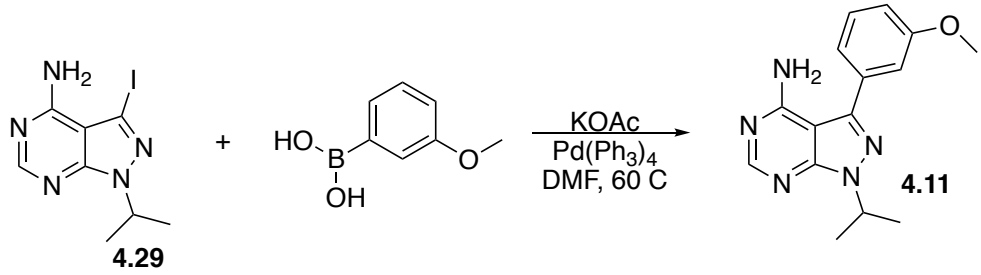

Scheme 4.5. Synthesis of Compound **4.11**

1-isopropyl-3-(3-methoxyphenyl)-1*H*-pyrazolo[3,4-*d*]pyrimidin-4-amine (**4.11**). In a 5 mL round bottom flack, **4.29** (10 mg, 0.03 mmol), (3-methoxyphenyl)boronic acid (4.5

mg, 0.03 mmol), potassium acetate (9 mg, 0.09 mmol), and tetrakis (4 mg, 0.003 mmol) was dissolved in 5 mL of dry DMF. The reaction was heated to 60 C, stirred for 16, cooled to room temperature, and immediately purified by reverse phase HPLC using a linear 30% - 90% ACN in H_2O gradient to afford **4.11** as a white solid (4 mg, 0.01 mmol), yield = 46%. ^{1}H NMR (500 MHz, dmso) δ 8.22 (s, 1H), 7.44 (t, *J* = 7.7, 7.7 Hz, 1H), 7.22 (d, *J* = 7.3 Hz, 1H), 7.16 (s, 1H), 7.03 (d, *J* = 8.1 Hz, 1H), 5.04 (p, *J* = 14.1, 7.1, 7.1 Hz, 1H), 3.81 (s, 3H), 1.48 (d, *J* = 6.5 Hz, 6H).

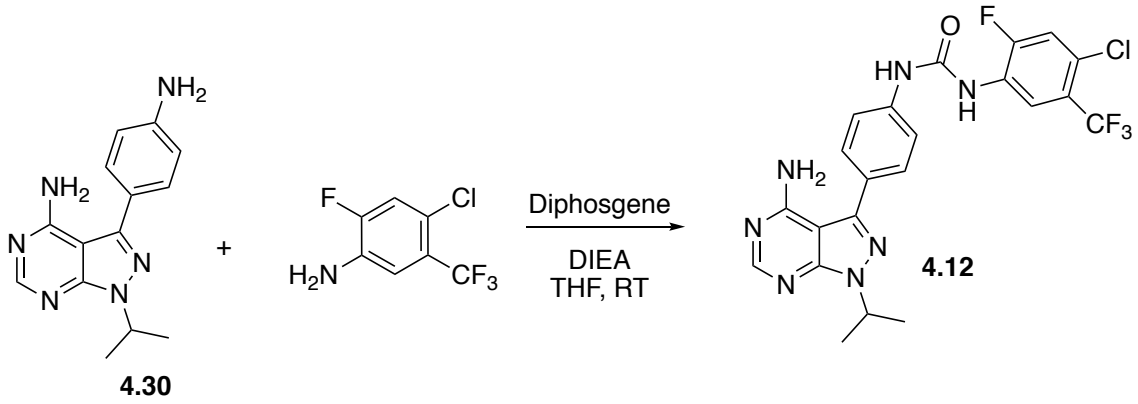

Scheme 4.6. Synthesis of Compound **4.12**

1-(4-(4-amino-1-isopropyl-1*H*-pyrazolo[3,4-*d*]pyrimidin-3-yl)phenyl)-3-(4-chloro-2-fluoro-5-(trifluoromethyl)phenyl)urea (**4.12**). To a 10 mL round bottom flask, 4-chloro-2-fluoro-5-(trifluoromethyl)aniline (19 mg, 0.09 mmol) was dissolved in 5 mL dry THF. Diphosgene (22 μL, 0.18 mmol) was added and the reaction was refluxed for 2 h, cooled to room temperature, and concentrated *in-vacuo*. The residue was resuspended in 5mL of dry THF in which **4.30** (25 mg, 0.09 mmol) and DIEA (31 μL, 0.18 mmol) was added and the reaction was allowed to stir at room temperature for 4 hours. The reaction was concentrated *in vacuo* and the residue was purified using reverse phase HPLC using a linear 30% - 90% ACN in H_2O to afford **4.12** as a white solid (10.5 mg, 0.02 mmol). Yield = 23%. ^{1}H NMR (500 MHz, DMSO-*d*6): ^{13}C NMR (126 MHz, dmso) δ 158.55, 155.81, 154.47, 153.71, 152.46, 152.32, 143.44, 139.66, 129.39, 127.96, 127.86, 127.69, 119.42, 119.23, 119.08, 97.84, 48.50, 22.24.

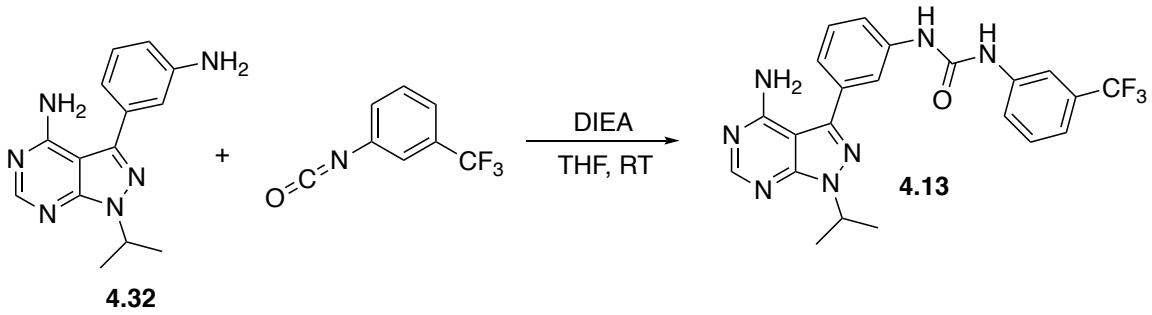

Scheme 4.7. Synthesis of Compound **4.13**

1-(3-(4-amino-1-isopropyl-1*H*-pyrazolo[3,4-*d*]pyrimidin-3-yl)phenyl)-3-(3-(trifluoromethyl)phenyl)urea (**4.13**). To a 10 mL round bottom flask, **4.32** (25 mg, 0.09 mmol) was dissolved in 5 mL dry THF. Compound **4.32** was synthesized previously as described.[37] 1-isocyanato-3-(trifluoromethyl)benzene (13 μL, 0.09 mmol) and DIEA (31 μL, 0.18 mmol) was added and the reaction was stirred at room temperature for 4 h and concentrated *in vacuo*. The residue was purified using reverse phase HPLC using a linear 30% - 90% ACN in H_2O to afford **4.13** as a white solid (27 mg, 0.06 mmol). Yield = 67%. ^{1}H NMR (500 MHz, DMSO-*d*6) δ 9.13 (s, 1H), 9.06 (s, 1H), 8.23 (s, 1H), 7.98 (s, 1H), 7.78 (s, 1H), 7.61 (d, *J* = 7.9 Hz, 1H), 7.51 (d, *J* = 7.6 Hz, 2H), 7.45 (t, *J* = 7.7 Hz, 1H), 7.30 (s, 2H), 5.06 (p, *J* = 13.1, 6.4 Hz, 1H), 1.48 (d, *J* = 6.6 Hz, 6H). ^{13}C NMR (126 MHz, dmso) δ 158.46, 155.88, 153.77, 153.15, 143.57, 140.94, 140.32, 134.11, 130.36, 130.13, 122.55, 122.43, 119.22, 118.87, 118.61, 114.65, 97.86, 48.57, 40.88, 22.24.

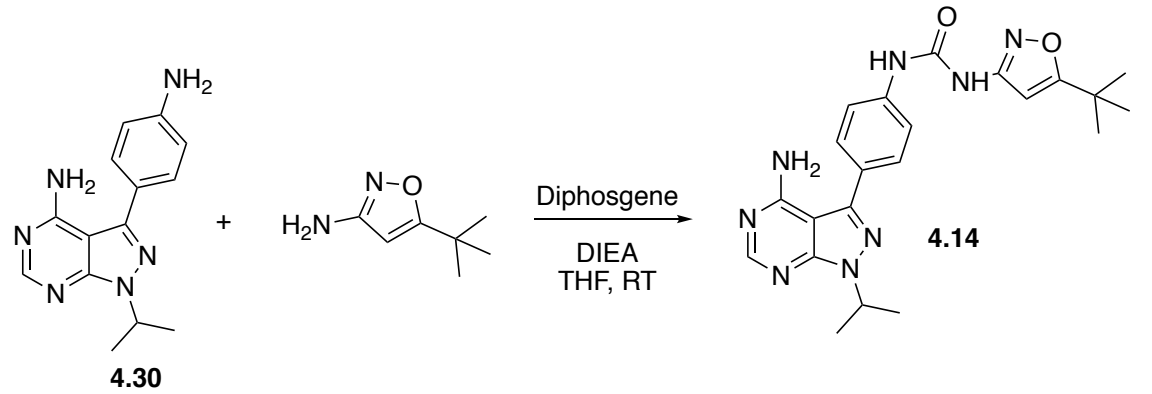

Scheme 4.8. Synthesis of Compound **4.14**

1-(4-(4-amino-1-isopropyl-1*H*-pyrazolo[3,4-*d*]pyrimidin-3-yl)phenyl)-3-(5-(*tert*-butyl)isoxazol-3-yl)urea (**4.14**). To a 10 mL round bottom flask, 5-(*tert*-butyl)isoxazol-3-amine (13 mg, 0.09 mmol) was dissolved in 5 mL dry THF. Diphosgene (22 µL, 0.18 mmol) was added and the reaction was refluxed for 2 h, cooled to room temperature, and concentrated *in vacuo*. The residue was resuspended in 5mL of dry THF in which **4.30** (25 mg, 0.09 mmol) and DIEA (31 µL, 0.18 mmol) was added and the reaction was allowed to stir at room temperature for 4 hours. The reaction was concentrated *in vacuo* and the residue was purified using reverse phase HPLC using a linear 30% - 90% ACN in H_2O to afford **4.14** as a white solid (5 mg, 0.04 mmol). Yield = 34%.

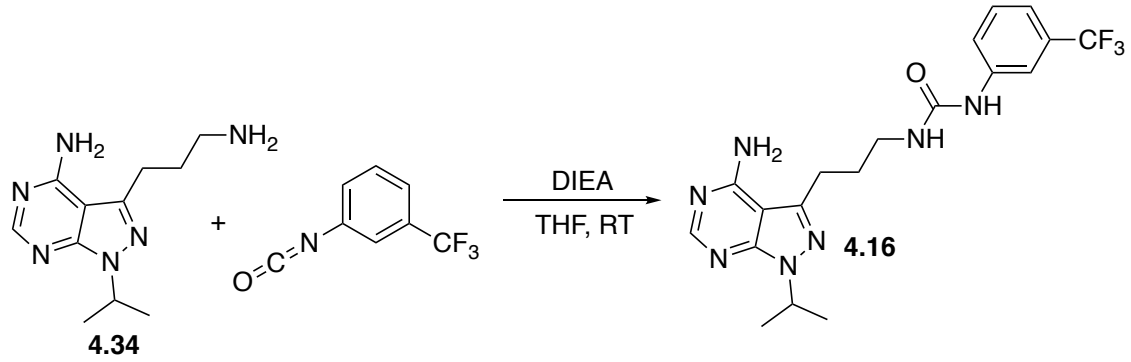

Scheme 4.9. Synthesis of Compound **4.16**

1-(3-(4-amino-1-isopropyl-1*H*-pyrazolo[3,4-*d*]pyrimidin-3-yl)propyl)-3-(3-(trifluoromethyl)phenyl)urea (**4.16**). To a 10 mL round bottom flask, **4.34** (21 mg, 0.09 mmol) was dissolved in 5 mL dry THF. Compound **4.34** was synthesized previously as described. 1-isocyanato-3-(trifluoromethyl)benzene (13 µL, 0.09 mmol) and DIEA (31 µL, 0.18 mmol) was added and the reaction was stirred at room temperature for 4 h and concentrated *in vacuo*. The residue was purified using reverse phase HPLC using a linear 30% - 90% ACN in H_2O to afford **4.16** as a white solid (15 mg, 0.04 mmol). Yield = 67%. ^{1}H NMR (500 MHz, dmso) δ 8.82 (s, 1H), 8.13 (d, J = 2.0 Hz, 1H), 7.94 (s, 1H), 7.48 (d, J = 8.3 Hz, 1H), 7.42 (t, J = 7.9, 7.9 Hz, 1H), 7.19 (d, J = 7.7 Hz, 1H), 6.35 (t, 1H), 4.91 (p, J = 12.5, 7.1, 7.1 Hz, 1H), 3.15 (q, J = 6.8, 6.8, 6.8 Hz, 2H), 3.00 – 2.94 (m, 2H), 1.78 (t, J = 7.6, 7.6 Hz, 2H), 1.39 (d, J = 6.7 Hz, 6H).

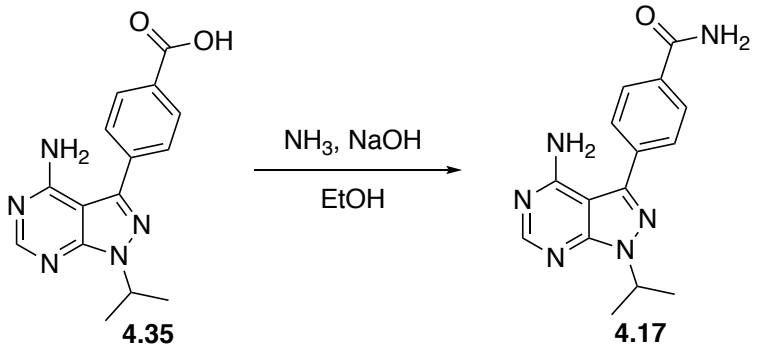

4.35 **4.17**

Scheme 4.10. Synthesis of Compound **4.17**

4-(4-amino-1-isopropyl-1*H*-pyrazolo[3,4-*d*]pyrimidin-3-yl)benzamide (**4.17**). To a 10 mL round bottom flask, **4.35** (25 mg, 0.08 mmol), ammonium chloride (4.5 mg, 0.09 mmol), and water (10 mL) was dissolved in 5 mL EtOH and cooled to 0 C. Compound **4.35** was synthesized previously as described.[37] A chilled (0 C) 10 M aqueous solution of NaOH (10 mL) was added drop-wise causing precipitation of a white solid. The resulting slurry was stirred for 5 mins. The solid was filtered washed with diethyl ether and water and dried *in-vacuo* to afford **4.17** as a white solid (18 mg, 0.06 mmol). Yield = 75%.

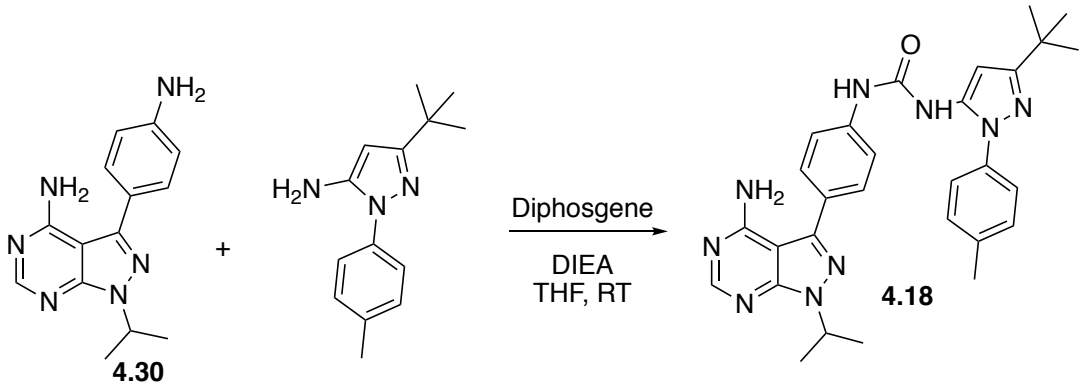

4.30 **4.18**

Scheme 4.11. Synthesis of Compound **4.18**

1-(4-(4-amino-1-isopropyl-1*H*-pyrazolo[3,4-*d*]pyrimidin-3-yl)phenyl)-3-(3-(*tert*-butyl)-1-(*p*-tolyl)-1*H*-pyrazol-5-yl)urea (**4.18**). To a 10 mL round bottom flask, 3-(*tert*-butyl)-1-(*p*-tolyl)-1*H*-pyrazol-5-amine (21 mg, 0.09 mmol) was dissolved in 5 mL dry THF. Diphosgene (22 µL, 0.18 mmol) was added and the reaction was refluxed for 2 h, cooled to room temperature, and concentrated *in vacuo*. The residue was resuspended in 5mL of

dry THF in which **4.30** (25 mg, 0.09 mmol) and DIEA (31 μL, 0.18 mmol) was added and the reaction was allowed to stir at room temperature for 4 hours. The reaction was concentrated *in vacuo* and the residue was purified using reverse phase HPLC using a linear 30% - 90% ACN in H_2O to afford **4.18** as a white solid (15 mg, 0.03 mmol). Yield = 32%. ^{1}H NMR (400 MHz, Chloroform-*d*) δ 8.32 (s, 1H), 7.61 (d, *J* = 8.4 Hz, 2H), 7.48 (d, *J* = 8.5 Hz, 2H), 7.30 (d, *J* = 7.4 Hz, 2H), 7.19 – 7.07 (m, 2H), 6.57 (s, 1H), 6.38 (s, 1H), 5.44 (s, 2H), 5.15 (p, *J* = 13.4, 6.7 Hz, 1H), 2.37 (s, 3H), 1.57 (d, *J* = 6.8 Hz, 6H), 1.36 (s, 9H).

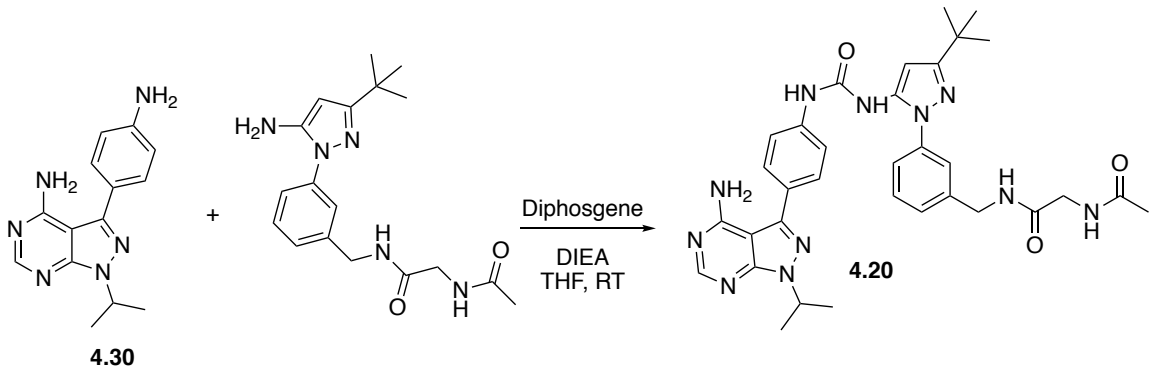

Scheme 4.12. Synthesis of Compound **4.20**

2-acetamido-*N*-(3-(5-(3-(4-(4-amino-1-isopropyl-1*H*-pyrazolo[3,4-*d*]pyrimidin-3-yl)phenyl)ureido)-3-(*tert*-butyl)-1*H*-pyrazol-1-yl)benzyl)acetamide (**4.20**). To a 10 mL round bottom flask, 2-acetamido-*N*-(3-(5-amino-3-(*tert*-butyl)-1*H*-pyrazol-1-yl)benzyl)acetamide (31 mg, 0.09 mmol) was dissolved in 5 mL dry THF. Diphosgene (22 μL, 0.18 mmol) was added and the reaction was refluxed for 2 h, cooled to room temperature, and concentrated *in vacuo*. The residue was resuspended in 5mL of dry THF in which **4.30** (25 mg, 0.09 mmol) and DIEA (31 μL, 0.18 mmol) was added and the reaction was allowed to stir at room temperature for 4 hours. The reaction was concentrated *in vacuo* and the residue was purified using reverse phase HPLC using a linear 30% - 90% ACN in H_2O to afford **4.20** as a white solid (6 mg, 0.01 mmol). Yield = 11%. ^{1}H NMR (400 MHz, Chloroform-*d*) δ 8.68 (s, 1H), 8.31 (s, 1H), 7.69 (s, 1H), 7.55 (d, *J* = 8.3 Hz, 2H), 7.49 (d, *J* = 8.5 Hz, 2H), 7.43 – 7.30 (m, 3H), 7.26 (d, *J* = 6.8 Hz, 1H), 7.14 (d, *J* = 7.4 Hz, 1H), 6.74 (t, *J* = 5.6 Hz, 1H), 6.51 (s, 1H), 5.55 (s, 2H), 5.14 (p,

J = 6.8 Hz, 1H), 4.36 (d, *J* = 6.0 Hz, 2H), 3.74 (d, *J* = 5.8 Hz, 2H), 1.96 (s, 3H), 1.56 (d, *J* = 6.7 Hz, 6H), 1.33 (s, 9H). ^{13}C NMR (126 MHz, dmso) δ 170.08, 169.50, 161.16, 158.46, 155.54, 153.43, 149.67, 147.41, 140.82, 129.50, 129.28, 124.99, 122.01, 121.47, 120.61, 114.51, 87.18, 48.27, 42.59, 42.38, 40.87, 30.65, 22.97, 22.25.

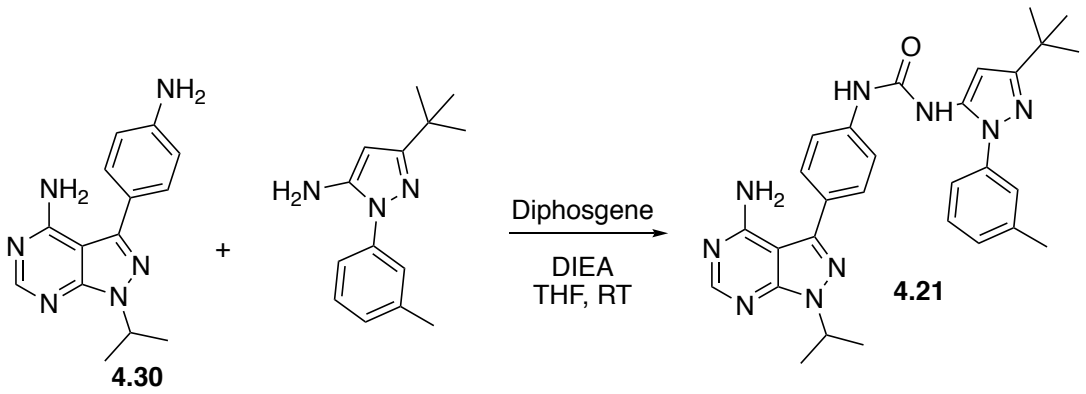

Scheme 4.13. Synthesis of Compound **4.21**

1-(4-(4-amino-1-isopropyl-1*H*-pyrazolo[3,4-*d*]pyrimidin-3-yl)phenyl)-3-(3-(*tert*-butyl)-1-(*m*-tolyl)-1*H*-pyrazol-5-yl)urea (**4.21**). To a 10 mL round bottom flask, 3-(*tert*-butyl)-1-(*m*-tolyl)-1*H*-pyrazol-5-amine (21 mg, 0.09 mmol) was dissolved in 5 mL dry THF. Diphosgene (22 μL, 0.18 mmol) was added and the reaction was refluxed for 2 h, cooled to room temperature, and concentrated *in vacuo*. The residue was resuspended in 5mL of dry THF in which **4.30** (25 mg, 0.09 mmol) and DIEA (31 μL, 0.18 mmol) was added and the reaction was allowed to stir at room temperature for 4 hours. The reaction was concentrated *in vacuo* and the residue was purified using reverse phase HPLC using a linear 30% - 90% ACN in H_2O to afford **4.21** as a white solid (18 mg, 0.04 mmol). Yield = 40%. ^{1}H NMR (400 MHz, Chloroform-*d*) δ 8.27 (s, 1H), 7.58 (d, *J* = 8.4 Hz, 2H), 7.51 (s, 1H), 7.45 (d, *J* = 8.4 Hz, 2H), 7.28 (d, *J* = 8.1 Hz, 2H), 7.15 (d, *J* = 8.1 Hz, 2H), 6.91 (s, 1H), 6.38 (s, 1H), 5.56 (s, 2H), 5.13 (p, *J* = 13.4, 6.7 Hz, 1H), 2.29 (s, 3H), 1.56 (d, *J* = 6.7 Hz, 6H), 1.32 (s, 9H).

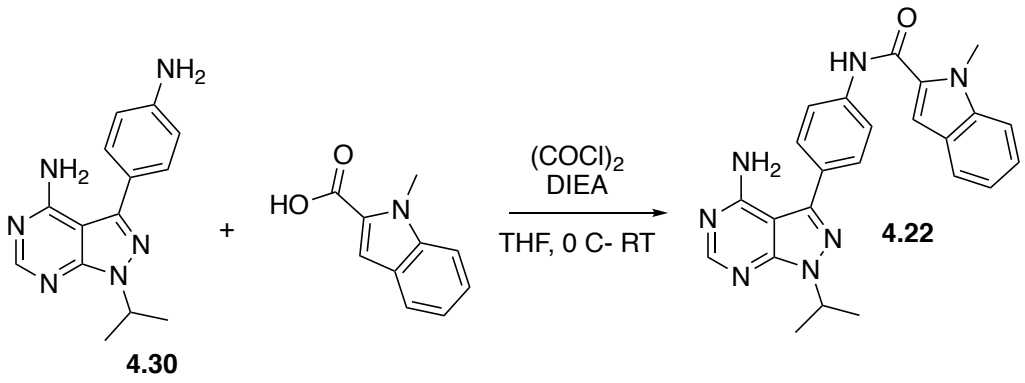

Scheme 4.14. Synthesis of Compound **4.22**

N-(4-(4-amino-1-isopropyl-1*H*-pyrazolo[3,4-*d*]pyrimidin-3-yl)phenyl)-1-methyl-1*H*-indole-2-carboxamide (**4.22**). To a 10 mL round bottom flask, 1-methyl-1*H*-indole-2-carboxylic acid (16 mg, 0.09 mmol) was dissolved in 5 mL dry THF. Oxalyl chloride (23 μL, 0.27 mmol) was added and the reaction was refluxed for 2 h, cooled to room temperature, and concentrated *in vacuo*. The residue was resuspended in 5mL of dry THF in which **4.30** (25 mg, 0.09 mmol) and DIEA (31 μL, 0.18 mmol) was added and the reaction was allowed to stir at room temperature for 4 hours. The reaction was concentrated *in vacuo* and the residue was purified using reverse phase HPLC using a linear 30% - 90% ACN in H_2O to afford **4.22** as a white solid (27 mg, 0.06 mmol). Yield = 70%. ^{1}H NMR (500 MHz, DMSO-*d*6) δ 10.52 (s, 1H), 8.24 (s, 1H), 7.99 (d, *J* = 8.7 Hz, 2H), 7.72 (d, *J* = 7.9 Hz, 1H), 7.66 (d, *J* = 8.7 Hz, 2H), 7.59 (d, *J* = 8.5 Hz, 1H), 7.37 (s, 1H), 7.33 (t, *J* = 8.2 Hz, 1H), 7.19 – 7.11 (m, 1H), 5.07 (p, *J* = 6.7 Hz, 1H), 4.04 (s, 3H), 1.50 (d, *J* = 6.7 Hz, 6H).^{13}C NMR (126 MHz, DMSO) δ 160.99, 158.49, 155.75, 153.68, 143.51, 139.85, 139.20, 132.34, 129.10, 128.63, 125.88, 124.49, 122.22, 120.79, 111.07, 106.27, 97.86, 48.53, 42.53, 31.92, 22.26.

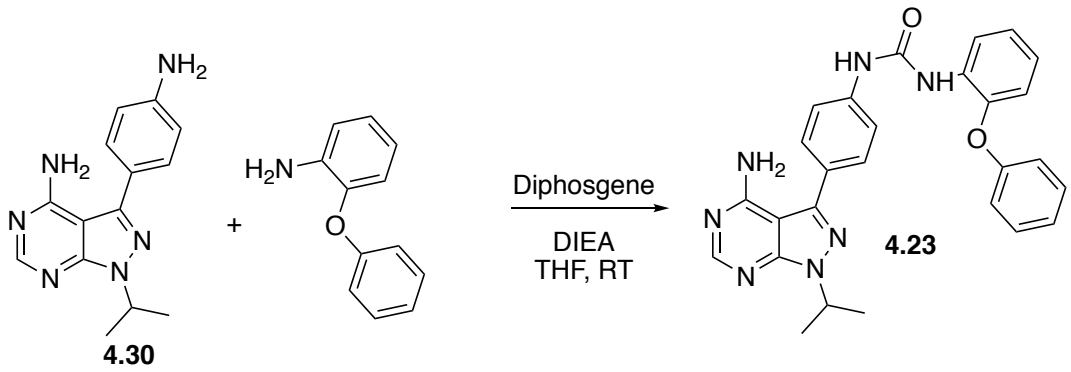

Scheme 4.15. Synthesis of Compound **4.23**

1-(4-(4-amino-1-isopropyl-1*H*-pyrazolo[3,4-*d*]pyrimidin-3-yl)phenyl)-3-(2-phenoxyphenyl)urea (**4.23**). To a 10 mL round bottom flask, 2-phenoxyaniline (17 mg, 0.09 mmol) was dissolved in 5 mL dry THF. Diphosgene (22 µL, 0.18 mmol) was added and the reaction was refluxed for 2 h, cooled to room temperature, and concentrated *in vacuo*. The residue was resuspended in 5mL of dry THF in which **4.30** (25 mg, 0.09 mmol) and DIEA (31 µL, 0.18 mmol) was added a3nd the reaction was allowed to stir at room temperature for 4 hours. The reaction was concentrated *in vacuo* and the residue was purified using reverse phase HPLC using a linear 30% - 90% ACN in H_2O to afford **4.23** as a white solid (13 mg, 0.03 mmol). Yield = 30%. ^{1}H NMR (500 MHz, DMSO-*d*6): (500 MHz, DMSO-*d*6) δ 10.19 (s, 1H), 8.37 (s, 2H), 7.76 (d, *J* = 7.9 Hz, 2H), 7.57 (d, *J* = 7.7 Hz, 2H), 5.07 (p, *J* = 13.3, 6.5 Hz, 1H), 2.98 (s, 3H), 1.48 (d, *J* = 6.4 Hz, 6H).

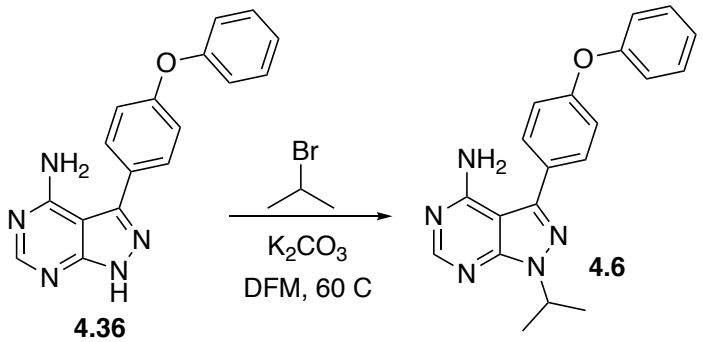

Scheme 4.16. Synthesis of Compound **4.6**

1-isopropyl-3-(4-phenoxyphenyl)-1*H*-pyrazolo[3,4-*d*]pyrimidin-4-amine (**4.6**). To a 10 mL round bottom flask, compound **4.36** (10 mg, 0.03 mmol) and potassium carbonate (12

mg, 0.09 mmol) was dissolved in 5 mL of dry DMF. Compound **4.36** was synthesized as previously described.[38] 2-bromopropane (3 μL, 0.04 mmol) was added and the reaction was stirred at 60 C for 6 h. The reaction was cooled to room temperature and immediately purified using reverse phase HPLC using a linear 30% - 90% ACN in H_2O to afford **4.6** as a white solid (7 mg, 0.02 mmol). Yield = 65%. ^{1}H NMR (500 MHz, DMSO-*d*6): δ 8.35 (s, 1H), 7.64 (d, J = 8.0 Hz, 2H), 7.36 (t, J = 7.7, 7.7 Hz, 2H), 7.14 (t, J = 8.5 Hz, 3H), 7.06 (d, J = 8.6 Hz, 2H), 5.58 (s, 3H), 5.16 (p, J = 6.7 Hz, 1H), 1.58 (d, J = 6.7 Hz, 6H). ^{13}C NMR (500 MHz, DMSO-*d*6): δ 162.35, 160.73, 159.59, 158.97, 158.04, 147.34, 145.34, 132.74, 132.66, 130.86, 126.37, 121.62, 121.54, 50.69, 24.41.

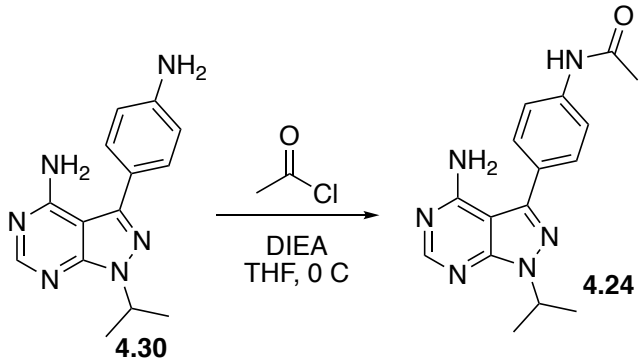

Scheme 4.17. Synthesis of Compound **4.24**

(**4.24**). To a 10 mL round bottom flask, **4.30** (25 mg, 0.09 mmol) was dissolved in 5 mL dry THF. Acetyl Chloride (7 μL, 0.09 mmol) and DIEA (31 μL, 0.18 mmol) was added, the reaction was stirred at 0 C for 4 h, and concentrated *in vacuo*. The residue was purified using reverse phase HPLC using a linear 30% - 90% ACN in H_2O to afford **4.24** as a white solid (22 mg, 0.07 mmol). Yield = 80%. ^{1}H NMR (500 MHz, DMSO-*d*6) δ 10.19 (s, 1H), 8.37 (s, 2H), 7.76 (d, *J* = 7.9 Hz, 2H), 7.57 (d, *J* = 7.7 Hz, 2H), 5.07 (p, *J* = 13.3, 6.5 Hz, 1H), 2.98 (s, 3H), 1.48 (d, *J* = 6.4 Hz, 6H) ^{13}C NMR (126 MHz, dmso) δ 169.03, 152.22, 145.18, 140.54, 129.67, 129.21, 126.99, 119.78, 97.31, 49.20, 42.55, 22.19.

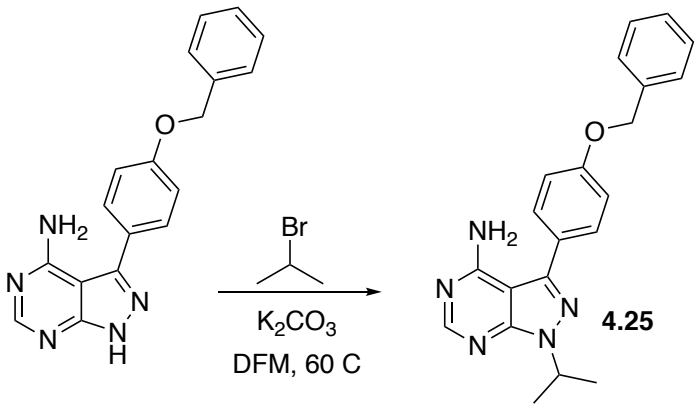

Scheme 4.18. Synthesis of Compound **4.25**

3-(4-(benzyloxy)phenyl)-1-isopropyl-1*H*-pyrazolo[3,4-*d*]pyrimidin-4-amine (**4.25**). To a 10 mL round bottom flask, compound 3-(4-(benzyloxy)phenyl)-1*H*-pyrazolo[3,4-*d*]pyrimidin-4-amine (9.5 mg, 0.03 mmol) and potassium carbonate (12 mg, 0.09 mmol) was dissolved in 5 mL of dry DMF. 2-bromopropane (3 μL, 0.04 mmol) was added and the reaction was stirred at 60 C for 6 h. The reaction was cooled to room temperature and immediately purified using reverse phase HPLC using a linear 30% - 90% ACN in H_2O to afford **4.25** as a white solid (7.6 mg, 0.02 mmol). Yield = 71%. ^{1}H NMR (500 MHz, DMSO-*d*6): δ 8.22 (s, 1H), 7.59 (d, J = 8.7 Hz, 2H), 7.49 (d, J = 7.2 Hz, 2H), 7.41 (t, J = 7.6 Hz, 2H), 7.35 (t, J = 7.3 Hz, 1H), 7.28 (d, J = 8.7 Hz, 2H), 5.18 (s, 2H), 5.04 (p, J = 6.7 Hz, 1H), 1.47 (d, J = 6.7 Hz, 6H). ^{13}C NMR (500 MHz, DMSO-*d*6): δ 159.06, 158.56, 155.81, 153.64, 143.44, 137.34, 130.03, 128.92, 128.35, 128.20, 126.17, 115.82, 97.84, 69.78, 48.44, 22.24.

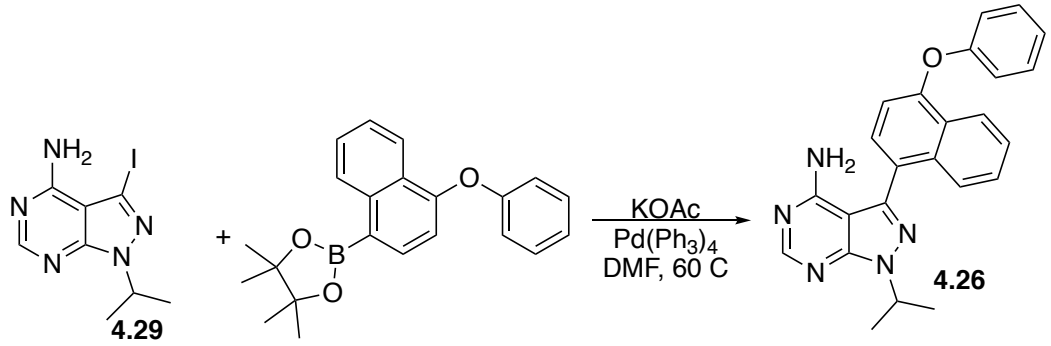

Scheme 4.19. Synthesis of Compound **4.26**

1-isopropyl-3-(4-phenoxynaphthalen-1-yl)-1*H*-pyrazolo[3,4-*d*]pyrimidin-4-amine (**4.26**). In a 5 mL round bottom flack, **4.29** (10 mg, 0.03 mmol), 4,4,5,5-tetramethyl-2-(4-phenoxynaphthalen-1-yl)-1,3,2-dioxaborolane (10 mg, 0.03 mmol), potassium acetate (9 mg, 0.09 mmol), and tetrikis (4 mg, 0.003 mmol) was dissolved in 5 mL of dry DMF. The reaction was heated to 60 C, stirred for 16, cooled to room temperature, and immediately purified by reverse phase HPLC using a linear 30% - 90% ACN in H_2O gradient to afford **4.26** as a white solid (2 mg, 0.005 mmol), yield = 18%. ^{1}H NMR (500 MHz, DMSO-*d*6): ^{13}C NMR (500 MHz, DMSO-*d*6): δ 158.30, 156.04, 153.38, 153.33, 141.70, 133.45, 130.57, 129.12, 127.92, 126.97, 126.83, 126.22, 126.16, 124.06, 122.27, 118.98, 113.57, 48.62, 42.55, 40.88, 22.33.

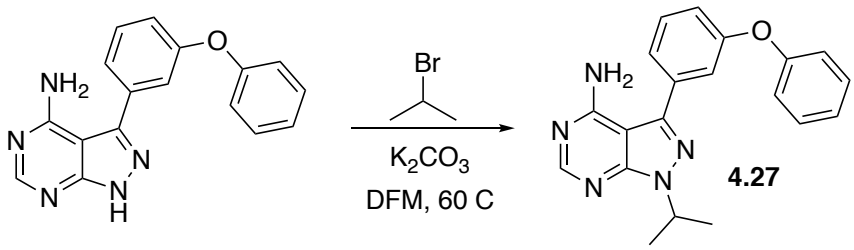

Scheme 4.20. Synthesis of Compound **4.27**

1-isopropyl-3-(3-phenoxyphenyl)-1*H*-pyrazolo[3,4-*d*]pyrimidin-4-amine (**4.27**). To a 10 mL round bottom flask, compound 3-(3-phenoxyphenyl)-1*H*-pyrazolo[3,4-*d*]pyrimidin-4-amine (10 mg, 0.03 mmol) and potassium carbonate (12 mg, 0.09 mmol) was dissolved in 5 mL of dry DMF. 2-bromopropane (3 μL, 0.04 mmol) was added and the reaction was stirred at 60 C for 6 h. The reaction was cooled to room temperature and immediately purified using reverse phase HPLC using a linear 30% - 90% ACN in H_2O to afford **4.27** as a white solid (4.7 mg, 0.013 mmol). Yield = 45%. ^{1}H NMR (500 MHz, Chloroform-*d*) δ 8.37 (s, 1H), 7.49 (t, *J* = 7.8 Hz, 1H), 7.44 (d, *J* = 7.6 Hz, 1H), 7.38 (t, *J* = 7.9 Hz, 2H), 7.34 (s, 1H), 7.16 (t, *J* = 7.4 Hz, 1H), 7.10 (t, *J* = 8.4 Hz, 3H), 5.58 (s, 2H), 5.19 (p, *J* = 6.7 Hz, 1H), 1.60 (d, *J* = 6.7 Hz, 6H).

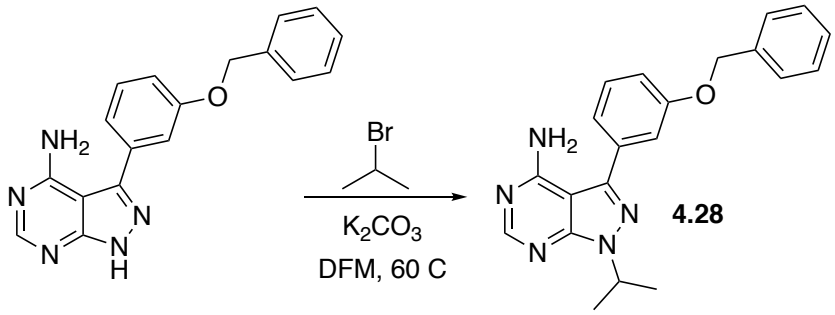

Scheme 4.21. Synthesis of Compound **4.28**

3-(3-(benzyloxy)phenyl)-1-isopropyl-1*H*-pyrazolo[3,4-*d*]pyrimidin-4-amine (**4.28**). To a 10 mL round bottom flask, compound 3-(3-(benzyloxy)phenyl)-1*H*-pyrazolo[3,4-*d*]pyrimidin-4-amine (9.5 mg, 0.03 mmol) and potassium carbonate (12 mg, 0.09 mmol) was dissolved in 5 mL of dry DMF. 2-bromopropane (3 μL, 0.04 mmol) was added and the reaction was stirred at 60 C for 6 h. The reaction was cooled to room temperature and immediately purified using reverse phase HPLC using a linear 30% - 90% ACN in H_2O to afford **4.28** as a white solid (5.3 mg, 0.015 mmol). Yield = 50%. ^{1}H NMR (500 MHz, Chloroform-*d*) δ 8.37 (s, 1H), 7.46 (t, *J* = 6.4 Hz, 3H), 7.42 (t, *J* = 7.6 Hz, 2H), 7.36 (t, *J* = 6.9 Hz, 1H), 7.32 – 7.28 (m, 2H), 7.11 (dd, *J* = 8.3, 2.5 Hz, 1H), 5.42 (s, 2H), 5.24 – 5.15 (m, 3H), 1.62 (d, *J* = 6.7 Hz, 6H).

Individual Contributions

Dr. Kristin Ko aided greatly in the design and sythesis of a number of pyrazolopyrimidine c-Src Inhibitors.

References:

1. Zhang J, Yang PL, Gray NS. Targeting Cancer with Small Molecule Kinase Inhibitors. *Nature Reviews Cancer***. 2009**, 9(1), 28.
2. Arora A, Scholar EM. Role of Tyrosine Kinase Inhibitors in Cancer Therapy. *Journal of Pharmacology and Experimental Therapeutics*. **2005**, 315(3), 971-9.
3. Shawver LK, Slamon D, Ullrich A. Smart Drugs: Tyrosine Kinase Inhibitors in Cancer Therapy. *Cancer Cell*. **2002**, 1(2), 117-23.
4. Kung JE, Jura N. Structural Basis for the Non-catalytic Functions of Protein Kinases. *Structure*. **2016**, 24(1):7-24.
5. Moran MF, Koch CA, Anderson D, Ellis C, England L, Martin GS, Pawson T. Src Homology Region 2 Domains Direct Protein-protein Interactions in Signal Transduction. *Proceedings of the National Academy of Sciences*. **1990**, 87(21), 8622-6.
6. Bergeron JJ, Di Guglielmo GM, Baass PC, Authier F, Posner BI. Endosomes, Receptor Tyrosine Kinase Internalization and Signal Transduction. *Bioscience Reports*. **1995**, 15(6), 411-8.
7. Lin JH, Li H, Yasumura D, Cohen HR, Zhang C, Panning B, Shokat KM, LaVail MM, Walter P. IRE1 Signaling Affects Cell Fate During the Unfolded Protein Response. *Science***. 2007**, 318(5852), 944-9.
8. Wang S, Kaufman RJ. The Role of IRE1a in Lipid Homeostasis. *Experimental and Clinical Endocrinology & Diabetes*. **2012**, 120(10), A37.
9. Paschen W, Mengesdorf T. Endoplasmic Reticulum Stress Response and Neurodegeneration. *Cell Calcium*. **2005**, 38(3), 409-15.
10. Cubillos-Ruiz JR, Glimcher LH. Targeting Abnormal ER Stress Responses in Tumors: A New Approach to Cancer Immunotherapy. *Oncoimmunology*. **2016** , 5(3), e1098802.
11. Yoshida H, Matsui T, Yamamoto A, Okada T, Mori K. XBP1 mRNA is Induced by ATF6 and Spliced by IRE1 in Response to ER Stress to Produce a Highly Active Transcription Factor. *Cell*. **2001**, 107(7), 881-91.
12. Maly DJ, Papa FR. Druggable Sensors of the Unfolded Protein Response. Nature Chemical Biology. **2014**, 10(11), 892-901.
13. Malumbres M, Barbacid M. Cell cycle, CDKs and Cancer: a Changing Paradigm. *Nature Reviews. Cancer.* **2009**, 9(3), 153.
14. Jeffrey PD, Russo AA, Polyak K, Gibbs E, Hurwitz J, Massagué J, Pavletich NP. Mechanism of CDK Activation Revealed by the Structure of a CyclinA-CDK2 Complex. *Nature*. **1995**, 376(6538), 313-20.
15. Jeffrey PD, Tong L, Pavletich NP. Structural Basis of Inhibition of CDK–cyclin Complexes by INK4 Inhibitors. *Genes & Development*. **2000**, 14(24), 3115-25.
16. Novotny CJ, Pollari S, Park JH, Lemmon MA, Shen W, Shokat KM. Overcoming Resistance to HER2 Inhibitors through State-specific Kinase Binding. *Nature Chemical Biology*. **2016**, 12(11), 923.
17. Leonard SE, Register AC, Krishnamurty R, Brighty GJ, Maly DJ. Divergent Modulation of Src-family Kinase Regulatory Interactions with ATP-competitive Inhibitors. *ACS Chemical Biology*. **2014**, 9(8), 1894-905.

18. Kwarcinski FE, Brandvold KR, Phadke S, Beleh OM, Johnson TK, Meagher JL, Seeliger MA, Stuckey JA, Soellner MB. Conformation-selective Analogues of Dasatinib Reveal Insight into Kinase Inhibitor Binding and Selectivity. *ACS Chemical Biology*. **2016**, 11(5), 1296-304.
19. MacFarlane RJ, Gelmon KA. Lapatinib for Breast Cancer: a Review of the Current Literature. *Expert Opinion on Drug Safety*. **2011**, 10(1). 109-21.
20. Paez JG, Jänne PA, Lee JC, Tracy S, Greulich H, Gabriel S, Herman P, Kaye FJ, Lindeman N, Boggon TJ, Naoki K. EGFR Mutations in Lung Cancer: Correlation with Clinical Response to Gefitinib Therapy. *Science*. **2004**, 304(5676), 1497-500.
21. Akinleye A, Chen Y, Mukhi N, Song Y, Liu D. Ibrutinib and Novel BTK Inhibitors in Clinical Development. *Journal of Hematology & Oncology*. **2013**, 6(1), 59.
22. Hanke JH, Gardner JP, Dow RL, Changelian PS, Brissette WH, Weringer EJ, Pollok BA, Connelly PA. Discovery of a Novel, Potent, and Src Family-selective Tyrosine Kinase Inhibitor Study of Lck-and FynT-dependent T Cell Activation. *Journal of Biological Chemistry*. **1996**, 271(2), 695-701.
23. Wu P, Nielsen TE, Clausen MH. Small-molecule Kinase Inhibitors: an Analysis of FDA-approved Drugs. *Drug Discovery Today*. **2016**, Jan 31, 21(1):5-10.
24. Agius MP, Soellner MB. Modulating Noncatalytic Function with Kinase Inhibitors. *Chemistry & Biology*. **2014**, 21(5), 569-71.
25. Araujo J, Logothetis C. Dasatinib: a Potent SRC Inhibitor in Clinical Development for the Treatment of Solid Tumors. *Cancer Treatment Reviews*. **2010**, 36(6), 492-500.
26. Frankfurt O, Licht JD. Ponatinib—a step Forward in Overcoming Resistance in Chronic Myeloid Leukemia. *Clinical Cancer Research***. 2013**, 19(21), 5828-34.
27. Vultur A, Buettner R, Kowolik C, Liang W, Smith D, Boschelli F, Jove R. SKI-606 (bosutinib), a Novel Src Kinase Inhibitor, Suppresses Migration and Invasion of Human Breast Cancer Cells. *Molecular Cancer Therapeutics*. **2008**, 7(5), 1185-94.
28. Heusschen R, Muller J, Binsfeld M, Marty C, Plougonven E, Dubois S, Mahli N, Moermans K, Carmeliet G, Léonard A, Baron F. SRC Kinase Inhibition with Saracatinib Limits the Development of Osteolytic Bone Disease in Multiple Myeloma. *Oncotarget*. **2016,** 7(21), 30712.
29. Dhawan NS. Small Molecule Stabilization of the KSR Inactive State Antagonizes Oncogenic Ras Signalling. *Nature.* **2016**, 537(7618), 112.
30. Apsel B, Blair JA, Gonzalez B, Nazif TM, Feldman ME, Aizenstein B, Hoffman R, Williams RL, Shokat KM, Knight ZA. Targeted Polypharmacology: Discovery of Dual Inhibitors of Tyrosine and Phosphoinositide Kinases. *Nature Chemical Biology*. **2008**, 4(11), 691-9.
31. Dar AC, Lopez MS, Shokat KM. Small Molecule Recognition of c-Src via the Imatinib-binding Conformation. *Chemistry & Biology*. **2008**, 15(10), 1015-22.
32. Murphy RC, Ojo KK, Larson ET, Castellanos-Gonzalez A, Perera BG, Keyloun KR, Kim JE, Bhandari JG, Muller NR, Verlinde CL, White Jr AC. Discovery of Potent and Selective Inhibitors of CDPK1 from C. parvum and T. gondii. *ACS Medicinal Chemistry Letters*. **2010**, 1(7):331-5.
33. Klein M, Morillas M, Vendrell A, Brive L, Gebbia M, Wallace IM, Giaever G, Nislow C, Posas F, Grøtli M. Design, Synthesis and Characterization of a Highly Effective Inhibitor for Analog-sensitive (as) Kinases. *PloS one.* **2011**, 6(6), e20789.

34. Dar AC, Das TK, Shokat KM, Cagan RL. Chemical Genetic Discovery of Targets and Anti-targets for Cancer Polypharmacology. *Nature***. 2012**, 486(7401), 80.
35. Vidadala RS, Ojo KK, Johnson SM, Zhang Z, Leonard SE, Mitra A, Choi R, Reid MC, Keyloun KR, Fox AM, Kennedy M. Development of Potent and Selective Plasmodium Falciparum Calcium-dependent Protein Kinase 4 (PfCDPK4) Inhibitors that Block the Transmission of Malaria to Mosquitoes. *European Journal of Medicinal Chemistry*. **2014**, 74, 562-73.
36. Shieh WC, McKenna J, Sclafani JA, Xue S, Girgis M, Vivelo J, Radetich B, Prasad K. Syntheses of a Triad of Flt3 Kinase Inhibitors: from Bench to Pilot Plant. *Organic Process Research & Development*. **2008**, 12(6), 1146-55.
37. Garske AL, Peters U, Cortesi AT, Perez JL, Shokat KM. Chemical Genetic Strategy for Targeting Protein Kinases Based on Covalent Complementarity. *Proceedings of the National Academy of Sciences*. **2011,** 108(37), 15046-52.
38. Wu H, Aoli Wang ZQ, Li X, Chen C, Yu K, Zou F, Hu C, Wang W, Zhao Z, Wu J, Liu J. Discovery of a highly potent FLT3 Kinase Inhibitor for FLT3-ITD-positive AML. *Leukemia*. **2016**, (10), 2112.

CHAPTER V

Identification of Allosteric Hotspots that can Modulate the Global Conformation of c-Src Kinase

Abstract

Conformation selective ATP competitive c-Src inhibitors can uniquely inhibit both catalytic and non-catalytic functions simultaneously. Unfortunately, these ATP-competitive inhibitors face a number of challenges including: achieving suitable potency, selectivity, and displaying efficacy for inhibitor resistance mutations. Development of a c-Src allosteric modulator that will stabilize the closed conformation and inhibitor catalytic function is a unique strategy that can overcome these developmental challenges. However, we first must identify allosteric sites that can be probes via small molecule modulator. Herin, we utilize MixMD simulation, developed by the Carlson Lab, to identify potential 'hotspot' on c-Src. Using mutagenesis, we incorporated tryptophan residues in these sites to elucidate the 'druggability' of each site. Using selective proteolysis methodology, we found two mutations that stabilize the closed conformation, Q365W and T293W. These sites can now be used in future docking studies to begin designing or screening for novel allosteric c-Src modulators.

Introduction

All FDA approved kinase inhibitors to date bind in the ATP binding site and inhibit catalytic activity.[1] Designing ATP competitive inhibitors have become increasingly simple as the ATP pocket is well defined, highly conserved, and a number of diverse chemical scaffolds are available as promising starting points.[2, 3] Unfortunately, there still remain a number of pitfalls with inhibitors that bind the ATP binding site. Firstly, since all kinases are defined by having a kinase domain responsible for downstream phosphorylation, gaining inhibitor selectively among the kinome has been no simple task.[4] Methods for achieving inhibitor selective include: entropic strategies via

steric clashes with off target amino acids, enthalpy strategies via interactions with target specific side chins, and irreversible strategies via electrophilic targeting of non-conserved cysteine residues.[5-7] However, to date only a small percentage of the kinome can be targeted with exquisite selectivity. Furthermore, ATP competitive inhibitors must compete with high intracellular levels of ATP, making potent (K_d <100 nM) essential for displaying efficacy at non-toxic dosages. While these strategies remain effective, a number of cancers have been successful in using mutations to evade inhibitor treatments, including the common 'gatekeeper mutation,' which is a common resistance mechanism across the kinome.[8-10]

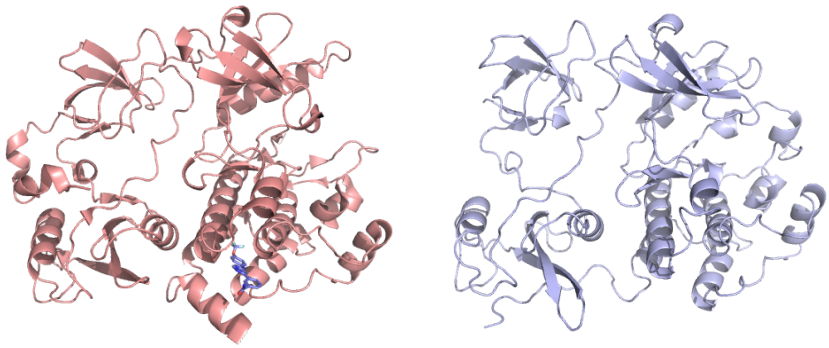

Figure 5.1. (Left) c-Abl bound to the allosteric inhibitor GNF-2 (blue), which can inhibit catalytic function and stabilize c-Abl in the closed conformation. (Right) c-Src has no known allosteric modulators, however is structurally similar to c-Abl.

In order to combat these pitfalls of using ATP competitive inhibitors, we hypothesized that identification of allosteric modulators of c-Src that stabilized the closed kinase conformation, would be highly advantageous. Data in chapter III has uncovered that all closed mutations of c-Src also display large decreases in catalytic activity. Thus, an allosteric modulator of c-Src that can stabilize a closed c-Src conformation would be highly advantageous. Such a molecule would have a high degree of selectivity to c-Src or Src family kinases, as areas outside the ATP binding site will be less conserved. Furthermore, there is no competition for binding ATP, thus allosteric modulators may be

efficacious with only modest binding affinity to the site. Finally, used alone or in combination with an ATP competitive inhibitor, an allosteric modulator can avoid common resistance mechanism as seen with c-Abl.[11] However, more importantly an allosteric modulator that stabilizes the closed kinase conformation would additionally inhibit c-Src's non-catalytic functions, in addition to the catalytic functions.

Allosteric inhibitors of kinases have shown great promise in the literature and in the clinic. For example, the allosteric c-Abl inhibitor, GNF-2, is currently being investigated for the treatment of CML.[12, 13] GNF-2 binds in the myristate pocket of c-Abl and inhibits catalytic activity through a large global conformational change.[14] Selective proteolysis data in Chapter II show that GNF-2 stabilizes c-Abl in the closed conformation, similarly to that of c-Src. While c-Src also has a myristate binding pocket, probing this site has yet to show that stabilization of a closed kinase conformation is obtainable. However, due to the conformational similarities in the auto-regulated states (closed conformation), such a molecule for c-Src may have similar successes of that as GNF-2 (Figure 5.1). Thus, the first step towards identifying an allosteric modulator of c-Src requires the identification of potential ligand binding sites that can stabilize the closed global conformation. Towards this goal we collaborated with the Carlson Lab who have developed a computational method, known as MixMD, that can successfully identify ligand-binding sites ('hotspots') distal to the ATP binding site.

MixMD to Identify Allosteric Hotspots

MixMD, a molecular dynamics technique, developed by the Carlson Lab, identifies critical binding sub-sites on protein surfaces ('hotspots'). Proteins are simulated in explicit water and 5% miscible, organic cosolvents. Molecular dynamics (MD) incorporates full flexibility and allows the protein to adapt to the presence of the organic probes (Figure 5.2). Moreover, the probes must compete with water to occupy sites on the protein surface, clearly identifying regions that prefer drug-like functional groups over water molecules. MixMD has superior performance over similar methods like MacKerrel's SILCS and Barril's MDmix, as detailed in literature publications. Other methods are plagued by many spurious, misleading, "extra" sites that score as strongly as real hotspots in real binding sites, which greatly hinders prospective applications.

MixMD eliminates these noisy "bad" sites by enabling complete protein flexibility, using lower concentrations of probe solvent, and averaging over more simulations.

We have established a rigorous protocol to identify and rank the binding hotspots on a protein surface.[16] Our approach requires binding sites to be mapped by more than one type of probe at a high signal-to-noise ratio. Using MixMD, simulations of 5% acetonitrile, isopropanol, and pyrimidine, the Carlson Lab recently reported the successful detection of both ortho- and allo-steric binding sites within several protein kinases (including c-Abl, PDK1, and CHK1).[16, 17] Each of these kinases had a previously known (and druggable) allosteric binding site, however, simple pocket finding algorithms would not yield the allosteric pocket. MixMD's results were compared to FTMap another approach to hotspot mapping. FTMap did not identify the allosteric sites in PDK1 and c-Abl.[18, 19] FTMap also produced many spurious hotspots identified outside the known sites, which would greatly hamper a prospective study. Especially challenging is the allosteric pocket in c-Abl, which requires the αI'-helix of c-Abl to spontaneously reorganize in the presence of the probe molecules.

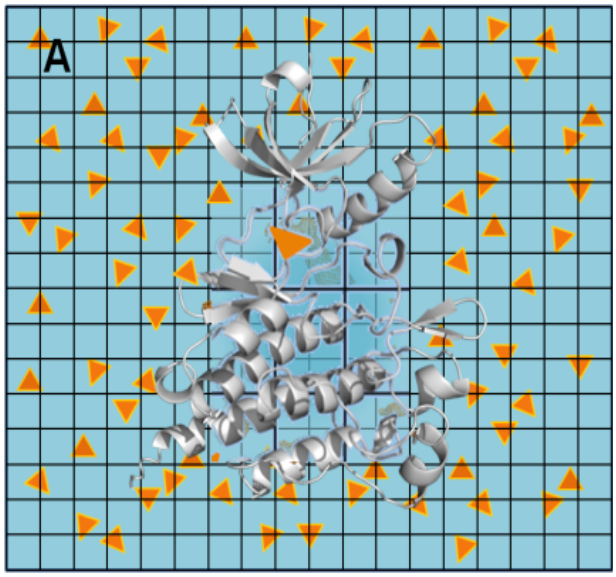

Figure 5.2. MixMD simulations rely on clustering of small organic solvents (triangles), including acetonitrile, isopropanol, and pyrimidine, to identify potential ligand binding 'hotspots.'

The protein simulations are setup using MOE and the tleap suite of AmberTools.[20, 21] A layer of probe molecules is added around the protein using tleap followed by the addition of a sufficient number of TIP3P water molecules as necessary to create a 5% v/v ratio of probe to water.[22] Probe solvents include acetonitrile (ACN), isopropanol (IPA), acetone, N-methylacetamide (NMA), imidazole (IMI), pyrimidine (PYR), and methylammonium plus acetate (MAI/ACE). The parameters for the probes and simulation protocol have been established in previous work. For c-Src, we will use the FF14SB forcefield and AMBER for the MD simulations.[23, 24] For each probe cosolvent, 10 independent simulations of 20 ns will be carried out, resulting in 200 ns of cumulative production simulation time for each probe. A total time of 1.2 μs is had across all probes.

The location of all probe atoms from the last 5 ns of the ten runs are binned onto a grid of 0.5-Å spacing, using the ptraj module from AmberTools.[21] A higher value for a particular location on the grid signifies a higher residence time for a probe molecule at that particular location across all ten MixMD simulation runs. These maps are visualized in PyMOL.[25]

Identification of Novel Druggable Hotspots of c-Src

Our previous MixMD studies of kinases successfully identified known active and allosteric sites, including the ATP-binding site, the myristate binding pocket, and the SH2 domain binding interface of ABL kinase.[16, 17] When applied to c-Src kinase, MixMD readily identified the ATP-binding site (Site 2). Interestingly, the interface between the kinase domain and SH-3 and SH-2 domains were identified as hotspots (Sites 5 and 6, respectively) (Figure 5.3).

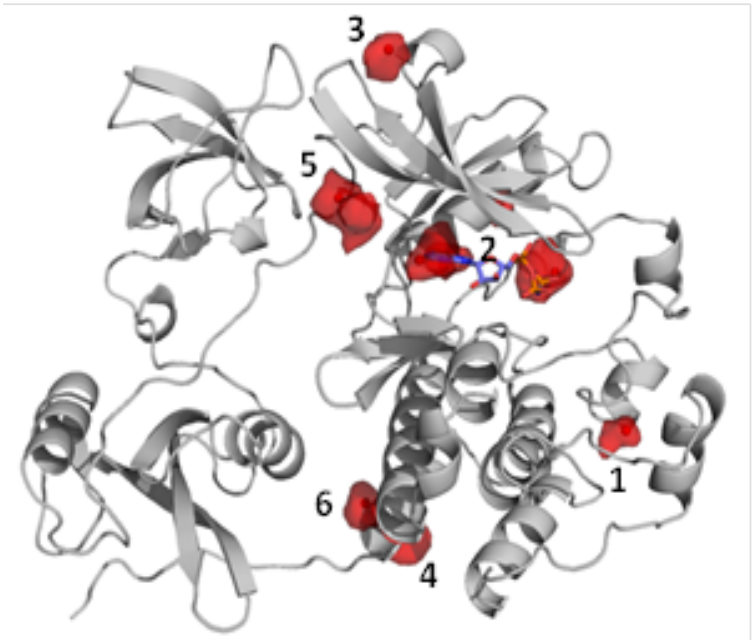

Figure 5.3. MixMD simulations on c-Src afforded 6 potential 'hotspot.' Hotspots 4,5, and 6 will be specifically probed using tryptophan mutations due to their optimal location between the kinase domain and its regulatory SH2/SH3 domains.

We next used experimental mutagenesis to probe the 'ligandability' of each pocket. For each pocket, we identified an amino acid residue that, when mutated to Trp would occupy the allosteric site. For example, Asp-365 is pointing toward putative allosteric site 6 and replacement with a Trp fills the predicted allosteric pocket. Similarly, replacement of Thr-293 is predicted to occupy the allosteric site 5. This panel of tryptophan mutants was achieved through site-directed mutagenesis. Unfortunately, many of these mutants could not be obtained through typical expression and purification protocols. We hypothesize this to be from the destabilization of changing a small amino acid residues being mutated into the large and hydrophobic tryptophan residue. We centered our screen to probe pockets 4,5, and 6. These 'hotspots' lie at the interface of the kinase domain and SH2/SH3 domains, and it could be speculated that these would likely showcase the largest perturbations. Pockets 1,2, and 3 all lie near or in the ATP-binding site and while these pockets may perturb the global conformation of c-Src, they

may be doing so through perturbation of the ATP site itself. Thus, we set our initial screen to targeted allosteric hotspots 4,5, and 6.

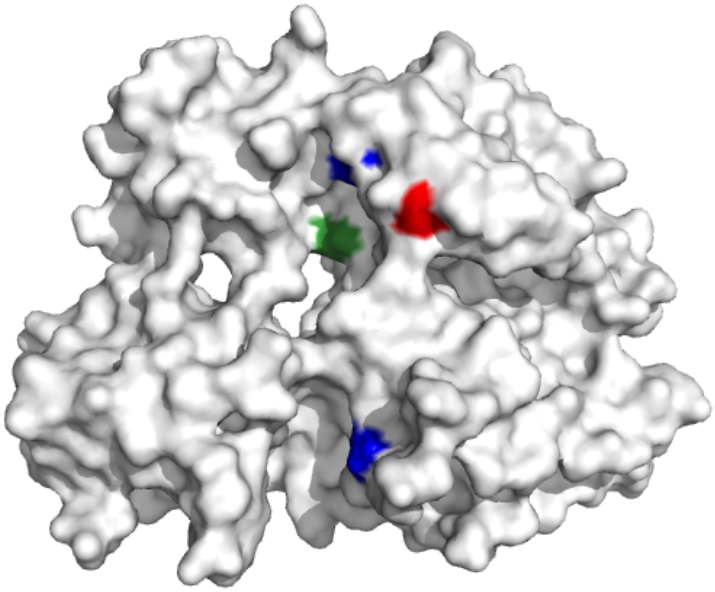

Figure 5.4. Selective proteolysis of 6 tryptophan c-Src mutants. Q365W and T293W (blue) both stabilized the closed conformation and validated pockets 5 & 6 as potential allosteric sites. Q254W (green) displayed no change in conformation. Mutations is red could not be expressed.

Although production of the entire panel could not be obtained, we were successful in identifying two mutations that stabilized the closed c-Src conformation (Figure 5.4). Q365W and T293W with half-lives of 250 and 80 mins respectfully. This data suggests that these 'hotspot' are not only novel sites where ligands can bind, but could have a biological affected when probed with a small molecule. The c-Src mutation Q254W was not observed to see a change in half-life however these pockets, showcasing that the tryptophan residue may not be able to accommodate or stabilize the closed kinase conformation. 3 tryptophan mutations: V367W, M286W, and L258W were not able to be purified. We speculate that the locations of these residues are highly crowded and the addition of a tryptophan may be highly disfavorable for optimal protein folding. As Q365W had the longest half-life, it is speculated that this site may be superior in terms of

stabilizing the closed conformation. Toward the possibility of identifying allosteric small molecule modulators, these 'hotspot' can now be used in *in-silico* experiments toward the identification of novel allosteric c-Src Modulators.

Conclusions

Towards identifying allosteric modulators of c-Src, we successfully identified two novel sites on c-Src that may be able to be probed with a small molecule. These site's were identified utilizing MixMD simulations which can identify 'hotspots' on target proteins through molecular dynamic simulations with added organic solvent molecules.[15] The clustering of these molecules afford 6 unique 'hotspots' on c-Src. However, pockets 4,5, and 6 were targeted as they encompassed the space between the kinase domain and its regulatory domains. Tryptophan screening of these hotspot identified pockets 5 and 6 having the potential to be druggable sites. Q365W (pocket 5) and T293W (pocket 6) showed the longest half-life in the selective proteolysis method, indicative of stabilizing the closed kinase conformation.

These data provide valuable insight into novel sites that can be drugged that exist outside the kinase domain. Without having developed selective proteolysis methodology we would have to rely on catalytic based assays and would have missed the opportunity to identify site's that stabilized the closed kinase conformation. These sites will provide us the opportunity to use classical docking models, PH4 model construction, and *in-silio* screening to identify small molecule allosteric modulators. We can next determine if these modulators will affect either, or both, conformation and catalytic activity. Such probes may be useful as potential therapeutics for c-Src dependent cancer, and will be exciting probes to better elucidate the impact non-catalytic functions have on cell signaling pathways.

Materials and Methods

Protocol for MixMD Simulation

The crystal structures used as the starting conformations for the MixMD simulations for the closed c-Src conformation was PDB: 2SRC. The protein structures

were stripped of water molecules and any cofactors or active-site ligands. This was followed by the addition of hydrogen atoms using Protonate 3D in MOE. The asparagine and glutamine residues were flipped as necessary to achieve optimal hydrogen bonding. Histidine tautomers were corrected when required. A sufficient number of sodium or chloride ions were added to neutralize each system using the tleap suite of AmberTools.A layer of probe molecules was added around the protein using tleap followed by the addition of a sufficient number of TIP3P water molecules as necessary to create a 5% v/v ratio of probe to water. The force field parameters for the probes acetonitrile, isopropanol, and pyrimidine were from our previous work. Methylammonium + acetate is a new probe set for MixMD. MD simulations were carried out in AMBER 1118 using the FF99SB force field. The SHAKE algorithm was used to restrain bonds to hydrogen atoms, and a time step of 2 fs was used. Particle Mesh Ewald as implemented for the GPUs (PMEMDCUDA) was used. The non-bonded cutoff was 10 Å, and the Andersen Thermostat was used to maintain temperature at 300 K. Using this approach, three separate simulations with the probes acetonitrile, isopropanol, and pyrimidine were set up for each protein target. The systems were then subjected to an equilibration protocol to gradually increase the temperature and allow proper relaxation of all the atoms in the system as described previously. This was followed by a simulation of 20 ns. For each protein and probe pair, 10 independent simulations were carried out resulting in 200 ns of cumulative production simulation time.

Processing MixMD Results

The locations of all probe atoms from the last 5 ns of the 10 runs were binned onto a grid of 0.5 Å spacing, using the ptraj module from AmberTools. The raw bin counts (x) in each of the grid points were converted to σ values using the equation $(x - \mu)/\sigma$ where μ is the mean of all the binned grid data and σ is the standard deviation of all the binned grid data. This allows us to represent the location of the probes in a manner commonly implemented for electron density from X-ray crystallography. The resulting maps were contoured at various σ values and examined in the presence of the average protein structure to identify locations of maximal occupancy. A higher σ value for a particular location on the grid signifies a higher residence time for a probe molecule at

that particular location across all 10 MixMD simulation runs. The maps in this study have been color coded as orange for acetonitrile, blue for isopropanol, and magenta for pyrimidine to represent the respective MixMD simulations from which they have been derived. These maps were visualized in PyMOL

Production of c-Src Mutants

Human c-Src 3-domain in pET28a, modified with a TEV protease cleavable N-terminal 6x-His tag was prepared as previously reported.[26] The desired mutations were added to this plasmid using iterative rounds of mutagenesis using the Agilent QuikChange II kit. The plasmid was transformed by electroporation into Bl21DE3 electrocompetent cells containing YopH in pCDFDuet-1. Cell growth, expression, and protein purification were performed using modified literature protocols for expression of wild-type c-Src 3-domain.

Selective Proteolysis of c-Src Tryptophan Mutations

c-Src tryptophan mutants were diluted in proteolysis buffer (50 mM Tris-HCl pH 8.0, 100 mM NaCl, 0.5 mM $CaCl_2$) to yield a final protein concentration of 2 μM. If inhibitor was being used, 1 μL of a 10 mM DMSO stock was added and incubated with c-Src for 15 mins at room temperature. Thermolysin (purchased from Promega, catalog number: V4001) from a 3.8 μM stock solution was added to the reaction mixture to a final concentration of 60 nM. 15 μL of the proteolysis reaction was added to 5 μL of 50 mM EDTA to quench proteolysis at various time points (0, 2, 5, 10, 30, 60, 90, 120, 180, and 240 mins) and stored at -20 °C. The quenched samples were analyzed by SDS-PAGE (12 % Bis-Tris gel in MES running buffer, staining with comassie blue). Band intensities were analyzed by ImageJ imaging software. Percent protein remaining was plotted against time and fit to an exponential decay equation using GraphPad Prism 6 software to obtain half-lifes of each protein. The Exponential Decay curve for each protein was fit using the equation Y=(Y0 - Plateau)*exp(-K*X) + Plateau X = time(mins) and Y = normalized band intensity.

References

1. Wu P, Nielsen TE, Clausen MH. Small-molecule Kinase Inhibitors: an Analysis of FDA-approved Drugs. *Drug Discovery Today*. **2016**, 21(1), 5-10.
2. Zhang J, Yang PL, Gray NS. Targeting Cancer with Small Molecule Kinase Inhibitors. *Nature Reviews. Cancer*. **2009**, 9(1):28.
3. Noble ME, Endicott JA, Johnson LN. Protein Kinase Inhibitors: Insights into Drug Design from Structure. *Science*. **2004,** 303(5665), 1800-5.
4. Norman RA, Toader D, Ferguson AD. Structural Approaches to Obtain Kinase Selectivity. *Trends in Pharmacological Sciences*. **2012**, 33(5), 273-8.
5. Uitdehaag JC, Zaman GJ. A Theoretical Entropy Score as a Single Value to Express Inhibitor Selectivity. *BMC Bioinformatics*. **2011**, 12(1), 94.
6. Kawasaki Y, Freire E. Finding a Better Path to Drug Selectivity. *Drug Discovery Today*. **2011,** 16(21), 985-90.
7. Liu Q, Sabnis Y, Zhao Z, Zhang T, Buhrlage SJ, Jones LH, Gray NS. Developing Irreversible Inhibitors of the Protein Kinase Cysteinome. *Chemistry & Biology*. **2013**, 20(2), 146-59.
8. Lee F, Fandi A, Voi M. Overcoming Kinase Resistance in Chronic Myeloid Leukemia. *The International Journal of Biochemistry & Bell Biology*. **2008**, 40(3), 334-43.
9. Azam M, Seeliger MA, Gray NS, Kuriyan J, Daley GQ. Activation of Tyrosine Kinases by Mutation of the Gatekeeper Threonine. Nature Structural & Molecular Biology. **2008**, 15(10), 1109-18.
10. Gazdar A. Activating and Resistance Mutations of EGFR in Non-small-cell Lung Cancer: Role in Clinical Response to EGFR Tyrosine Kinase Inhibitors. *Oncogene*. **2009**, 28(Suppl 1), S24.
11. Zhang J, Adrián FJ, Jahnke W, Cowan-Jacob SW, Li AG, Iacob RE, Sim T, Powers J, Dierks C, Sun F, Guo GR. Targeting Wild-type and T315I Bcr-Abl by Combining Allosteric with ATP-site Inhibitors. *Nature*. **2010,** 463(7280), 501.
12. Adrián FJ, Ding Q, Sim T, Velentza A, Sloan C, Liu Y, Zhang G, Hur W, Ding S, Manley P, Mestan J. Allosteric Inhibitors of Bcr-abl-dependent Cell Proliferation. *Nature Chemical Biology*. **2006**, 2(2), 95.
13. O'Hare T, Eide CA, Deininger MW. New Bcr-Abl Inhibitors in Chronic Myeloid Leukemia: Keeping Resistance in Check. *Expert Opinion on Investigational Drugs*. **2008**, 17(6), 865-78.
14. Skora L, Mestan J, Fabbro D, Jahnke W, Grzesiek S. NMR Reveals the Allosteric Opening and Closing of Abelson Tyrosine Kinase by ATP-site and Myristoyl Pocket Inhibitors. *Proceedings of the National Academy of Sciences*. **2013**, 110(47), E4437-45.
15. Patwardhan P, Resh MD. Myristoylation and Membrane Binding Regulate c-Src Stability and Kinase Activity. *Molecular and Cellular Biology*. **2010**, 30(17), 4094-107.
16. Ghanakota P, Carlson HA. Moving Beyond Active-Site Detection: MixMD Applied to Allosteric Systems. *The Journal of Physical Chemistry B*, **2016**, 120, 8685-95.
17. Ung PM, Ghanakota P, Graham SE, Lexa KW, Carlson HA. Identifying Binding Hot Spots on Protein Surfaces by Mixed-solvent Molecular Dynamics: HIV-1 Protease as a test case. *Biopolymers,* **2016,** 105*,* 21-34.

18. Buhrman G, Casey O, Zerbe B, Kearney BM, Napoleon R, Kovrigina EA, Vajda S, Kozakov D, Kovrigin EL, Mattos C. Analysis of Binding Site Hot Spots on the Surface of Ras GTPase. *Journal of Molecular Biology*, **2011**, 413, 773-89.
19. Hall DH, Grove LE, Yueh C, Ngan CH, Kozakov D, Vajda S. Robust Identification of Binding Hot Spots using Continuum Electrostatics: Application to Hen egg-white Lysozyme. J*ournal of the American Chemical Society*, **2011**, 133, 20668-71.
20. *Molecular Operating Environment*; Chemical Computing Group Inc.: Montreal, Canada, 2010.
21. Case DA, Darden TA, Cheatham TE, Simmerling CL, Wang J, Duke RE, Luo R, Crowley M, Walker R, Zhang W, Merz K. AMBER 11; **2011**, University of California: San Francisco, CA.
22. Jorgensen WL, Chandrasekhar J, Madura JD, Impey RW, Klein ML. Comparison of Simple Potential Functions for Simulating Liquid Water. *The Journal of Chemical Physics,* **1983**, 79, 926-35.
23. Maier JA, Martinez C, Kasavajhala K, Wickstrom L, Hauser KE, Simmerling C. ff14SB: Improving the Accuracy of Orotein Side Chain and Backbone Parameters from ff99SB. *Journal of Chemical Theory and Computation,* **2015**, 11, 3696-713.
24. Case DA, Betz RM, Cerutti DS, Cheatham TE, Darden TA, Duke RE, Giese TJ, Gohlke H, Goetz AW, Homeyer N, Amber 16; **2016**, University of California
25. *The PyMOL Molecular Graphics System*; Schrödinger, LLC.
26. Seeliger MA, Young M, Henderson MN, Pellicena P, King DS, Falick AM, Kuriyan J. High Yield Bacterial Expression of Active c-Abl and c-Src Tyrosine Kinases. *Protein Science*. **2005**, 14(12), 3135-9.

CHAPTER VI

The Future of Inhibiting Kinase Signaling: Modulating both the Catalytic and Non-Catalytic Functions

Abstract

The work herein highlights methods, both ligand and mutation induced, to modulate the global conformation of c-Src kinase. Characterization of these conformational changes was possible due to the development of our novel 'Selective Proteolysis' methodology that we have expanded to other diverse kinases. This work demonstrates that inhibitors, if designed strategically, can be used to modulate both signaling arms simultaneous. Additionally, clinical mutations may be activating mutations through stabilization of district protein conformations. We hope that others use this work as a stepping-stone towards developing the next generation of kinase targeted therapies with improved signaling modulation.

Introduction

Throughout this dissertation, examples of modulating the non-catalytic function of kinases has been portrayed with the kinases IRE1α, Erk2, Her2, Cdk, and c-Src.[1-5] Such a small panel of kinases showcases the approach of targeting non-catalytic functions still remain in its infancy. The difficulty in targeting non-catalytic functions lies in the basis that these functions are often governed through protein-protein interactions. The ease of measuring chemical reactions, i.e. that of a kinase phosphorylating a downstream target, has paved the way for the primary focus to be on their catalytic function. In order for more researchers to begin considering non-catalytic functions, the development of simple and robust tools to observe conformational changes must first be accomplished.

We previously identified the kinase c-Src to be a highly validated kinase target in triple-negative breast cancer.[6-8] Thus we recognized that in order to inhibit the entirety c-Src signaling, we must consider modulating both the catalytic and non-catalytic

functions. The tools available for observing changes in protein conformation required advanced biophysical techniques that were not suited to be used in a high-throughput fashion.[9-11] Additionally, the only biochemical technique reported could not be used with our c-Src mutation panel in chapter III. This led us to seek our own solution toward identifying the conformational changes of c-Src. The success of developing such a method has enabled our group to begin probing how to best modulate the global conformations of c-Src, and how these changes may impact cellular signaling. Additionally, its ability to be expanded to other diverse kinases make this method a unique drop-in platform technology that we hope researchers take advantage of when targeting kinases, including the highly targeted c-Abl and Btk.

Selective Proteolysis of c-Src as a Potential Drop-in Platform Technology

In Chapter II we revealed the development of a novel method to monitor changes in the global conformation of c-Src kinase. This method takes advantage of an observation made in 1989 when the inactive, pY530 Src, showed loss of sensitivity to the bacterial protease, thermolysin.[12] We were not only fortunate that thermolysin displayed 'selective' cleavage of c-Src (with only one dominate cut site), but that this single cut site was located on a linker that changed in accessibility between the open and closed conformation. We validated our method with using c-Src constructs previously reported in literature (via advanced biophysical techniques) with both phosphorylated constructs and ligand bound c-Src.[9, 11] Performing an alignment of the SH2-linker with other diverse kinases afforded 9 possible targets, in which one was confirmed using c-Abl.

The expansion of this assay does not end with only these 9 potential kinases. With the many commercially available proteases, kinases that may not be cleaved by thermolysin could be tested by any number of proteases. Although the kinase in question will need to be expressed and purified as recombinant protein, it expands the utility of this method to cover a greater percentage of the kinome. A similar method, limited proteolysis, can be used in tandem with mass spectrometry to identify regions of the protein that had changes in accessibility.[13] When expanding the scope of this method using alternative proteases, 'selective proteolysis' does not necessarily need to be observed, and limited proteolysis can be used as a substitution. Finally, the same report

in 1989 also reported activation loop sensitivity of c-Src by the protease trypsin. As the activation loop conformation has been shown to change accessibility when bound to conformation-selective inhibitors, this method could also be utilized to access conformational changes in the activation loop conformation (or any important kinase loops).

The kinases c-Abl and Btk have been highly validated targets for CML and lymphomas respectfully, and are still significant targets today.[14,15] As this method is applicable to these proteins, it will provide researchers the tools to begin designing improved targeted therapies, as the FDA approved inhibitors for c-Abl and Btk are already conformation selective, it may be important for clinical efficacy.

Kinase Mutations as Genetic Tools for Elucidating Signaling Pathways

In Chapter III we first utilized the power of our selective proteolysis methodology to characterize clinical mutations of c-Src. These mutations could easily be characterized catalytically, but their affects on the global conformation could not be accomplished in a high-throughput fashion. With our method, many of these mutations had altered the global conformation of c-Src, revealing the intricacy of the hydrogen bond network that governs protein conformation. Activating kinase mutations are typically thought to impact catalytic function. For example, L858R in EGFR is an activating mutation in lung cancer as this mutation renders a constitutively active kinase.[16] The same can be said for Braf mutation V600E.[17] Characterization of the clinical mutations reveal that 'activation' may also occur through stabilization of the 'active' protein conformation, versus affecting solely catalytic function. Herin we identified the mutation W121R to stabilize the open conformation, be highly catalytically active, and have the ability to escape down regulation by Csk. While it is unsure if this mutation is transforming, active pY419 c-Src is a common feature of malignant tumors and we may have revealed a constituently active kinase mutant.[18]

With the emerging utility of CRISPR-Cas9 gene editing technology, we can start to begin to understand the impacts these mutations have on signaling functions. It is studies such as these that can showcase the effect the clinical mutations have on promoting tumor growth and metastasis. Furthermore, we now have genetic tools to

being understanding how global c-Src conformation affects signaling pathways. As overexpression techniques in mammalian cells often lead to non-physiological levels of kinases, CRISPR-Cas9 would fit as the preferred method.[19] The mutation F408G in c-Src showed no affect on conformation but would render a 'kinase-dead' construct. Additionally, adding a mutation that affected the global conformation in tandem, we could finally begin to understand which signaling pathways of c-Src are dependent on conformation alone, and which require catalytic function to progress (Figure 6.1). Additionally, there has been reported a number of Imatinib restraint mutations of c-Abl and we speculate that this resistance is due from stabilization of contradicting global c-Abl conformations.[20] This methodology can be utilized to reveal how protein conformation can perturb not only signaling pathways, but additionally be utilized as a method for escaping inhibitor treatment.

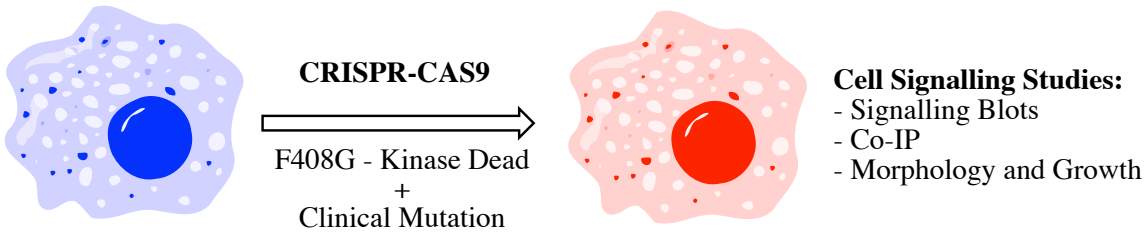

Figure 6.1. Studies to study the effect of global conformational changes independent of catalytic function be carried out utilizing CRISPR-CAS9 technology.

Modulating Global Conformation with Kinase Inhibitors

Only a few examples in literature show how conformation-selective inhibitors can influence the non-catalytic function of kinases.[1-5] Unfortunately, due to the infancy of this approach, previously developed kinase inhibitors that display promising efficacy may already have this characteristic. Nearly all reported cases of influencing non-catalytic kinase functions involved modulation of the αC-helix. Thus the αC-helix remains one of the most underappreciated regulatory motifs of protein kinases. Stabilization of the αC-helix-in or αC-Helix-out conformations has been the basis for targeting these non-

catalytic functions. The insight with our tunable conformation-selective inhibitors provides researchers the ability to module the αC-helix movement of any kinase of interest.

In Chapter IV we revealed a series of pyrazolopyrimidine inhibitors that can stabilize various open and closed conformations of c-Src. Thus we have a series of inhibitors with 'tunable' degrees of interaction to the αC-helix of c-Src. Additionally, we show that these design elements can be transposed onto FDA approved inhibitor scaffolds including conformation-selective Dasatinib analogs and conformation-selective Lapatinib analogs. These data showcase that any kinase may be targeted in a conformation-selective fashion and require a selective starting scaffold and a conformation-selective element that can be utilized from any one of the 23 characterized inhibitors (Figure 6.2). This panel can now provide starting points for developing conformation-selective inhibitors for any kinase toward targeting their non-catalytic functions.

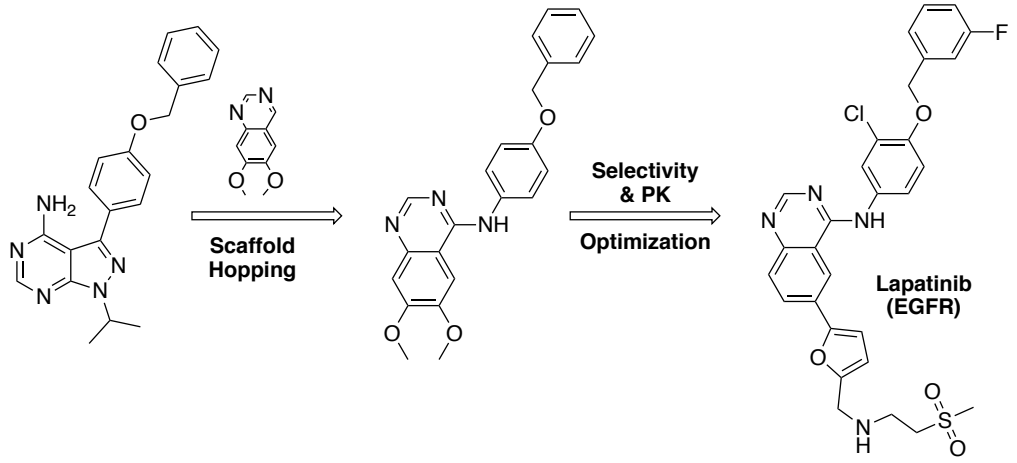

Figure 6.2. 'Tunable' ATP competitive inhibitors can be utilized and adapted to target any kinase of interest.

Identifying Allosteric Inhibitors of c-Src Kinase

The challenges with the ATP competitive inhibitors in chapter IV are due to the difficulty in obtaining kinase selective.[21] The conserved nature of the ATP binding site

among the kinome makes designing a perfectly selective inhibitor a nearly impossible task. Additionally, our published data showcase that the conformation-selective portion of the kinase inhibitor does not alter inhibitor selectivity to a significant degree.[22] Thus, the development of allosteric c-Src inhibitors would be of great use. In chapter V we collaborated with the Carlson Lab and utilized a novel 'hotspot' ID technique, MixMD that involved molecular dynamic simulations of organic solvent molecules in solution.[23] The results of the MixMD simulation afforded 6 unique 'hotspots' that may be able to be probed with a small molecule. Through mutagenesis, we introduced tryptophan mutations in these pockets in order to mimic that of a small fragment binding. Surprisingly, two of the hotspots were verified as allosteric sites as the tryptophan mutants Q365W and T298W were found to stabilized the closed conformations. These are the first identified computationally, and validated biochemically, allosteric sites on c-Src that can stabilize the closed conformation.

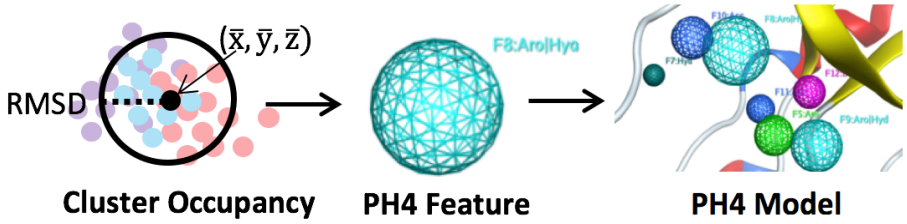

Figure 6.3. Identified hotspots can be used to generate PH4 models in which *in-silico* docking experiments can be performed to find allosteric modulators of c-Src.

Towards identifying allosteric inhibitors of c-Src, we now have two novel allosteric sites that small molecule docking can be implemented. PH4 models can be generated using these sites and *in-silico* screens can now begin toward identifying allosteric inhibitors of c-Src (Figure 6.3). It can be speculated that these inhibitors can also inhibit catalytic function, as all closing mutations in chapter II all had a decrease in catalytic activity. However, finding allosteric inhibitors that only modulated global conformation would also be incredibly valuable. As these inhibitors can be used to elucidate how changing kinase conformation impacts signaling independent of catalytic

function, and in a dose dependent manner. Additionally, these sites are much less conserved than the ATP binding pocket and it can be speculated that these allosteric inhibitors will have exquisite selectivity for c-Src or other Src family kinases.

Conclusions

The work herein highlights the discovery of orthogonal methods, both mutation and ligand induced, to modulate the global conformation of c-Src kinase. This work could not be possible without the development of novel, selective-proteolysis methodology that could be so easy implemented by our group. We have showcased that the global conformation of c-Src is perturbed in a number of clinical mutations. Furthermore, that these conformational changes are used as an activating mechanism, and have discovered W121R to be a possible activating c-Src mutant. We have developed a series of small molecule inhibitors that can 'tune' the global conformation of c-Src and can be transferred onto any inhibitor scaffold to target any kinase of interest. We identified allosteric 'hotspots' of c-Src distal the ATP binding pocket that can be used to probe the global conformation and increase inhibitor selectivity. Finally, we have shown a unique targeting strategy of matching inhibitor conformation to protein conformation to better drug c-Src mutations that affect global conformation.

These data highlight number of themes that should be considered when studying or targeting any of the 513 kinases. Firstly, kinases' signaling pathways involve both its catalytic function (via post-translational phosphorylation), and its ability to participate in key protein-protein interactions. Secondly, small molecule inhibitors can target both catalytic and non-catalytic functions simultaneously, right within the ATP binding pocket (often by modulation of the αC-Helix). Finally, clinical mutations of kinases can be activating, not through changes in catalytic function, but rater through stabilizing distinct protein conformations. These themes are applicable across many protein families, and remind us about the intricacies of cellular signaling pathways.

References:

1. Maly DJ, Papa FR. Druggable Sensors of the Unfolded Protein Response. *Nature Chemical Biology*. **2014**, 10(11), 892-901.
2. Hari SB, Merritt EA, Maly DJ. Conformation-selective ATP-competitive Inhibitors Control Regulatory Interactions and Noncatalytic Functions of Mitogen-Activated Protein Kinases. *Chemistry & Biology*. **2014**, 21(5), 628-35.
3. Novotny CJ, Pollari S, Park JH, Lemmon MA, Shen W, Shokat KM. Overcoming Resistance to HER2 Inhibitors Through State-specific Kinase Binding. *Nature Chemical Biology*. **2016,** 12(11), 923.
4. Jeffrey PD, Tong L, Pavletich NP. Structural Basis of Inhibition of CDK–cyclin Complexes by INK4 Inhibitors. *Genes & Development*. **2000**, 14(24), 3115-25.
5. Leonard SE, Register AC, Krishnamurty R, Brighty GJ, Maly DJ. Divergent Modulation of Src-family Kinase Regulatory Interactions with ATP-competitive Inhibitors. *ACS Chemical Biology*. **2014,** 9(8), 1894-905.
6. Cleator S, Heller W, Coombes RC. Triple-negative Breast Cancer: Therapeutic Options. The Lancet Oncology. **2007**, 8(3), 235-44.
7. Gilani RA, Phadke S, Bao LW, Lachacz EJ, Dziubinski ML, Brandvold KR, Steffey ME, Kwarcinski FE, Graveel CR, Kidwell KM, Merajver SD. UM-164: a Potent c-Src/p38 Kinase Inhibitor with in vivo Activity Against Triple-Negative Breast Cancer. *Clinical Cancer Research***. 2016**, 22(20), 5087-96.
8. Ottenhoff-Kalff AE, Rijksen G, Van Beurden EA, Hennipman A, Michels AA, Staal GE. Characterization of Protein Tyrosine Kinases from Human Breast Cancer: Involvement of the c-Src Oncogene Product. *Cancer Research*. **1992**, 52(17), 4773-8.
9. Xu W, Harrison SC, Eck MJ. Three-dimensional Structure of the Tyrosine Kinase c-Src. *Nature*. **1997**, 385(6617), 595.
10. Bernadó P, Pérez Y, Svergun DI, Pons M. Structural Characterization of the Active and Inactive States of Src Kinase in Solution by Small-angle X-ray Scattering. *Journal of Molecular Biology*. **2008**, 376(2), 492-505.
11. Krishnamurty R, Brigham JL, Leonard SE, Ranjitkar P, Larson ET, Dale EJ, Merritt EA, Maly DJ. Active Site Profiling Reveals Coupling Between Domains in SRC-Family Kinases. *Nature Chemical Biology*. **2013**, 9(1), 43-50.
12. MacAuley AL, Cooper JA. Structural Differences Between Repressed and Derepressed forms of p60c-src. Molecular and Cellular Biology. **1989**, 9(6), 2648-56.
13. Hubbard SJ. The Structural Aspects of Limited Proteolysis of Native Proteins. *Biochimica et Biophysica Acta (BBA)-Protein Structure and Molecular Enzymology*. **1998**, 1382(2), 191-206.
14. Ren R. Mechanisms of BCR-ABL in the Pathogenesis of Chronic Myelogenous Leukaemia. *Nature Reviews. Cancer*. **2005**, 5(3), 172.
15. Wang ML, Rule S, Martin P, Goy A, Auer R, Kahl BS, Jurczak W, Advani RH, Romaguera JE, Williams ME, Barrientos JC. Targeting BTK with Ibrutinib in Relapsed or Refractory Mantle-cell Lymphoma. *New England Journal of Medicine*. **2013** , 369(6), 507-16.

16. Gazdar A. Activating and Resistance Mutations of EGFR in Non-small-cell Lung Cancer: Role in Clinical Response to EGFR Tyrosine Kinase Inhibitors. *Oncogene*. **2009**, 28(Suppl 1), S24.
17. Prahallad A, Sun C, Huang S, Di Nicolantonio F, Salazar R, Zecchin D, Beijersbergen RL, Bardelli A, Bernards R. Unresponsiveness of Colon Cancer to BRAF (V600E) Inhibition through Feedback Activation of EGFR. *Nature*. **2012**, 483(7387), 100.
18. Irby RB, Yeatman TJ. Role of Src Expression and Activation in Human Cancer. *Oncogene*. **2000**, 19(49), 5636.
19. Maeder ML, Linder SJ, Cascio VM, Fu Y, Ho QH, Joung JK. CRISPR RNA-Guided Activation of Endogenous Human Genes. *Nature Methods.* **2013**, 10(10), 977-9.
20. Gorre ME, Mohammed M, Ellwood K, Hsu N, Paquette R, Rao PN, Sawyers CL. Clinical Resistance to STI-571 Cancer Therapy Caused by BCR-ABL Gene Mutation or Amplification. *Science*. **2001**, 293(5531), 876-80.
21. Davis MI, Hunt JP, Herrgard S, Ciceri P, Wodicka LM, Pallares G, Hocker M, Treiber DK, Zarrinkar PP. Comprehensive Analysis of Kinase Inhibitor Selectivity. *Nature Biotechnology*. **2011**, 29(11), 1046-51.

Appendix A
Supplemental Data for Chapter II

Mass Spectrometry Data for Selective Proteolysis

Figure A.1. Mass Spectrometry Data for Selective Proteolysis

A. Deconvuluted Mass Spectrum of WT Src + 0nM Thermolysin
Calculated 3D-Src = 51880.0
Experimental = 51884.0

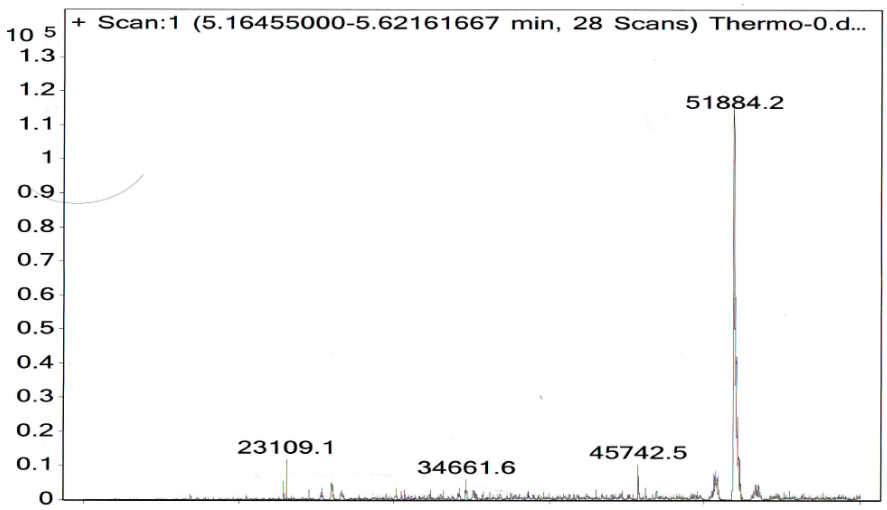

B. Deconvuluted Mass Spectra of WT Src + 60nM Thermolysin
Calculated m/z (M + H) = 19952.3
Experimental m/z (M + H) = 19953.0

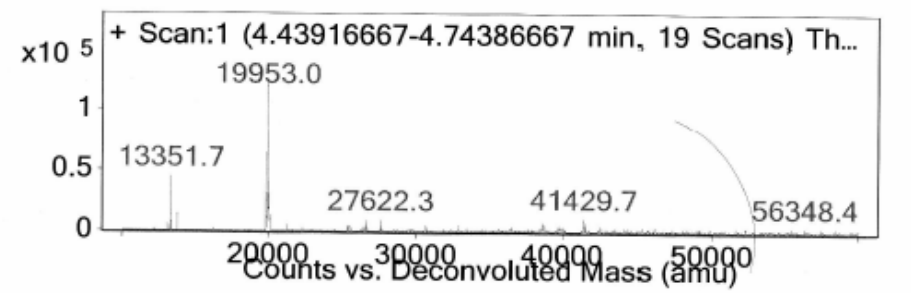

Calculated m/z (M + H) = 31946.1
Experimental m/z (M + H) = 31950.0

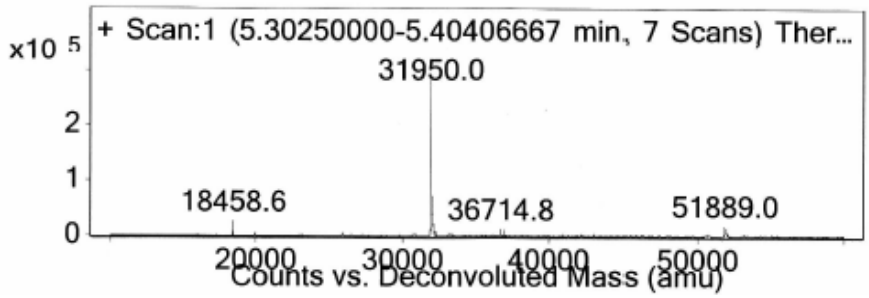

Analytical Data for Half-Life Determination of c-Src Constructs

Figure A.2. Half-Life Determination of c-Src Constructs

A. 2 μM WT Src treated with 60 nM Thermolysin $T_{1/2}$ = 33 mins

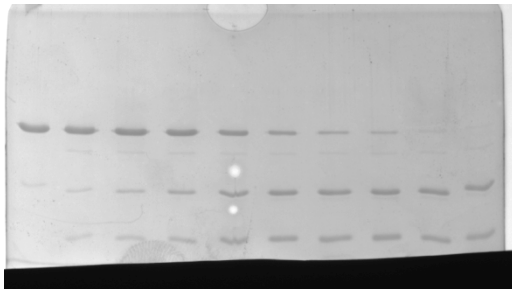

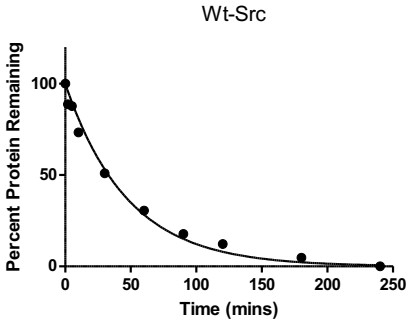

Half Life	32.96

B. 2 μM pY419 Src (Y530F) with 60 nM Thermolysin $T_{1/2}$ = 12 mins

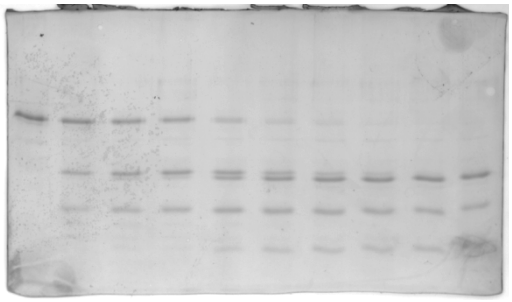

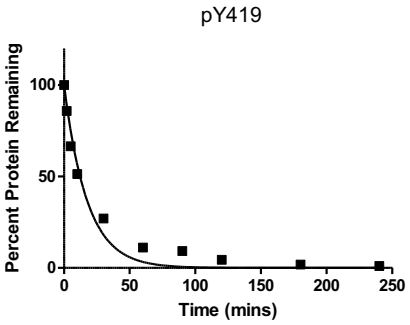

	pY419
Half Life	12.21

C. 2 μM pY530 Src (Y419F) with 60 nM Thermolysin $T_{1/2}$ = 241 mins

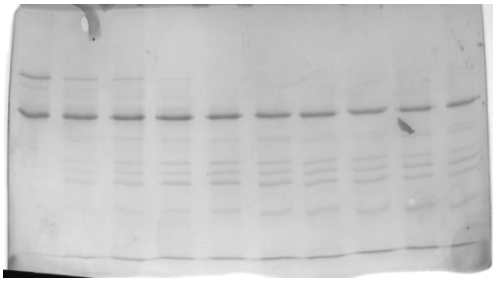

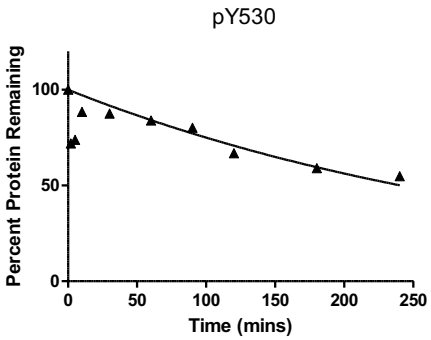

	pY530
Half Life	240.9

D. 2 μM Src^{SH2Eng} with 60 nM Thermolysin. $T_{1/2}$ = 356 mins

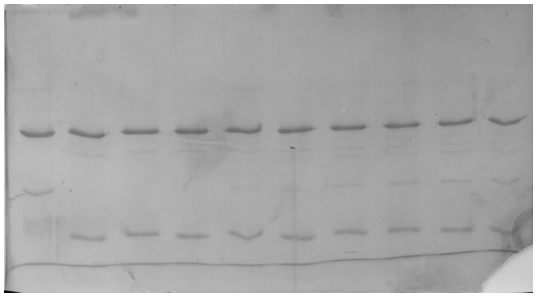

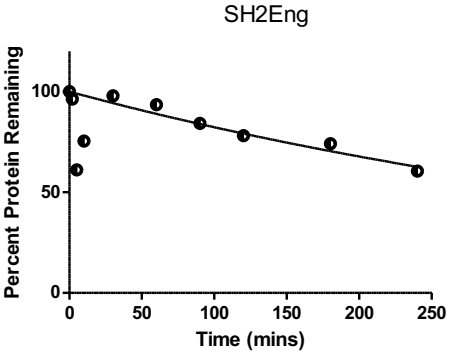

	SH2Eng
Half Life	356.4

Analytical Data for 2.1 & 2.2 bound c-Src

Figure A.3. Half-Life Curves for Compounds **2.1** and **2.2** bound c-Src

A. wt-Src + 25 μM **2.1** with 60 nM Thermolysin $T_{1/2}$ = 2.7 mins

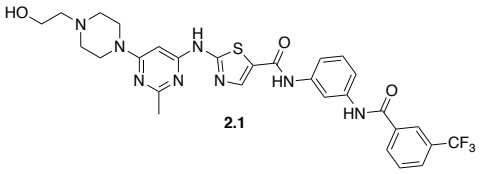

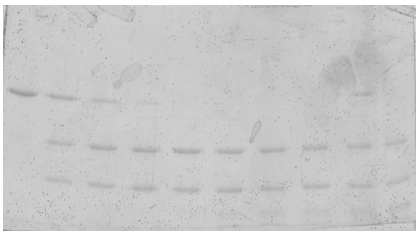

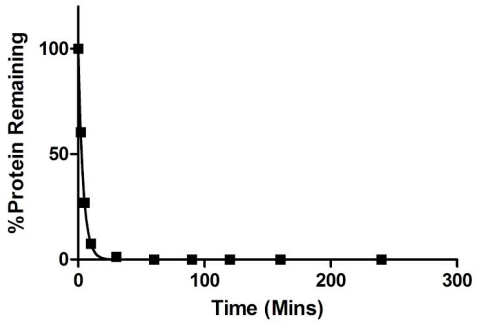

	2.1
Half Life	2.7

B. wt -Src + 25 μM **2.2** with 60 nM Thermolysin $T_{1/2}$ = 80 mins

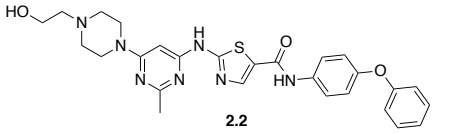

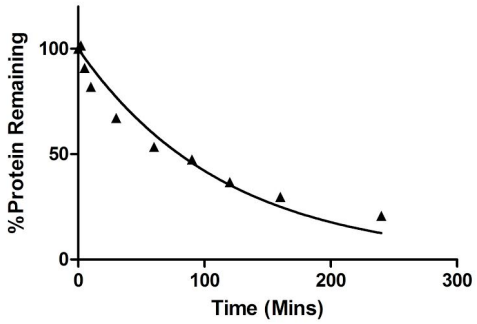

	2.2
Half Life	80

Analytical Data for Small Molecules bound c-Abl

Figure A.4. Half-Life Curves for small molecules bound to c-Abl

A. 2 µM c-Abl with 20 nM Thermolysin $T_{1/2}$ = 30 mins

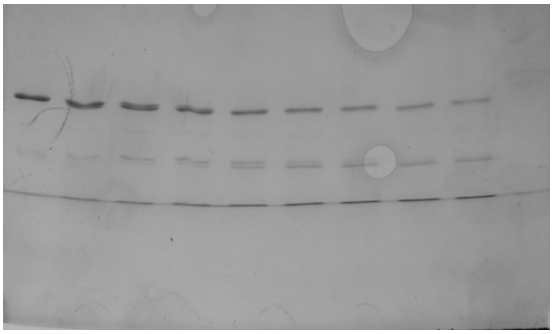

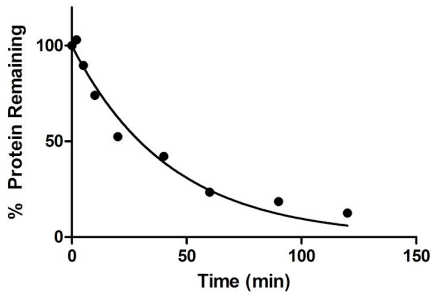

	3 Domain Abl
Half Life	30

B. c-Abl + 25 µM Imatinib with 20 nM Thermolysin $T_{1/2}$ = 3.3 mins

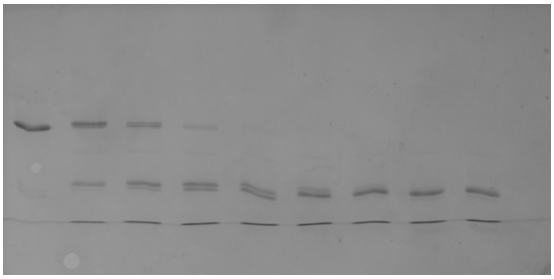

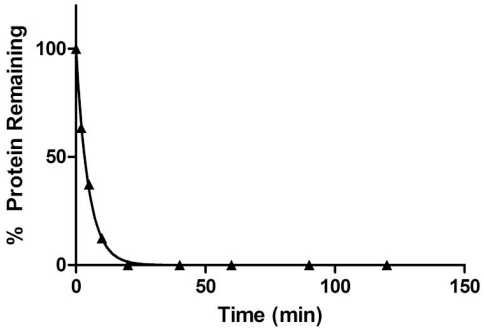

	+ Imatinib
Half Life	3.3

C. c-Abl + 25 µM Myristate Peptide with 20 nM Thermolysin $T_{1/2}$ = 192 mins

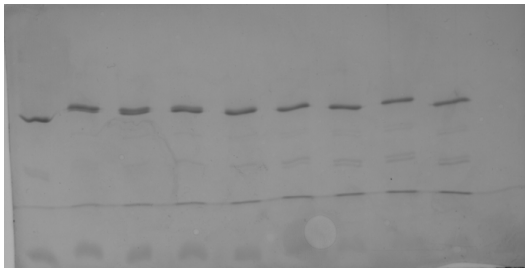

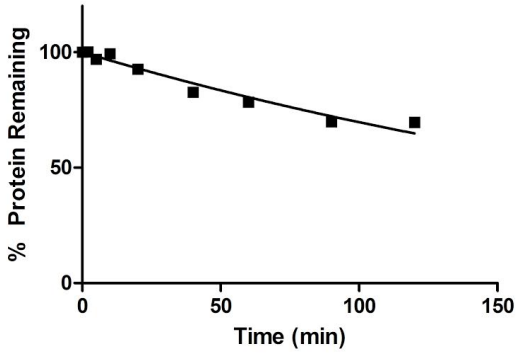

	+ Myristate
Half Life	192

D. c-Abl + 25 μM **2.1** with 20 nM Thermolysin $T_{1/2}$ = 2.2

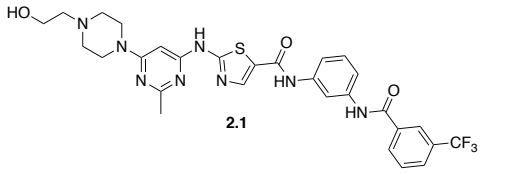

2.1

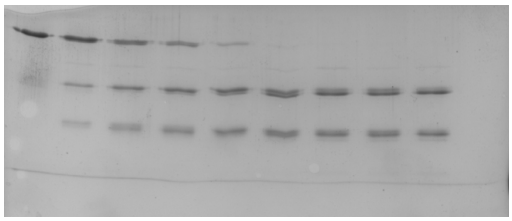

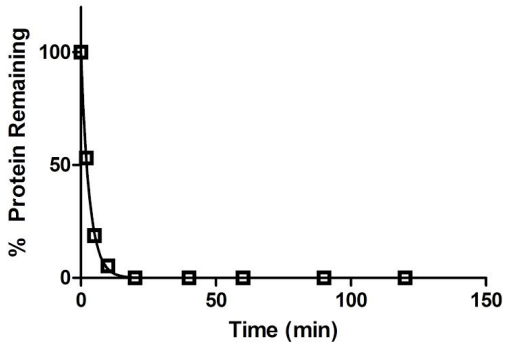

	+ 2.1
Half Life	2.2

E. c-Abl + 25 μM **2.2** with 20 nM Thermolysin $T_{1/2}$ = 47 mins

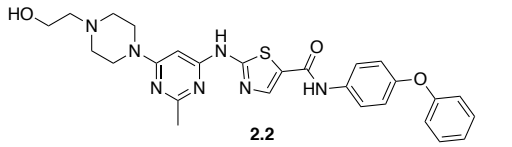

2.2

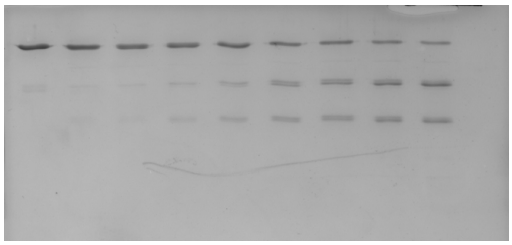

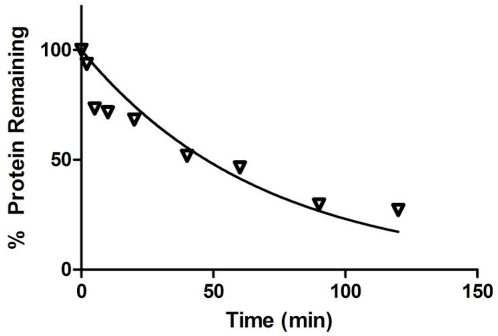

	+ 2.2
Half Life	47

F. c-Abl + 25 μM GNF-2 with 20 nM Thermolysin $T_{1/2}$ = 173 mins

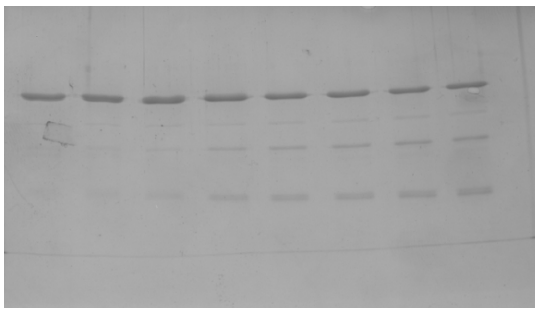

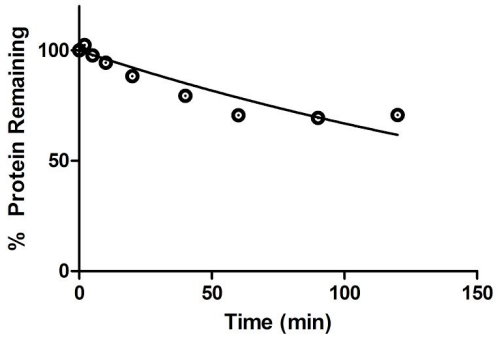

	+ GNF
Half Life	173

Appendix B

Analytical Data and Supplemental Information for Chapter III

Selective Proteolysis for Clinical Mutations

Figure B.1. Selective Proteolysis for Clinical Mutations

A) I113F with 60 nM Thermolysin. $T_{1/2}$ = 31 mins

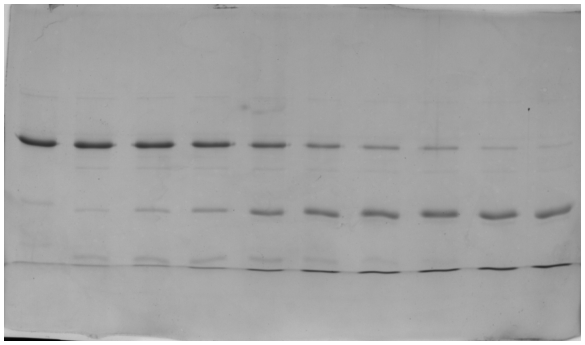

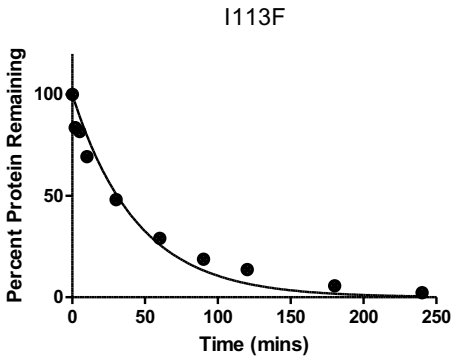

	I113F
Half Life	30.86

B) W121R with 60 nM Thermolysin. $T_{1/2}$ = 2 mins

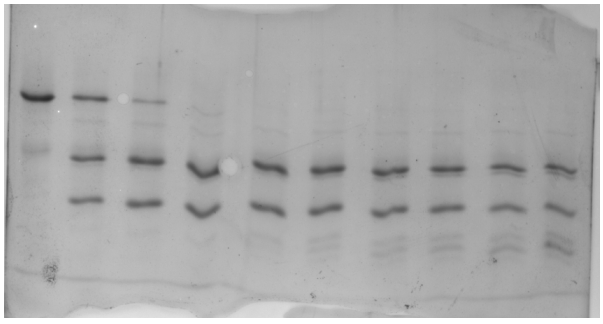

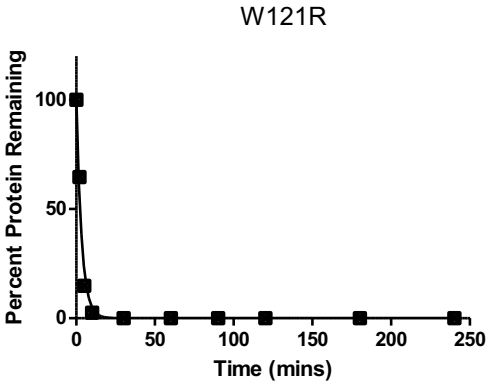

	W121R
Half Life	2.342

C) V140M with 60 nM Thermolysin. $T_{1/2}$ = 29 mins

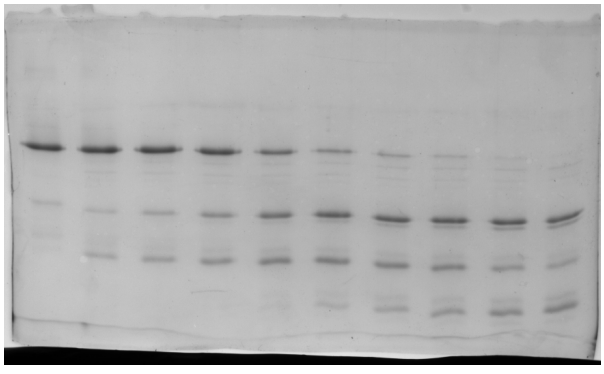

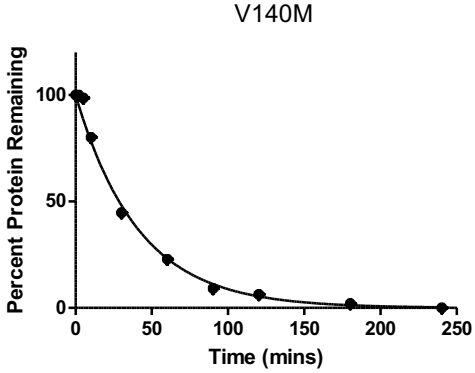

	V140M
Half Life	28.51

D) R163W with 60 nM Thermolysin. $T_{1/2}$ = 4 mins

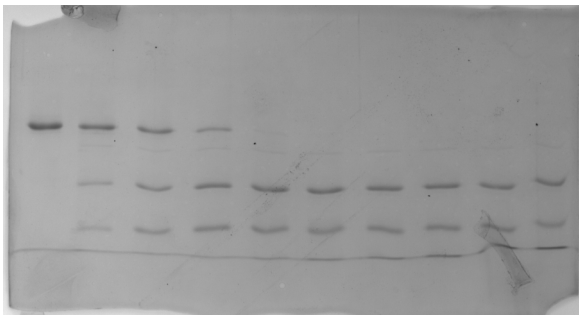

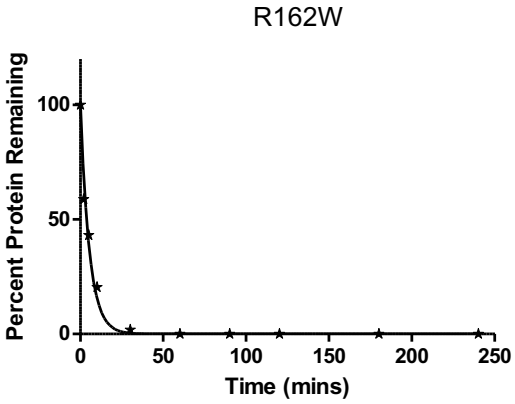

	R162W
Half Life	3.756

E) P171Q with 60 nM Thermolysin. $T_{1/2}$ = 41 mins

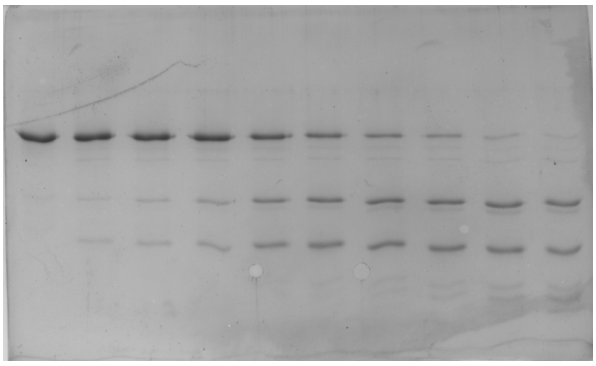

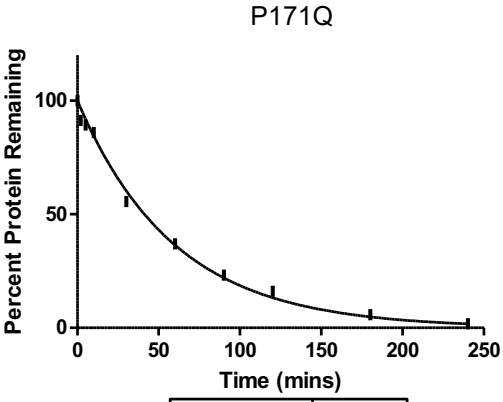

	P171Q
Half Life	41.19

F) K298E with 60 nM Thermolysin. $T_{1/2}$ = 67 mins

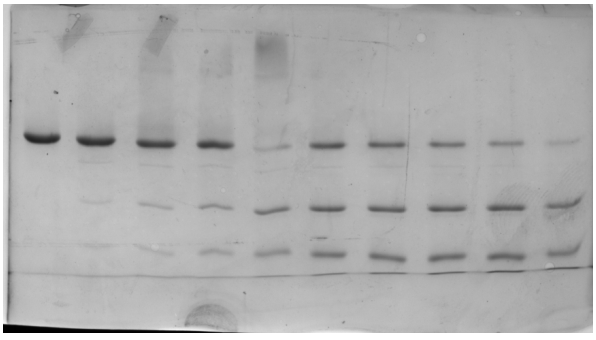

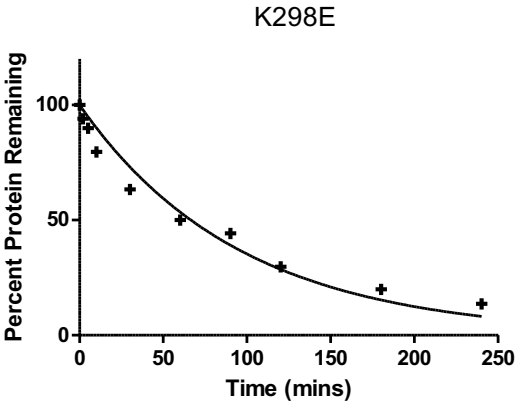

	K298E
Half Life	66.51

G) P307R with 60 nM Thermolysin. $T_{1/2}$ = 62 mins

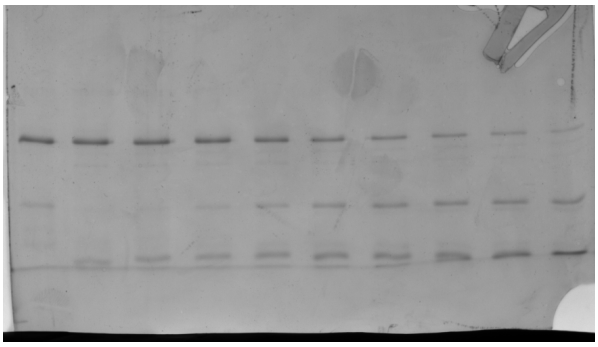

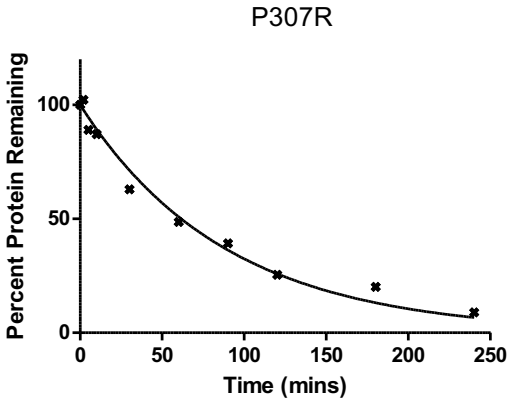

	P307R
Half Life	61.57

H) T341R with 60 nM Thermolysin. $T_{1/2}$ = 106 mins

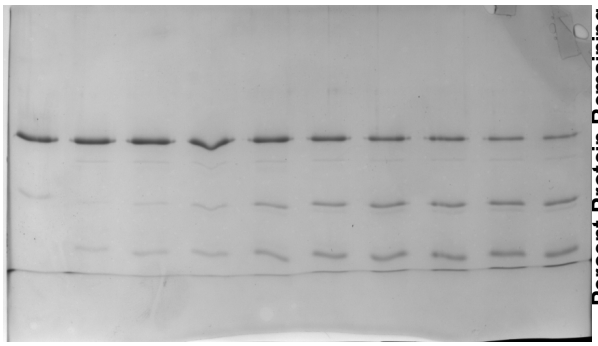

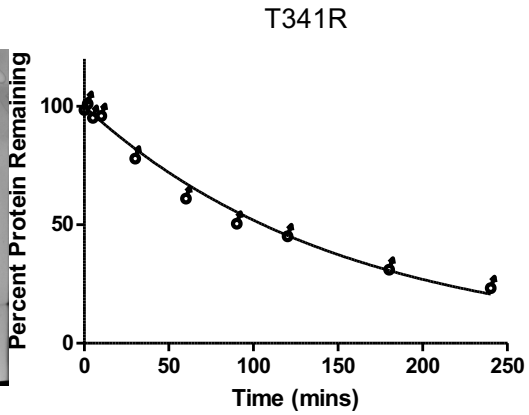

	T341R
Half Life	105.7

I) D407H with 60 nM Thermolysin. $T_{1/2}$ = 13 mins

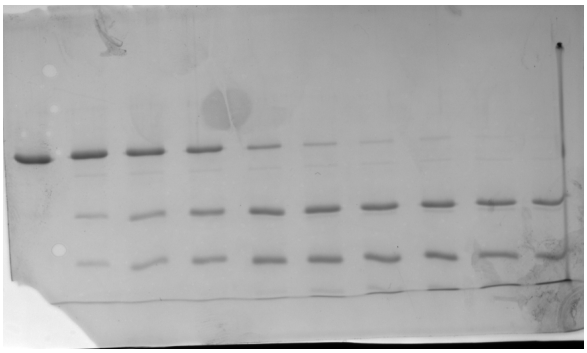

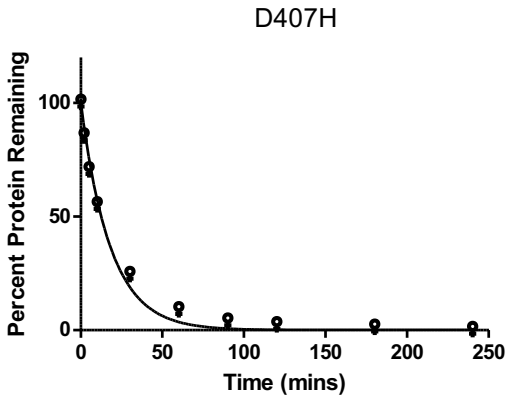

	D407H
Half Life	12.53

J) D521N with 60 nM Thermolysin. $T_{1/2}$ = 37 mins

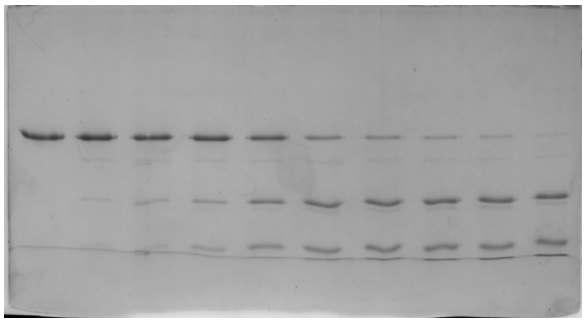

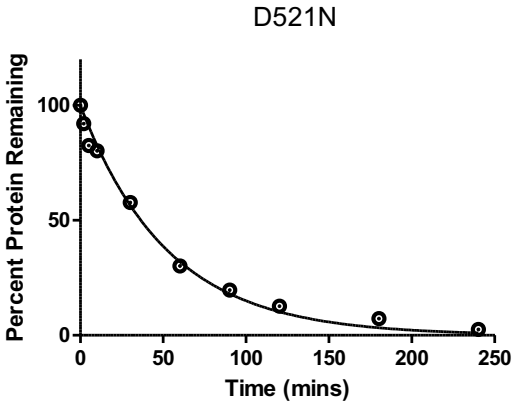

	D521N
Half Life	36.50

K) E527K with 60 nM Thermolysin. $T_{1/2}$ = 50 mins

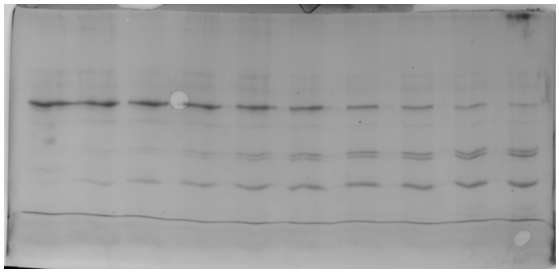

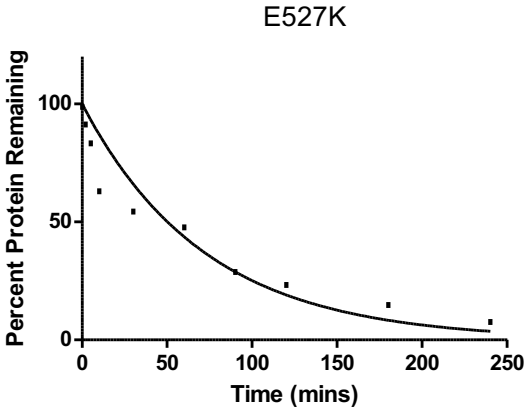

	E527K
Half Life	50.21

L) Q529H with 60 nM Thermolysin. $T_{1/2}$ = 141 mins

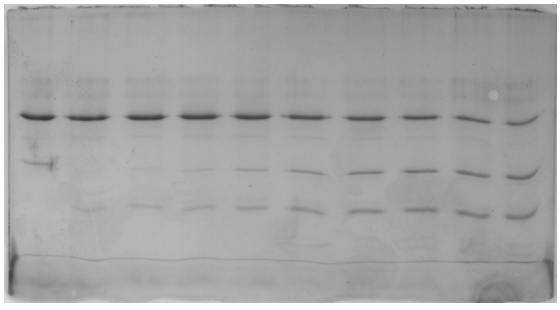

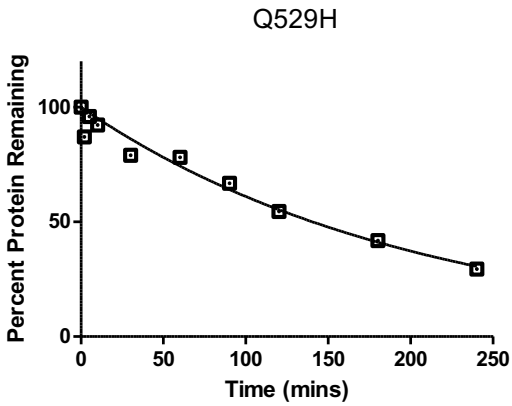

	Q529H
Half Life	140.5

Selective Proteolysis for Non-Clinical Mutations & Complexes

Figure B.2. Selective Proteolysis for Non-Clinical Mutations and Complexes

A) R98W with 60 nM Thermolysin. $T_{1/2}$ = 12 mins

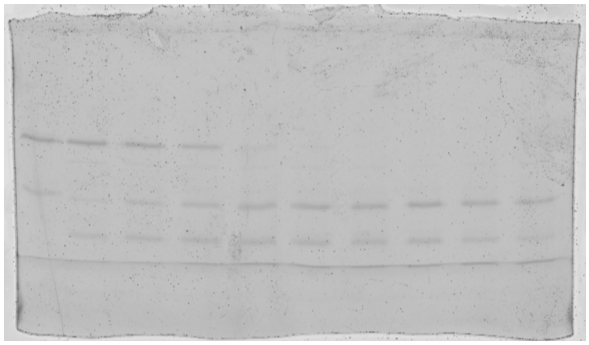

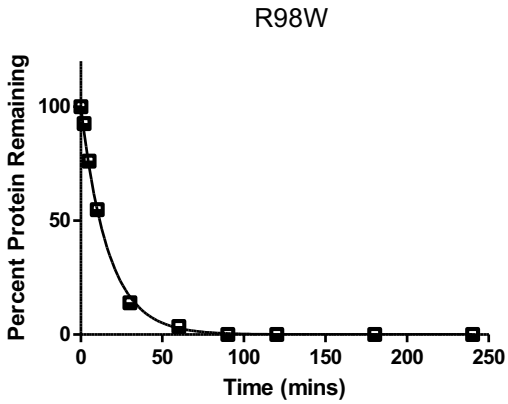

	R98W
Half Life	11.63

B) D120N with 60 nM Thermolysin. $T_{1/2}$ = 11 mins

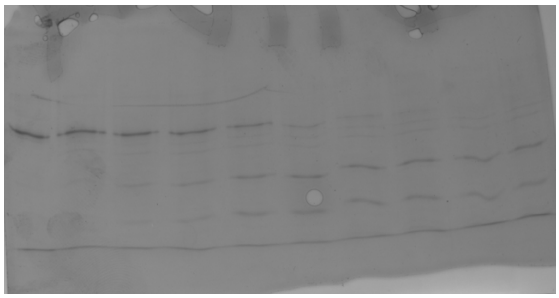

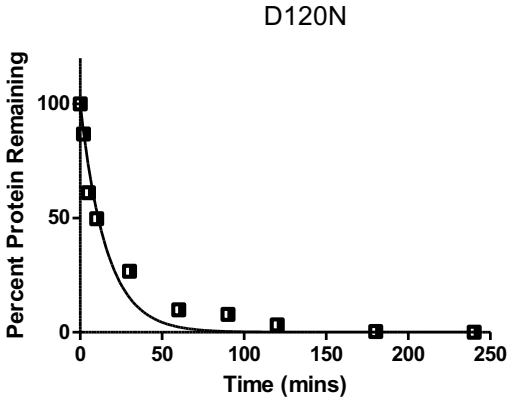

	D120N
Half Life	11.06

C) W263A with 60 nM Thermolysin. $T_{1/2}$ = 3.3 mins

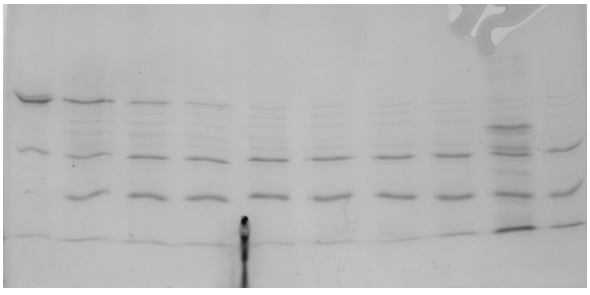

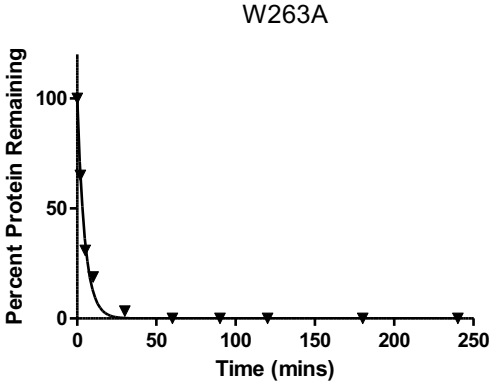

	W263A
Half Life	3.312

D) K298M with 60 nM Thermolysin. $T_{1/2}$ = 11 mins

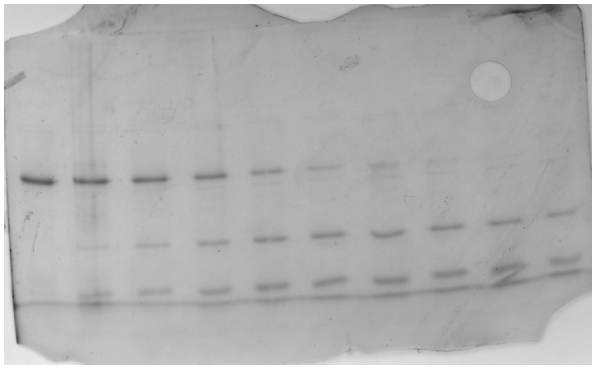

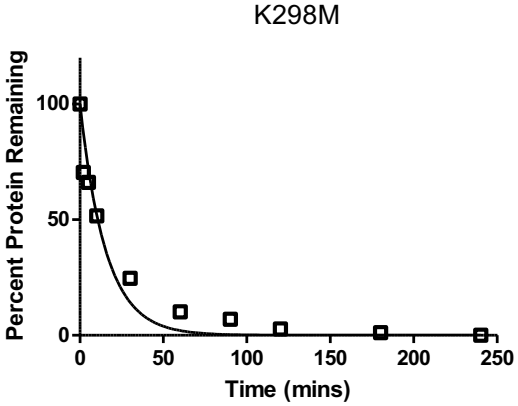

	K298M
Half Life	10.70

E) T341I with 60 nM Thermolysin. $T_{1/2}$ = 35 mins

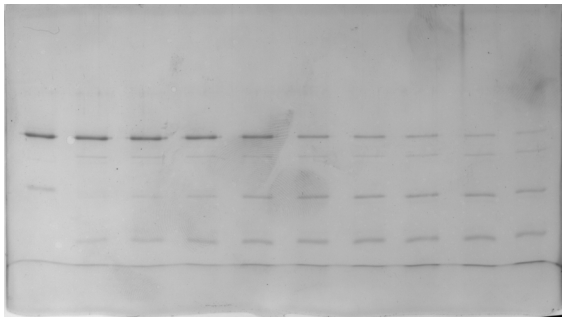

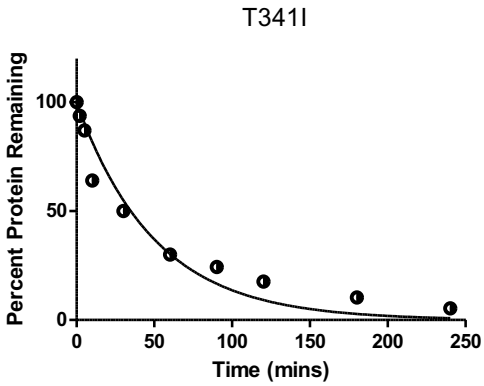

	T341I
Half Life	34.82

F) T341G with 60 nM Thermolysin. $T_{1/2}$ = 71 mins

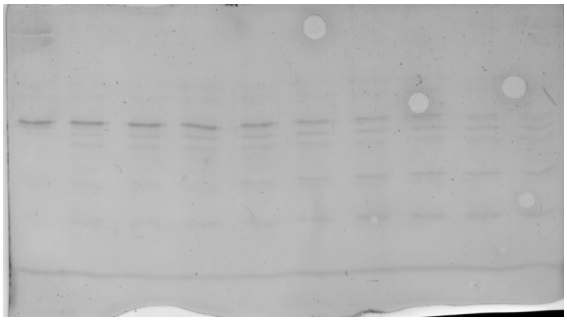

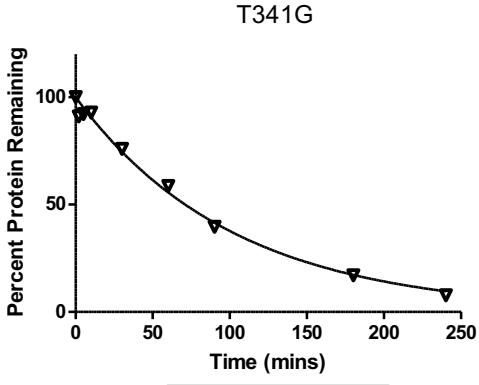

	T341G
Half Life	71.02

G) T341M with 60 nM Thermolysin. $T_{1/2}$ = 43 mins

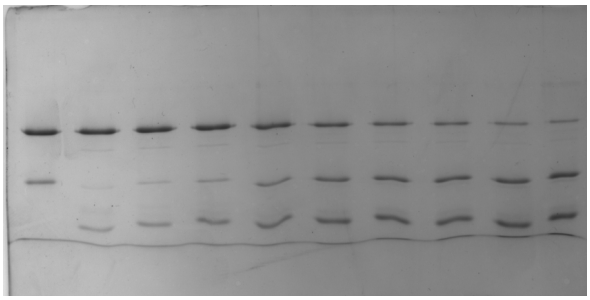

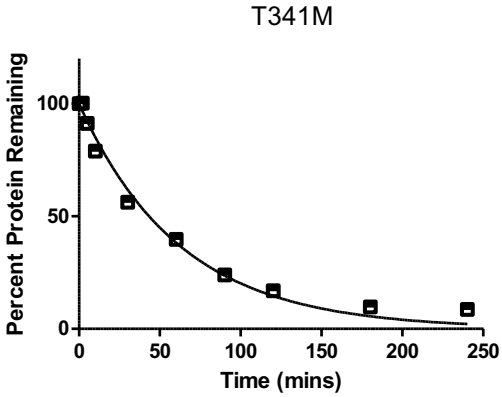

	T341M
Half Life	43.30

H) T341R with 60 nM Thermolysin. $T_{1/2}$ = 106 mins

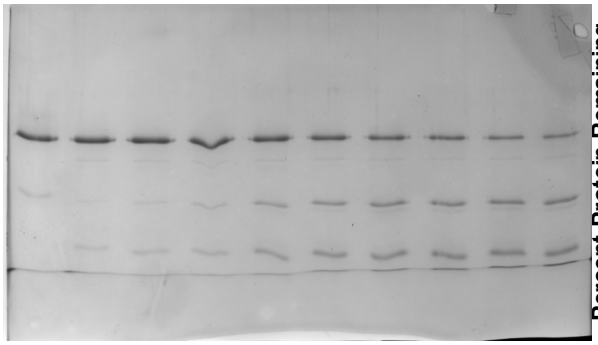

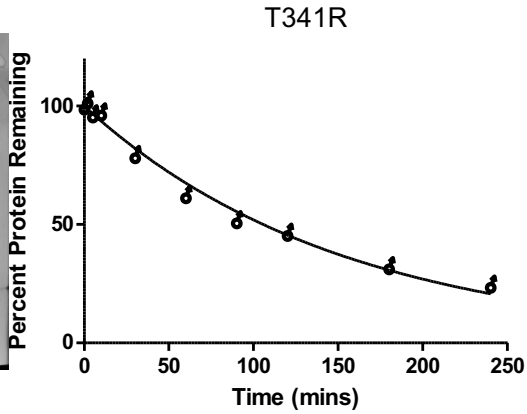

	T341R
Half Life	105.7

I) F408A with 60 nM Thermolysin. $T_{1/2}$ = 192 mins

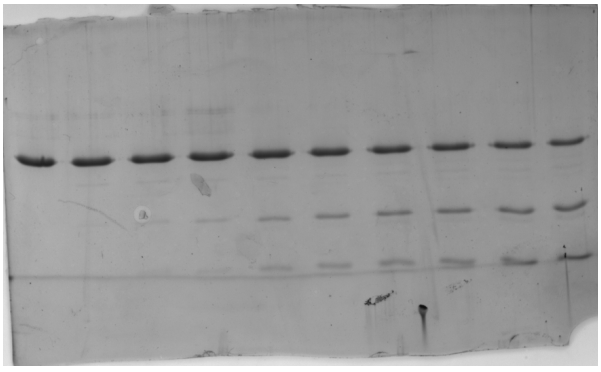

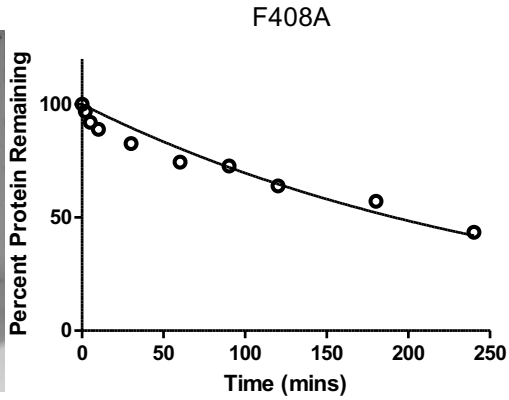

	F408A
Half Life	191.6

J) F408G with 60 nM Thermolysin. $T_{1/2}$ = 31 mins

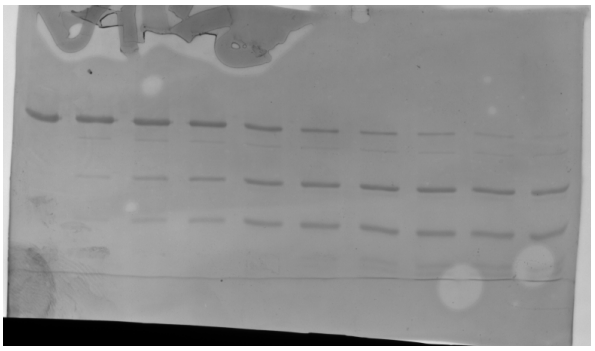

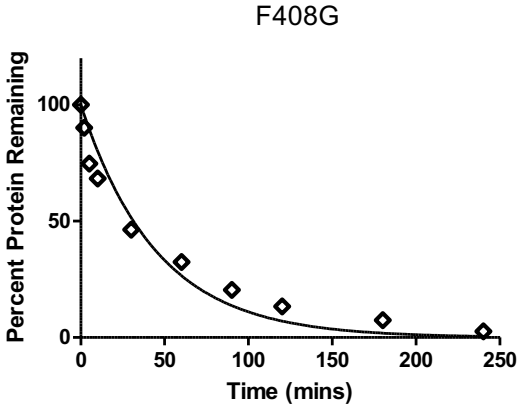

	F408G
Half Life	31.40

K) Y419F with 60 nM Thermolysin. $T_{1/2}$ = 19 mins

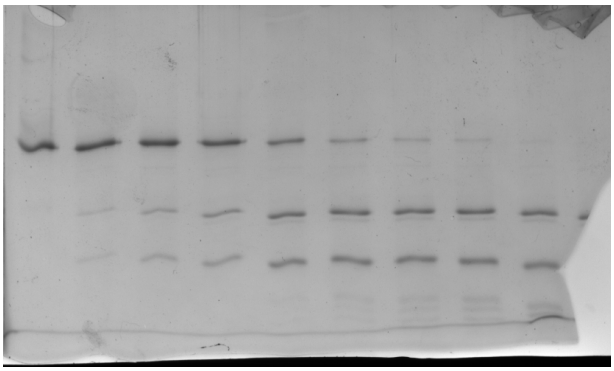

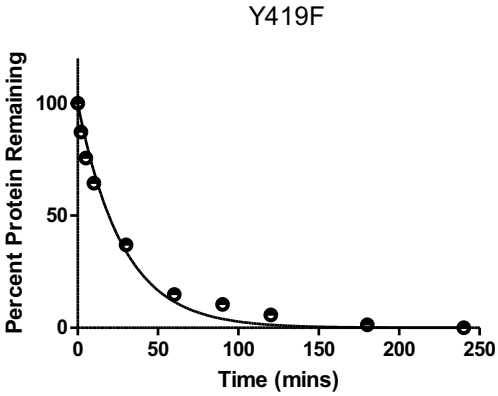

	Y419F
Half Life	19.33

L) Y530F with 60 nM Thermolysin. $T_{1/2}$ = 35 mins

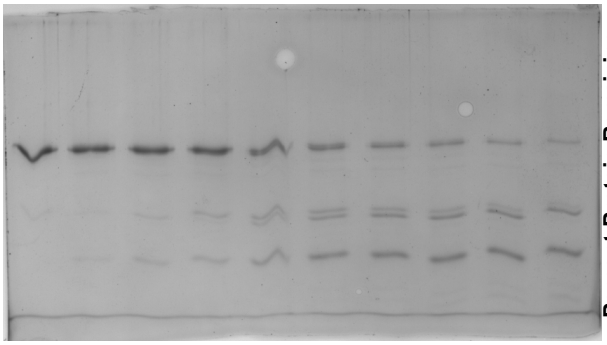

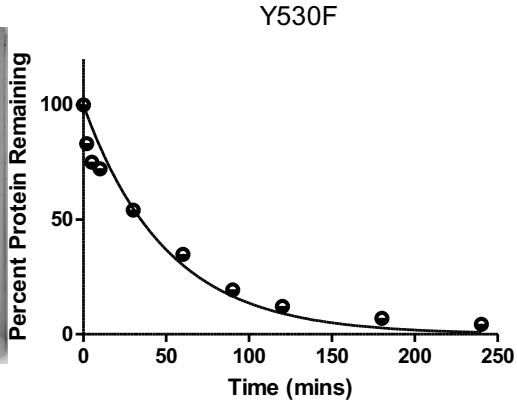

	Y530F
Half Life	34.72

M) SH2Eng with 60 nM Thermolysin. $T_{1/2}$ = 356 mins

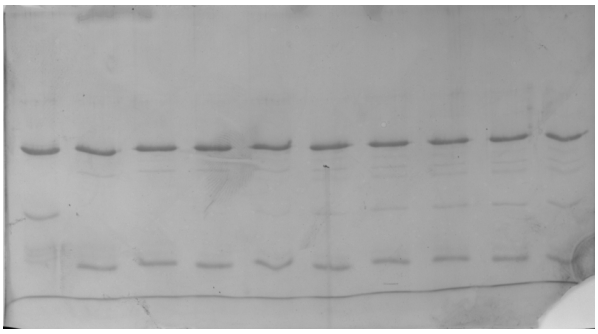

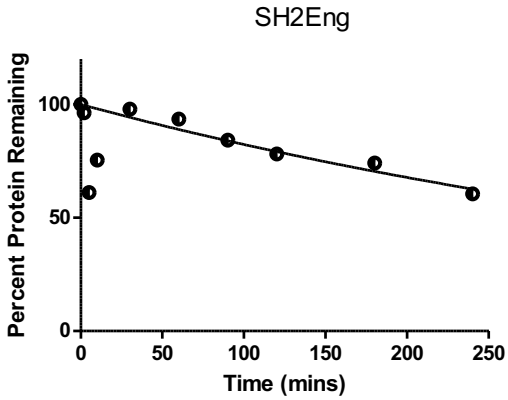

	SH2Eng
Half Life	356.4

N) T341M^{SH2Eng} with 60 nM Thermolysin. $T_{1/2}$ = 279 mins

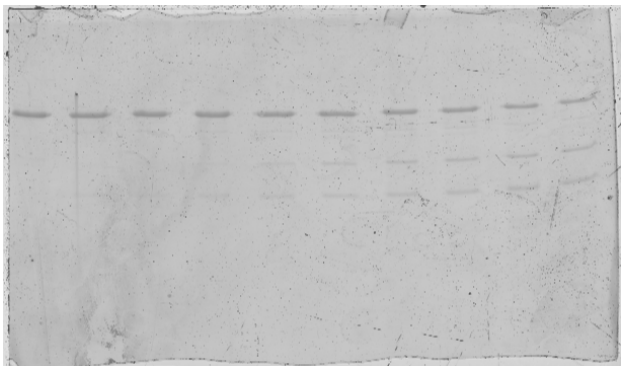

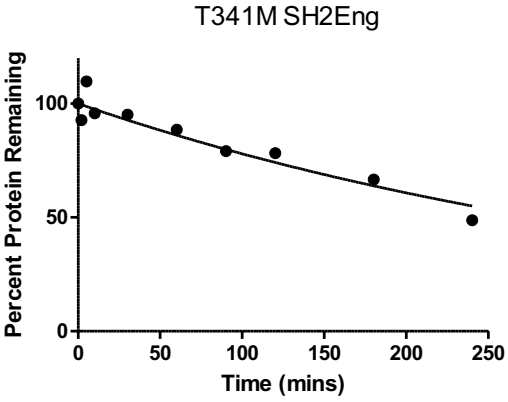

	T341M SH2 ENG
Half Life	278.6

O) R98W^{SH2Eng} with 60 nM Thermolysin. $T_{1/2}$ = 38 mins

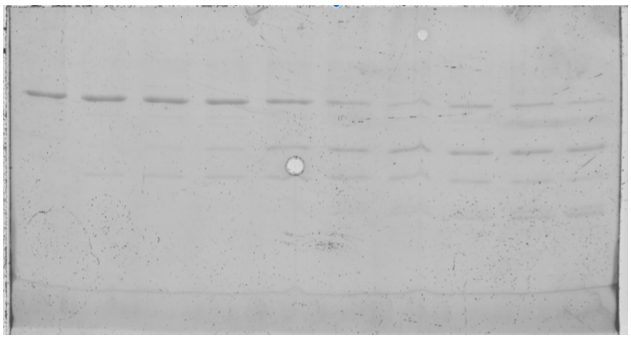

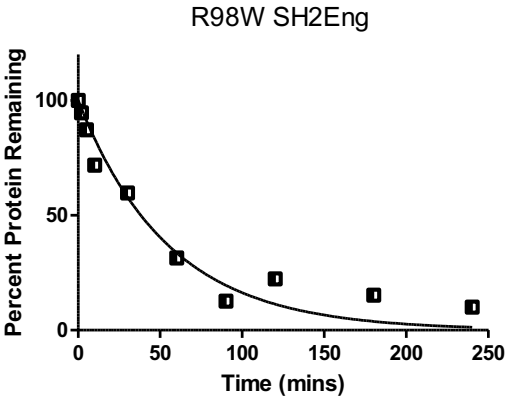

	R98W SH2 Eng
Half Life	38.21

P) W121R^{SH2Eng} with 60 nM Thermolysin. $T_{1/2}$ = 4 mins

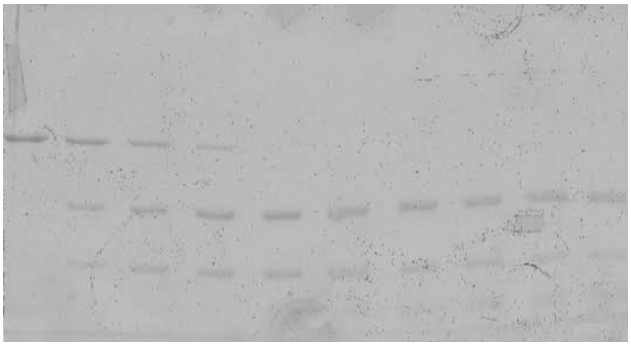

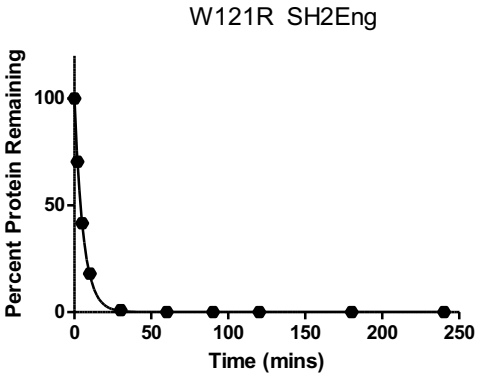

	W121R SH2Eng
Half Life	3.990

Q) Src-**3.1** Complex with 60 nM Thermolysin. $T_{1/2}$ = 13 mins

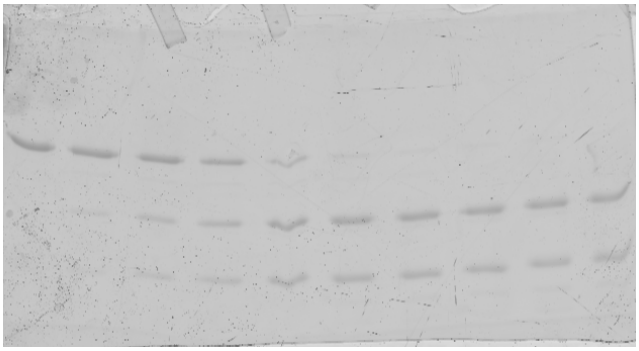

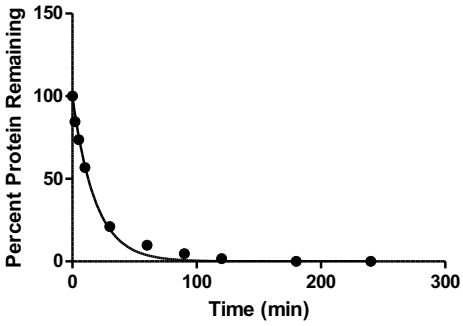

	3D Src (1)
Half Life	12.75

R) Src-**3.2** Complex with 60 nM Thermolysin. $T_{1/2}$ = 141 mins

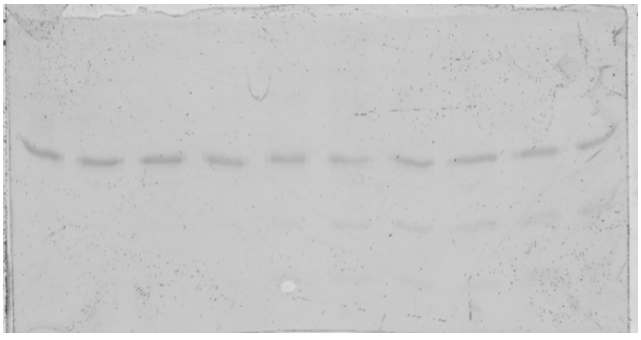

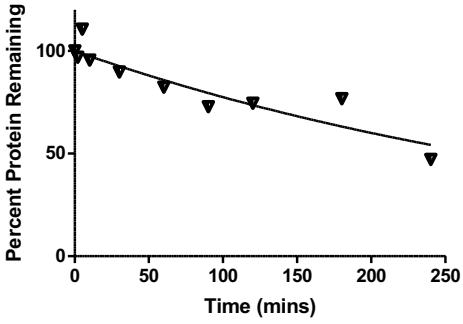

	3D-Src (2)
Half Life	271.9

S) Src^{Y530F}-**3.1** Complex with 60 nM Thermolysin. $T_{1/2}$ = 18 mins

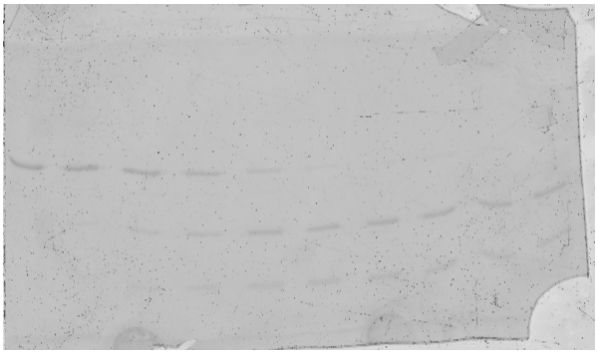

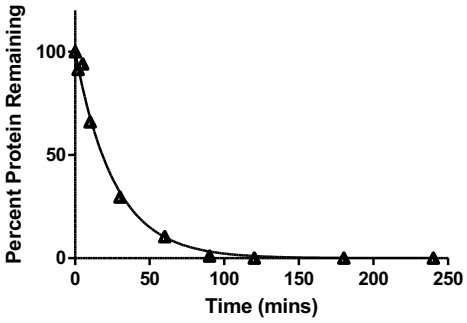

	Y530F (1)
Half Life	18.26

T) Src^{Y530F}-**3.2** Complex with 60 nM Thermolysin. $T_{1/2}$ = 141 mins

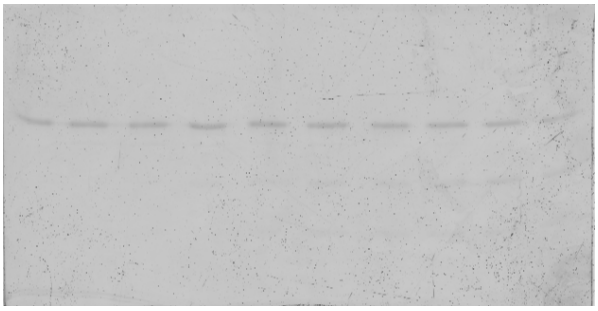

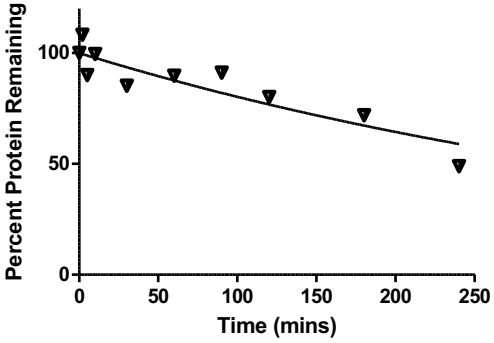

	Y530F (2)
Half Life	315.0

U) K298R with 60 nM Thermolysin $T_{1/2}$ = 92 mins

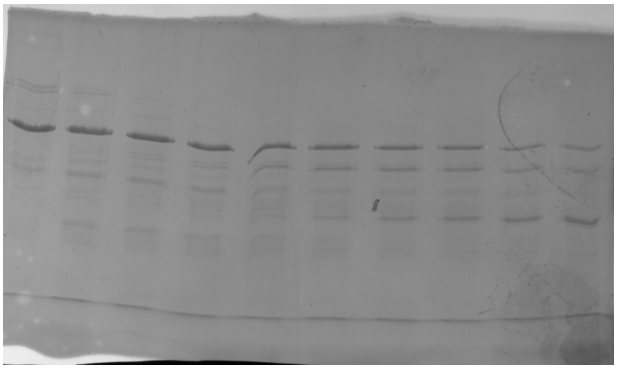

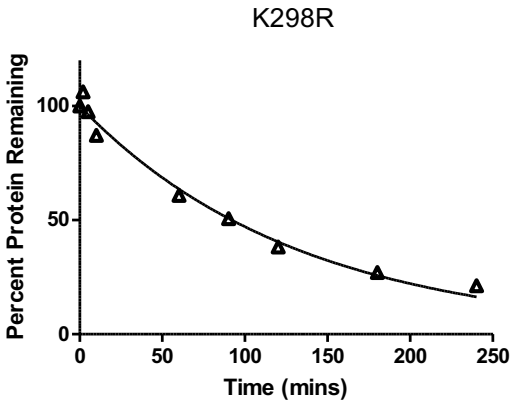

	K298R
Half Life	92.01

Table B.1. Comprehensive Half-Life Table for All Mutations

c-Src Mutant	Half-Life (min)	c-Src Mutant	Half-Life (min)
WT-Src	33	I113F	31
pY419	12	W121R	2.3
pY530	241	T341R	106
W263A	3.3	D407H	13
D407N	13	E527K	50
F408A	192	P171Q	41
K298M	11	Y419F	19
K298R	92	Y530F	35
T341G	71	T341I	35
F408G	31	T341M	43
V140M	29	R98W	9
R163W	3.8	D120N	11
K298E	67	SH2 Eng	356
P307R	62	T341M SH2 Eng	283
D521N	37	R98W SH2 Eng	42
Q529H	141	W121R SH2 Eng	4
3D Src • 3.1	13	Y530F Src • 3.1	18
3D Src • 3.2	272	Y530F Src • 3.2	315

V_{max} & Substrate K_m Determinations for c-Src Mutations/Constructs

Figure B.3. V_{max} & Substrate K_m Determinations for c-Src Mutations/Constructs

A) WT-Src

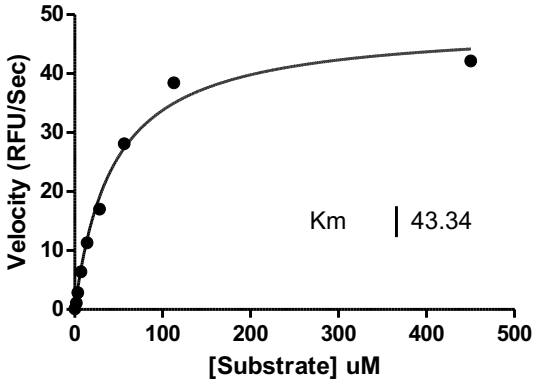

Substrate K_m (μM) = 43 ± 2

V_{max} (Rfu/min) = 56 ± 6

B) pY419 Src

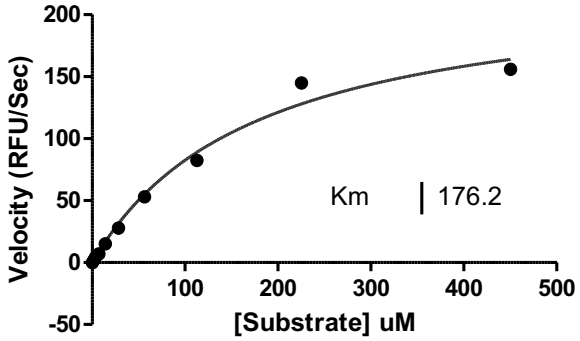

Substrate K_m (μM) = 215 ± 47

V_{max} (Rfu/min) = 239 ± 8

C) pY530 Src

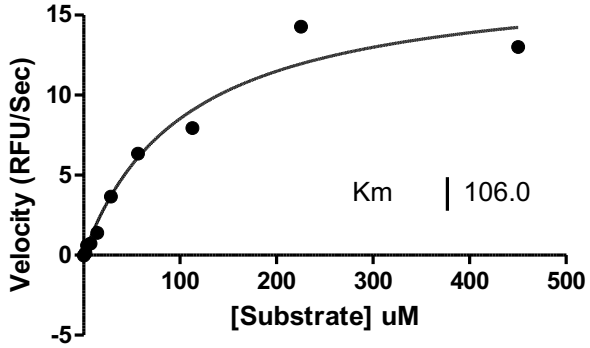

Substrate K_m (μM) = 108 ± 28

V_{max} (Rfu/min) = 25 ± 6

D) I113F

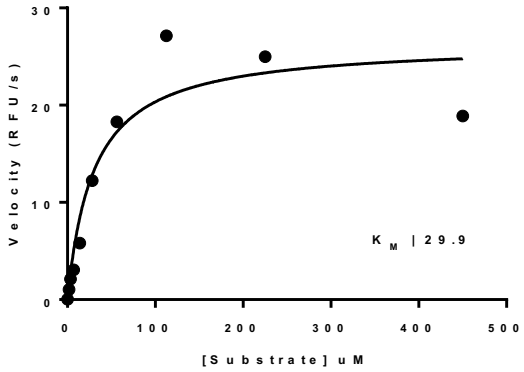

Substrate K_m (μM) = 24 ± 4

V_{max} (Rfu/min) = 30 ± 5

E) W121R

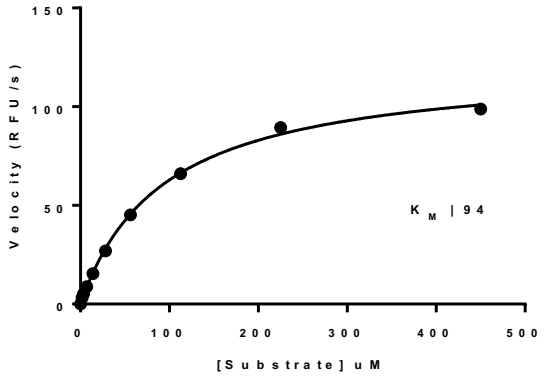

Substrate K_m (μM) = 101 ± 26

V_{max} (Rfu/min) = 128 ± 21

F) V140M

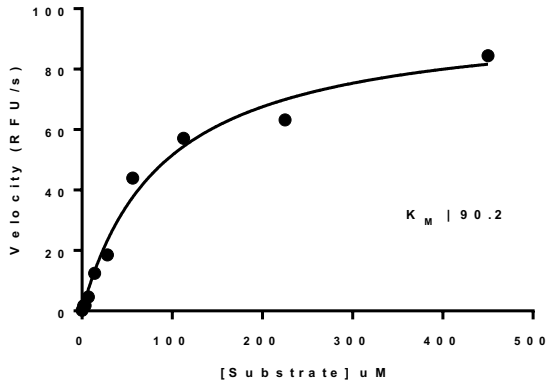

Substrate K_m (μM) = 104 ± 8

V_{max} (Rfu/min) = 152 ± 1

G) R163W

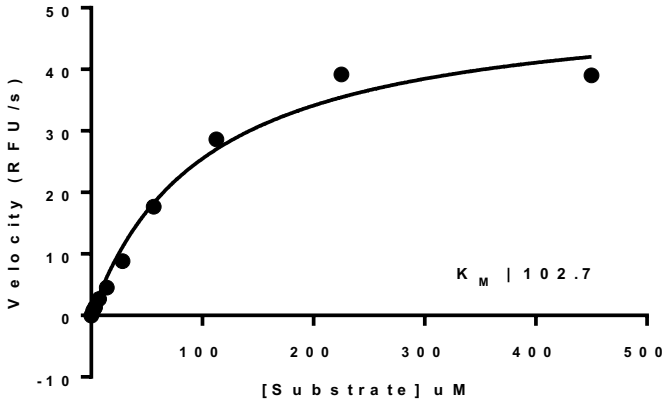

Substrate K_m (μM) = 102 ± 7

V_{max} (Rfu/min) = 50 ± 5

H) P171Q

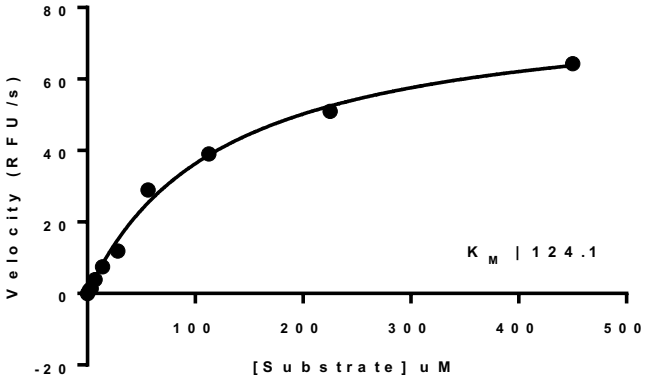

Substrate K_m (μM) = 142 ± 29

V_{max} (Rfu/min) = 115 ± 28

I) P307R

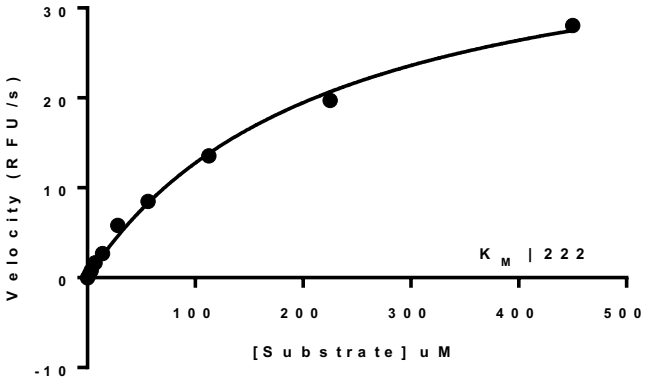

Substrate K_m (μM) = 222 ± 23

V_{max} (Rfu/min) = 23 ± 2

J) T341R

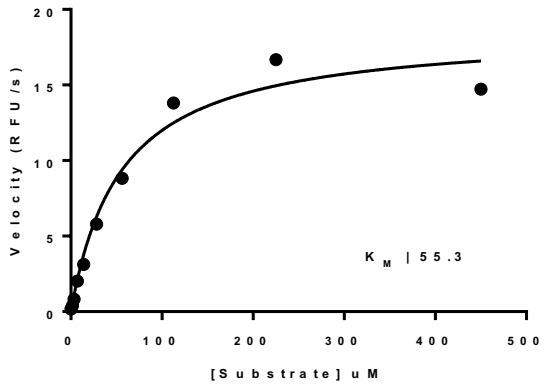

Substrate K_m (µM) = 48 ± 6

V_{max} (Rfu/min) = 17 ± 1.4

K) D521N

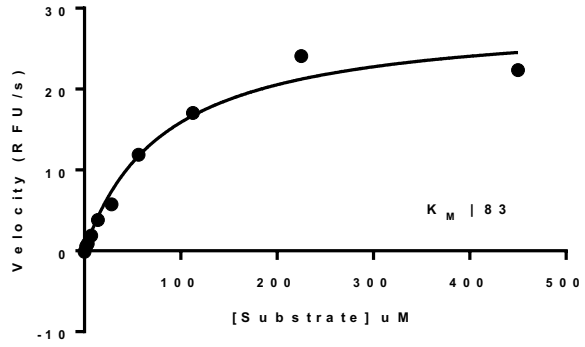

Substrate K_m (µM) = 83 ± 8

V_{max} (Rfu/min) = 29 ± 1

L) E527K

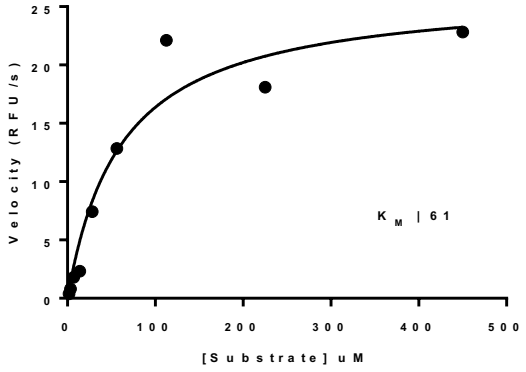

Substrate K_m (µM) = 78 ± 24

V_{max} (Rfu/min) = 28 ± 10

M) Q529H

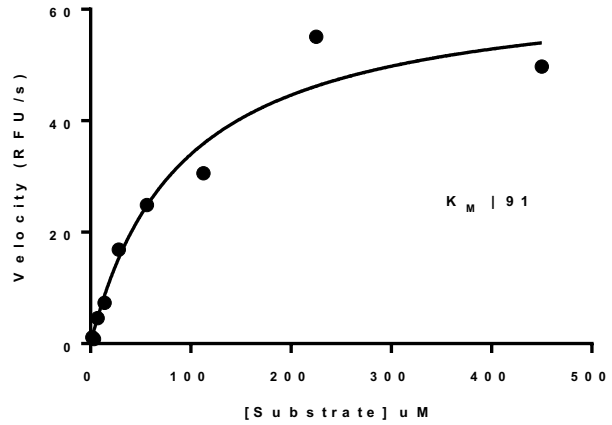

Substrate K_m (μM) = 89 ± 9

V_{max} (Rfu/min) = 49 ± 11

N) R98W

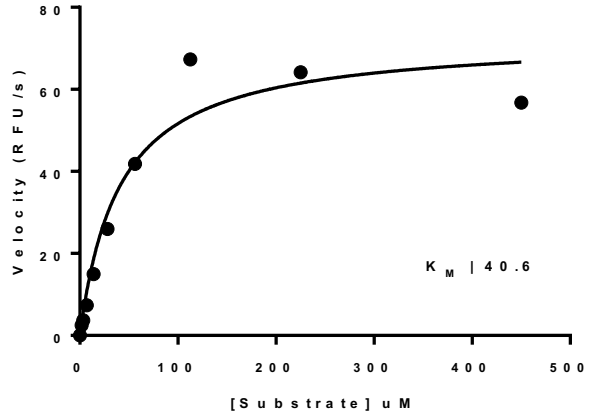

Substrate K_m (μM) = 42 ± 4

V_{max} (Rfu/min) = 74 ± 7

O) D120N

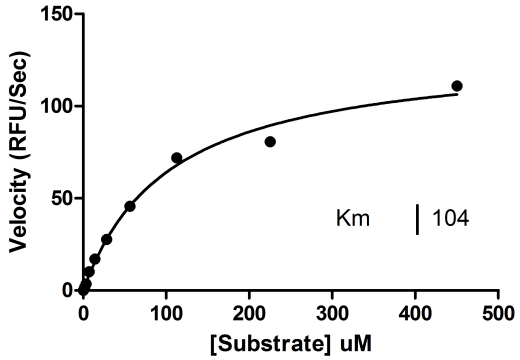

Substrate K_m (μM) = 110 ± 9

V_{max} (Rfu/min) = 126 ± 4

P) W263A

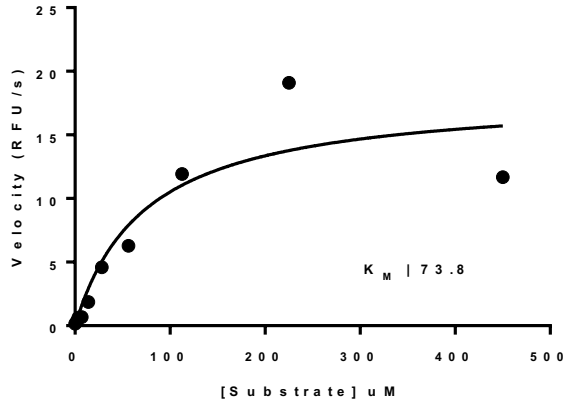

Substrate K_m (μM) = 65 ± 14

V_{max} (Rfu/min) = 16 ± 2

Q) T341I

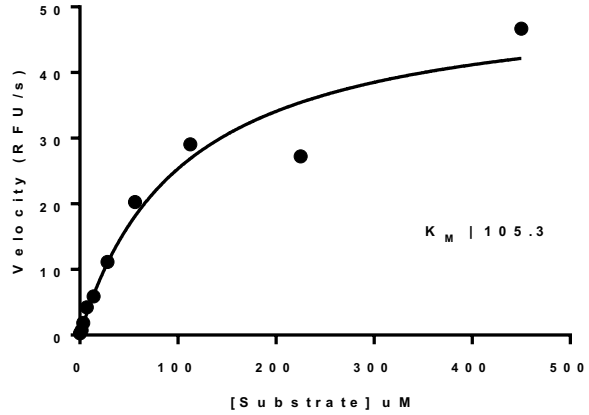

Substrate K_m (μM) = 106 ± 17

V_{max} (Rfu/min) = 58 ± 7

R) T341G

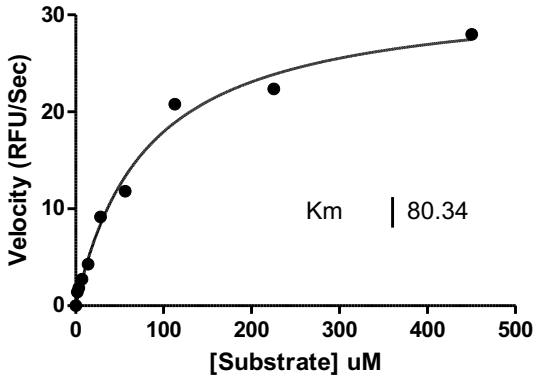

Substrate K_m (μM) = 72 ± 24

V_{max} (Rfu/min) = 25 ± 6

S) T341M

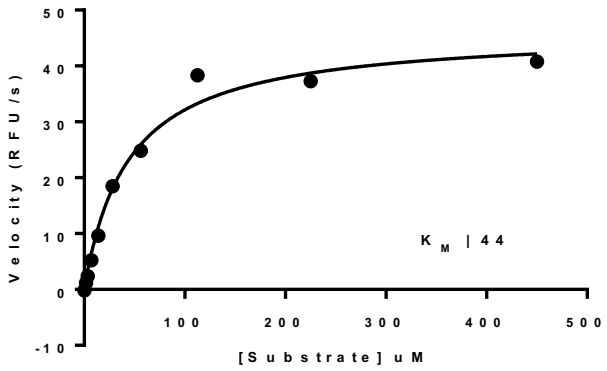

Substrate K_m (μM) = 53 ± 7

V_{max} (Rfu/min) = 54 ± 5

T) Y419F

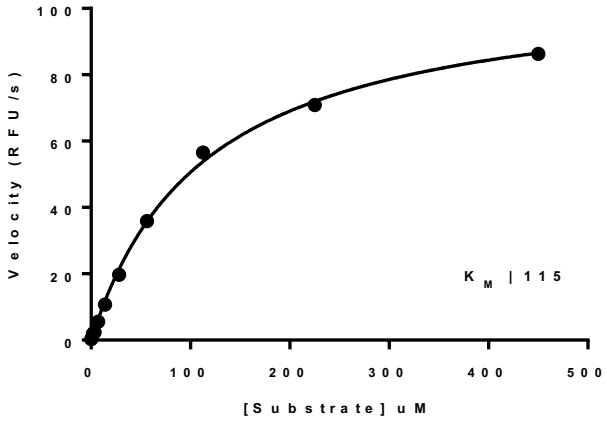

Substrate K_m (μM) = 99 ± 12

V_{max} (Rfu/min) = 126 ± 14

U) Y530F

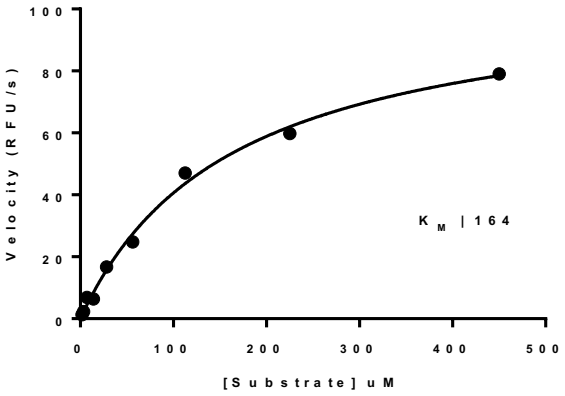

Substrate K_m (μM) = 155 ± 14

V_{max} (Rfu/min) = 106 ± 8

V) SH2Eng

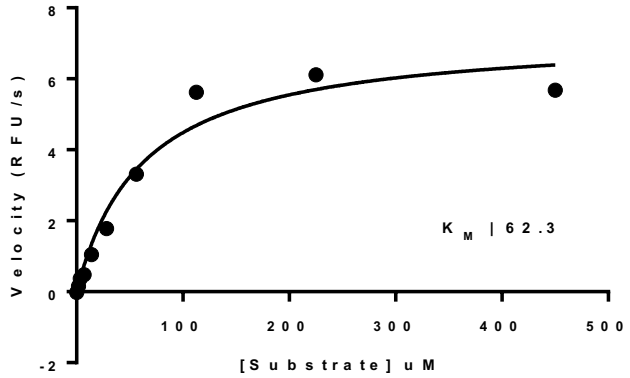

Substrate K_m (μM) = 58 ± 10

V_{max} (Rfu/min) = 6.5 ± 0.5

W) T341M^{SH2Eng}

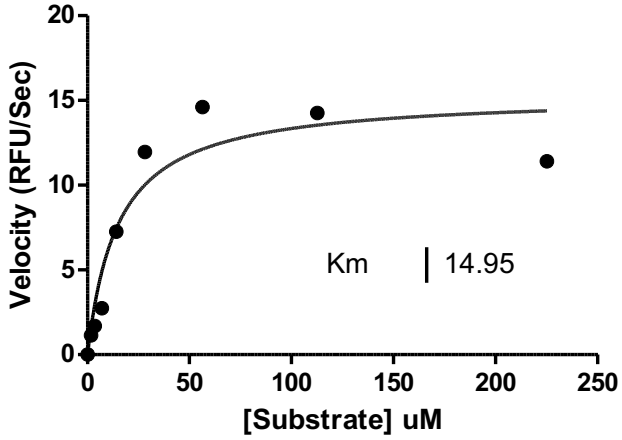

Substrate K_m (μM) = 14 ± 1

V_{max} (Rfu/min) = 11 ± 4

X) R98W^{SH2Eng}

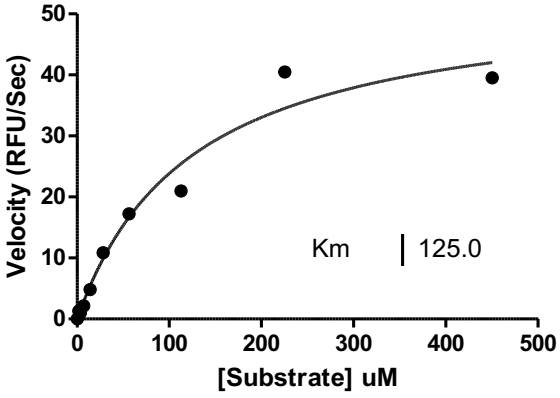

Substrate K_m (μM) = 130 ± 60

V_{max} (Rfu/min) = 70 ± 21

Y) W121R^{SH2Eng}

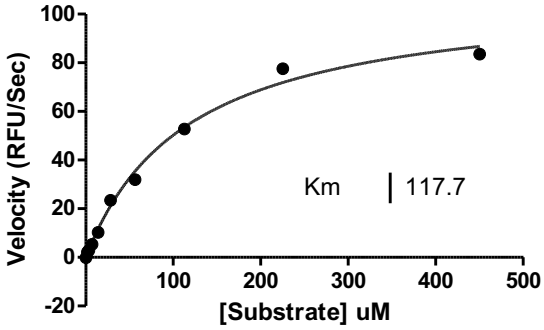

Substrate K_m (μM) = 130 ± 27

V_{max} (Rfu/min) = 118 ± 7

Table B.2. Comprehensive Table for V_{max} of c-Src Mutants

c-Src Mutant	Vmax (Rfu/Sec)	c-Src Mutant	Vmax (Rfu/Sec)
WT-Src	56 ± 6	**I113F**	30 ± 5
pY419	239 ± 8	**W121R**	128 ± 21
pY530	25 ± 6	**T341R**	17 ± 1.4
W263A	16 ± 2	**D407H**	Dead
D407N	Dead	**E527K**	28 ± 10
F408A	Dead	**P171Q**	115 ± 28
K298M	Dead	**Y419F**	126 ± 14
K298R	Dead	**Y530F**	106 ± 8
T341G	25 ± 6	**T341I**	58 ± 7
F408G	Dead	**T341M**	54 ± 5
V140M	152 ± 1	**R98W**	74 ± 7
R163W	50 ± 5	**D120N**	126 ± 4
K298E	Dead	**Src^{SH2ENG}**	6.5 ± 0.5
P307R	23 ± 2	**$T341M^{SH2ENG}$**	11 ± 4
D521N	29 ± 1	**$R98W^{SH2ENG}$**	70 ± 21
Q529H	49 ± 11	**$W121R^{SH2ENG}$**	118 ± 7

Table B.3. Comprehensive Table for Substrate K_m of c-Src Mutants

c-Src Mutant	Substrate K_m (μM)	c-Src Mutant	Substrate K_m (μM)
WT-Src	43 ± 2	**I113F**	24 ± 4
pY419	215 ± 47	**W121R**	101 ± 26
pY530	108 ± 28	**T341R**	48 ± 6
W263A	65 ± 14	**D407H**	Dead
D407N	Dead	**E527K**	78 ± 24
F408A	Dead	**P171Q**	142 ± 29
K298M	Dead	**Y419F**	99 ± 12
K298R	Dead	**Y530F**	155 ± 14
T341G	72 ± 24	**T341I**	106 ± 17
F408G	Dead	**T341M**	53 ± 7
V140M	104 ± 8	**R98W**	42 ± 4
R163W	102 ± 7	**D120N**	110 ± 9
K298E	Dead	**Src^{SH2ENG}**	58 ± 10
P307R	222 ± 23	**$T341M^{SH2ENG}$**	14 ± 1
D521N	83 ± 8	**$R98W^{SH2ENG}$**	130 ± 60
Q529H	89 ± 9	**$W121R^{SH2ENG}$**	130 ± 27

ATP K_m Determination for c-Src Mutants

Figure B.4. ATP K_m Determination for c-Src Mutants

A) Wt-Src

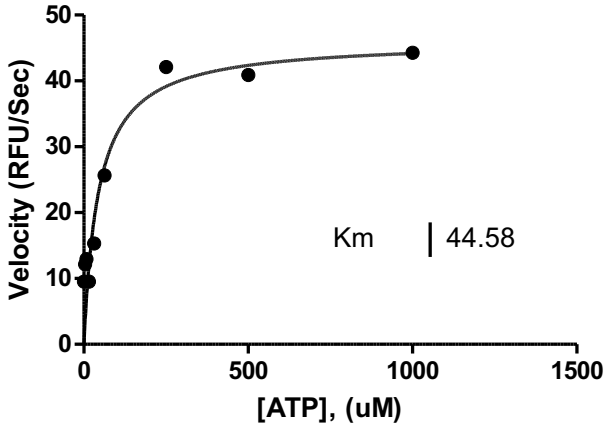

WT-Src
ATP K_m (μM) = 51 ± 14

B) pY419 Src

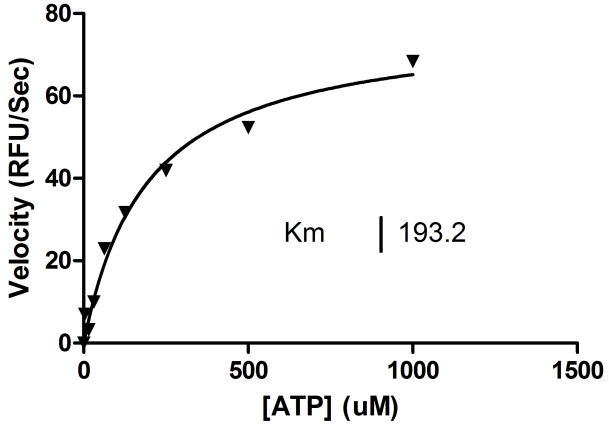

pY419 Src
ATP K_m (μM) = 170 ± 50

C) pY530 Src

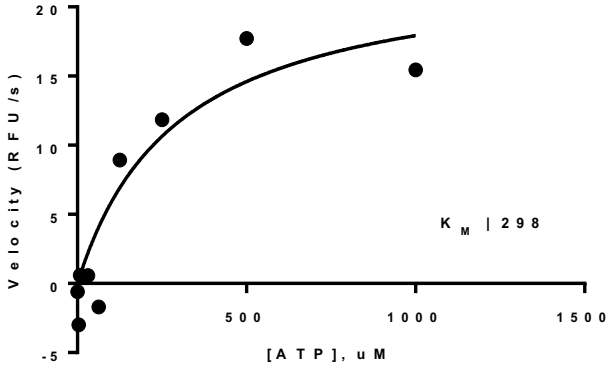

pY530 Src
ATP K_m (μM) = 340 ± 99

D) I113F

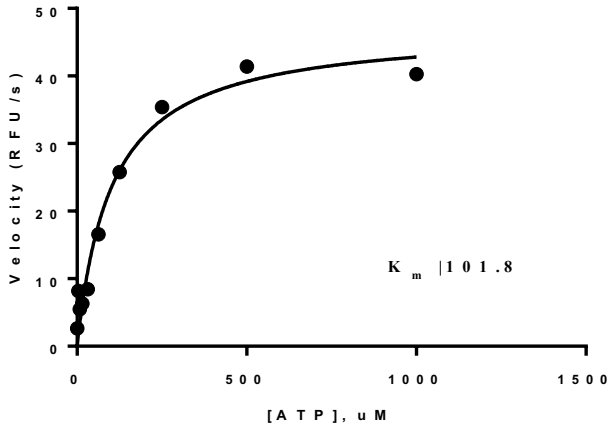

I113F Src
ATP K_m (μM) = 111 ± 12

E) W121R

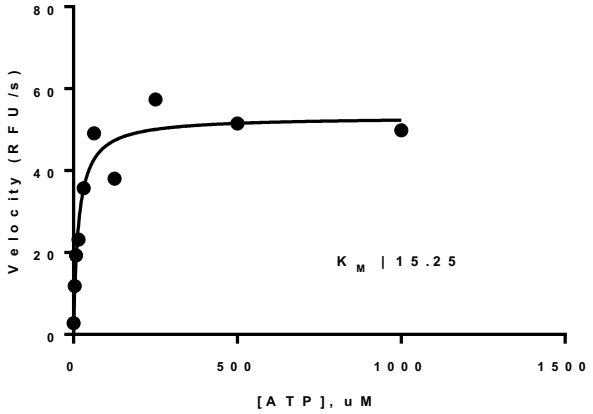

W121R Src
ATP K_m (μM) = 20 ± 4

F) V140M

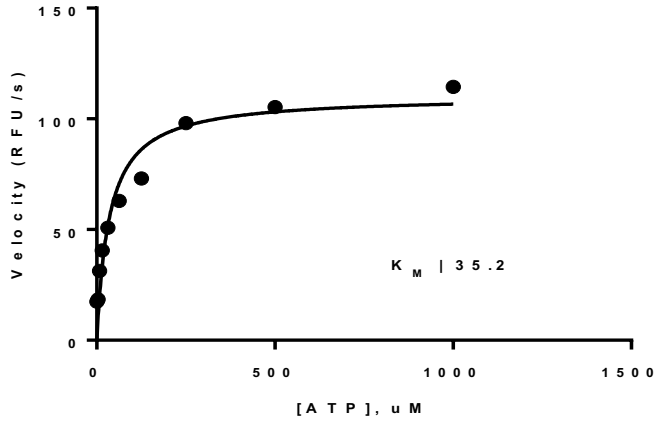

V140M Src
ATP K_m (μM) = 38 ± 3

G) R163W

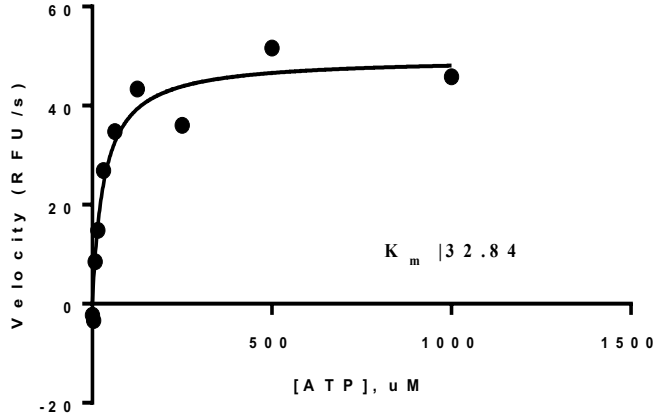

R163W Src
ATP K_m (μM) = 31 ± 4

H) P171Q

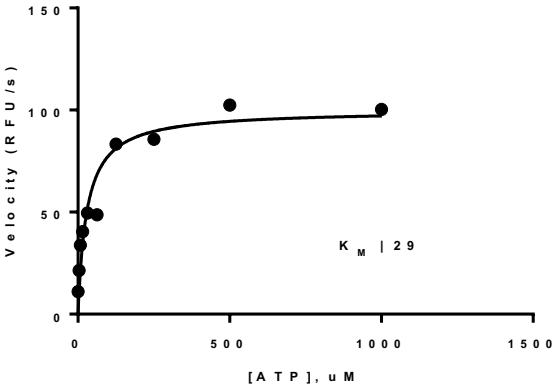

P171Q Src
ATP K_m (μM) = 22 ± 6

I) P307R

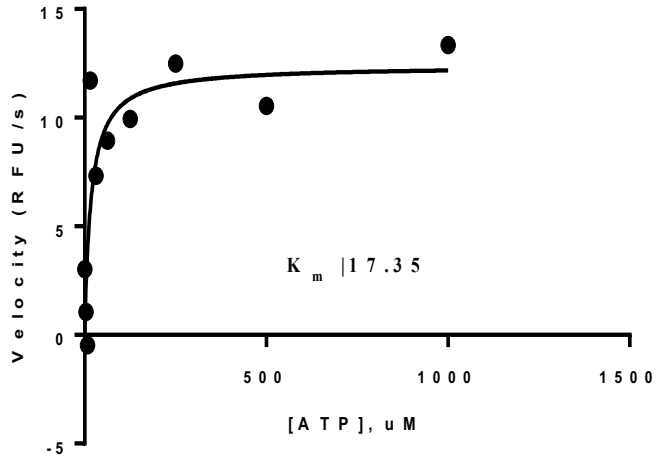

P307R Src
ATP K_m (μM) = 17 ± 5

J) T341R

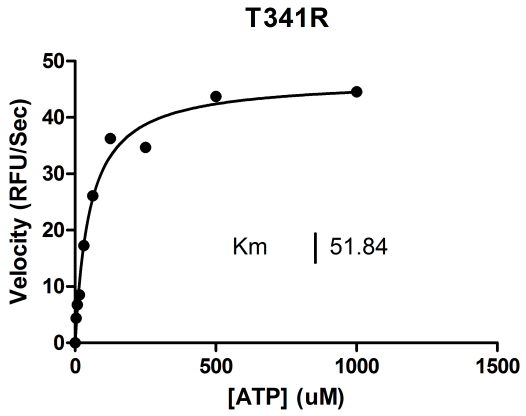

T341R Src
ATP K_m (μM) = 60 ± 10

K) D521N

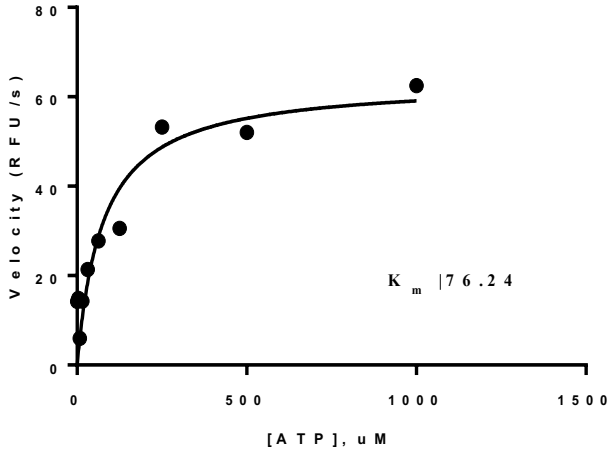

D521N Src
ATP K_m (μM) = 81 ± 9

L) E527K

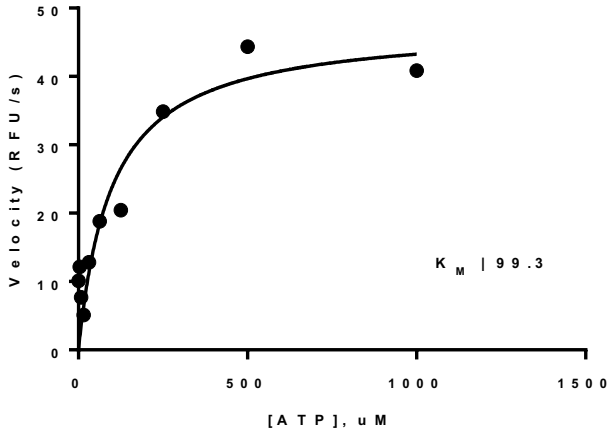

E527K Src
ATP K_m (μM) = 95 ± 5

M) Q529H

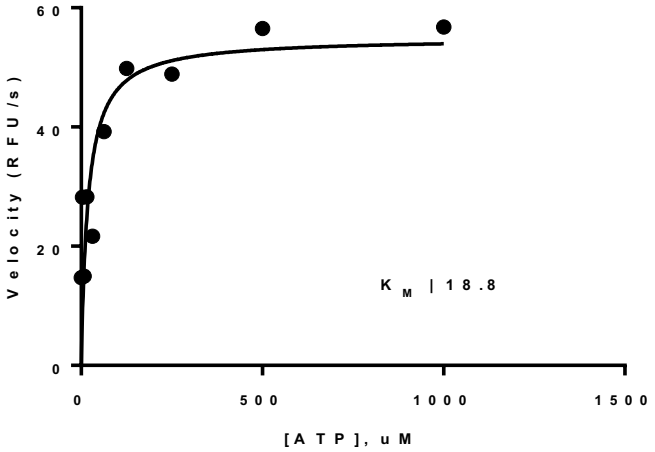

Q529H Src
ATP K_m (μM) = 14 ± 4

N) R98W

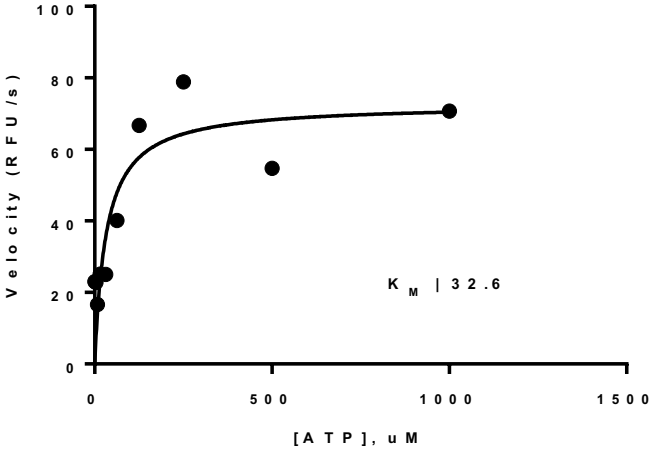

R98W Src
ATP K_m (μM) = 34 ± 5

O) D120N

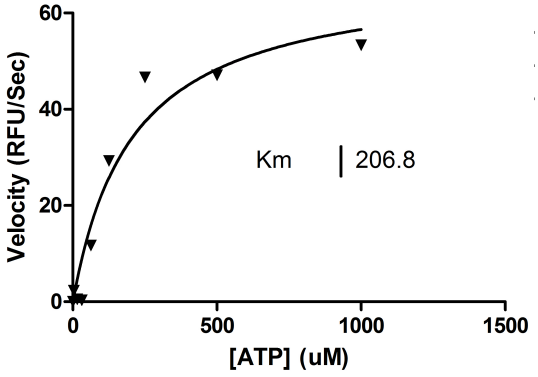

D120N Src
ATP K_m (μM) = 210 ± 5

P) W263A

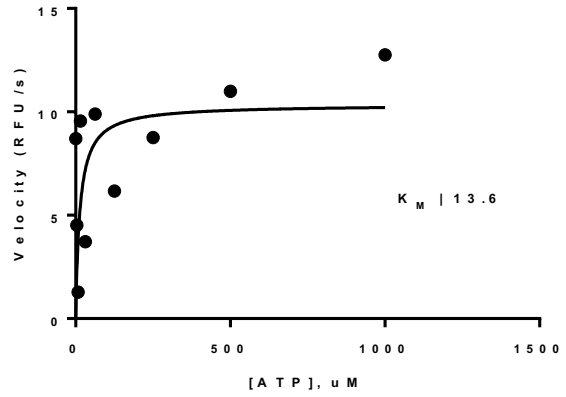

W263A Src
ATP K_m (μM) = 7 ± 3.5

Q) T341I

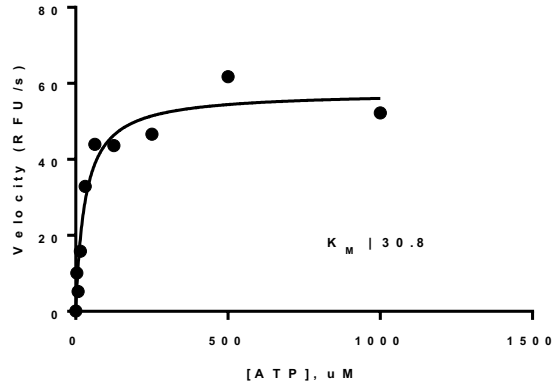

T341I Src
ATP K_m (μM) = 33 ± 4

R) T341G

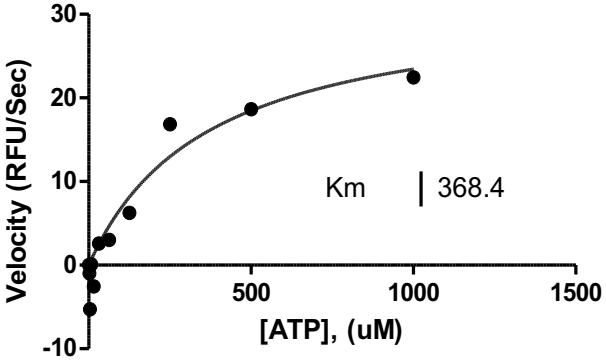

T341G Src
ATP K_m (μM) = 350 ± 30

S) T341M

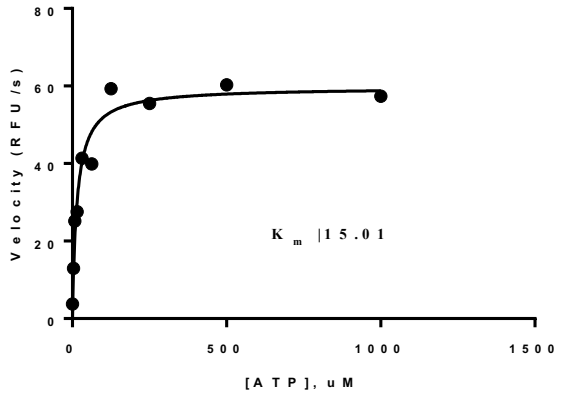

T341M Src
ATP K_m (μM) = 17 ± 3

T) Y419F

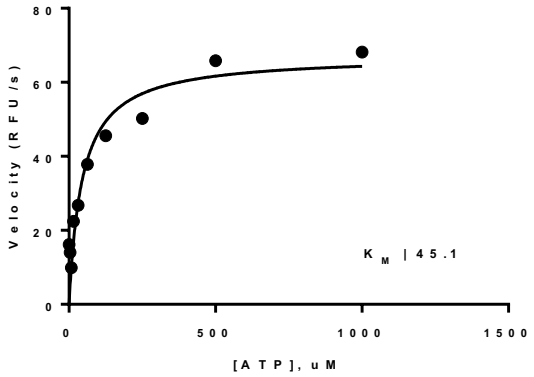

Y419F Src
ATP K_m (μM) = 46 ± 1

U) Y530F

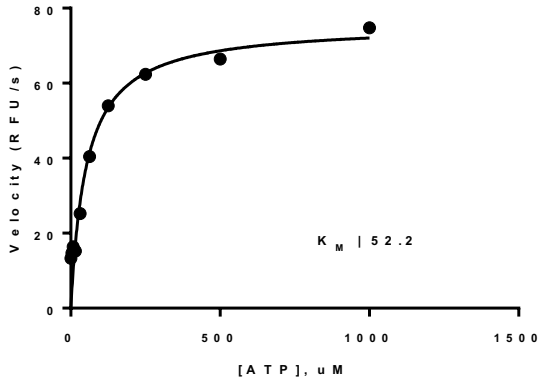

Y530F Src
ATP K_m(μM) = 54 ± 4

V) SH2Eng

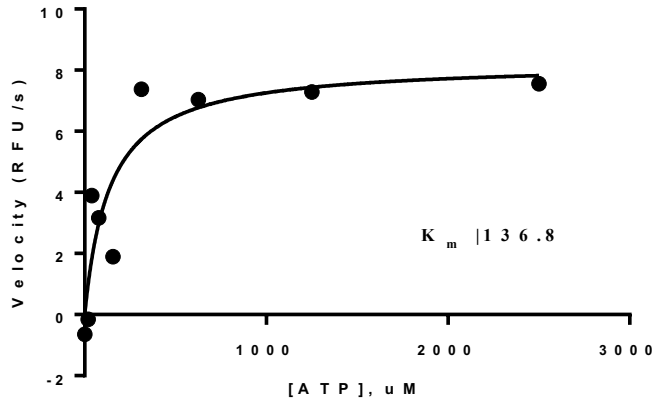

SH2Eng Src
ATP K_m (μM) = 140 ± 4

W) T341M^{SH2Eng}

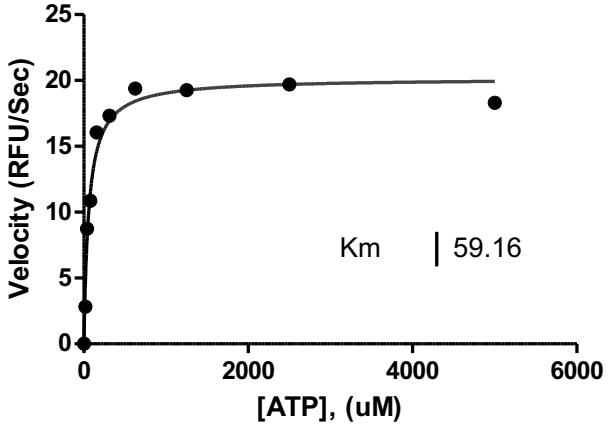

T341M^{SH2Eng} Src
ATP K_m (μM) = 50 ± 10

X) R98W^{SH2Eng}

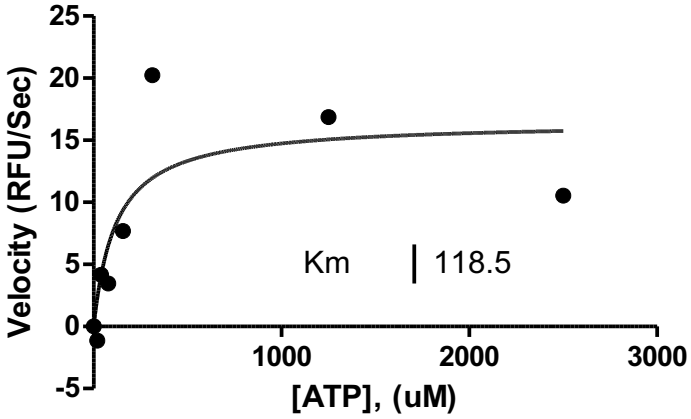

R98W^{SH2Eng} Src
ATP K_m (μM) = 120 ± 50

Y) W121R^{SH2Eng}

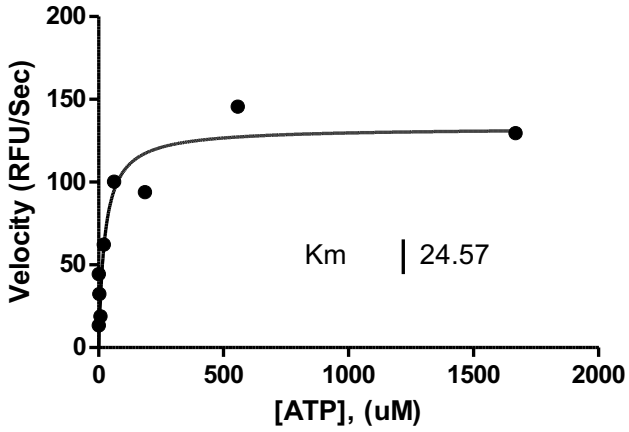

W121R^{SH2Eng} Src
ATP K_m (μM) = 20 ± 4

Table B.4. Comprehensive Table for ATP K_m of c-Src Mutants

c-Src Mutant	ATP K_m (μM)	c-Src Mutant	ATP K_m (μM)
WT-Src	51 ± 14	**I113F**	111 ± 12
pY419	170 ± 50	**W121R**	20 ± 4
pY530	340 ± 99	**T341R**	60 ± 10
W263A	7 ± 3.5	**D407H**	Dead
D407N	Dead	**E527K**	95 ± 5
F408A	Dead	**P171Q**	22 ± 6
K298M	Dead	**Y419F**	46 ± 1
K298R	Dead	**Y530F**	54 ± 4
T341G	350 ± 30	**T341I**	33 ± 4
F408G	Dead	**T341M**	17 ± 3
V140M	38 ± 3	**R98W**	34 ± 5
R163W	31 ± 4	**D120N**	210 ± 5
K298E	Dead	**Src^{SH2ENG}**	140 ± 4
P307R	17 ± 5	**$T341M^{SH2ENG}$**	50 ± 10
D521N	81 ± 9	**$R98W^{SH2ENG}$**	120 ± 50
Q529H	14 ± 4	**$W121R^{SH2ENG}$**	20 ± 4

Table B.5. Comprehensive Table for K_d of SH2-FITC Peptide with c-Src Mutants

c-Src Mutant	Peptide (3) Kd (nM)	c-Src Mutant	Peptide (3) Kd (nM)
WT-Src	729 ± 87	**W121R**	700 ± 150
pY419	> 10000	**T341R**	2100 ± 500
pY530	> 10000	**D407H**	146 ± 12
W263A	200 ± 90	**P171Q**	590 ± 40
F408A	500 ± 3	**Y419F**	682 ± 47
K298M	2126 ± 345	**T341M**	218 ± 44
K298R	> 5000	**R98W**	> 5000
T341G	140 ± 90	**D120N**	790 ± 90
F408G	1160 ± 130	**Src^{SH2ENG}**	> 10000
R163W	397 ± 89	**$T341M^{SH2ENG}$**	> 10000
Q529H	380 ± 20	**$R98W^{SH2ENG}$**	470 ± 80
		$W121R^{SH2ENG}$	290 ± 40

Table B.6. Comprehensive Table for c-Src Mutant Melting Temperatures

c-Src Mutant	Tm (°C)	c-Src Mutant	Tm (°C)
WT-Src	50.84 ± 0.34	**I113F**	48.60 ± 0.34
pY419	52.23 ± 0.30	**W121R**	46.95 ± 0.37
pY530	54.33 ± 0.14	**T341R**	N.T.
W263A	N.T.	**D407H**	N.T.
D407N	N.T.	**E527K**	50.66 ± 0.18
F408A	52.80 ± 0.12	**P171Q**	48.56 ± 0.61
K298M	N.T.	**Y419F**	51.13 ± 0.10
K298R	47.90 ± 0.20	**Y530F**	52.15 ± 0.06
T341G	54.22 ± 0.33	**T341I**	N.T.
F408G	48.00 ± 0.08	**T341M**	47.41 ± 0.07
V140M	N.T.	**R98W**	45.33 ± 0.33
R163W	50.59 ± 0.07	**D120N**	N.T.
K298E	44.52 ± 0.54	**Src^{SH2ENG}**	54.43 ± 0.10
P307R	N.T.	**T341M^{SH2ENG}**	51.22 ± 0.74
D521N	50.66 ± 0.40	**R98W^{SH2ENG}**	50.15 ± 0.14
Q529H	48.77 ± 0.26	**W121R^{SH2ENG}**	52.13 ± 0.55
Y530F Src • 1	53.08 ± 0.36	**Y530F Src • 2**	53.20 ± 0.42
Wt 3D-Src• 1	53.12 ± 0.35	**Wt 3D-Src • 2**	55.37 ± 0.88

N.T. = Not Tested

Phosphorylation Rate Determination of 3.1 & 3.2 Src Complexes

Figure B.5. Phosphorylation Rate Determination with **3.1** and **3.2** c-Src

ProQDiamond Stain (Left), SyproRuby Stain (Right)

A) Wt-Src – **3.1** + Csk

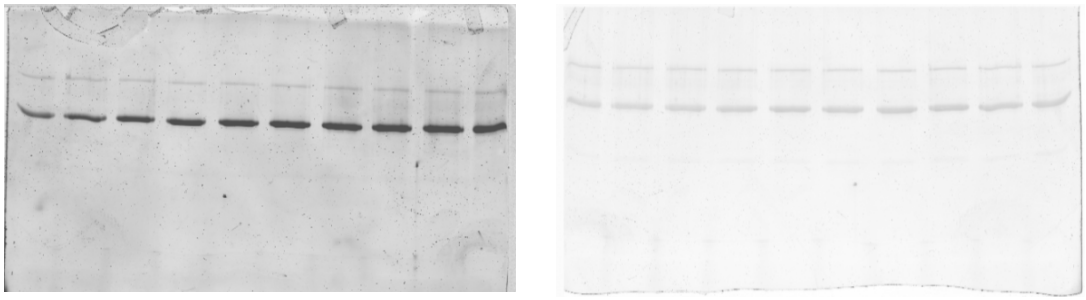

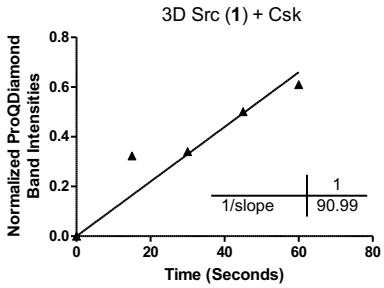

B) Wt-Src – **3.2** + Csk

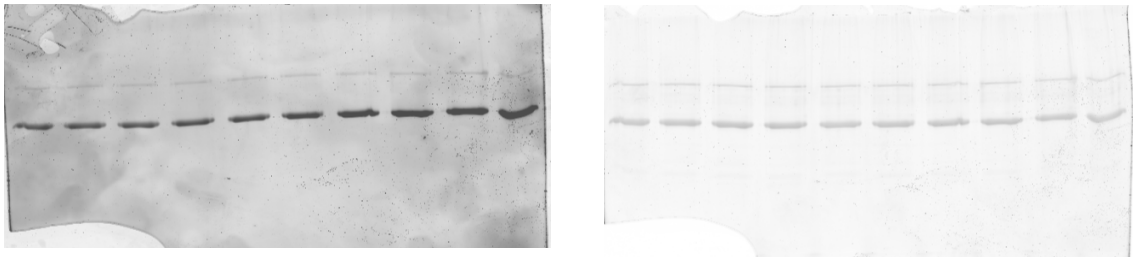

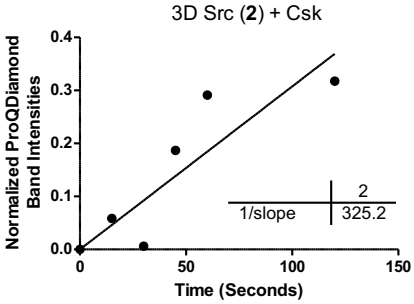

C) Src^{Y530F} – **3.1** + 3D-Hck

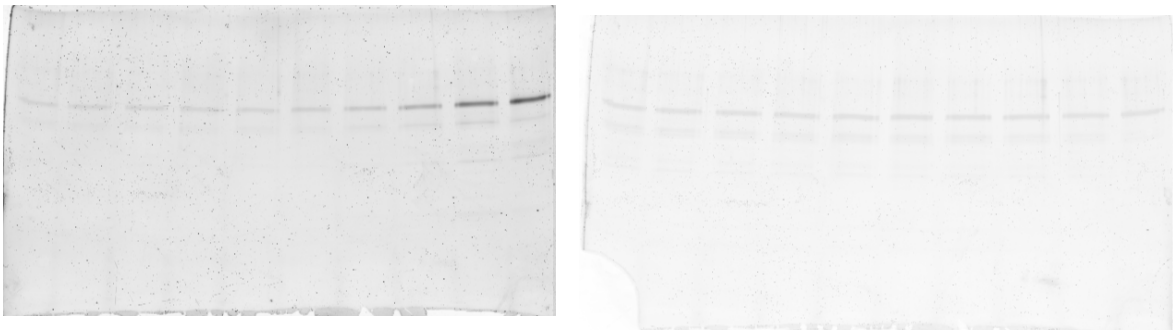

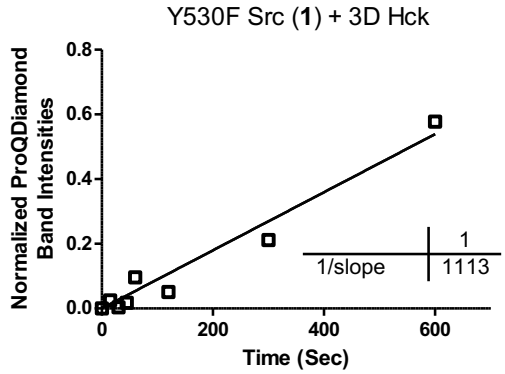

D) Src^{Y530F} – **3.2** + 3D-Hck

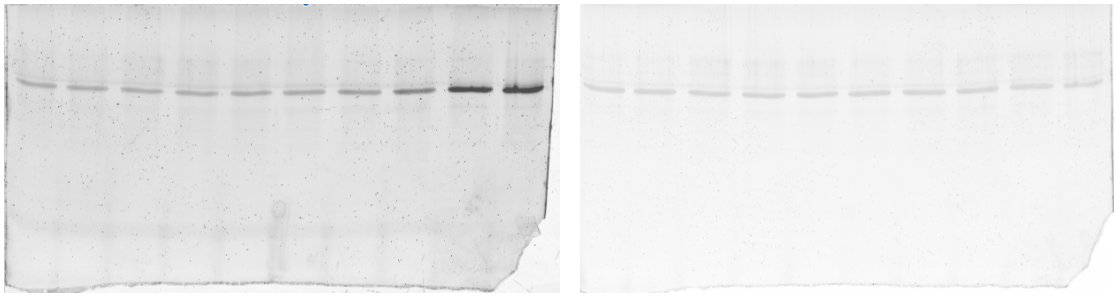

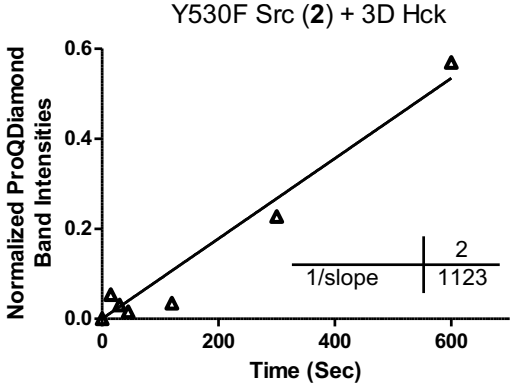

E) Src^{Y530F} – **3.1** + Kd-Hck

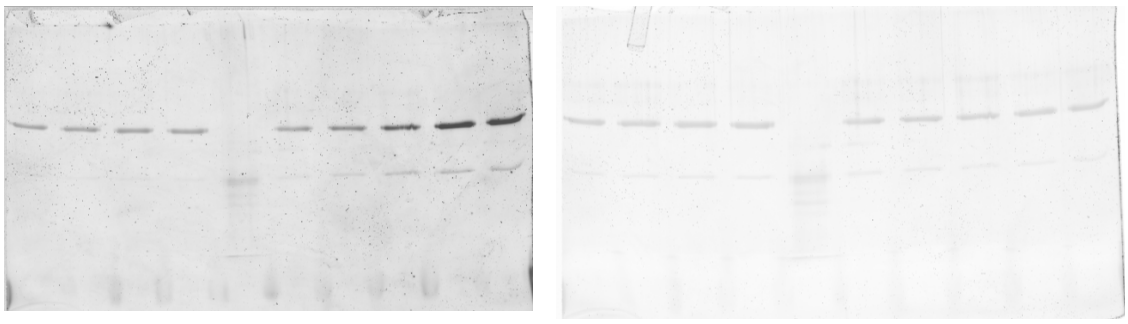

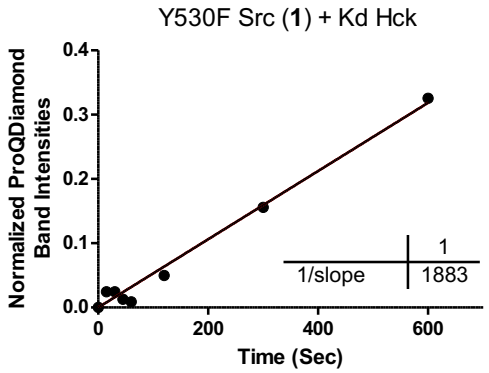

F) Src^{Y530F} – **3.2** + Kd-Hck

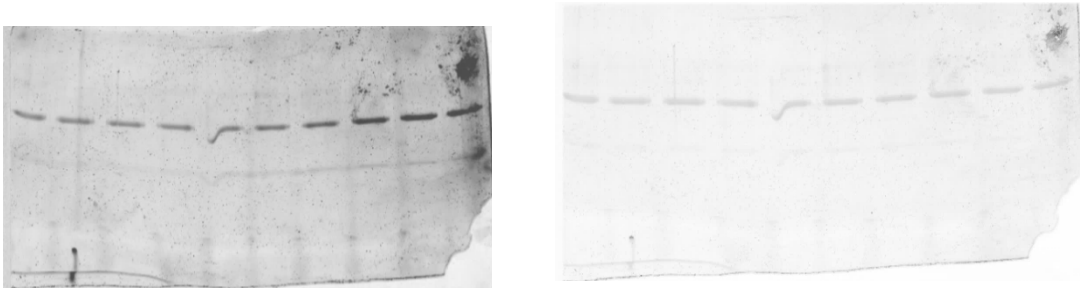

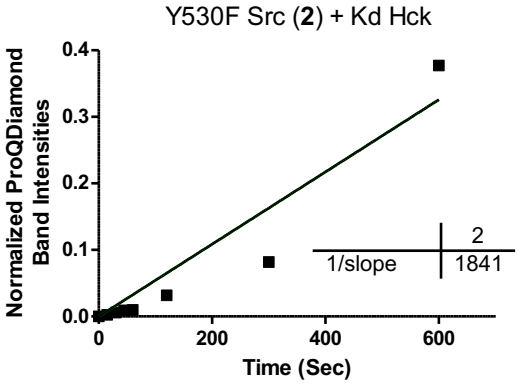

Table B.7. Initial Phosphorylation Rates of Irreversible Bound Constructs

	Src• 3.1 Kd Hck	Src• 3.2 Kd Hck	Src• 3.1 3D Hck	Src• 3.2 3D Hck	Src• 3.1 Csk	Src• 3.2 Csk
1/Slope	1883	1841	1113	1123	90.99	325.2

Spectral Data of Compounds 3.1, 3.2, 3.7, 3.9 – 3.12

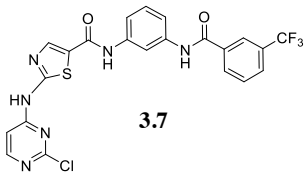

3.7

^{1}H:

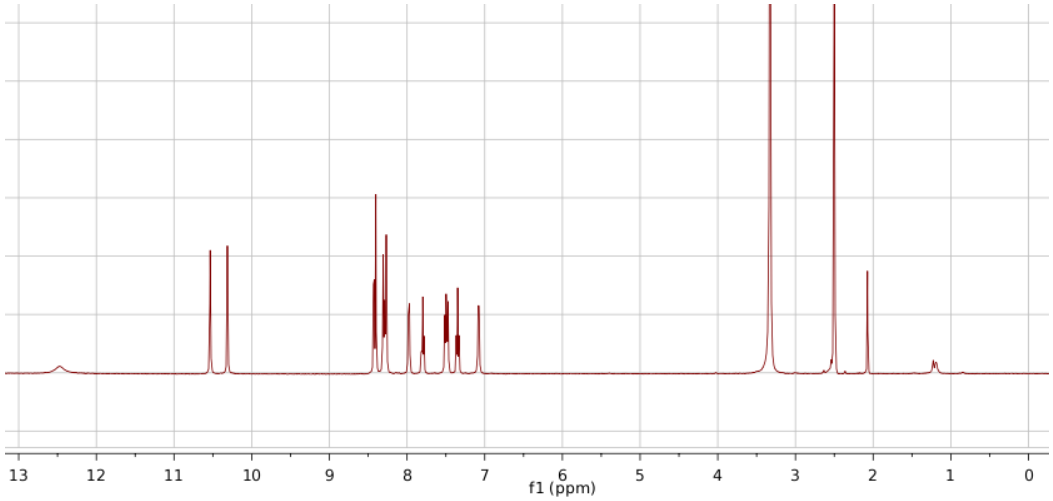

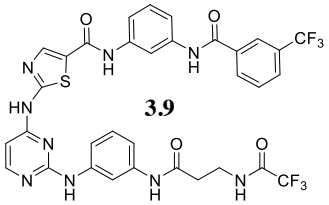

3.9

^{1}H:

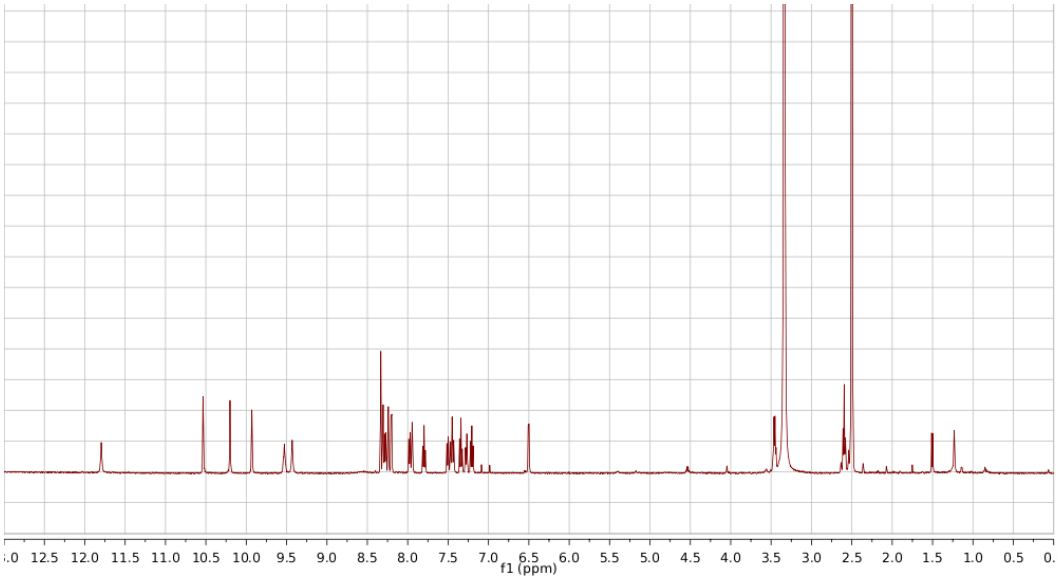

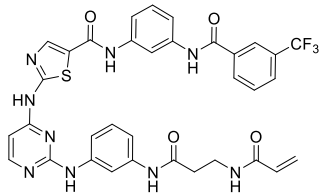

3.1

^{1}H:

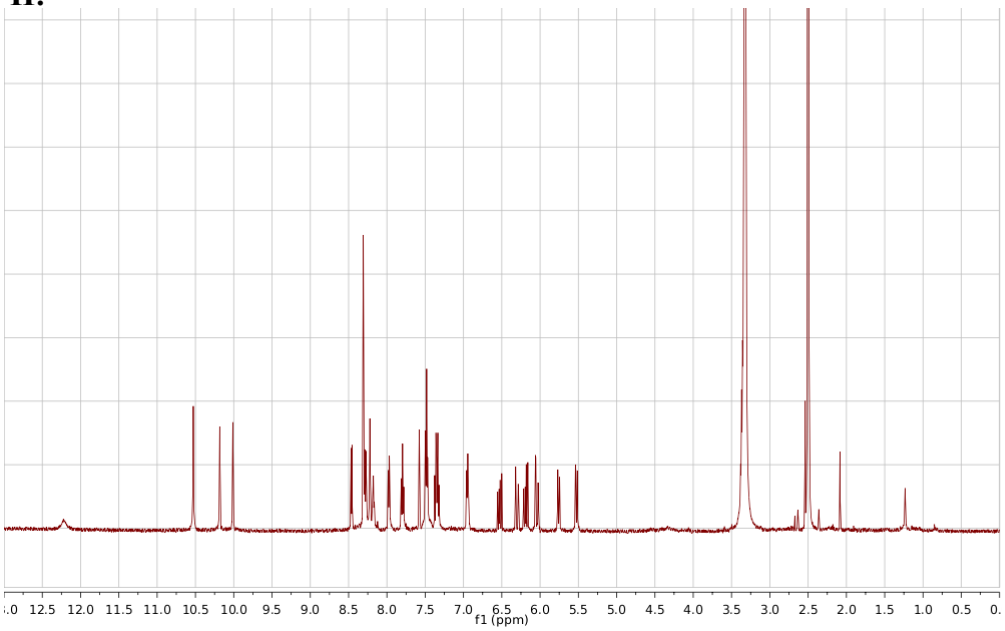
12.5 12.0 11.5 11.0 10.5 10.0 9.5 9.0 8.5 8.0 7.5 7.0 6.5 6.0 5.5 5.0 4.5 4.0 3.5 3.0 2.5 2.0 1.5 1.0 0.5
f1 (ppm)

^{13}C:

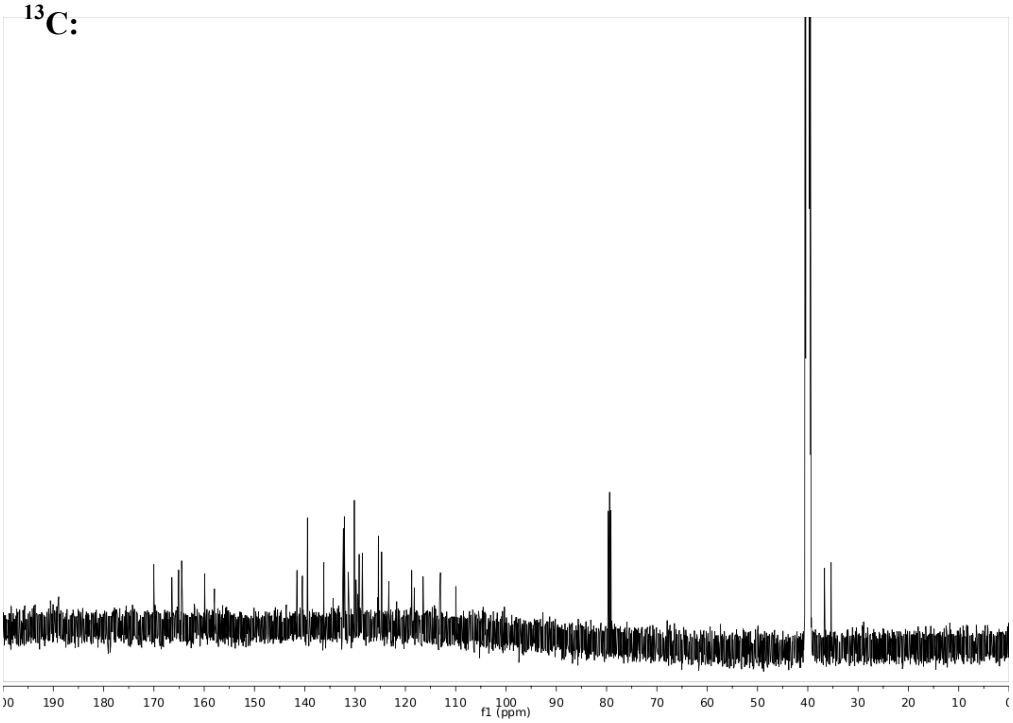
190 180 170 160 150 140 130 120 110 100 90 80 70 60 50 40 30 20 10
f1 (ppm)

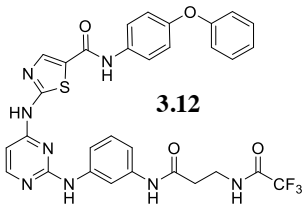

3.12

^{1}H:

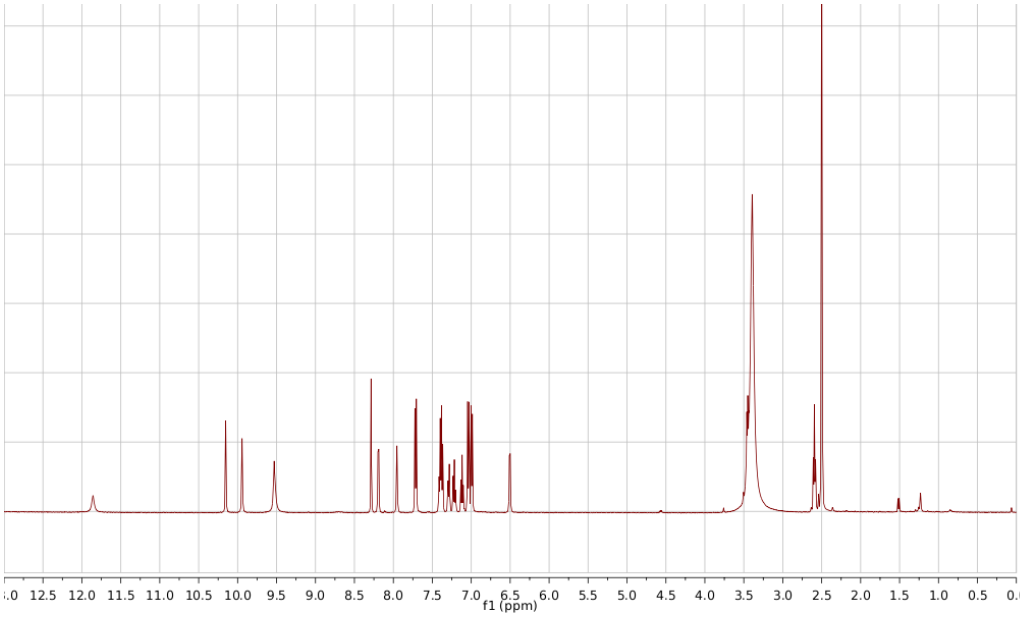

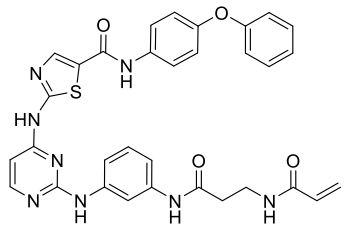

3.2

^{1}H:

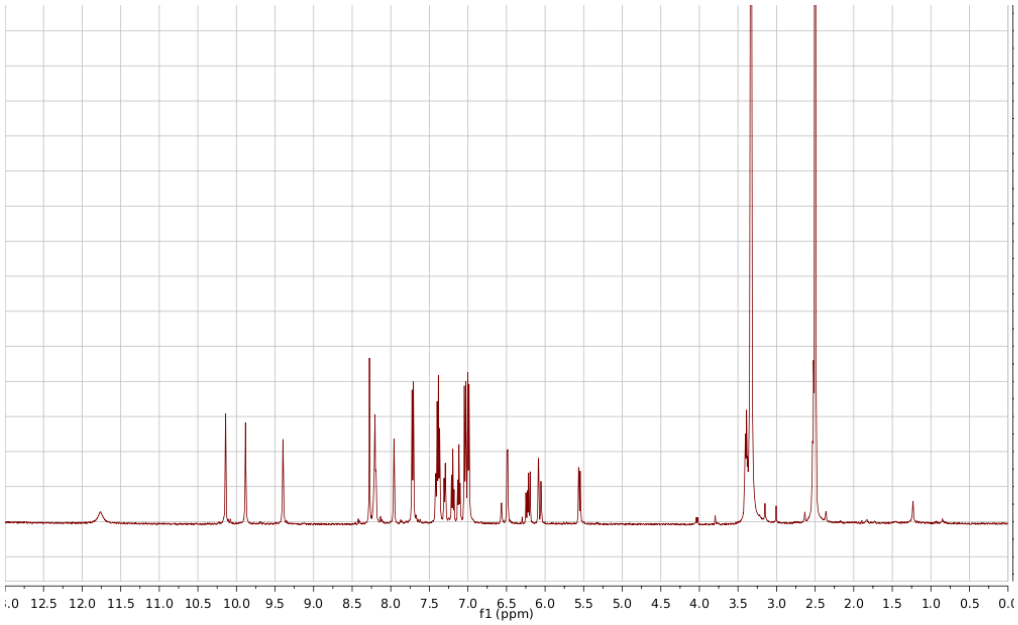

^{13}C:

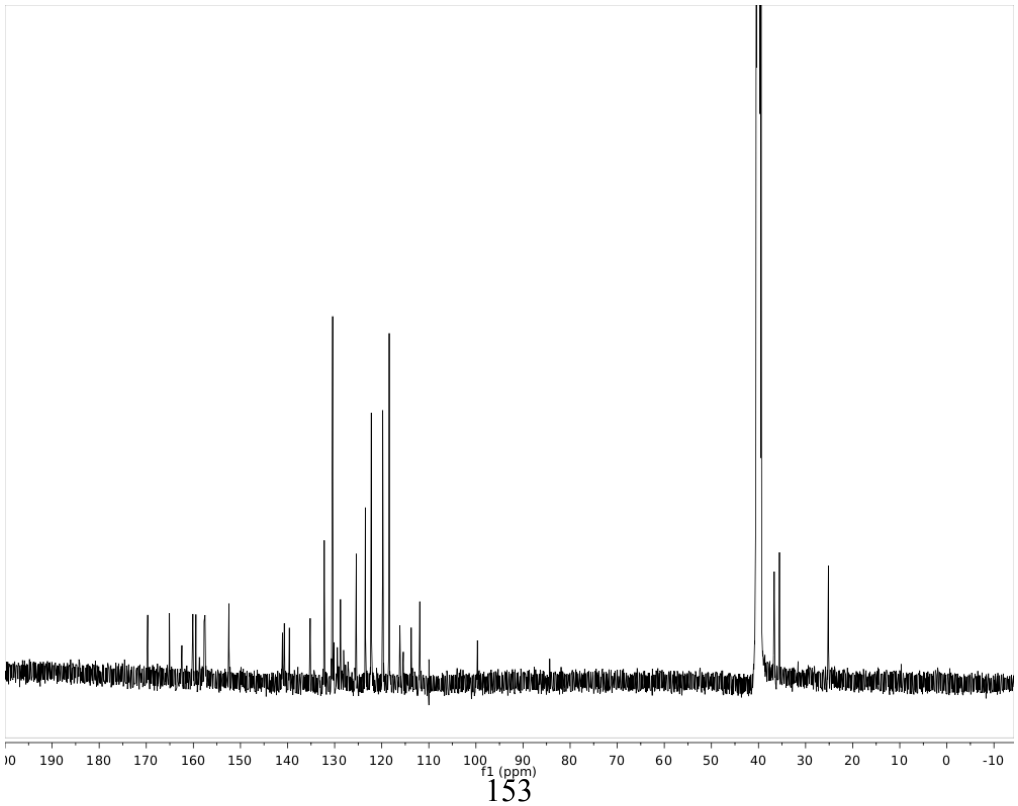

K_{off} Rates for BODIPY Compounds 3.3 & 3.4

Figure B.6. K_{off} Rates for BODIPY Compounds 3.3 & 3.4

A) Wt Src + **3.3** K_{off} = 0.0104 $M^{-1}min^{-1}$ $T_{1/2}$ = 67 mins

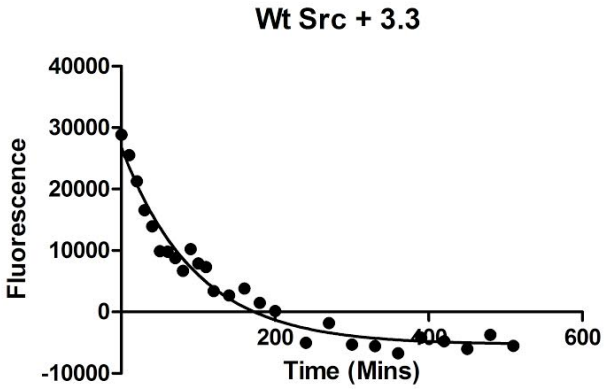

	Src + 3.3
K	0.01040
Half Life	66.65

B) Wt Src + **3.4** K_{off} = 0.0107 $M^{-1}min^{-1}$ $T_{1/2}$ = 65 mins

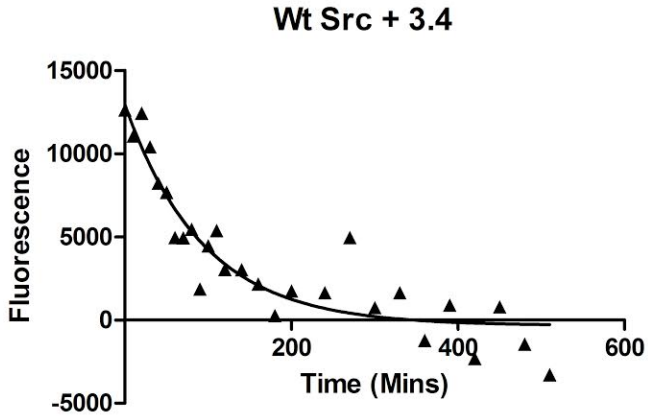

	Src + 3.4
K	0.01066
Half Life	65.04

C) pY419 Src + **3.3** K_{off} = 0.006 $M^{-1}min^{-1}$ $T_{1/2}$ = 119 mins

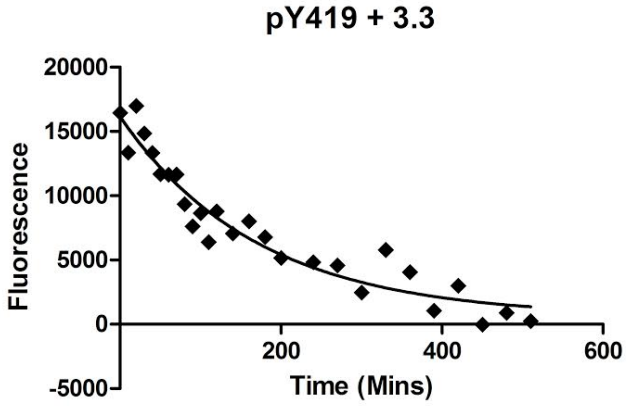

	pY419 + 3.3
K	0.005840
Half Life	118.7

D) pY419 Src + **3.4** K_{off} = 0.0101 $M^{-1}min^{-1}$ $T_{1/2}$ = 69 mins

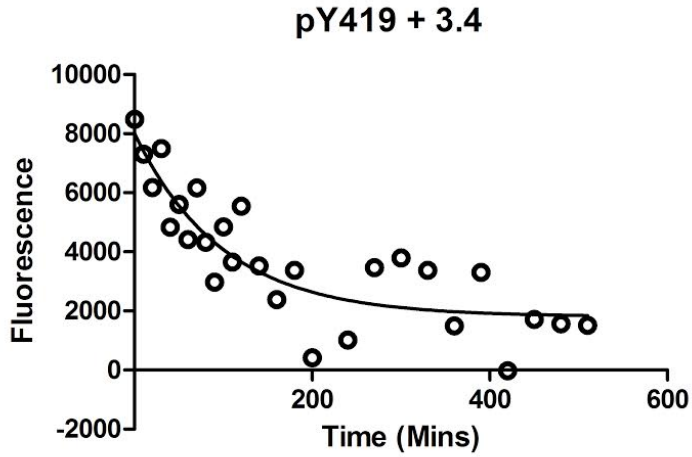

	pY419 + 3.4
K	0.01006
Half Life	68.88

E) pY530 + **3.3** K_{off} = 0.0253 $M^{-1}min^{-1}$ $T_{1/2}$ = 27 mins

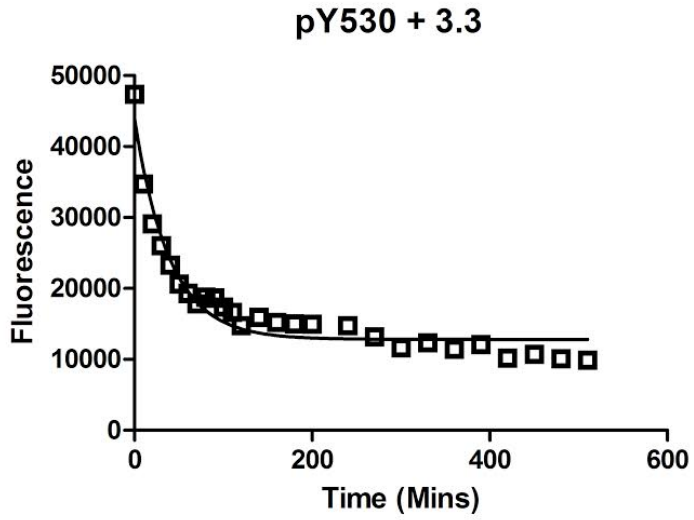

	pY530 + 3.3
K	0.02532
Half Life	27.37

F) pY530 + **3.4** K_{off} = 0.0217 $M^{-1}min^{-1}$ $T_{1/2}$ = 32 mins

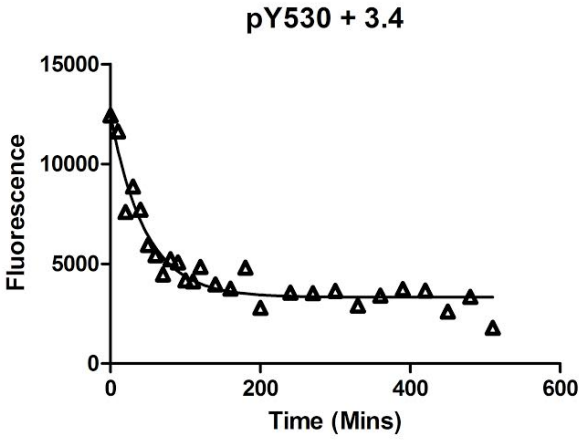

	pY530 + 3.4
K	0.02171
Half Life	31.92

K_d Determination for BODIPY Compounds 3.3 & 3.4

Figure B.7. K_d Determination for BODIPY Compounds 3.3 & 3.4

A) **3.3** + Wt-Src K_d Curve. **Average K_d = 10.5 nM**

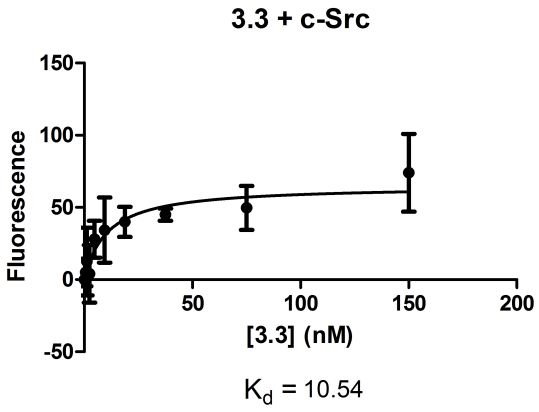

B) **3.4** + Wt-Src K_d Curve. **Average K_d = 5.8 nM**

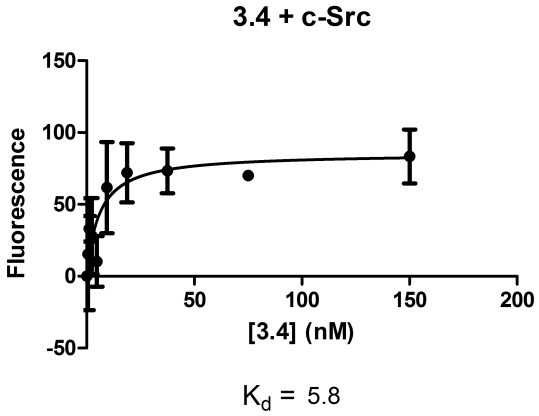

C) **3.3** + pY419 Src K_d Curve. **Average K_d = 3.1 nM**

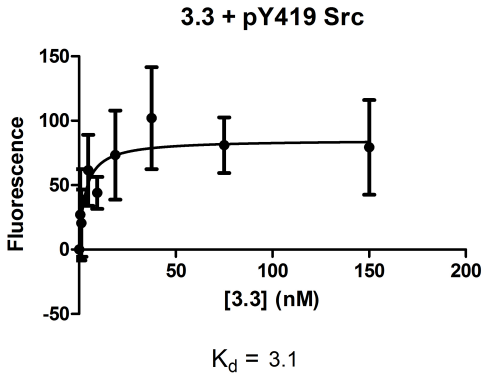

D) **3.4** + pY419 Src K_d Curve. **Average K_d = 2.4 nM**

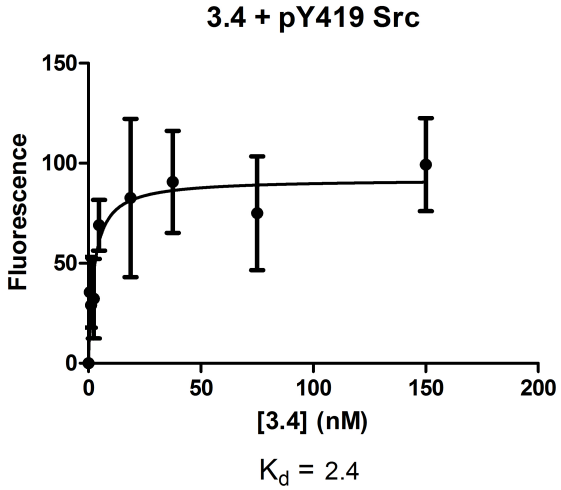

E) **3.3** + Src^{SH2Eng} K_d Curve. **Average K_d = 2.5 nM**

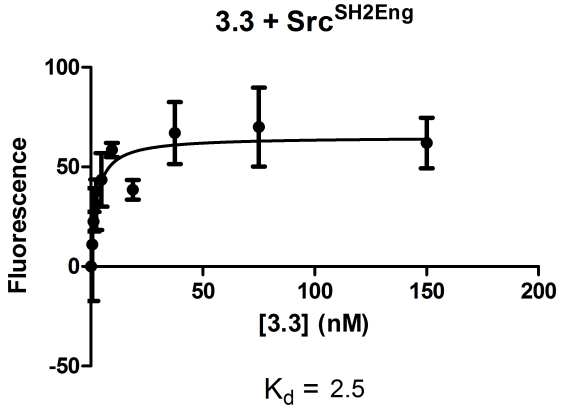

F) **3.4** + Src^{SH2Eng} K_d Curve. **Average K_d = 5.3 nM**

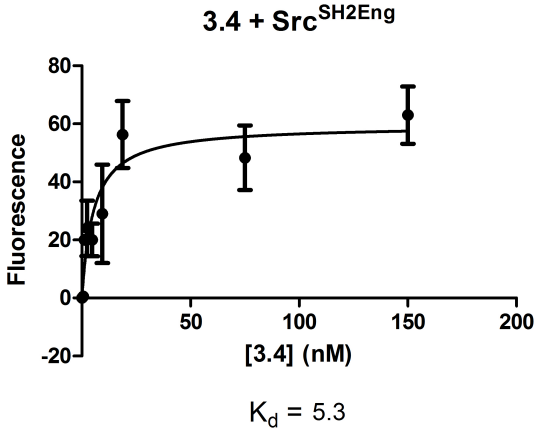

Appendix C

Analytical Data and Supplemental Information for Chapter IV

Selective Proteolysis Results for c-Src Inhibitors

Figure C.1. Selective Proteolysis Results for c-Src Inhibitors

A) Compound **4.1** (60 μM) with 2 μM c-Src & 60 nM Thermolysin $\mathbf{T_{1/2}}$ = **2.7 mins**

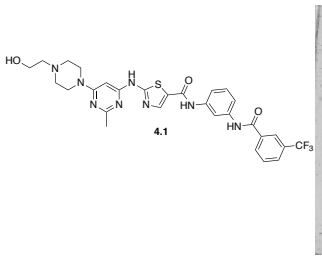

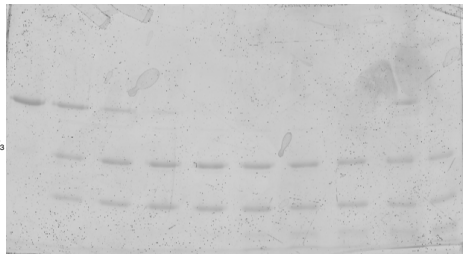

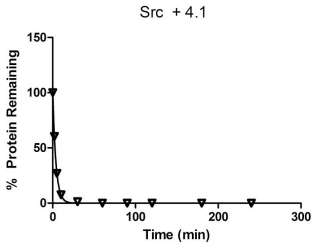

	4.1
Half Life	2.7

B) Compound **4.2** (60 μM) with 2 uM c-Src & 60 nM Thermolysin $\mathbf{T_{1/2}}$ = **82 mins**

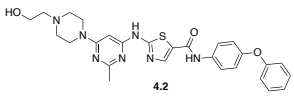

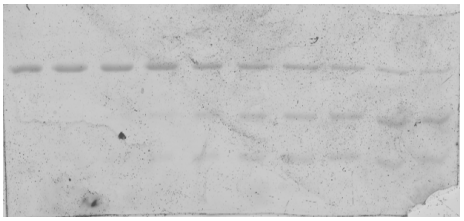

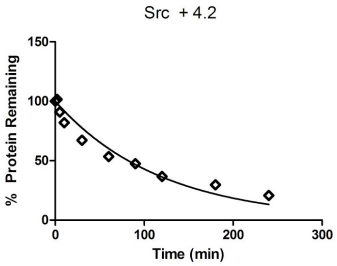

	4.2
Half Life	82

C) Compound **4.3** (60 μM) with 2 μM c-Src & 60 nM Thermolysin $\mathbf{T_{1/2}}$ = 4.5 mins

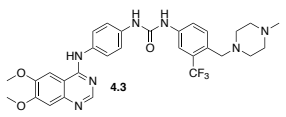

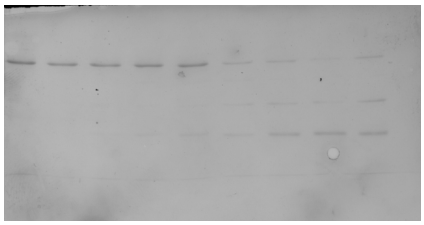

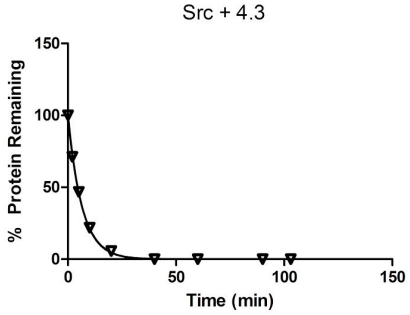

	4.3
Half Life	4.498

D) Compound **4.4** (60 μM) with 2 μM c-Src & 60 nM Thermolysin $\mathbf{T_{1/2}}$ = 100 mins

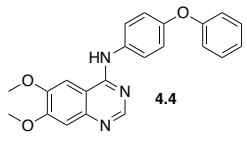

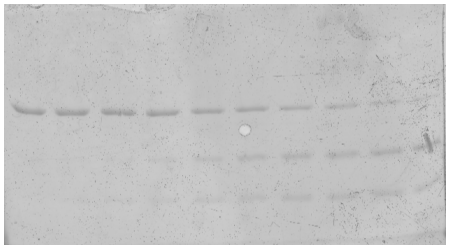

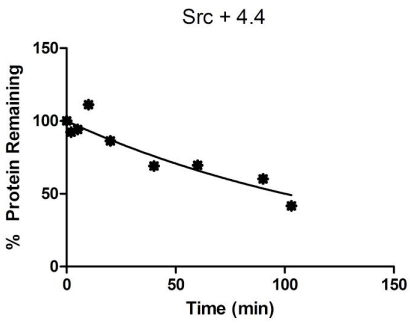

	4.4
Half Life	100.2

E) Compound **4.5** (60 μM) with 2 μM c-Src & 60 nM Thermolysin $\mathbf{T_{1/2}}$ **= 2.2 mins**

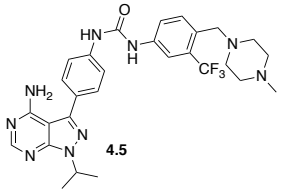

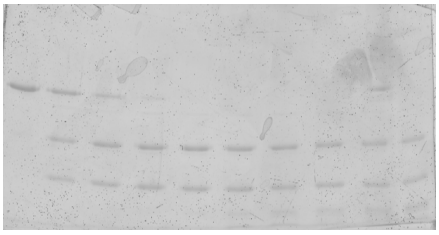

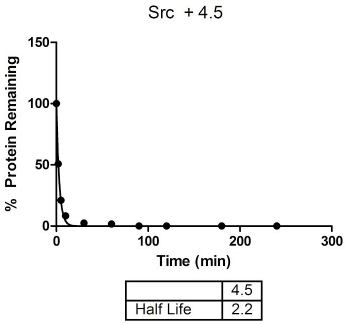

	4.5
Half Life	2.2

F) Compound **4.6** (60 μM) with 2 μM c-Src & 60 nM Thermolysin $\mathbf{T_{1/2}}$ **= 71 mins**

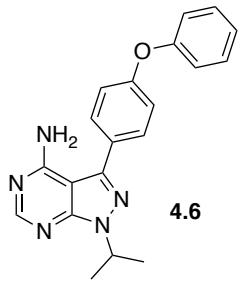

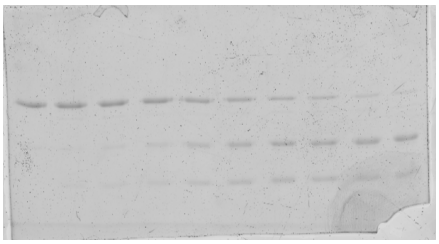

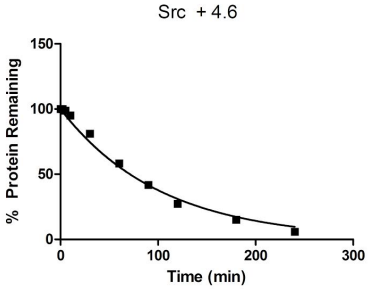

	4.6
Half Life	71

G) Compound **4.7** (60 μM) with 2 μM c-Src & 60 nM Thermolysin $\mathbf{T_{1/2}}$ **= 3.7 mins**

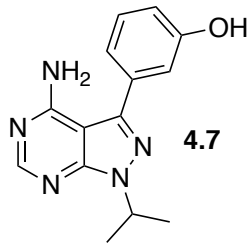

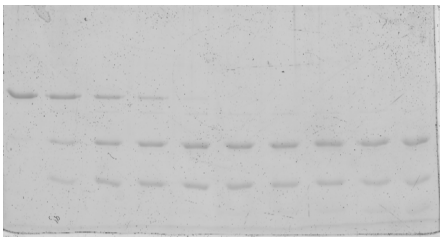

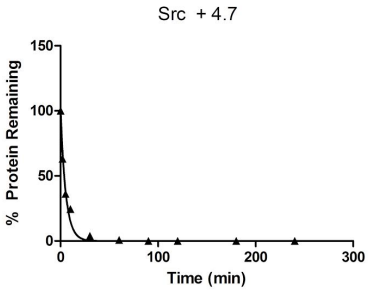

	4.7
Half Life	3.7

H) Compound **4.8** (60 μM) with 2 μM c-Src & 60 nM Thermolysin $\mathbf{T_{1/2}}$ **= 9.1 mins**

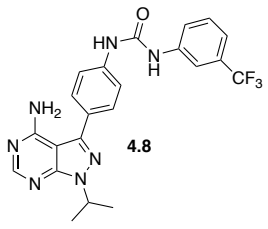

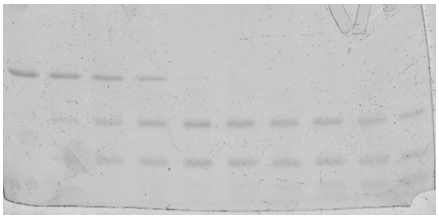

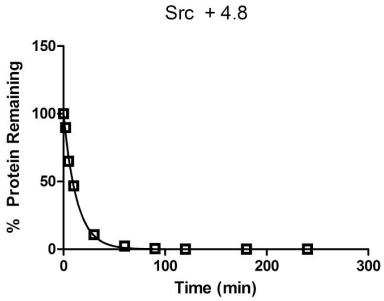

	4.8
Half Life	9.1

I) Compound **4.9** (60 μM) with 2 μM c-Src & 60 nM Thermolysin $\mathbf{T_{1/2}}$ **= 11 mins**

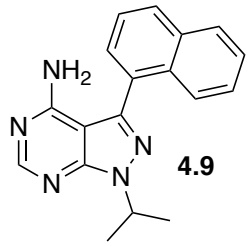

4.9

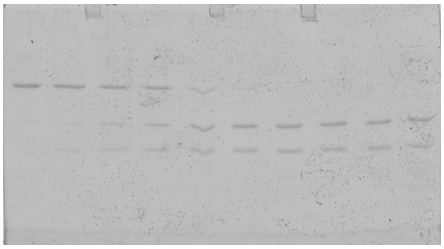

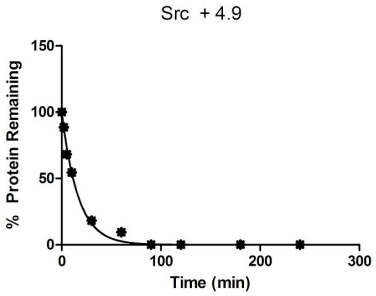

	4.9
Half Life	11

J) Compound **4.10** (60 μM) with 2 μM c-Src & 60 nM Thermolysin $\mathbf{T_{1/2}}$ **= 13 mins**

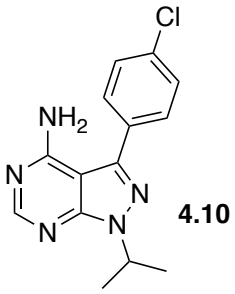

4.10

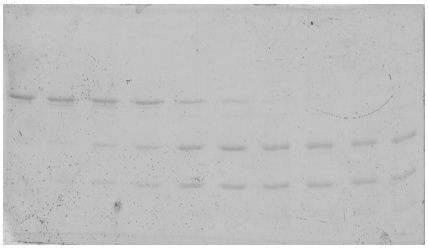

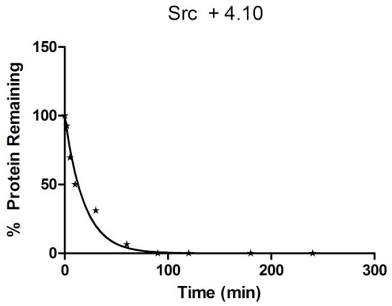

	4.10
Half Life	13

K) Compound **4.11** (60 μM) with 2 μM c-Src & 60 nM Thermolysin $\mathbf{T_{1/2}}$ **= 13 mins**

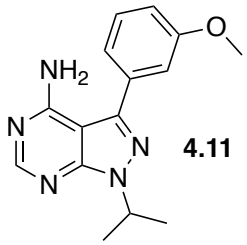

4.11

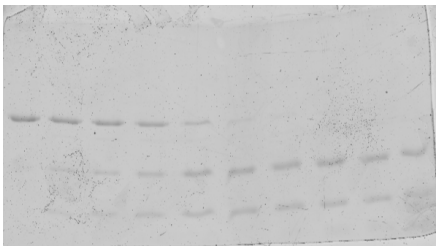

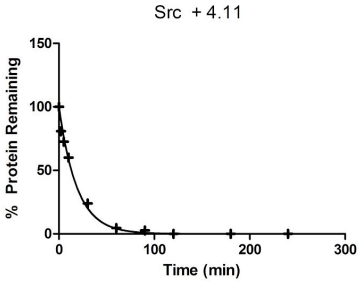

	4.11
Half Life	13

L) Compound **4.12** (60 μM) with 2 μM c-Src & 60 nM Thermolysin $\mathbf{T_{1/2}}$ **= 14 mins**

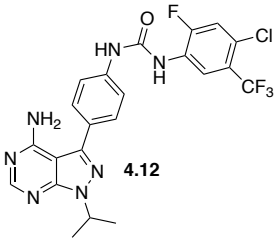

4.12

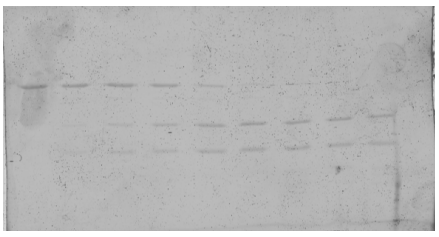

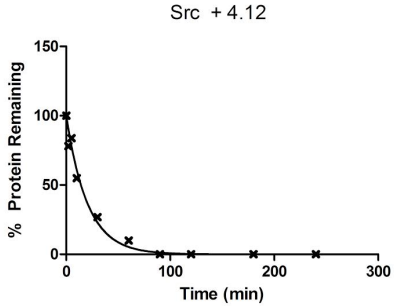

	4.12
Half Life	14

M) Compound **4.13** (60 μM) with 2 μM c-Src & 60 nM Thermolysin $\mathbf{T_{1/2}}$ **= 16 mins**

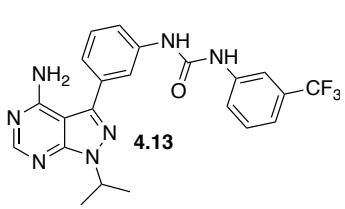

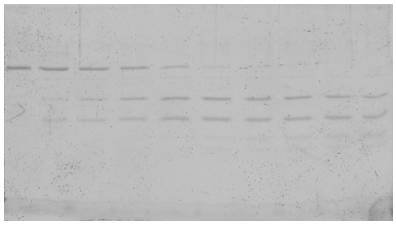

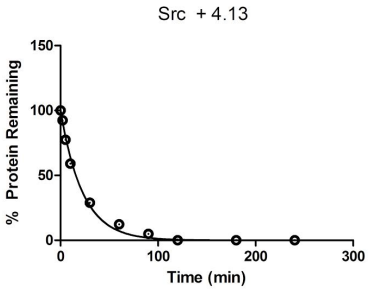

	4.13
Half Life	16

N) Compound **4.14** (60 μM) with 2 μM c-Src & 60 nM Thermolysin $\mathbf{T_{1/2}}$ **= 16 mins**

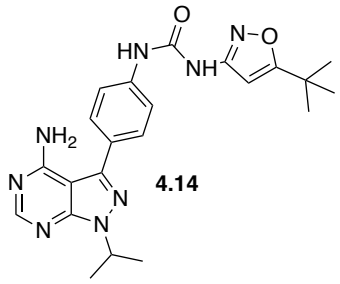

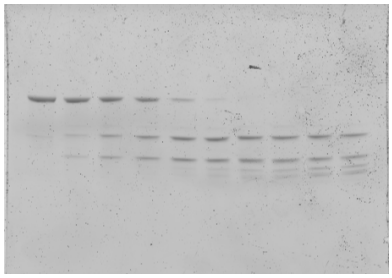

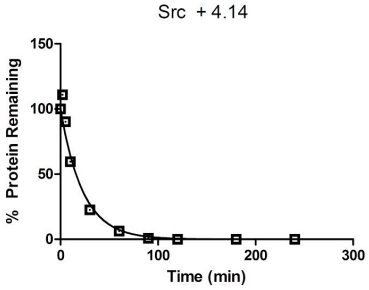

	4.14
Half Life	16

O) Compound **4.15** (60 μM) with 2 μM c-Src & 60 nM Thermolysin $\mathbf{T_{1/2}}$ **= 23 mins**

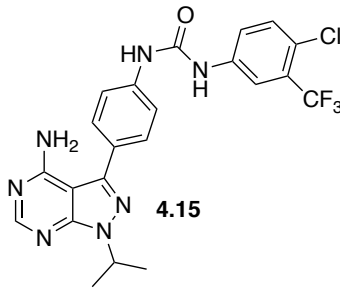

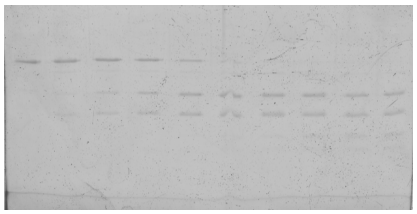

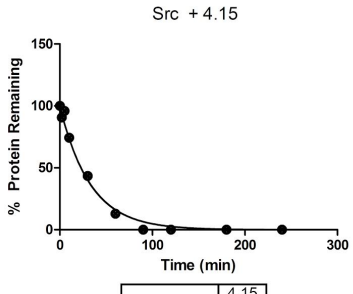

	4.15
Half Life	23

P) Compound **4.16** (60 μM) with 2 μM c-Src & 60 nM Thermolysin $\mathbf{T_{1/2}}$ **= 24 mins**

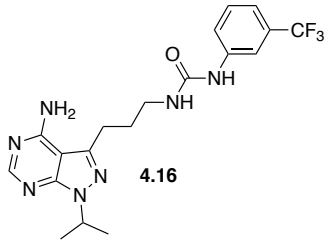

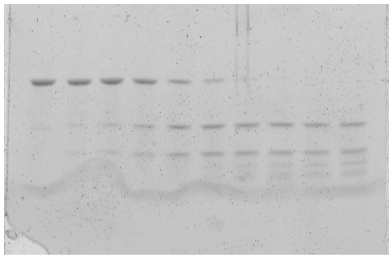

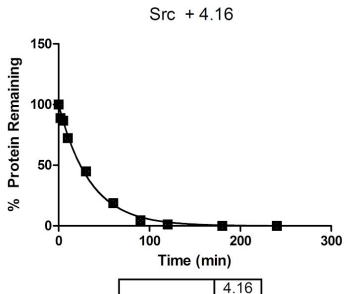

	4.16
Half Life	24

Q) Compound **4.17** (60 µM) with 2 µM c-Src & 60 nM Thermolysin $\mathbf{T_{1/2}}$ **= 36 mins**

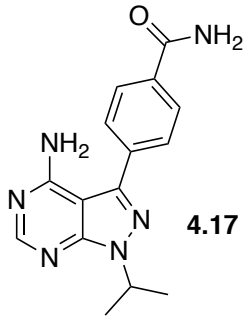

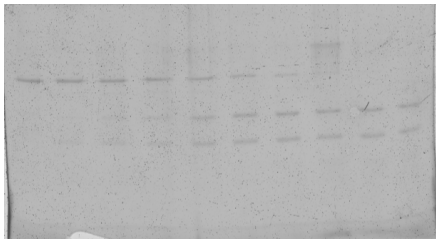

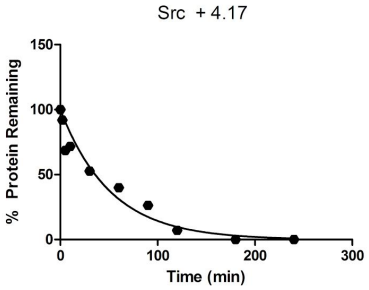

	4.17
Half Life	36

R) Compound **4.18** (60 µM) with 2 µM c-Src & 60 nM Thermolysın $\mathbf{T_{1/2}}$ **= 42 mins**

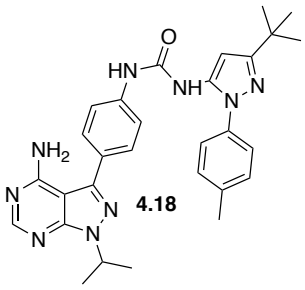

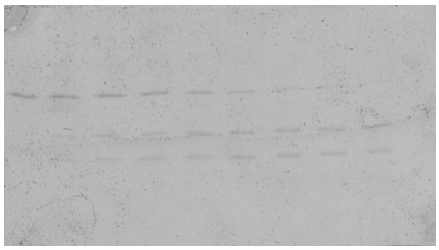

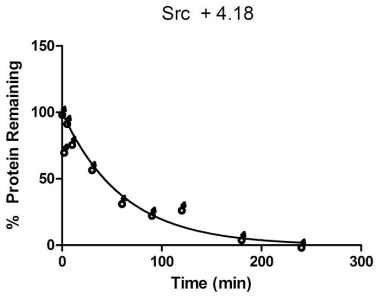

	4.18
Half Life	42

S) Compound **4.19** (60 µM) with 2 µM c-Src & 60 nM Thermolysin $\mathbf{T_{1/2}}$ **= 44 mins**

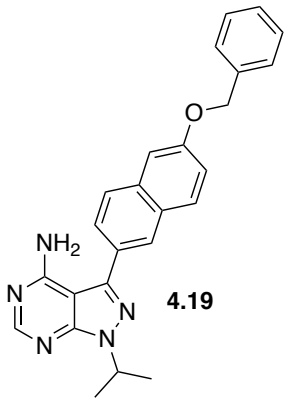

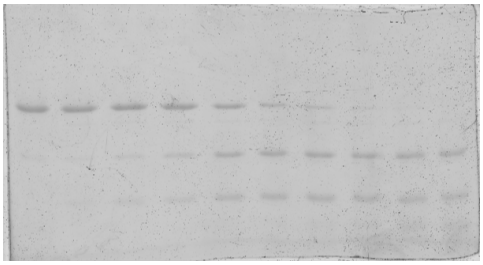

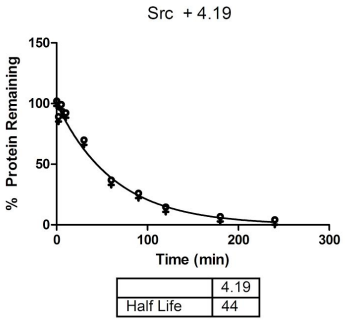

	4.19
Half Life	44

T) Compound **4.20** (60 µM) with 2 µM c-Src & 60 nM Thermolysin $\mathbf{T_{1/2}}$ **= 44 mins**

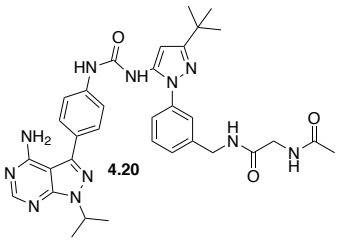

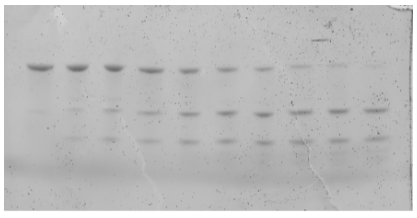

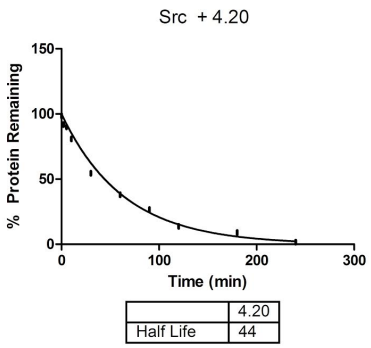

	4.20
Half Life	44

U) Compound **4.21** (60 μM) with 2 μM c-Src & 60 nM Thermolysin $\mathbf{T_{1/2}}$ **= 49 mins**

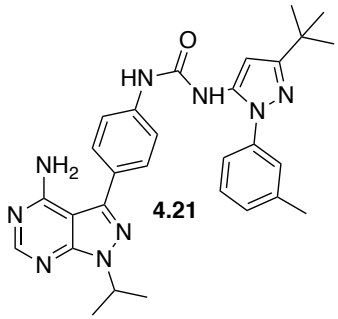

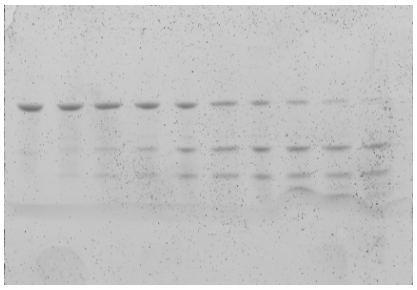

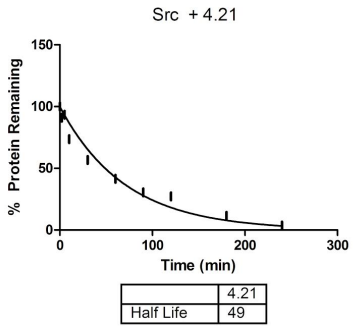

	4.21
Half Life	49

V) Compound **4.22** (60 μM) with 2 μM c-Src & 60 nM Thermolysin $\mathbf{T_{1/2}}$ **= 51 mins**

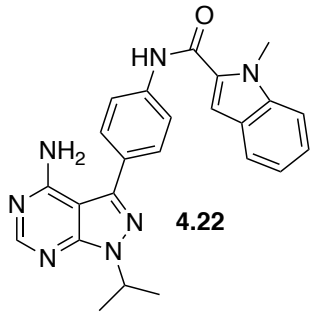

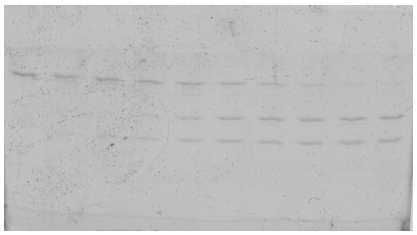

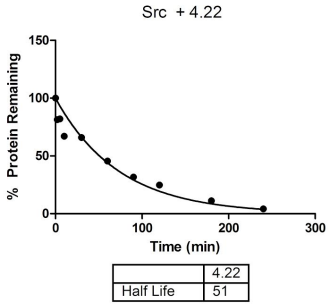

	4.22
Half Life	51

W) Compound **4.23** (60 μM) with 2 μM c-Src & 60 nM Thermolysin $\mathbf{T_{1/2}}$ **= 70 mins**

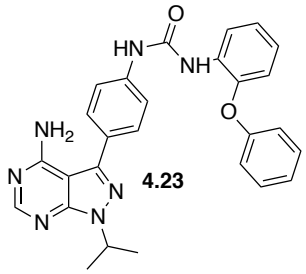

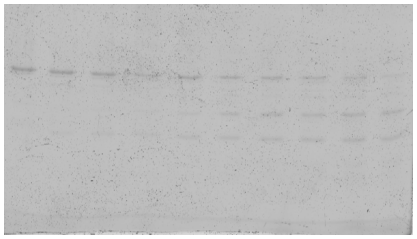

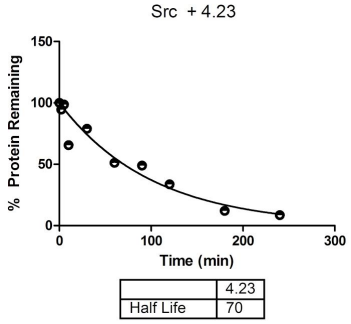

	4.23
Half Life	70

X) Compound **4.24** (60 μM) with 2 μM c-Src & 60 nM Thermolysin $\mathbf{T_{1/2}}$ **= 84 mins**

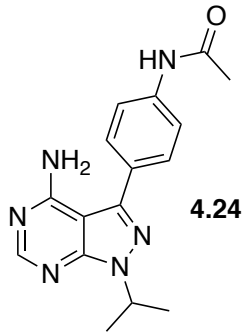

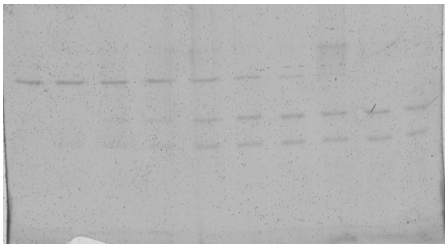

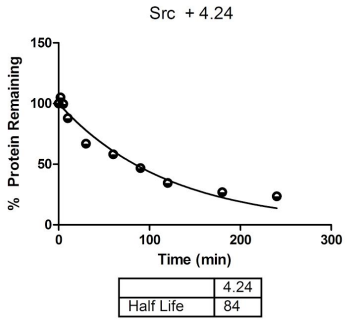

	4.24
Half Life	84

Y) Compound **4.25** (60 μM) with 2 μM c-Src & 60 nM Thermolysin $\mathbf{T_{1/2}}$ **= 85 mins**

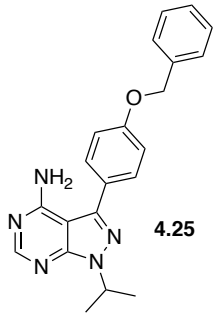

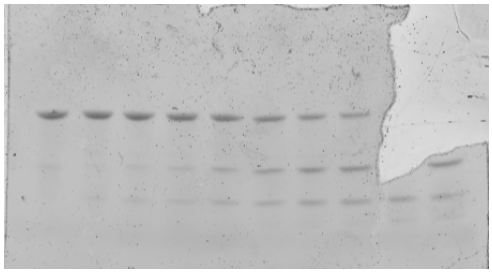

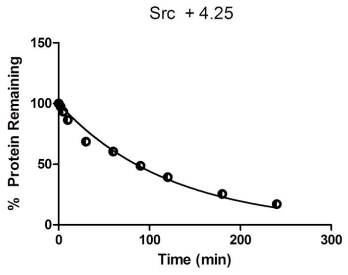

	4.25
Half Life	85

X) Compound **4.26** (60 μM) with 2 μM c-Src & 60 nM Thermolysin $\mathbf{T_{1/2}}$ **= 91 mins**

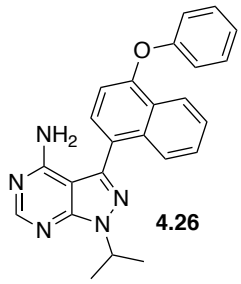

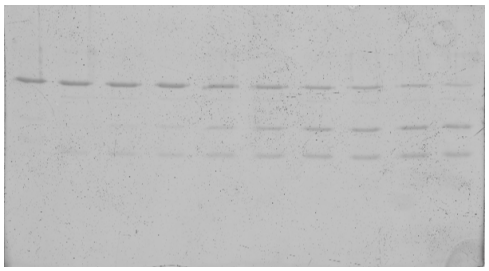

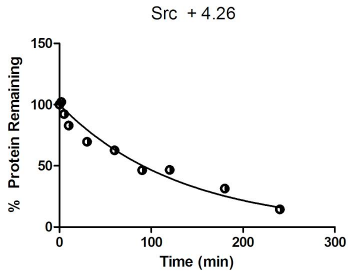

	4.26
Half Life	91

Y) Compound **4.27** (60 μM) with 2 μM c-Src & 60 nM Thermolysin $\mathbf{T_{1/2}}$ **= 94 mins**

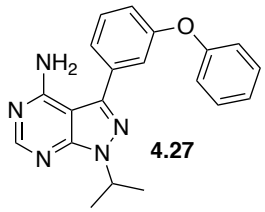

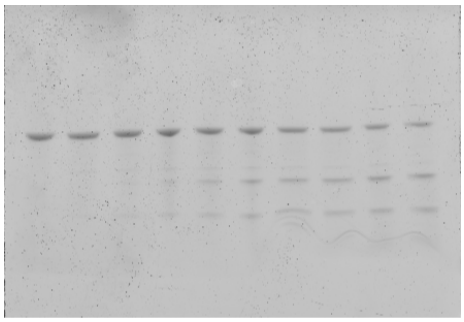

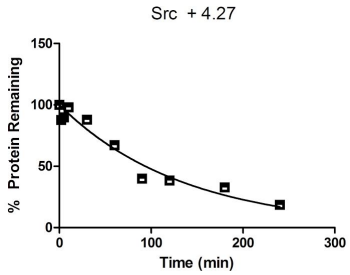

	4.27
Half Life	94

Z) Compound **4.28** (60uM) with 2 uM c-Src & 60 nM Thermolysin $\mathbf{T_{1/2}}$ **= 159 mins**

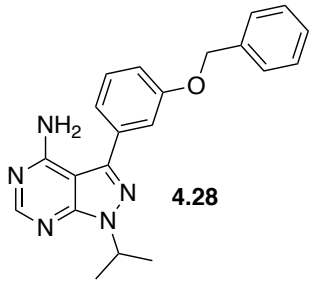

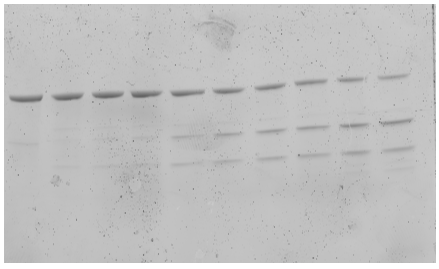

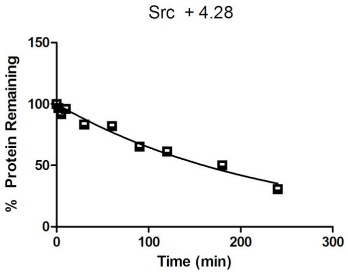

	4.28
Half Life	159

AA) **Dasatinib** (60 µM) with 2 µM c-Src & 60 nM Thermolysin $T_{1/2}$ = **3.1 mins**

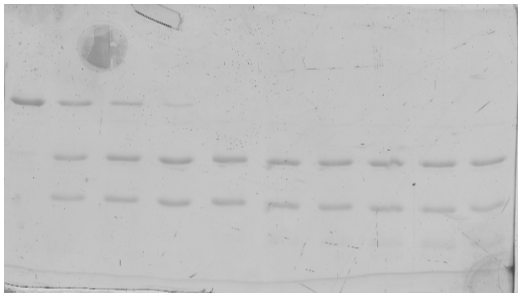

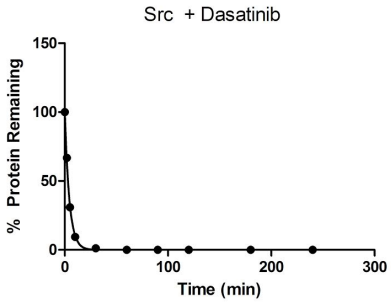

	Dasatinib
Half Life	3.1

BB) **Ponatinib** (60 µM) with 2 µM c-Src & 60 nM Thermolysin $T_{1/2}$ = **2.5 mins**

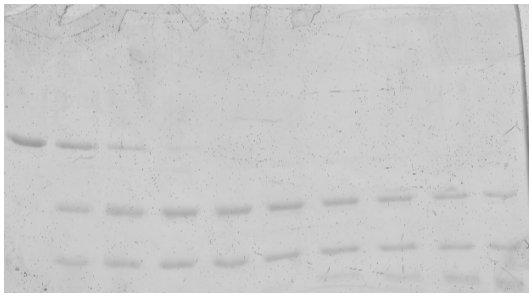

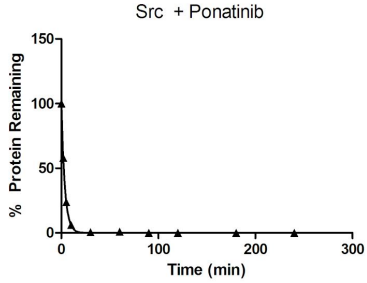

	Ponatinib
Half Life	2.5

CC) **Saracatinib** (60 µM) with 2 µM c-Src & 60 nM Thermolysin $T_{1/2}$ = **6.9 mins**

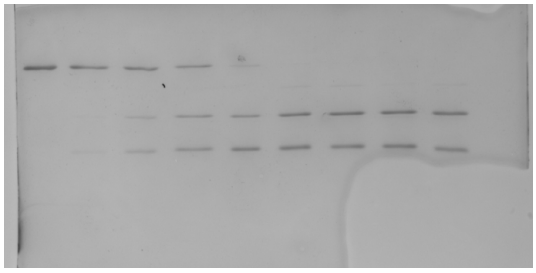

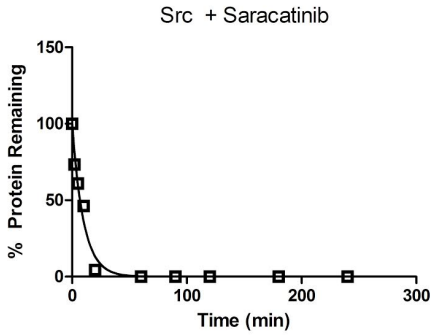

	Saracatinib
Half Life	6.9

DD) **Bousutinib** (60 µM) with 2 µM c-Src & 60 nM Thermolysin $T_{1/2}$ = **4.5 mins**

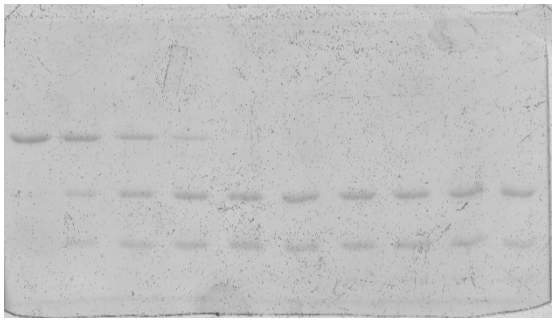

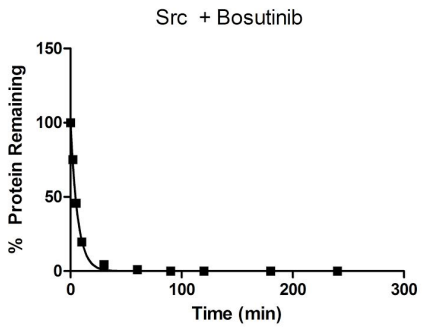

	Bosutinib
Half Life	4.5

Table C.1. Comprehensive Table of All Inhibitor Half-Lives

Compound	Half-Life (min)	Compound	Half-Life (min)
DMSO	33	4.16	24
4.1	2.7	4.18	42
4.2	82	4.19	44
4.3	4.5	4.20	44
4.4	100	4.21	49
4.5	2.2	4.22	51
4.6	71	4.23	70
4.7	3.7	4.24	80
4.8	9.1	4.25	85
4.9	11	4.26	91
4.10	13	4.27	94
4.11	13	4.28	159
4.12	14	Dasatinib	3.1
4.13	16	Ponatinib	4.5
4.14	16	Bosutinib	2.5
4.15	23	Saracatinib	6.9

Spectral Data for Compounds 4.5, 4.11 – 4.14, 4.16 – 4.18, 4.20 - 4.28

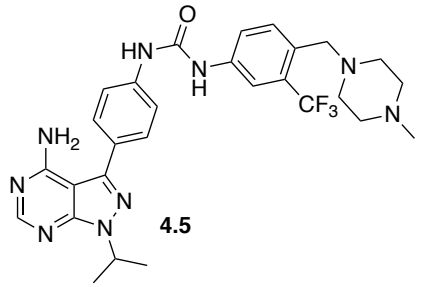

4.5

^{1}H NMR

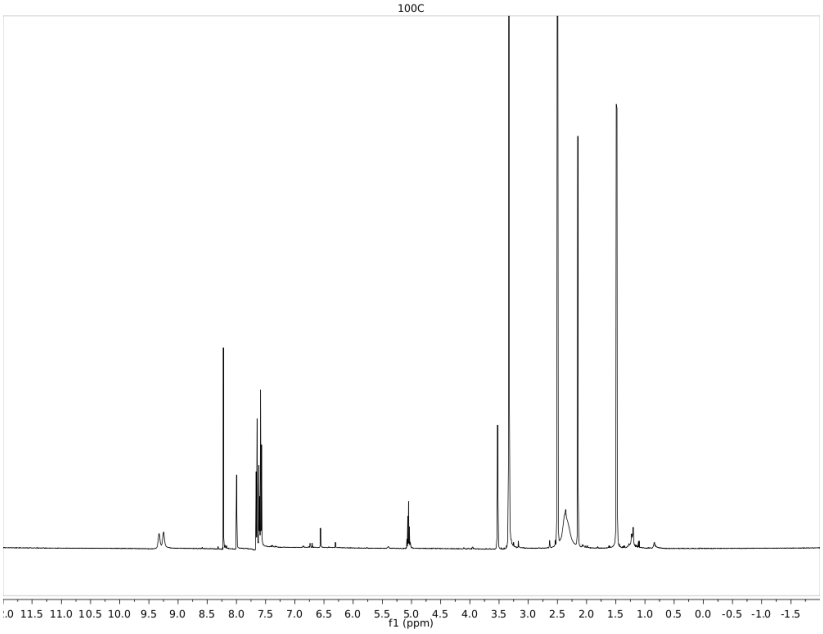

^{13}C NMR

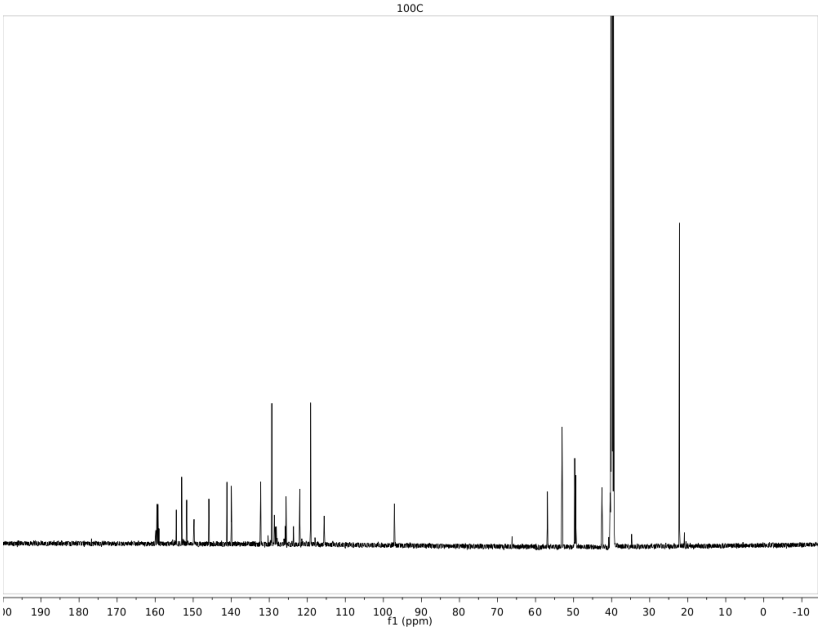

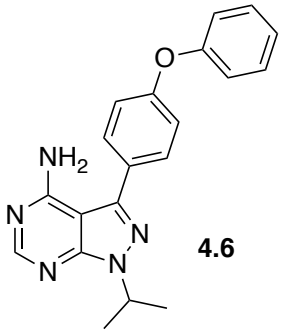

4.6

^{1}H NMR

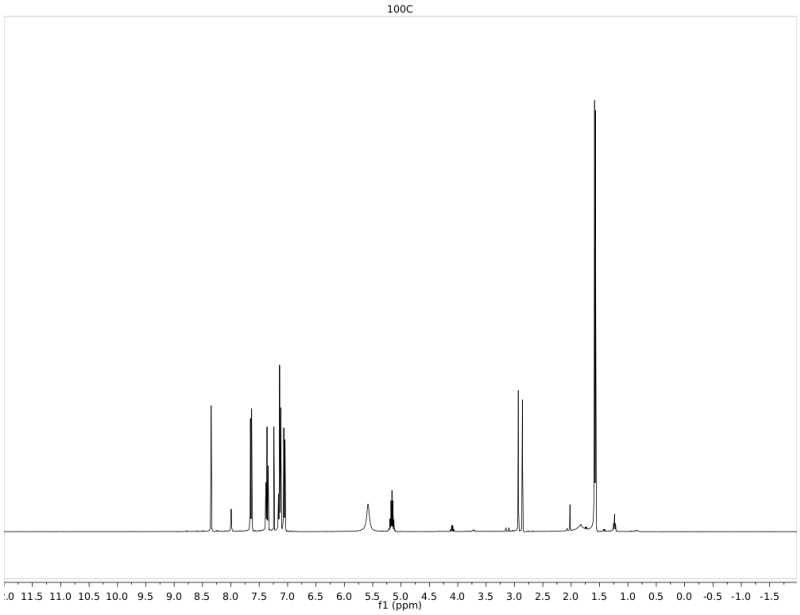

^{13}C NMR

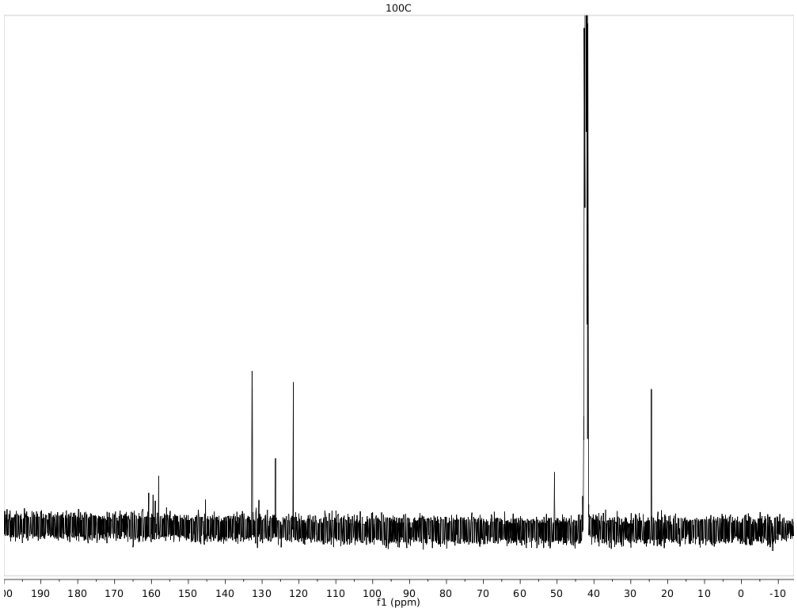

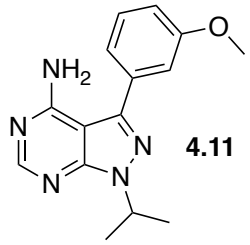

4.11

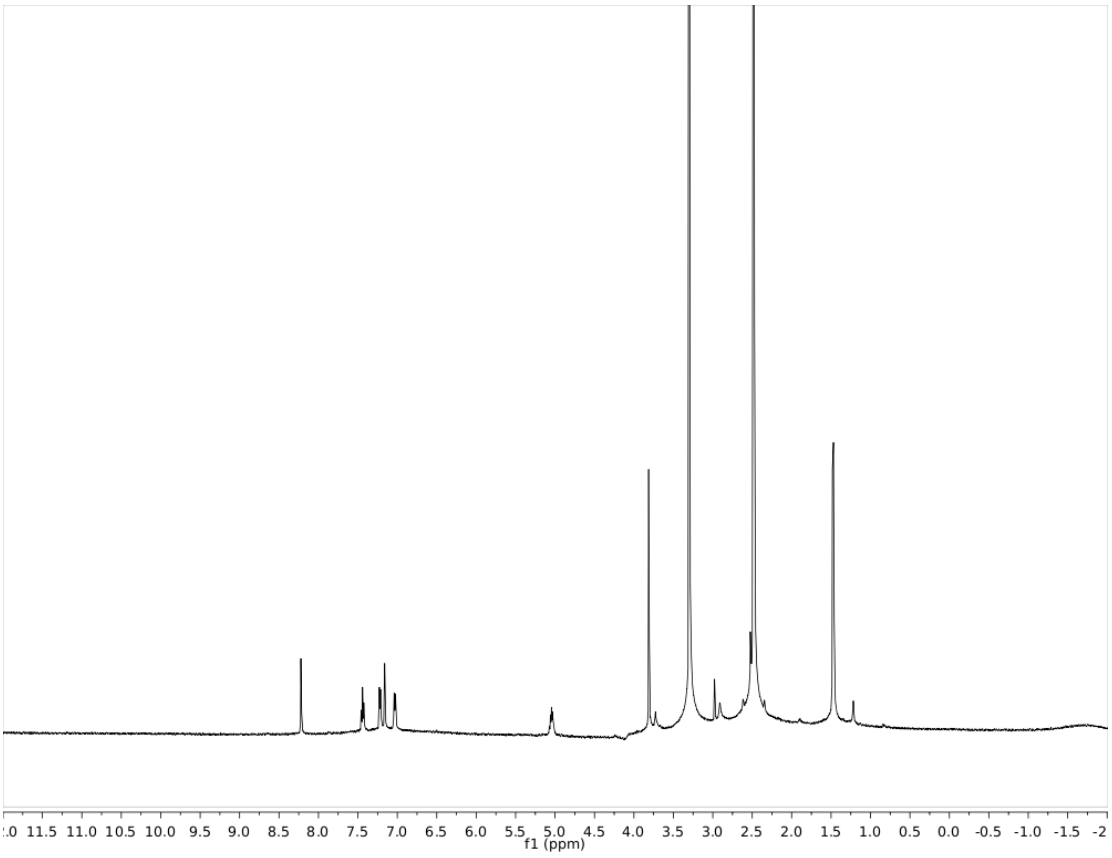

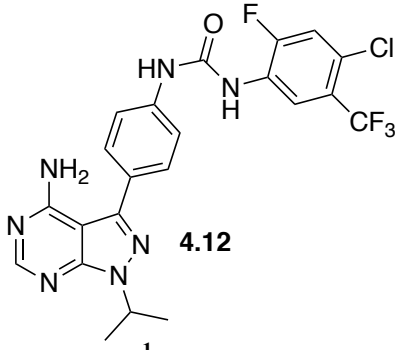

4.12

^{1}H NMR

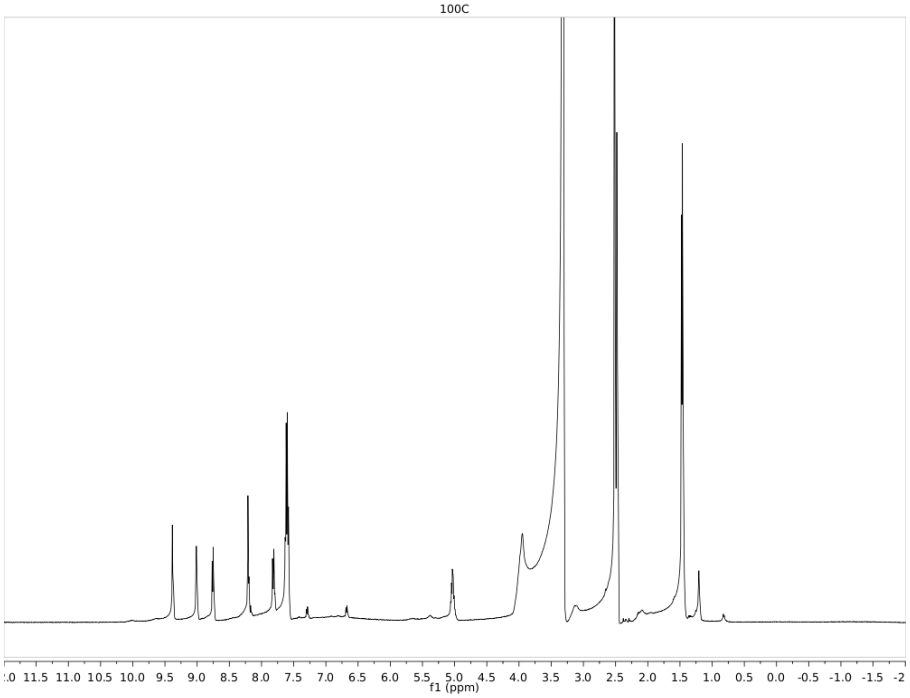

^{13}C NMR

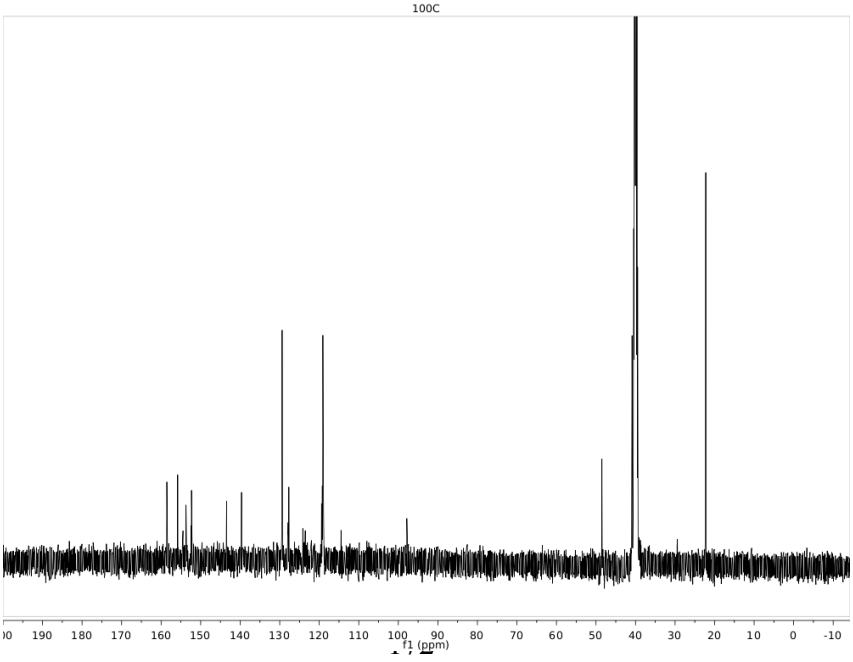

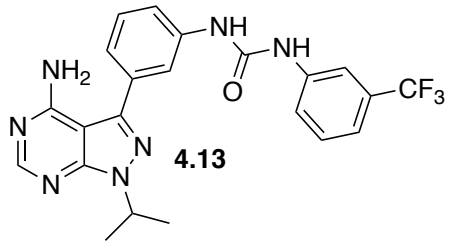

4.13

^{1}H NMR

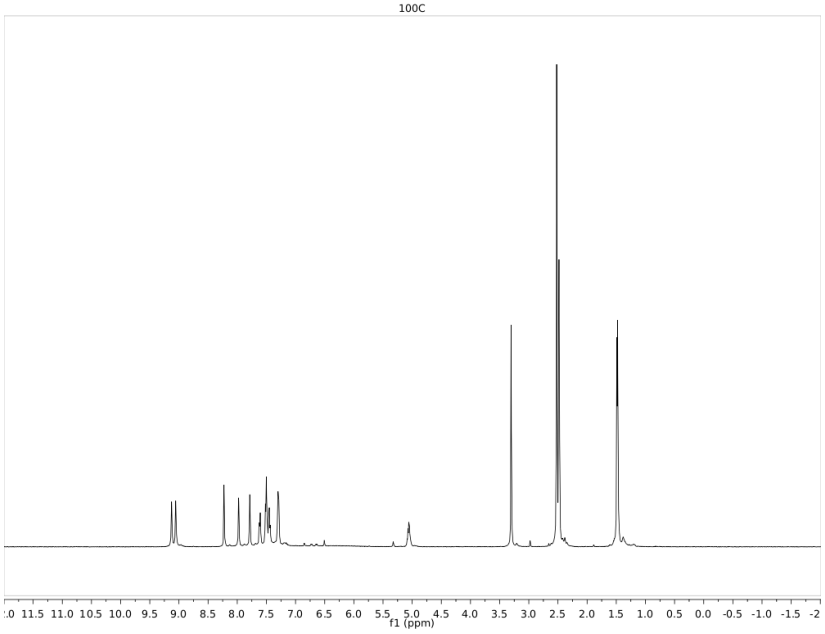

^{13}C NMR

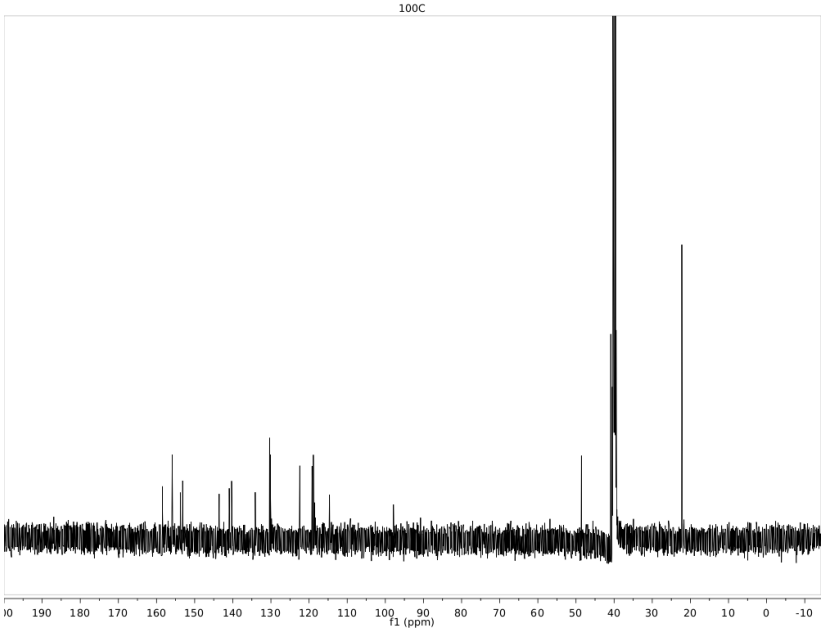

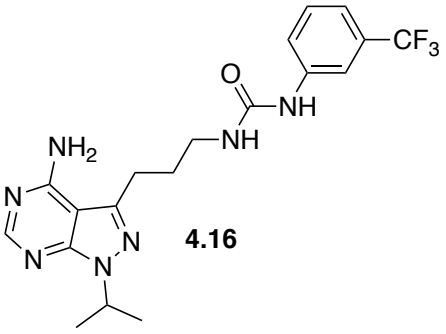
CF3
O
NH
NH
NH2
N
N
N
N

4.16

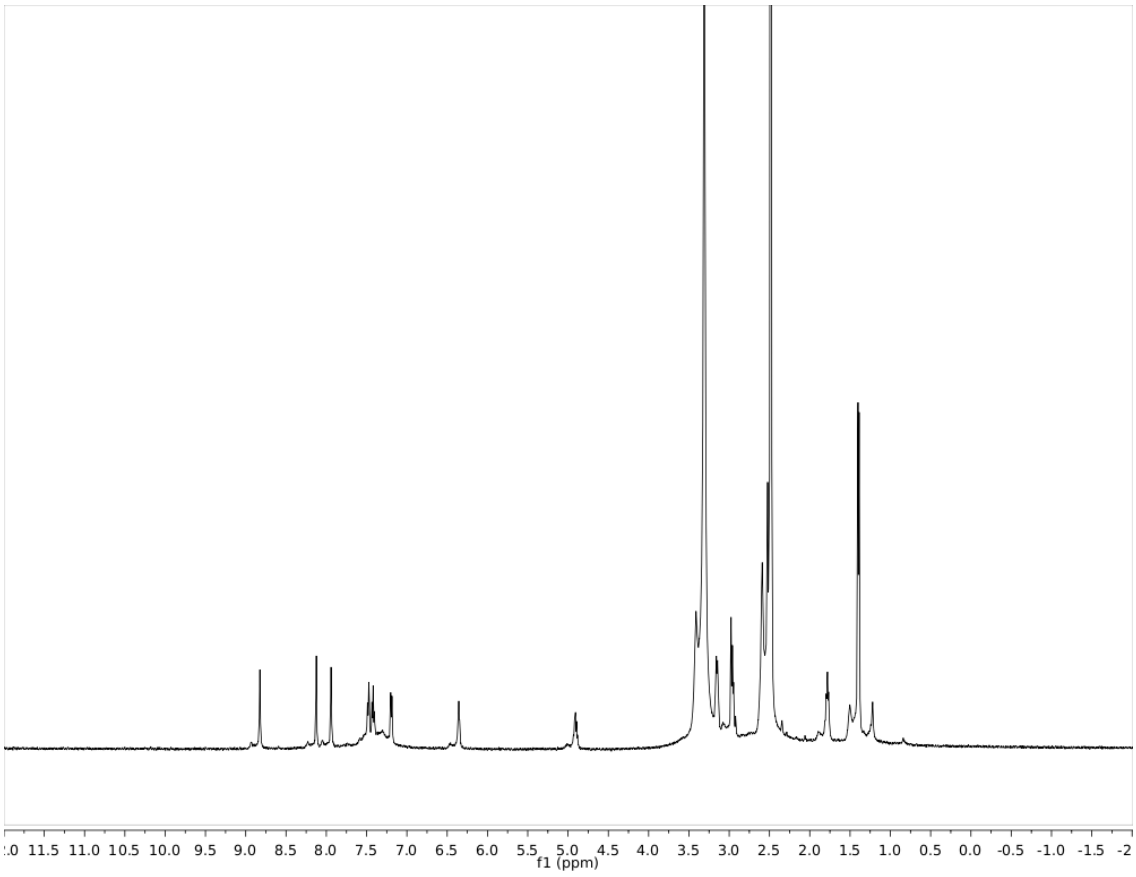
11.5 11.0 10.5 10.0 9.5 9.0 8.5 8.0 7.5 7.0 6.5 6.0 5.5 5.0 4.5 4.0 3.5 3.0 2.5 2.0 1.5 1.0 0.5 0.0 -0.5 -1.0 -1.5 -2
f1 (ppm)

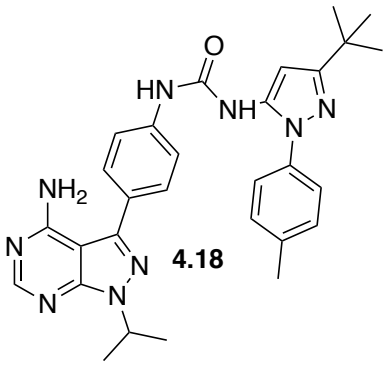
O
HN
NH
N
N
NH2
N
N
N
N

4.18

^{1}H NMR

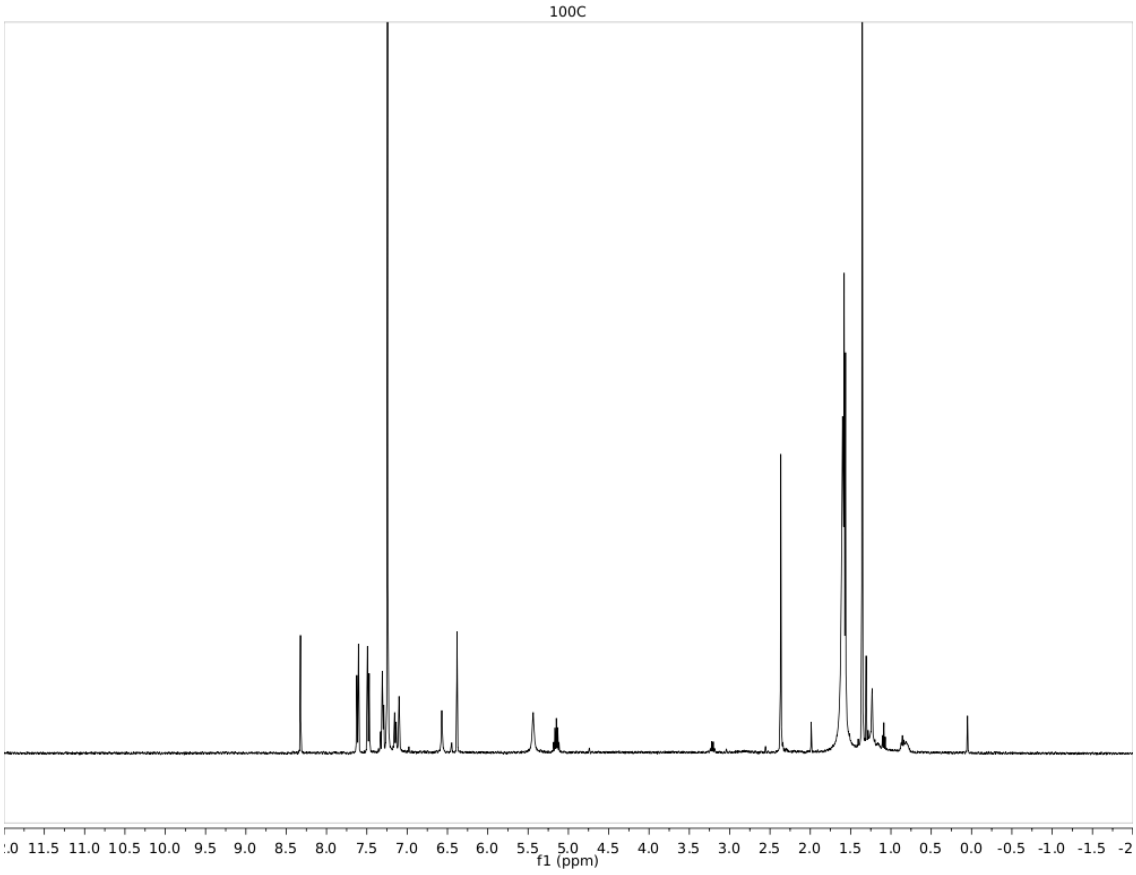
100C
11.5 11.0 10.5 10.0 9.5 9.0 8.5 8.0 7.5 7.0 6.5 6.0 5.5 5.0 4.5 4.0 3.5 3.0 2.5 2.0 1.5 1.0 0.5 0.0 -0.5 -1.0 -1.5 -2
f1 (ppm)

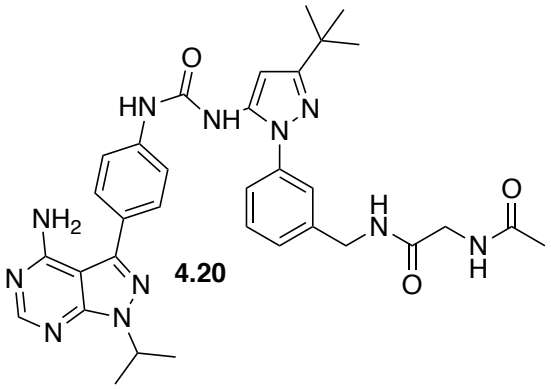

4.20

^{1}H NMR

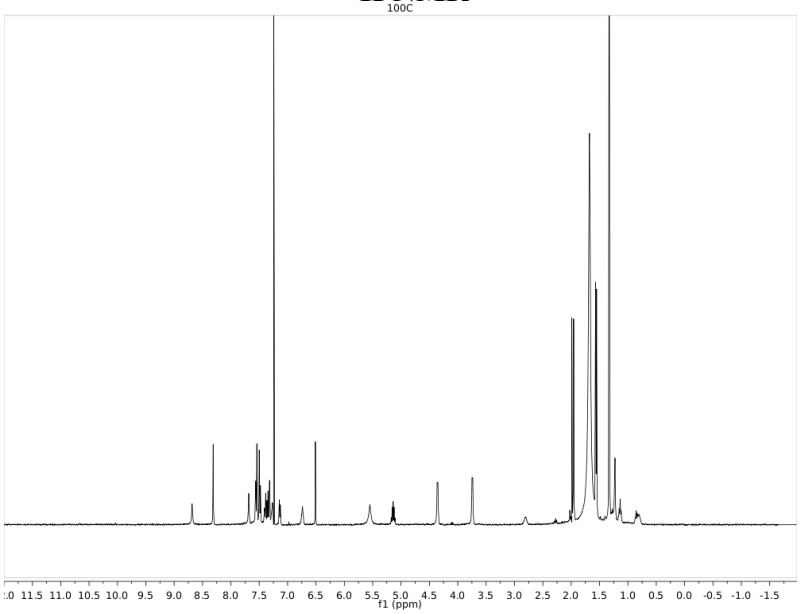

^{13}C NMR

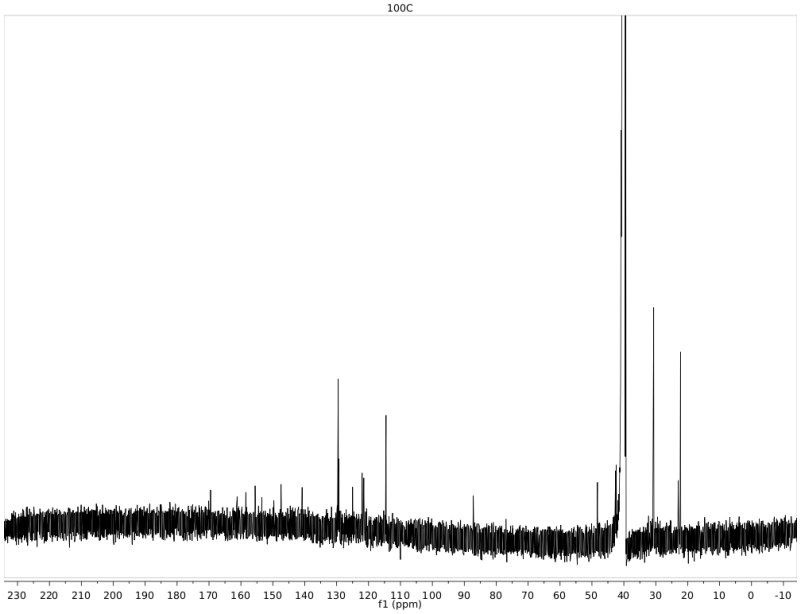

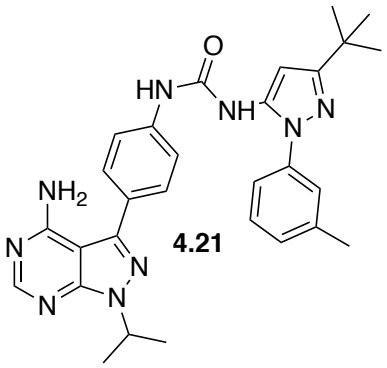
O
HN
NH
N
N
NH2
N
N
N
N

4.21

^{1}H NMR

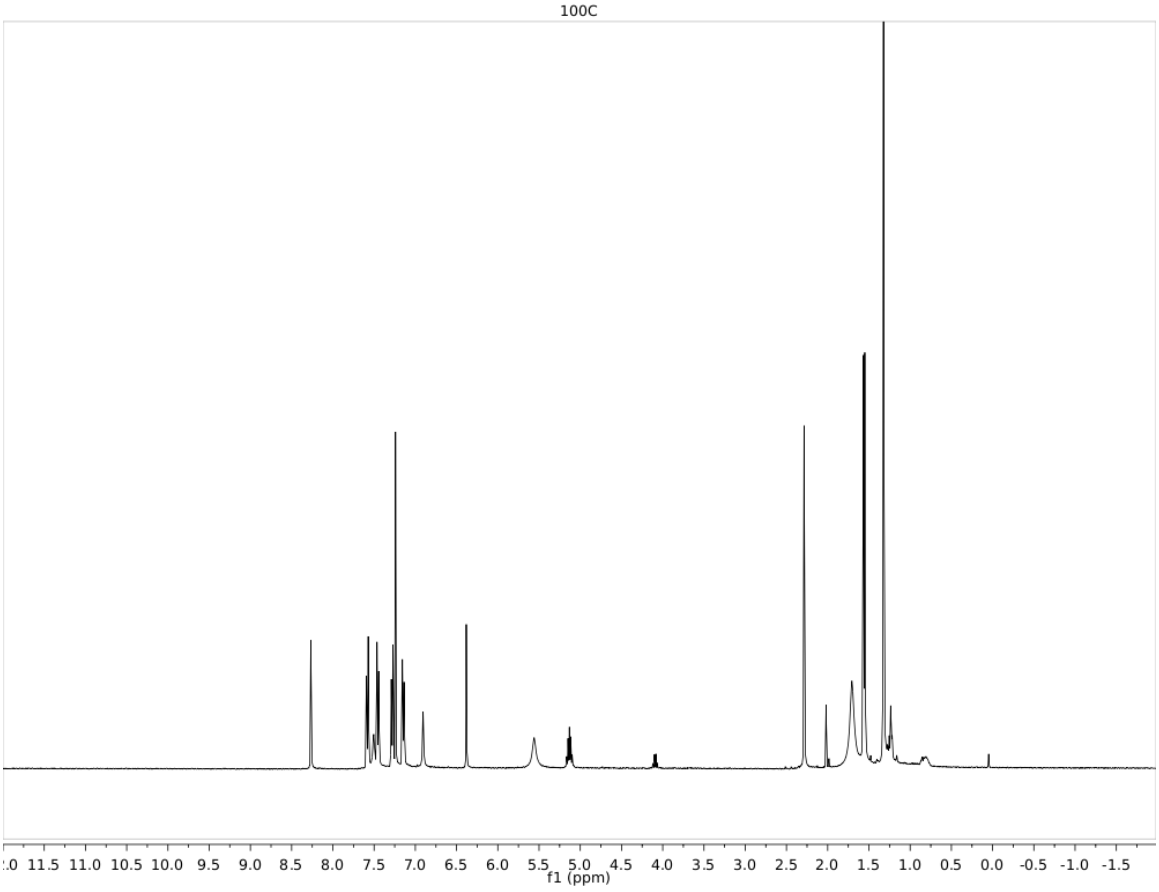
100C
11.5 11.0 10.5 10.0 9.5 9.0 8.5 8.0 7.5 7.0 6.5 6.0 5.5 5.0 4.5 4.0 3.5 3.0 2.5 2.0 1.5 1.0 0.5 0.0 -0.5 -1.0 -1.5
f1 (ppm)

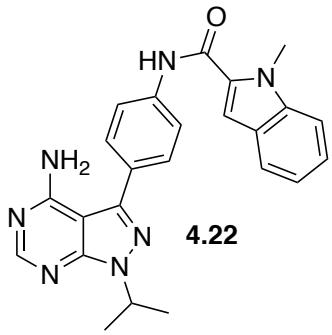

4.22

^{1}H NMR

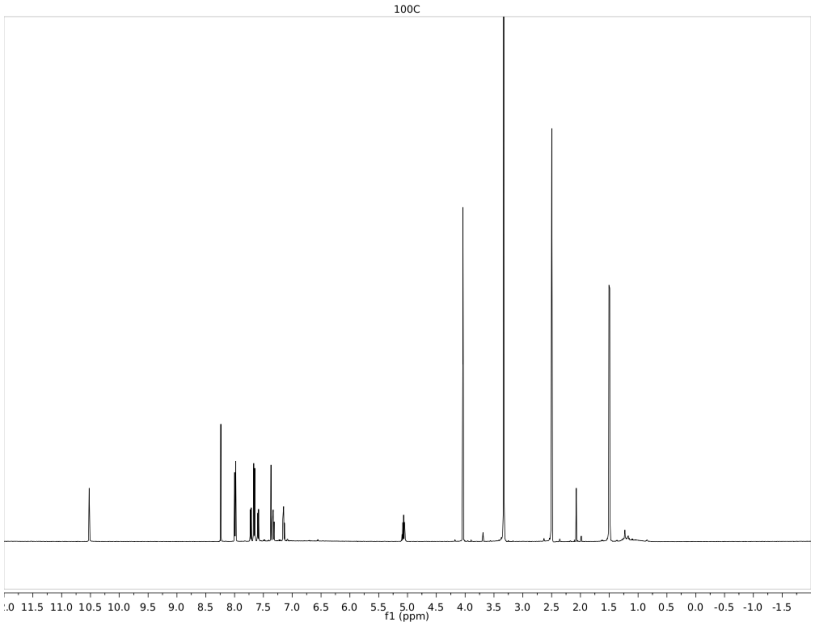

^{13}C NMR

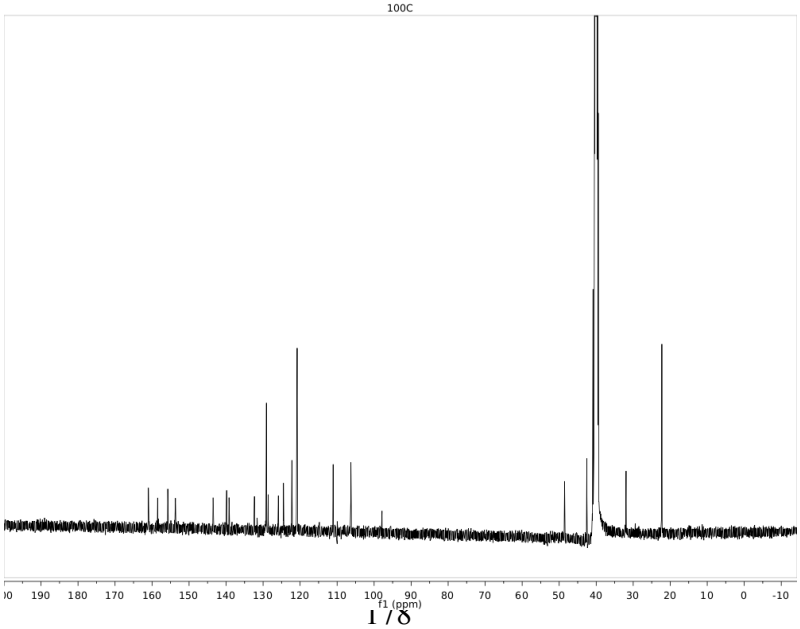

1 / δ

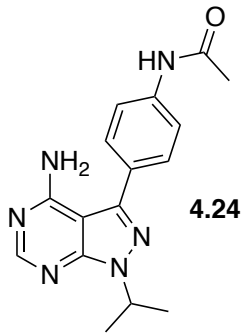

4.24

^{1}H NMR

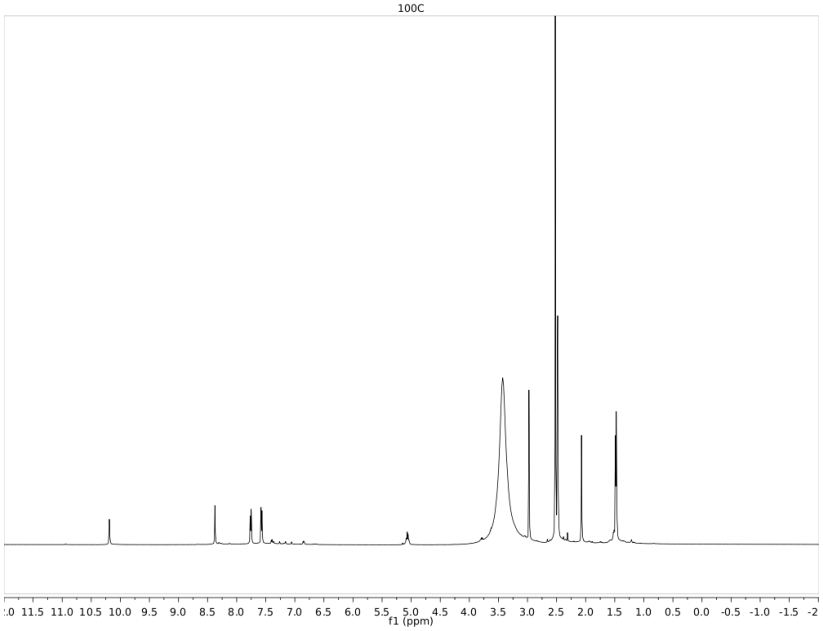

^{13}C NMR

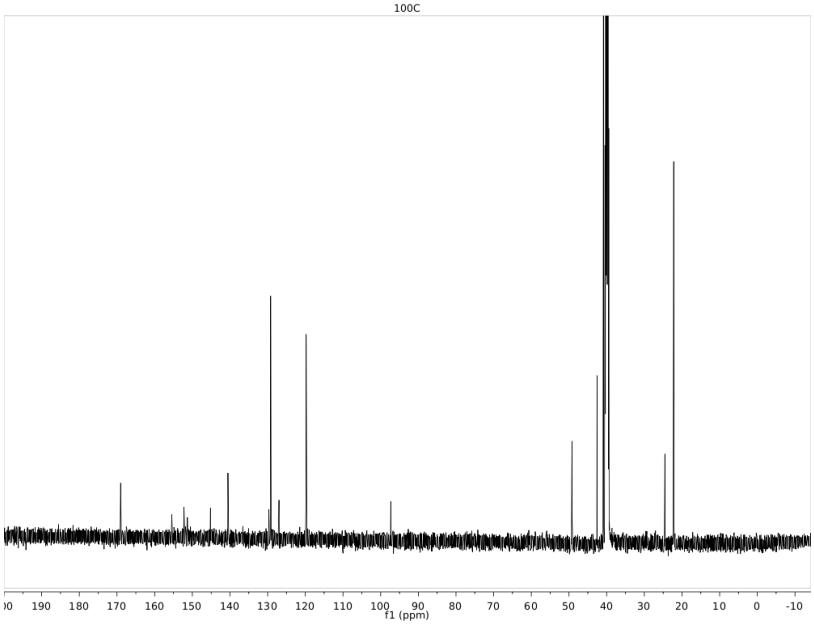

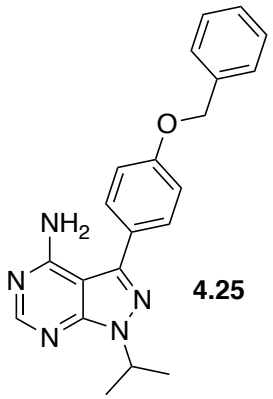

4.25

^{1}H NMR

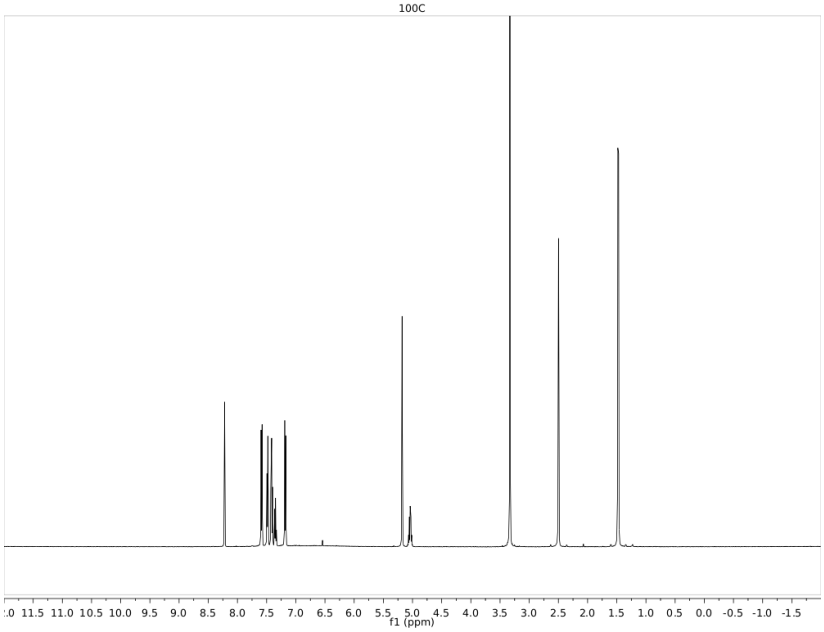

^{13}C NMR

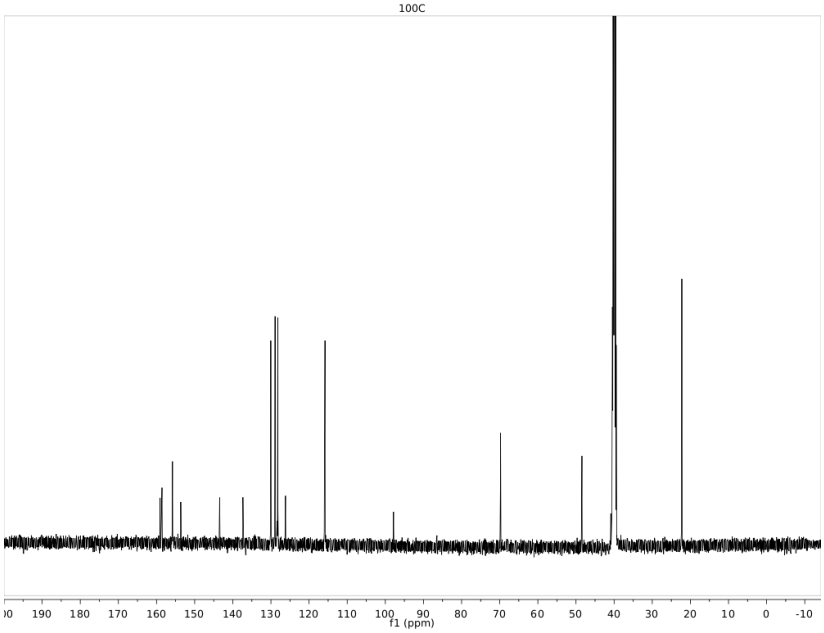

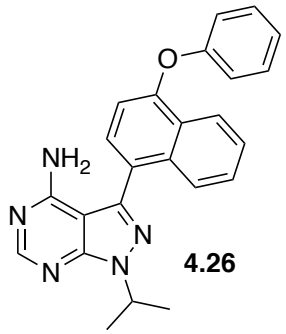

4.26

^{1}H NMR

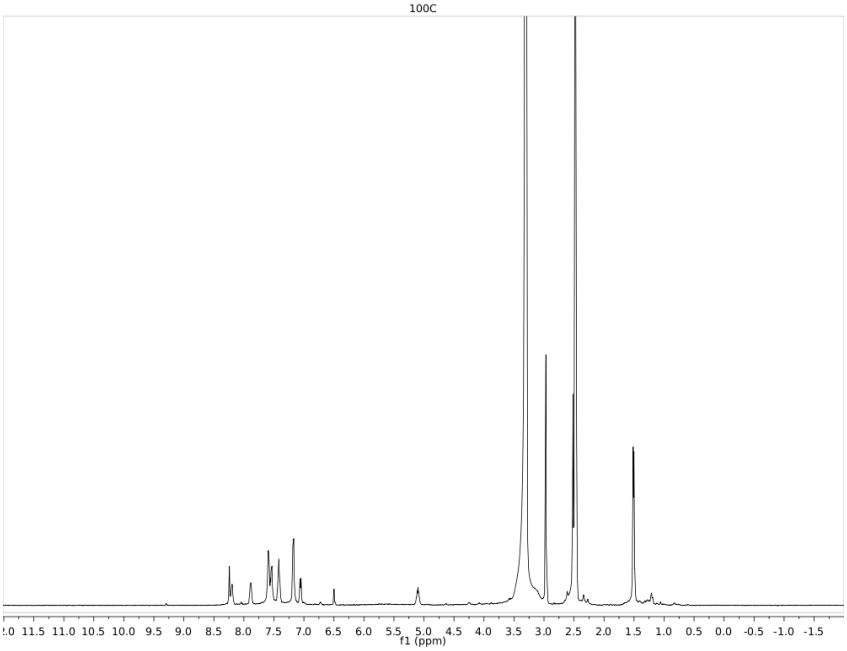

^{13}C NMR

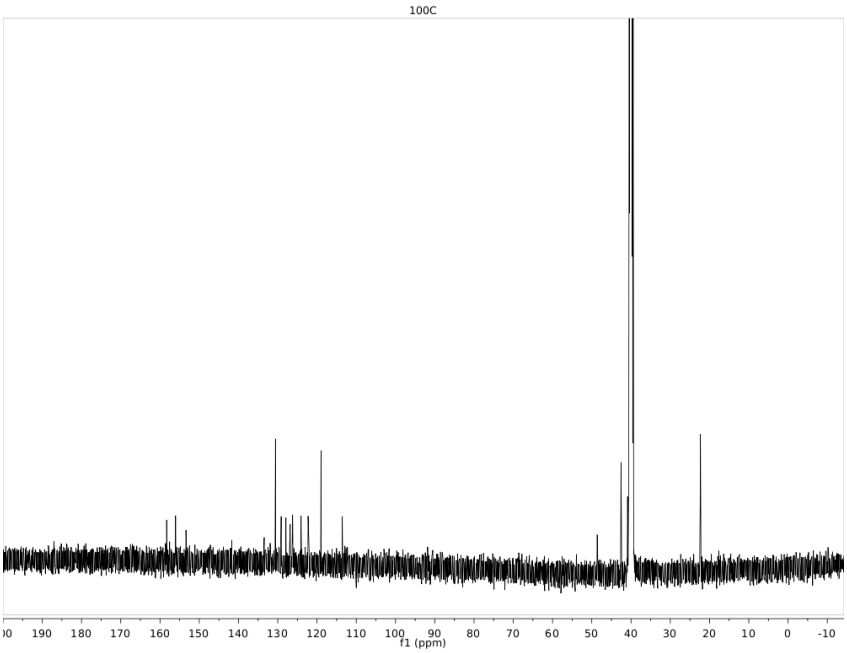

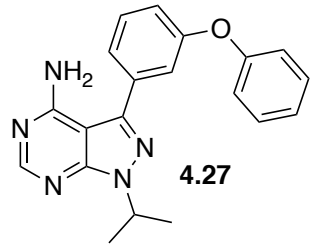
NH2
N
N
N
N
O

4.27

^{1}H NMR

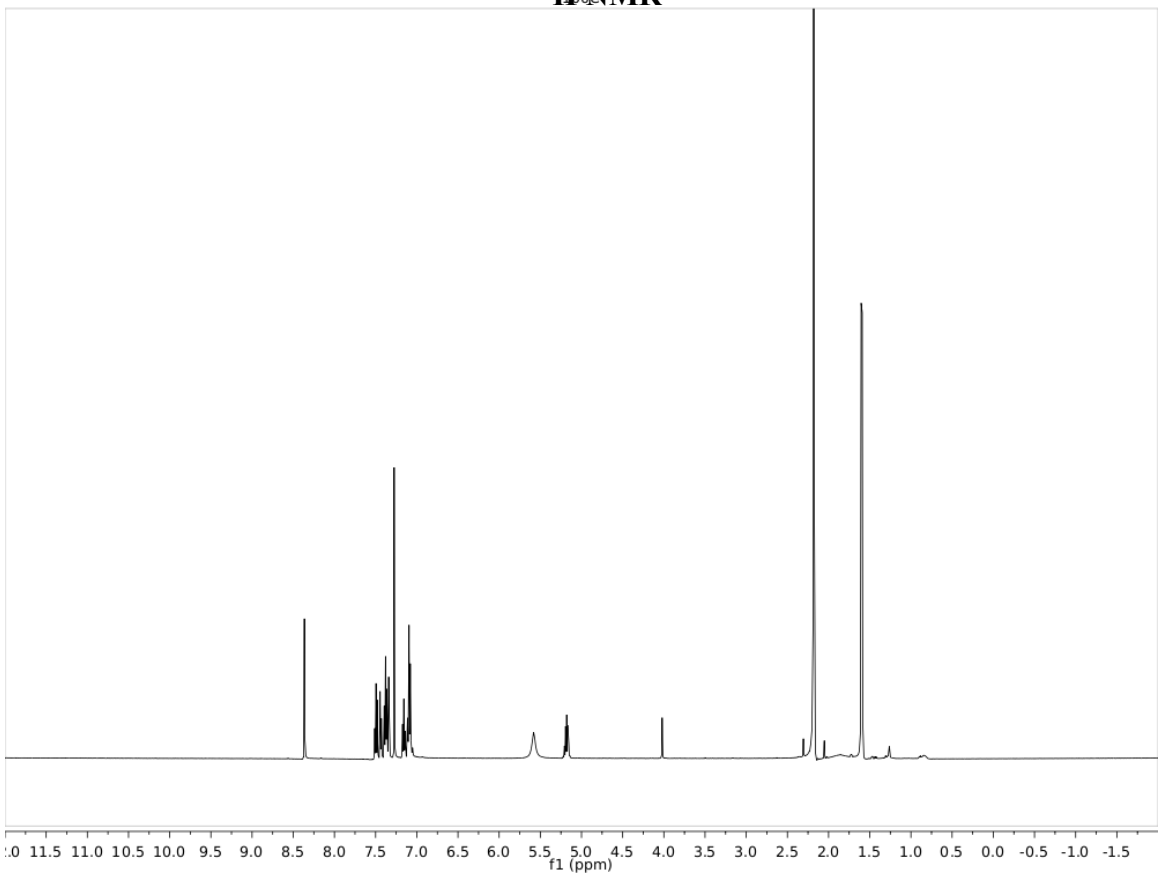
11.5 11.0 10.5 10.0 9.5 9.0 8.5 8.0 7.5 7.0 6.5 6.0 5.5 5.0 4.5 4.0 3.5 3.0 2.5 2.0 1.5 1.0 0.5 0.0 -0.5 -1.0 -1.5
f1 (ppm)

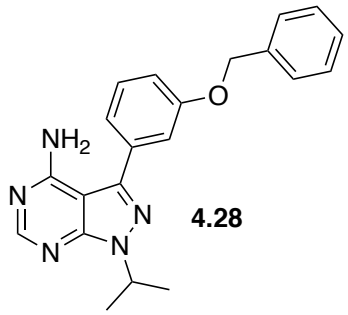

4.28

100C

^{1}H NMR

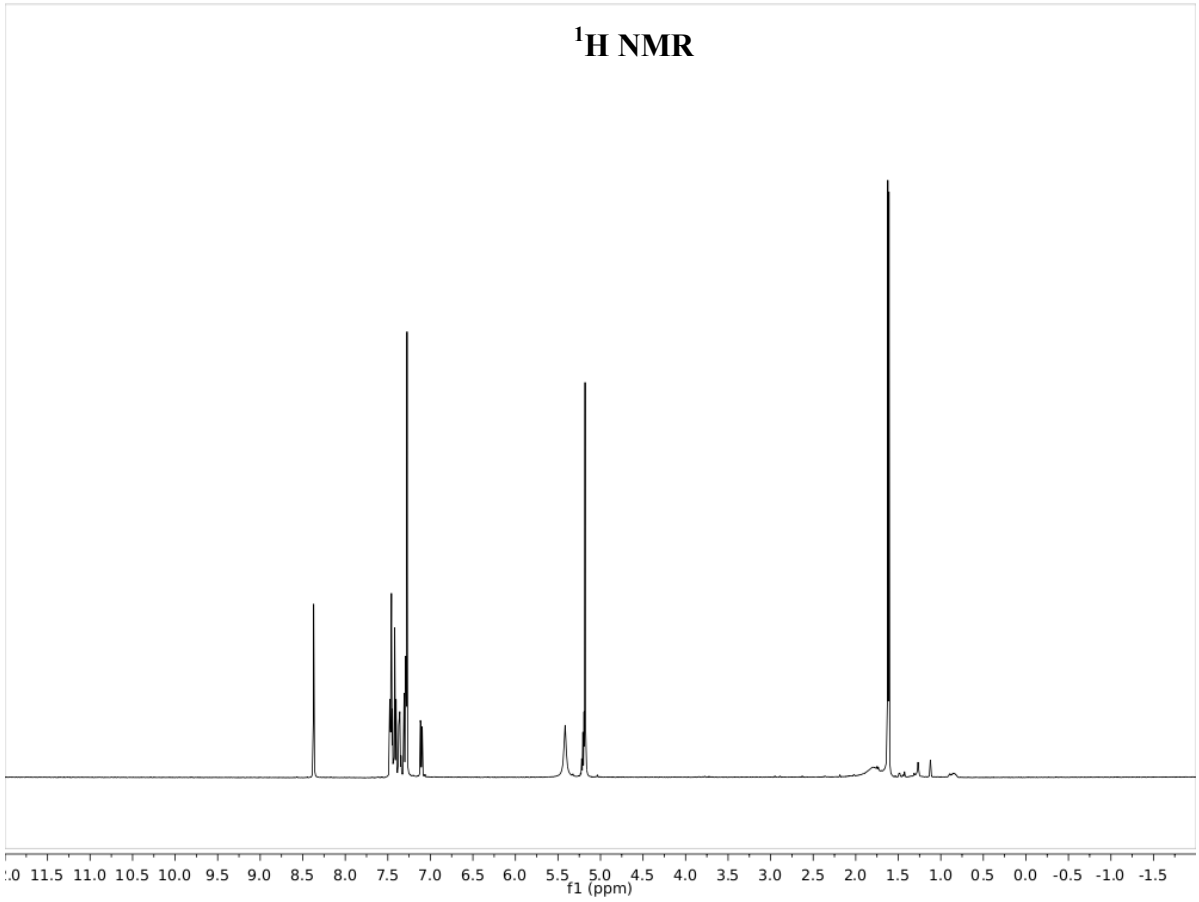

Appendix D

Supplemental Data for Chapter V

Analytical Data for Half-Life Determination of c-Src Mutants
Figure D.1. Analytical Data for Half-Life Determination of c-Src Mutants

A. 2 μM Q365W with 60 nM Thermolysin $T_{1/2}$ = 314 mins

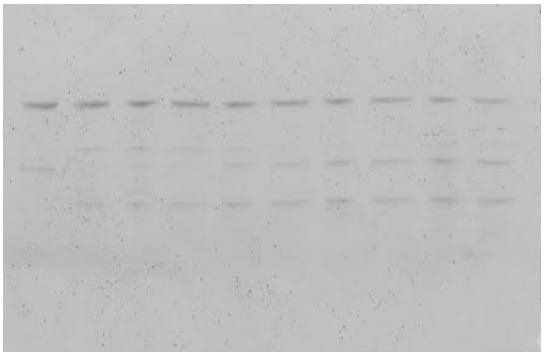

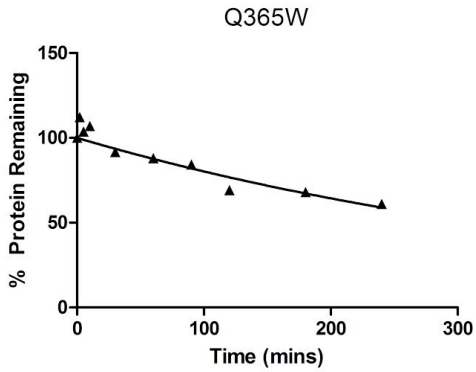

	Q365W
Half Life	314.4

B. 2 μM T293W with 60 nM Thermolysin $T_{1/2}$ = 80 mins

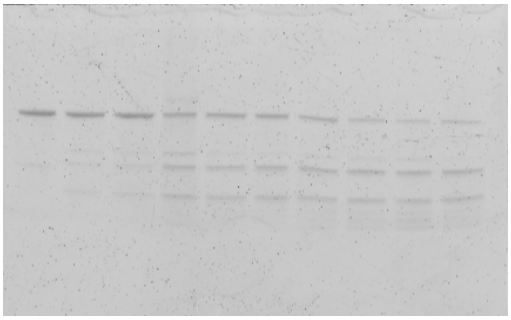

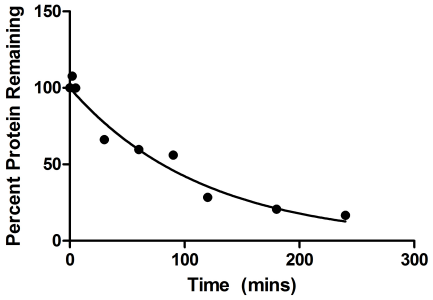

	T293W
Half Life	80

C. 2 μM Q254W with 60 nM Thermolysin $T_{1/2}$ = 30 mins

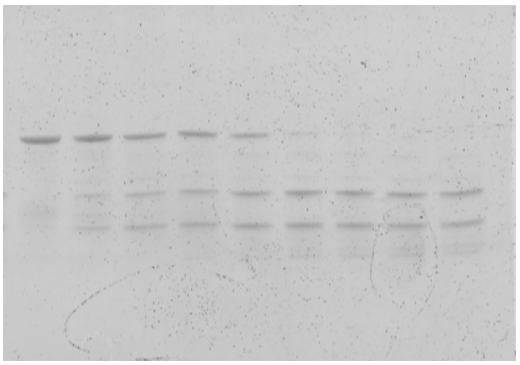

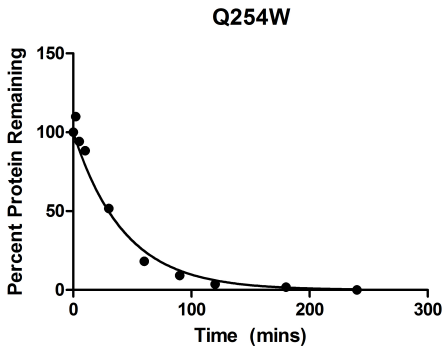

	Q254W
Half Life	30